



**CLIMATE & BIOTA** of the  
**EARLY PALEOGENE**

CBEP 2011

5<sup>th</sup> - 8<sup>th</sup> June, Salzburg/Austria

5 – 8 June 2011  
Salzburg  
Austria

# FIELD-TRIP GUIDEBOOK

Edited by: Hans Egger

## **BIBLIOGRAPHIC REFERENCE**

Hans Egger, 2011. Climate and Biota of the Early Paleogene, Field-Trip Guidebook, 5 – 8 June 2011, Salzburg, Austria. - Berichte der Geologischen Bundesanstalt, **86**, 132 p., Wien

ISSN 1017-8880

This work is subject to copyrights. All rights are reserved.

© Geologische Bundesanstalt, Neulinggasse 38, A 1030 Wien

[www.geologie.ac.at](http://www.geologie.ac.at)

Printed in Austria

Cover-Design by: Monika Brüggemann-Ledolter

Layout by: Markus Kogler

Verlagsort: Wien

Herstellungsort: Wien

Ziel der „Berichte der Geologischen Bundesanstalt“ ist die Verbreitung wissenschaftlicher Ergebnisse.

Die „Berichte der Geologischen Bundesanstalt“ sind im Handel nicht erhältlich.

Die einzelnen Beiträge sind auf der Website der Geologischen Bundesanstalt frei verfügbar.

Satz: Geologische Bundesanstalt

Druck: Offset-Schnelldruck Riegeltechnik, Piaristengasse 8, A 1080 Wien

Cover photo: Salzburg.info

## SPONSORS



Commission of the Stratigraphical and Palaeontological Research of Austria



Elektro-Optik-Service GmbH



Rohöl-Aufsuchungs AG

# LIST OF AUTHORS

(in alphabetic order)

## **Niels Andersen**

Leibniz Laboratory for Radiometric Dating and Stable Isotope Research, Christian-Albrechts-Universität Kiel, Max-Eyth-Str. 11, D-24118 Kiel, Germany

## **Peter Bijl**

Biomarine Sciences, Laboratory of Palaeobotany and Palynology, Institute of Environmental Biology, Utrecht University, Budapestlaan 4, 3584 CD Utrecht, the Netherlands

## **Henk Brinkhuis**

Biomarine Sciences, Laboratory of Palaeobotany and Palynology, Institute of Environmental Biology, Utrecht University, Budapestlaan 4, 3584 CD Utrecht, the Netherlands

## **Stjepan Coric**

Geological Survey of Austria, Neulinggasse 38, 1030 Vienna, Austria

## **Robert Darga**

Naturkundemuseum Siegsdorf, Auenstr. 2, D-83313 Siegsdorf, Germany

## **Katica Drobne**

Ivan Rakovec Institute of Paleontology ZRC SAZU, Novi trg 2, P.O.Box 306, SL-1000 Ljubljana, Slovenia

## **Hans Egger**

Geological Survey of Austria, Neulinggasse 38, 1030 Vienna, Austria

## **Juliane Fenner**

Bundesanstalt für Geowissenschaften und Rohstoffe, Stille Weg 2, D 30655 Hannover, Germany

## **Holger Gebhardt**

Geological Survey of Austria, Neulinggasse 38, 1030 Vienna, Austria

## **Claus Heilmann-Clausen**

Geologisk Institut, Aarhus Universitet, 8000 Aarhus C, Denmark

## **Christa Hofmann**

University of Vienna, Department of Palaeontology, Althanstr. 14, 1090 Vienna, Austria

## **Franz Ottner**

University of Natural Resources and Applied Life Sciences, Gregor-Mendel-Straße 33, 1180 Vienna, Austria

## **Omar Mohamed**

El-Minia University, Faculty of Science, Geology Department, El-Minia, Egypt.

## **Fred Rögl**

Museum of Natural History, Burgring 7, 1014 Vienna, Austria

## **Bettina Schenk**

Geological Survey of Austria, Neulinggasse 38, A-1030 Vienna, Austria

## **Birger Schmitz**

University of Lund, Sölvegatan 12, Lund, Sweden

## **Michael Wagreich**

Universität Wien, Department für Geodynamik und Sedimentologie, Althanstraße 14, 1090 Vienna, Austria

## **Winfried Werner**

Bavarian State Collection for Palaeontology and Geology, Richard-Wagner-Str. 10, D-80333 Munich, Germany

## **Erik Wolfgring**

Universität Wien, Department für Geodynamik und Sedimentologie, Althanstraße 14, A-1090 Vienna Austria

## **FIELD TRIP LEADERS**

**Stjepan Ćorić** (Geological Survey of Austria)

**Robert Darga** (Natural History Museum Siegsdorf)

**Hans Egger** (Geological Survey of Austria)

**Holger Gebhardt** (Geological Survey of Austria)

**Fred Rögl** (Museum of Natural History Vienna)

**Michael Wagneich** (University of Vienna)



# CONTENTS

<b>Introduction</b> .....	<b>9</b>
<b>Fieldtrip A1</b> .....	<b>17</b>
<b>Stop A1/1:</b> Untersberg Section near Fürstenbrunn .....	19
<b>Stop A1/2:</b> Anthering Section .....	27
<b>Stop A1/3:</b> Strubach Section .....	37
<b>Stop A1/4:</b> Southern Shelf of the European plate .....	39
<b>Fieldtrip A2</b> .....	<b>47</b>
<b>Stop A2/1:</b> Holzhäusl outcrop near Mattsee .....	49
<b>Stop A2/2:</b> Siegtsdorf Museum .....	59
<b>Stop A2/3:</b> Type locality of the Adelholzen beds (Primusquelle bottling plant) .....	61
<b>Stop A2/4:</b> Maastrichtian to Ypresian slope-basin deposits of the Ultrahelvetic nappe complex ..	73
<b>Fieldtrip A3</b> .....	<b>85</b>
<b>Stop A3/1:</b> GeoCentre at Gams .....	87
<b>Stop A3/2:</b> The Cretaceous-Paleogene (K/Pg) boundary at the Gamsbach section .....	89
<b>Stop A3/3:</b> Pichler section (Gams) .....	99
<b>Stop A3/4:</b> Photostop at the open cast mine Erzberg .....	107
<b>Overnight at St. Georgen am Längsee</b>	
<b>Stop A3/5:</b> Photostop at the Hochosterwitz Castle .....	109
<b>Stop A3/6:</b> Pemberger and Fuchsofen Quarries to the west of Klein St. Paul. ....	111
<b>Stop A3/7:</b> Outcrops along the Sonnberg forest road near Guttaring .....	119
<b>References</b> .....	<b>125</b>



## THE EARLY PALEOGENE HISTORY OF THE EASTERN ALPS

Hans Egger

The Eastern Alps, a 500 km long segment of the Alpine fold-and-thrust belt, originated from the northwestern Tethyan realm. The modern structure of the Eastern Alps is the result of the convergence between the European and the Adriatic plates (Fig. 1). Separation of these plates started by oblique rifting and spreading in the Permian and Triassic and continued during the Jurassic by the formation of oceanic lithosphere in the Penninic basin. The structural evolution of this basin was linked to the opening of the North Atlantic (e.g. Frisch, 1979; Stampfli et al., 2002). Due to the presence of lower Eocene sedimentary rocks in the Penninic units, it is clear that the final closure of the Penninic Ocean did not occur before the Eocene (see Neubauer et al., 2000 for a review).

As a result of the oblique collision of the European and Adriatic plates the elimination of the Penninic Ocean started in the West and prograded continuously to the East. E. g., thrusting in the Eastern Alps started at latest in the Middle Eocene whereas in the adjacent Western Carpathians the onset of thrust formation was around the Eocene-Oligocene boundary (see Decker & Peresson, 1996 for a review). In the Eastern Alps continuing convergence during the Miocene caused lateral tectonic escape of crustal wedges along strike slip faults, which strongly affected the nappe complex of the Eastern Alps. A recent review on the complicated structural development of the Eastern Alps is given by Brückl et al. (2010).

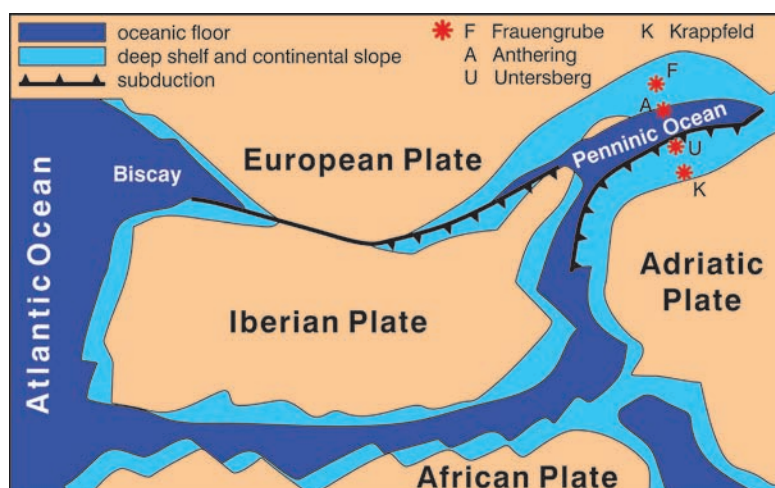


**Figure 1 ▲** Schematic paleogeographic map of the NW Tethys and neighbouring areas showing the location of the Alpine environmental areas in the early Paleogene (simplified and modified after Stampfli et al., 1998). Notice the location of the sections studied from the southern European plate margin until the northern Adriatic plate margin, with the Penninic Basin in between.

The northern rim of the Eastern Alps consists of detached Jurassic to Paleogene deposits, which tectonically overlie Oligocene to lower Miocene Molasse sediments. From north to south these thrust units originated from (1) the southern shelf of the European Plate (Helvetic nappe complex), (2) the adjacent passive continental margin (Ultrahelvetic nappe complex), (3) the abyssal Penninic Basin (Rhenodanubian nappe complex) and (4) the bathyal slope of the Adriatic Plate (nappe complex of the Northern Calcareous Alps). Thrusting and wrenching from the Upper Eocene on destroyed the original configuration of these depositional areas and, therefore, the original palinspastic distance

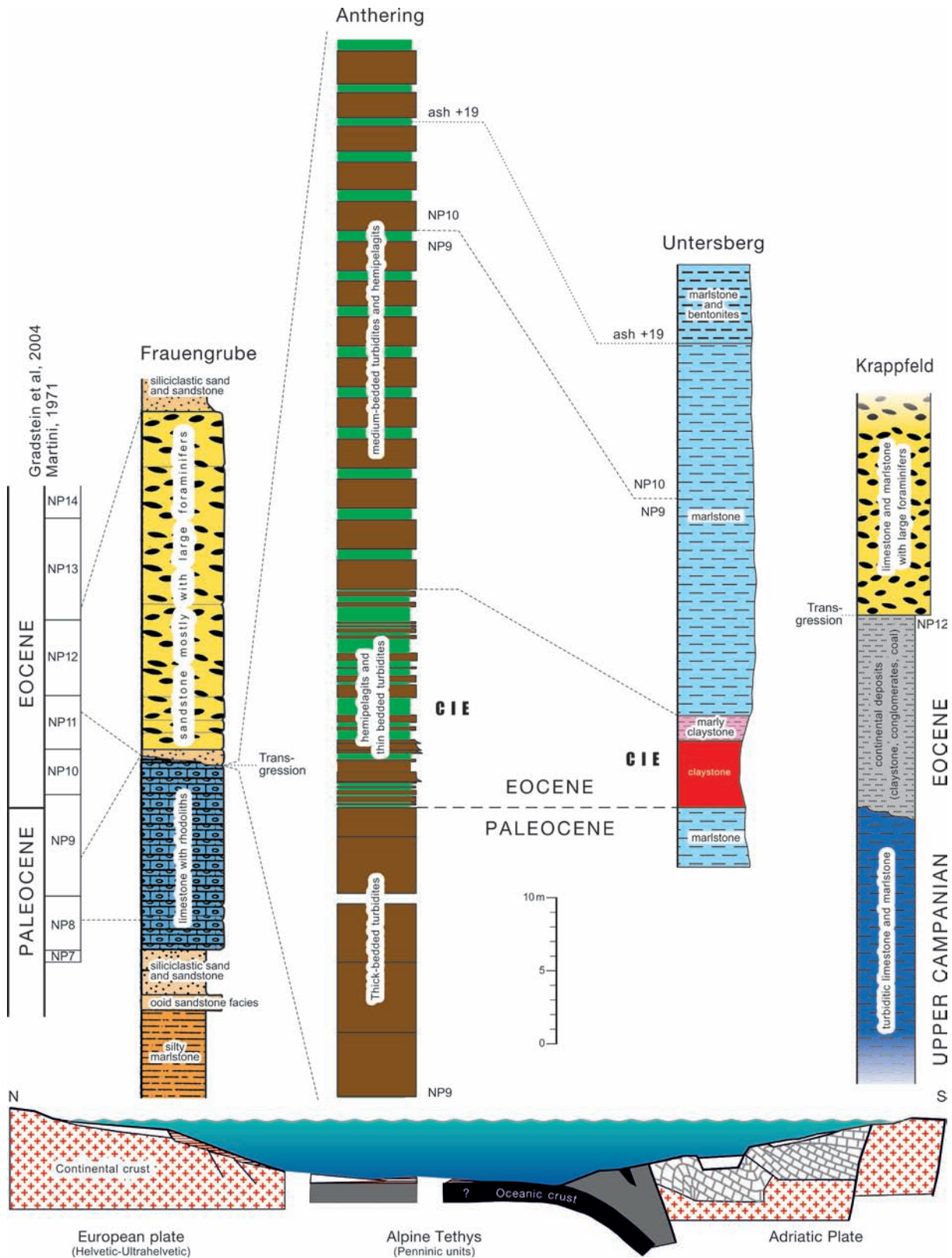


**Figure 2 ▲**  
Correlation and paleogeographic position of Paleogene sections across the Penninic Basin.



**Figure 3 ▲**

The transgressive contact between the Gerhardsreit Formation (Maastrichtian) and the glauconitic sandstone of the Adelholzen Formation (Lutetian) at the Wimmern section (Bavaria).

with an erosional unconformity overlies the Maastrichtian of the Gerhartsreith Formation (Fig. 3). The Adelholzen Beds are an equivalent of the Bürgen Formation in Switzerland (Schwerd, 2008) where an equivalent hiatus between the Cretaceous and the Eocene occurs (Menkveld-Gfeller, 1997). Basinward, this main hiatus is less extended and comprises only the uppermost Paleocene (upper part of Zone NP9) and the lowermost Eocene (Zones NP10 and NP11 - Egger et al., 2009b) in the southern part of the Helvetic shelf (Frauengrube section – STOP A1/4). A tectonically disturbed but continuous record exists across the K/Pg-boundary of the South-Helvetic domain (Kuhn & Weidich, 1987; Rasser & Piller, 1999).

Towards south, the Helvetic shelf gradually passed into the Ultrahelvetic continental slope. Depending on the paleodepth at this slope, the pelitic rocks of the Ultrahelvetic unit display varying contents of carbonate. Since Prey (1952), these pelitic deposits were assembled to the informal lithostratigraphic unit Buntmergelserie, which was thought to comprise Albian to upper Eocene. However, only very few small outcrops of Paleocene to middle Eocene (STOPA2/1 – Rögl & Egger, 2010) have been recognized and most of them have unclear tectonic positions due to a strong tectonic deformation.

Recently, Egger & Mohamed (2010) recognized a stratigraphic contact between upper Maastrichtian (calcareous nannoplankton Zone CC25) Buntmergelserie and the uppermost Maastrichtian (CC26) to lowermost Eocene (NP11, NP12?) turbidite succession of the Achthal Formation at the Goppling section (STOP A2/4). This 350 m thick formation is interpreted as the infill of a slope basin, which formed as a result of block faulting of the continental margin. Deposition took place partly below the planktonic foraminiferal lysocline and partly below the CCD.

Sedimentary successions rich in turbidites other than the Achthal Formation, are known from a number of Ultrahelvetic sites. In Vorarlberg (westernmost Austria), grey turbidites and hemipelagic marlstone (Kehlegg beds) were assigned to the Ultrahelvetic unit by Oberhauser (1991). The base of the Kehlegg beds is situated around the K/Pg-boundary. The unit comprises the entire Paleocene (Egger, unpublished) and its top is tectonically truncated by an overthrust. In a more southerly paleogeographic position on the slope, the deep-water system of the Feuerstätt thrust unit was deposited, exposed in Vorarlberg and southwestern Germany (see Schwerd and Risch, 1983 for a review). There, turbidites and intervening red claystone (“Rote Gschlif-Schichten”) of Paleocene and early Eocene age may represent the in-fills of adjacent slope basins at different paleodepths on the continental slope (Weidich and Schwerd, 1987; Schwerd, 1996). Farther to the east, in Lower Austria, Paleocene to Eocene turbidite successions associated with Buntmergelserie are reported by Prey (1957).

In summary, the style of early Paleogene turbidite sedimentation on the European continental margin seen at the Goppling section was not a unique phenomenon. Rather, it occurred at several sites along

between the sedimentary environments of the studied sections is not known. During the pre-conference field trips, Paleogene sections along a north-south transect within these four major nappe complexes will be visited. The shelf deposits of the Adriatic Plate (Gurktal nappe complex) will be visited during the post conference field trip in the Krappfeld area in Carinthia (Fig. 2).

The shallow water sedimentary record of the Helvetic shelf is punctuated by a number of stratigraphic gaps, which become more pronounced in direction to the coast of the European continent in the north. So, in the North-Helvetic realm, Paleocene deposits are absent because there, the basal Lutetian (calcareous nannoplankton Sub-Zone NP14b) of the Adelholzen beds (STOP A2/2)

the strike of the Ultrahelvetic thrust unit in the Eastern Alps. Nevertheless, it is unlikely that these deposits originated from the same basin. Instead, a number of small sub-basins can be assumed, which, due to the different subsidence histories and their different bathymetric positions, probably cannot be directly correlated.

The largely synchronous formation of different sub-basins along the strike of the Ultrahelvetic slope points to large-scale tectonic deformation of the European continental margin, starting in the late Maastrichtian. The subsidence of intra-slope basins can be related to an extensional tectonic regime. However, for the same period, Nachtmann and Wagner (1987), Wessely (1987), and Ziegler (2002) all document strong intra-plate compressional deformation of the foreland of the Eastern Alps. Together with the data from the Goppling section and other Ultrahelvetic sites, this implies that the southern European plate was simultaneously affected by extension and compression. Here, this style of deformation is typical for anastomosing strike-slip fault zones in convergent settings (e.g. Crowell, 1974).

The well-established contractional deformation event, which affected the European Plate in Late Cretaceous times, was explained by two different models. In the first one, strike-slip faulting was driven

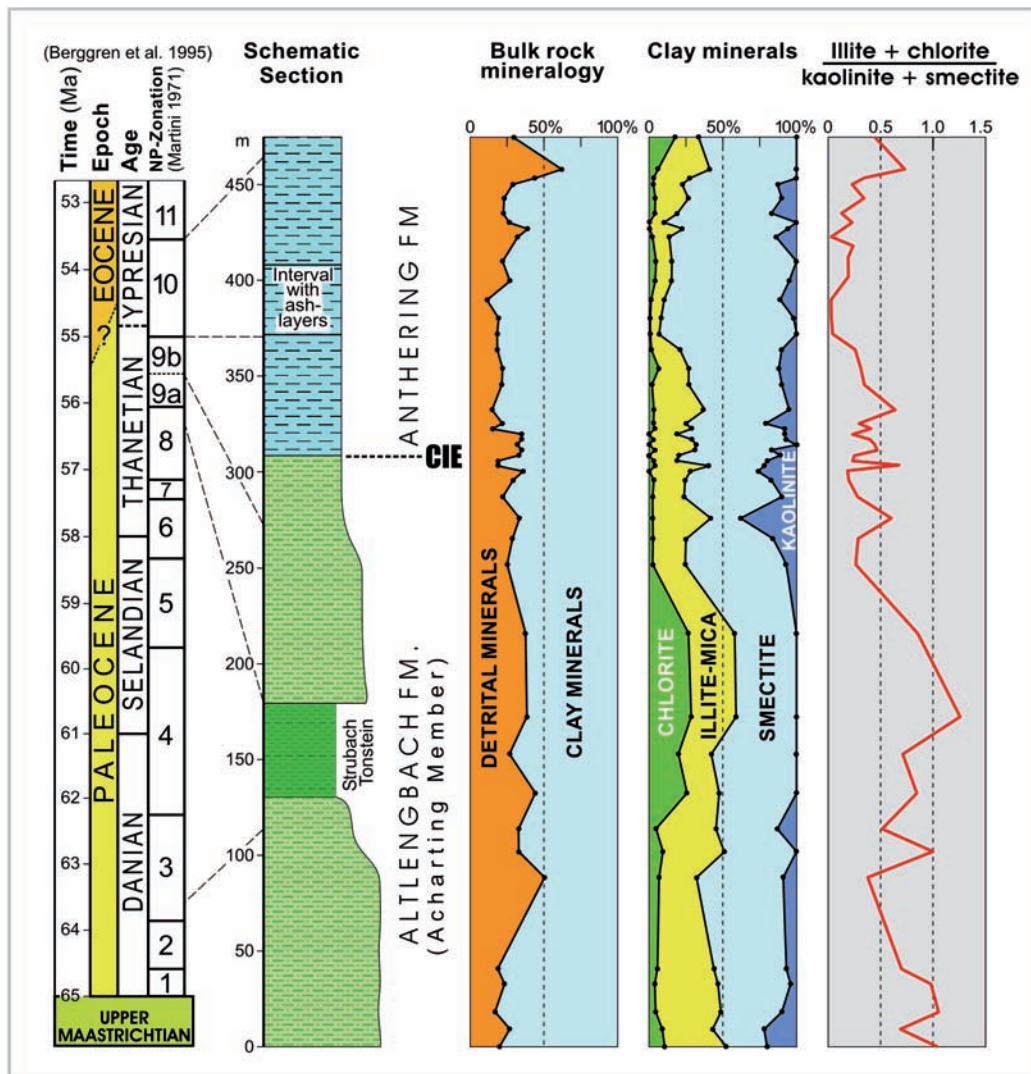


**Figure 4 ▲**  
 The Paleogene succession of the Rhenodanubian Flysch in Salzburg, including bulk rock mineralogy and composition of clay mineral assemblages of upper Maastrichtian to Ypresian hemipelagic shales. CIE: negative carbon isotope excursion (from Egger et al., 2002)

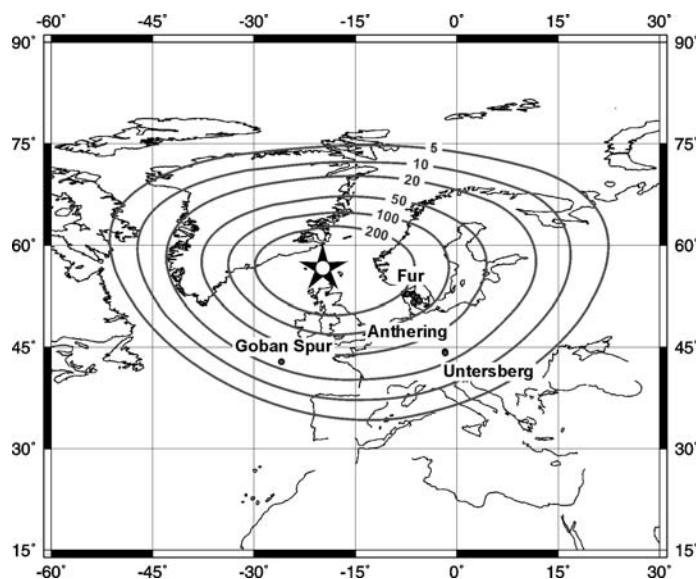


**Figure 5 ▲**

Map showing the plate tectonic situation at 54 Ma (rotated present day shore lines), the rotated locations where layer +19 has been found (solid spheres and locality names), and elliptical isopachs of layer +19 (grey contours, tephra thickness in mm) with the assumed NAIP-source (star) at one focus.

sedimentation (= Strubach-Tonstein, STOP A1/3) has been recognized in the Paleocene of the Rhenodanubian Group (Egger, 1995). This was interpreted to be the result of tectonic activity that caused a cut-off of the basin from its source areas (Egger et al., 2002). More precisely, the data presented suggest that structurally controlled slope-basins acted as sediment traps and prevented turbidity current by-pass to the main basin.

The Rhenodanubian Flyschzone constitutes an imbricated nappe complex trending NE parallel to the northern margin of the Eastern Alps. The deep-water sediments of Barremian to Ypresian age were formalized as Rhenodanubian Group (RG) by Egger and Schwerd (2008). The RG consists primarily of siliciclastic and calcareous turbidites but thin, hemipelagic claystone layers occur in all formations of the RG and indicate a deposition below the local calcite compensation depth, probably at palaeodepths > 3000 m (Butt, 1981; Hesse, 1975). Paleocurrents and the pattern of sedimentation suggest that the deposition occurred on a flat, elongate, weakly inclined abyssal basin plain (Hesse, 1982, 1995). Compared to other turbidite basins, the depositional area of the Rhenodanubian Group is characterized by low sedimentation rates. An average sedimentation rate for the Cretaceous basin fill, incorporating both turbidites and hemipelagites, of only 25 mm kyr<sup>-1</sup> has been calculated (Egger & Schwerd, 2008).

Lithostratigraphic classification of the Paleogene deposits of the Rhenodanubian Flysch has been proposed by Egger (1995) who distinguished three distinct lithological units in the area of Salzburg. A composite section of the ca. 500 m thick Paleocene to lowermost deposits of the Rhenodanubian Group in the Salzburg area is presented in Fig. 4. In the upper Maastrichtian and Danian the Acharting Member of the Altlengbach Formation is characterized by thin- to medium-bedded turbidites, which display base-truncated as well as complete Bouma sequences. Usually the upper part of the Bouma sequences consist of medium-grey clayey marl which represents c. 35 % of this member whereas the percentage of intervening green coloured hemipelagic shale layers is less than 15 %. A distinct feature of this turbidite facies is the intercalation of thick-bedded and coarse grained sandstones with high amounts of mica and quartz. These are marker beds for mapping the Altlengbach Formation. Calcareous nannoplankton zone NP3 was found in a sequence of very thin-bedded and fine-grained turbidites. Further up-section, hemipelagic claystone (Strubach Tonstein) becomes the dominant rock-type suggesting starvation of turbidite sedimentation. This claystone-rich interval is regarded as part of the Acharting Member.

The lower boundary of the 50 m thick Strubach Tonstein is within Zone NP3. New increased input of turbiditic material started within nannozone NP8 and continued until the upper part of zone NP10. In Zone NP8 and in the lower part of Zone NP9 the facies is very similar to that of the Danian part. In the

by the oblique convergence of the European and African plates resulting in a dextral transpressional tectonic regime subsequently to the onset of the collision (Ziegler, 1987). In the second model, this deformation is seen as the result of an important change in relative motion between the European and African plates causing pinching of Europe's lithosphere between Africa and Baltica (Kley and Voigt, 2008). This model explains better than the collision model the uniform N to NE intra-plate shortening of the European plate during the Late Cretaceous event and is also consistent with the NE-SW trending strike-slip faults, which affected the European margin and led to the formation of slope-basins.

Syn depositional faulting and the associated alteration in margin topography, changed sediment dispersal and accumulation not only on the slope but also in the adjacent "Rhenodanubian Flysch" of the Penninic basin. There, a dearth of turbidite

upper part of zone NP9 graded silty marls of the Anthering Formation become the predominant rock type at the expense of sandstones and siltstones. The base of the Anthering Formation is at the P/E-boundary, which is characterized by the common occurrence of hemipelagic claystone.

The rate of hemipelagic sedimentation in the Paleocene can be calculated using the Strubach Tonstein, which was deposited during a period of about 6 my between calcareous nannoplankton zones NP3 and NP8. Excluding the turbidites the rate of hemipelagic sedimentation has been calculated as ca. 8 mm ky<sup>-1</sup>. Similar values (7 mm ky<sup>-1</sup> resp. 9 mm ky<sup>-1</sup>) were assessed for the middle and upper part of Zone NP10, whereas a hemipelagic sedimentation rate of 49 mm ky<sup>-1</sup> has been calculated for the CIE-interval (Egger et al., 2003). From this it can be summarized that in the Penninic basin the CIE was associated with an increase in the sedimentation rate of siliciclastic hemipelagic material by a factor of six.

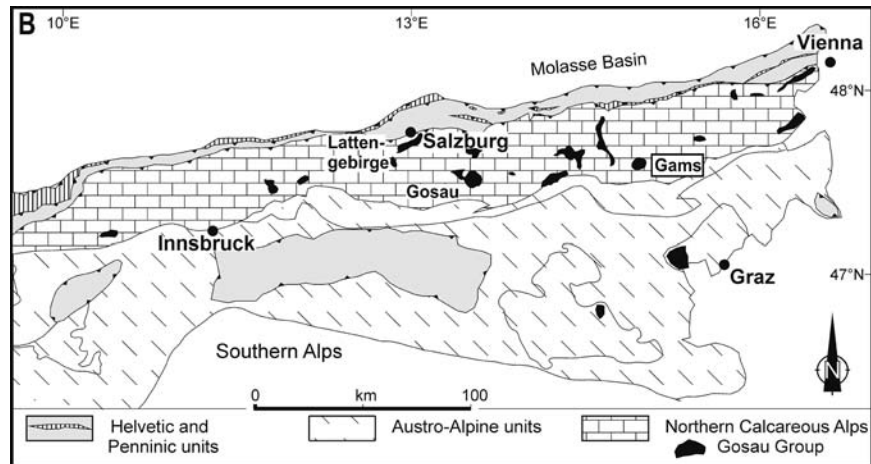


**Figure 6 ▲**  
Location of Gosau deposits in the Eastern Alps

In general, the input of terrestrially derived material into the basins increases during episodes of low sea-level as a result of enhanced topographical relief. In the Anthering section, the thickest turbidites of the Thanetian and Ypresian occur in the uppermost 13 m of the Thanetian (Egger et al., 2009). This suggests an episode of massive hinterland erosion, indicating a sea-level drop just prior to the onset of the CIE. This is consistent with data from the Atlantic region (Heilmann-Clausen, 1995; Knox, 1998; Steurbaut et al., 2003; Pujalte and Schmitz, 2006; Schmitz and Pujalte, 2007). The synchronicity of this sea-level drop in the Atlantic and Tethys regions indicates a eustatic fluctuation. Starting with the onset of the CIE, mainly fine-grained suspended material came into the basin and caused a strong increase in hemipelagic sedimentation rates. Such an increase associated with decreasing grain-sizes has been reported from P/E-boundary sections elsewhere and interpreted as an effect of a climate change at the level of the CIE, affecting the hydrological cycle and erosion (Schmitz et al., 2001).



**Figure 7 ▲**  
Image of the K/Pg-boundary at the Elendgraben section

In the lowermost Eocene of the eastern Alps (sub-Zone NP10a) twenty-three layers of altered volcanic ash (bentonites) originating from the North Atlantic Igneous Province have been recorded in lower Eocene deposits (calcareous nannoplankton Sub-Zone NP10a – STOPA1/2) at Anthering, about 1,900 km away from the source area (Egger et al., 2000). The Austrian bentonites are distal equivalents of the “main ash-phase” in Denmark and the North Sea basin. The total eruption volume of this series has been calculated as 21,000 km<sup>3</sup>, which occurred in 600,000 years (Egger and Brückl, 2006). The most pow-

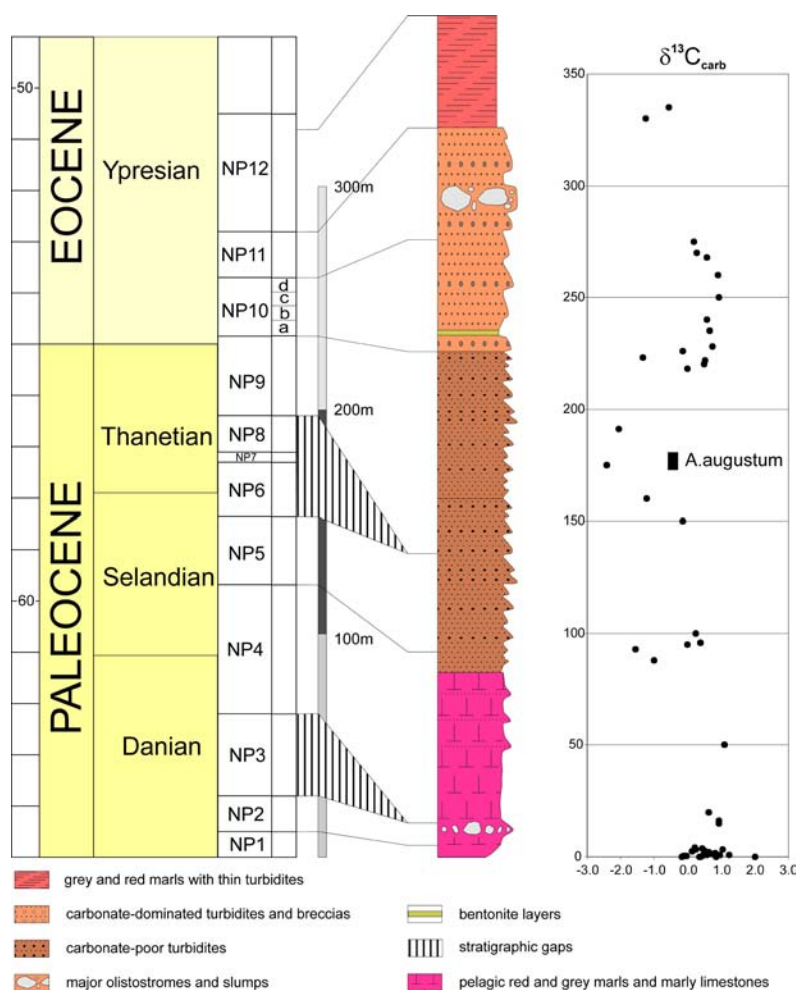


**Figure 8 ▲**

Stratigraphic and lithological log of the Paleogene part of the Gosau group at Gams, including bulk stable isotope values and the occurrences of *Apectodinium augustum* (Egger et al., 2009a).

can be divided into two parts – a lower part consisting of terrestrial and shallow-water sediments, including bauxites, coal seams, rudist biostromes, and several key stratigraphic horizons rich in ammonites and inoceramids (Lower Gosau Subgroup, Turonian to lower Campanian), and an upper part, comprising deep-water marlstone, claystone and turbidites (Upper Gosau Subgroup, upper Campanian to Priabonian). Deposition of the Gosau Group was the result of transtension, followed by rapid subsidence into deep-water environments due to subduction and tectonic erosion at the front of the Adriatic Plate (Wagreich, 1993).

The Cretaceous/Paleogene-boundary has been studied in five sections of the Nierental Formation of the Upper Gosau Subgroup of the Northern Calcareous Alps (Fig. 6). The first K/Pg boundary in the region was discovered in the Wasserfallgraben section of the Lattengebirge in Bavaria (Herm et al. 1981). Perch-Nielsen et al. (1982) reported on biostratigraphical and geochemical results, and Graup and Spettel (1989) measured bulk Ir contents of 4–5 ppb in the boundary clay from this section. The second K/Pg boundary site was identified in the Elendgraben section (Fig. 7) near the village of Rußbach in Salzburg (Preisinger et al. 1986; Stradner et al. 1987). The boundary is marked by a 2–4 mm thick yellowish clay layer, which contains up to 14.5 ppb iridium. The third K/Pg boundary site was recognized in the Knappengraben section at Gams (Stradner et al. 1987; see figs. 1B and 1C). Again, the boundary clay is of light yellow color and contains up to 7 ppb iridium. Lahodynsky (1988) studied the lithology of the Knappengraben and Elendgraben sections and interpreted their sedimentological and geochemical features as the result of extensive volcanic eruptions. Recently, Grachev et al. (2005, 2007, 2008) followed this interpretation. The fourth K/Pg boundary site has been described at the Rotwandgraben section also near the village of Gosau, about 2.5 km to the southeast of the Elendgraben section (Peryt et

erful single eruption of this series took place 54.0 million years ago (Ma) and ejected ca. 1,200 km<sup>3</sup> of ash material which makes it one of the largest pyroclastic eruptions in geological history. The clustering of eruptions must have significantly affected the incoming solar radiation in the early Eocene by the continuous production of stratospheric dust and aerosol clouds. This hypothesis is corroborated by oxygen isotope values which indicate a global decrease of sea surface temperatures between 1–2°C during this major phase of explosive volcanism.

Equivalents of these bentonites were found also in the sedimentary record of the northern Adriatic Plate within the succession of the Northern Calcareous Alps at Untersberg (STOP A1/1, Egger et al., 1996) and Gams (Egger et al., 2004). The Cretaceous to Paleogene deposits of the Adriatic Plate lithostratigraphically are formalized as Gosau Group. This Group comprises mainly siliciclastic and mixed siliciclastic-carbonate strata deposited after Early Cretaceous thrusting. The Gosau Group of the Northern Calcareous Alps

al. 1993, 1997). The maximum Ir content in the boundary clay has been determined to be 7 ppb. During the post-conference fieldtrip we will visit the Gamsbach section (STOP A3/1) near Gams (Egger et al., 2009), which is the best accessible and best exposed K/Pg-boundary site in the Eastern Alps.

In the Northern Calcareous Alps, Paleocene/Eocene-boundary sections were studied at Untersberg near Salzburg (Egger et al., 2005) and Gams in Styria (Egger et al., 2009; Wagreich et al., 2011). At the Untersberg section the P/E-boundary is characterized by grey and red claystone intercalated into the dominating marlstone of the succession. At its top, the claystone displays a gradual increase in calcium carbonate contents. This transition zone from the red claystone to the overlying grey marlstone indicates a deposition within the lysocline. The gradual change of carbonate content within the transition zones suggests a slow shift of the level of the lysocline and CCD at the end of the CIE and has been described also from other sections (e.g. Zachos et al., 2005).

Whereas turbidites are exceedingly rare at the Untersberg section, they are the dominant rock type at the Pichler section near Gams. There, 122 m of turbidite-dominated psammitic to pelitic deposits of the Zwieselalm Formation are exposed. Occasionally, thin layers and concretions occur consisting essentially of early diagenetic siderite. The Paleocene/Eocene-boundary at the base of the Pichler section is characterized by a negative excursion of carbon isotope values (CIE), the occurrences of the dinoflagellate cyst *Apectodinium augustum* and the calcareous nannoplankton species *Discoaster araneus* and *Rhomboaster* spp.. Foraminiferal assemblages are predominantly allochthonous and indicate deposition below the calcite compensation depth in the lower to middle part of the section. High sedimentation rates of ca. 20 cm kyr<sup>-1</sup> are estimated. The pronounced input of sand fraction is different from most other sections showing the Paleocene-Eocene transition (e.g. Schmitz & Pujalte, 2007) and can be interpreted as a result of regional tectonic activity overprinting the effects of global environmental perturbations.

Like on the Helvetic shelf in the north of the Penninic basin (see above), a major stratigraphic gap exists in the sedimentary record of the shelf of the Adriatic plate at the southern rim of the basin. Lower Eocene deposits rest with an erosional unconformity on Upper Campanian marlstone of the *Tranolithus phacelosus* Zone (Sub-Zone CC23a). In the Pemberger quarry (unfortunately, this outcrop was destroyed by recultivation of the quarry during the last winter), from the base of the marine deposits *Assilina placentula*, *Nummulites burdigalensis kuepperi*, *Nummulites increscens*, and *Nummulites bearnensis* were described (Schaub, 1981; Hillebrandt, 1993). This fauna is indicative of the lower part of shallow benthic zone SBZ10, which has been correlated with calcareous nannoplankton zone NP12 (Serra-Kiel et al. 1998).

Due to their similar stratigraphic positions, Egger et al. (2009) assumed that the Ypresian transgressions at the shelves of the European and Adriatic Plates originated from the same eustatic event, which was the highstand of the TA2 supercycle in the global sea-level curve (Haq et al., 1988). At the Adriatic Plate, at the base of the marine transgression, black shales occur containing a rich and well preserved tropical palynoflora, indicating *Nypa*-dominated mangrove type forests, which reflect the early Eocene climate optimum (Zetter and Hofmann, 2001). The onset of this episode of tropical climate was near the top of magnetic Chron 24, which coincides with the NP11/NP12 zonal boundary (Collinson, 2000; Gradstein et al., 2004).

The youngest deposits of the Gosau Group at Krappfeld are of Lutetian age. Hillebrandt (1993) reported both *Nummulites hilarionis* and *Nummulites boussaci*, which indicate shallow benthic zone SBZ14, and *Nummulites millecaput*, which is indicative for shallow benthic zone SBZ15. These foraminiferal zones can be correlated with the upper part of calcareous nannoplankton Zone NP15 and the lower part of Zone NP16 (Serra-Kiel et al., 1998).

## Paleocene/Eocene-boundary sections and a Selandian section in a transect through the Penninic Basin

### Introduction

Today we will visit outcrops at a transect from the southern paleo-slope (Untersberg) of the Penninic Basin through the center of this basin (Anthering) to the northern shelf (St. Pankraz). We first head to the western outskirts of Salzburg. Close to the village of Fürstenbrunn we will stop at the bathyal Untersberg section of the nappe complex of the Northern Calcareous Alps. After visiting outcrops of the P/E-boundary and the lower Eocene containing volcanic ash-layers, we will travel north to the village of Anthering, where we will see an abyssal succession of the same age like at Untersberg but showing different facies (nappe complex of the Rhenodanubian Flysch Zone). Only a short bus ride from the Anthering outcrop we will stop at an abyssal Danian - Selandian section along the course of a creek. This section can be only visited if there are dry weather conditions. The last set of outcrops is in shallow water deposits from the northern rim of the Penninic Basin (South Helvetic nappe complex).

### Notes:

- Arrange your own breakfast and assemble at the carpark of St. Virgil (Ernst-Grein-Straße 14, 5026 Salzburg; Tel. +43-662-65901-516) for departure at 8.30 a.m. sharp.
- Buffet lunch will be arranged at the Reinthal- inn (Tel+43-6223-20 300) at Anthering after visiting the Anthering section.
- Route: Salzburg (St. Virgil) – Fürstenbrunn – Anthering – Acharting – St. Pankraz – Salzburg (St. Virgil)
- Accomodation at Salzburg has to be arranged by the participants.

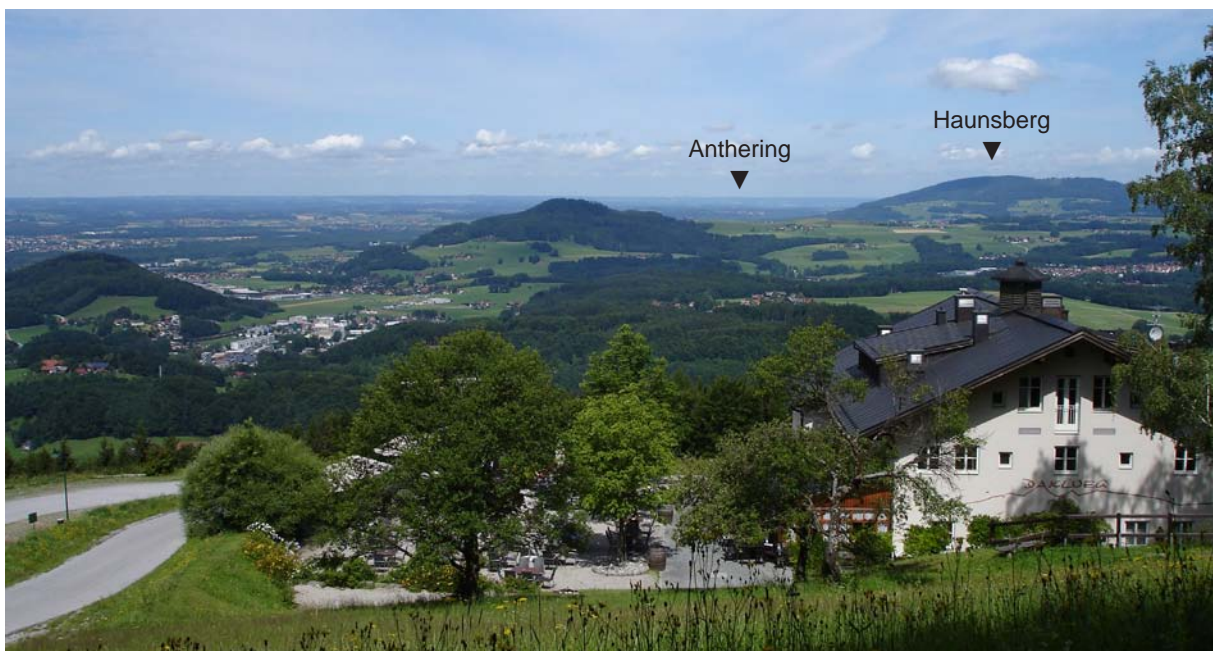


**Figure A1.1 ▲**  
View from Heuberg to north

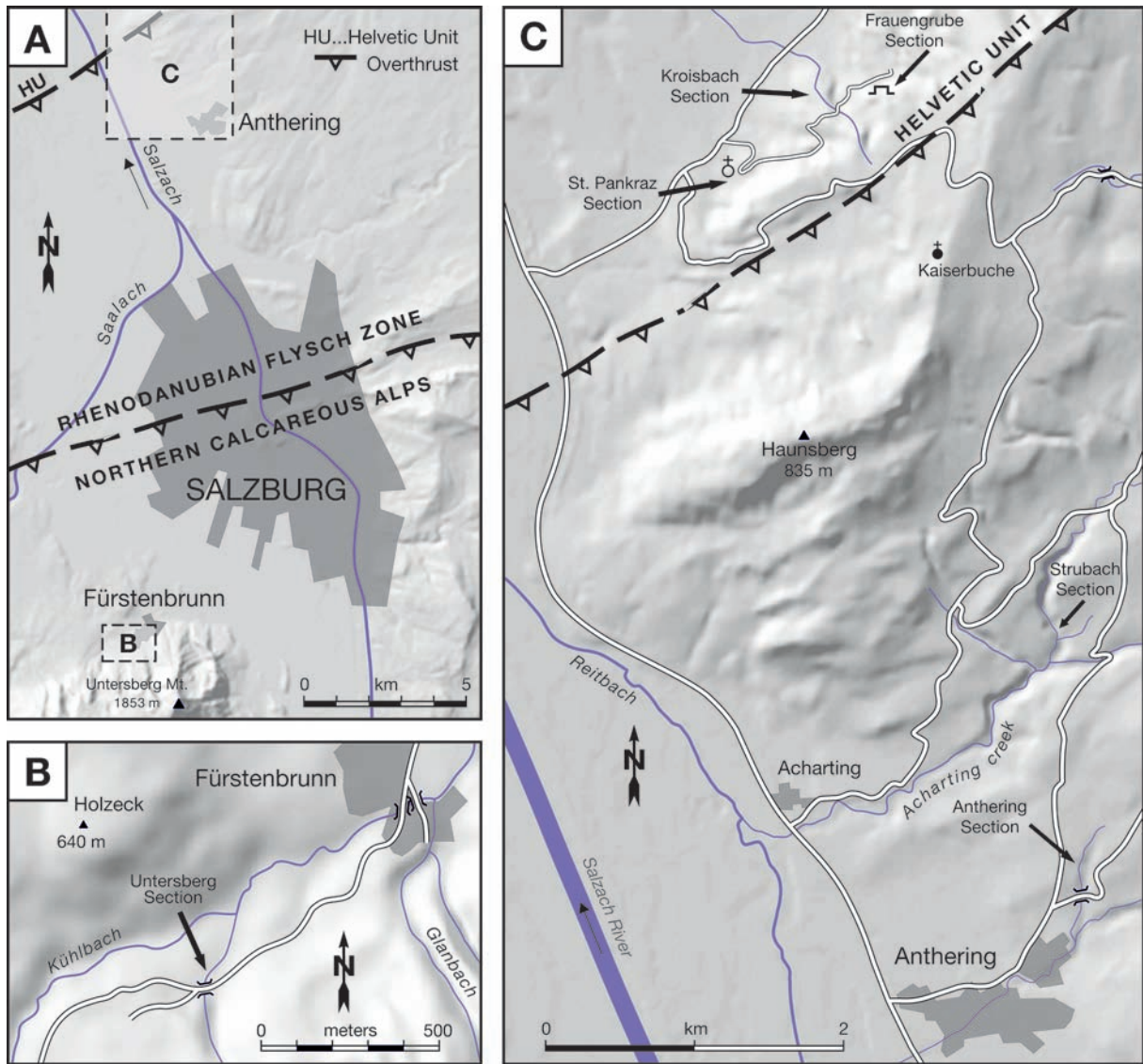


**Figure A1.2 ▲**  
Route maps for Field Trip A1

## UNTERSBERG SECTION NEAR FÜRSTENBRUNN

Hans Egger, Fred Rögl

**Topics:**

Paleocene/Eocene-boundary and lower Eocene bentonites in bathyal marlstone and claystone

**Tectonic unit:**

Northern Calcareous Alps

**Lithostratigraphic units:**

Gosau Group, Nierental Formation

**Chronostratigraphic units:**

Upper Paleocene to Lower Eocene

**Biostratigraphic units:**

Calcareous Nannoplankton Zones NP9 and NP10a; Planktonic Foraminifera Zones P5 to E3

**Location:**

Tributary of the Kühlbach near Fürstenbrunn

**Coordinates:**

47° 44' 19" N, 012° 59' 04" E

**References:**

Egger et al. (2005), Egger & Brückl (2006), Hillebrandt (1962), Hagn et al. (1981)

### **Outcrop 1a: Paleocene/Eocene-boundary**

From the bus stop it is a 10 minutes downhill walk through the forest (no trail!) to reach the outcrops, which are located along the course of a creek. Estimated duration of the stop is 1.5 hours.

The Paleogene deposits of the Untersberg region were examined by von Hillebrandt (1962 and in Hagn et al., 1981). The more than 1000 m thick Paleogene succession of the Untersberg area consists predominantly of marlstone displaying carbonate contents between 40 wt% and 50 wt%. Abundant planktonic foraminifera and calcareous nannoplankton are the main source of the carbonate. Von Hillebrandt (1962) already recognized the importance of the benthic foraminiferal extinction at the end of the Paleocene and Egger et al. (2005) re-examined this outcrop. However, at that time the exposure was worse and only part of the CIE-interval was outcropping. In 2010, a flood event due to torrential rain significantly improved the outcrop situation and revealed also minor faults along the dipping planes.



**Figure A1.3 ▲**

Photograph of the outcrop 1a at Untersberg showing the grey and red claystone of the CIE-interval

At the base of the new outcrop (Fig. A1.3) grey marlstone shows a sharp contact to grey claystone, which is overlain by red claystone. The claystone at the P/E-boundary indicates a deposition below the CCD. Excluding the carbonate content, the mean percentages of the siliciclastic components are almost identical below and above the CIE-interval: 16.3% quartz and feldspar and 83.7% clay minerals from the interval above the CIE and 16.6% quartz and feldspar and 83.4% clayminerals below the CIE. Within the CIE-interval, however, the mean percentage of quartz and feldspar is 24.8%, which is equivalent to an increase of 49% in relation to the other parts of the section.

The clay mineral assemblage at Untersberg is strongly dominated by smectite (72 wt%), followed by illite (18 wt%), kaolinite (6 wt%) and chlorite (4 wt%). The abundance of smectite throughout the studied section, together with the absence of mixed-layers, indicates that the rocks of the Untersberg section were not affected by deep-burial diagenesis. Consequently, diagenetic effects on the composition of clay mineral assemblages can be ruled out.

At its top, this claystone displays a gradual increase in calcium carbonate contents (Fig. A1.5) already documented by Egger et al. (2005). This transition zone to the overlying grey marlstone indicates a deposition within the lysocline, which is the water depth where carbonate dissolution rates are greatly accelerated (Berger, 1970). The gradual change of carbonate content within the transition zones suggests a slow shift of the level of the lysocline and CCD at the end of the CIE and has been described also from sections elsewhere (Zachos et al., 2005).

### **Calcareous nannoplankton**

Calcareous nannofossils were found in the marlstone and in the transition zones (marly claystone) between the marlstone and the shale. They are abundant (> 30 specimens per field of view) in the samples from the marlstone, whereas their abundance is low (< 10 specimens per field of view) in the samples from the transition zones. The preservation of nannofossils is moderate in the marlstone and poor in the transition zone according to the classification of Steinmetz (1979). In the moderately preserved sam-

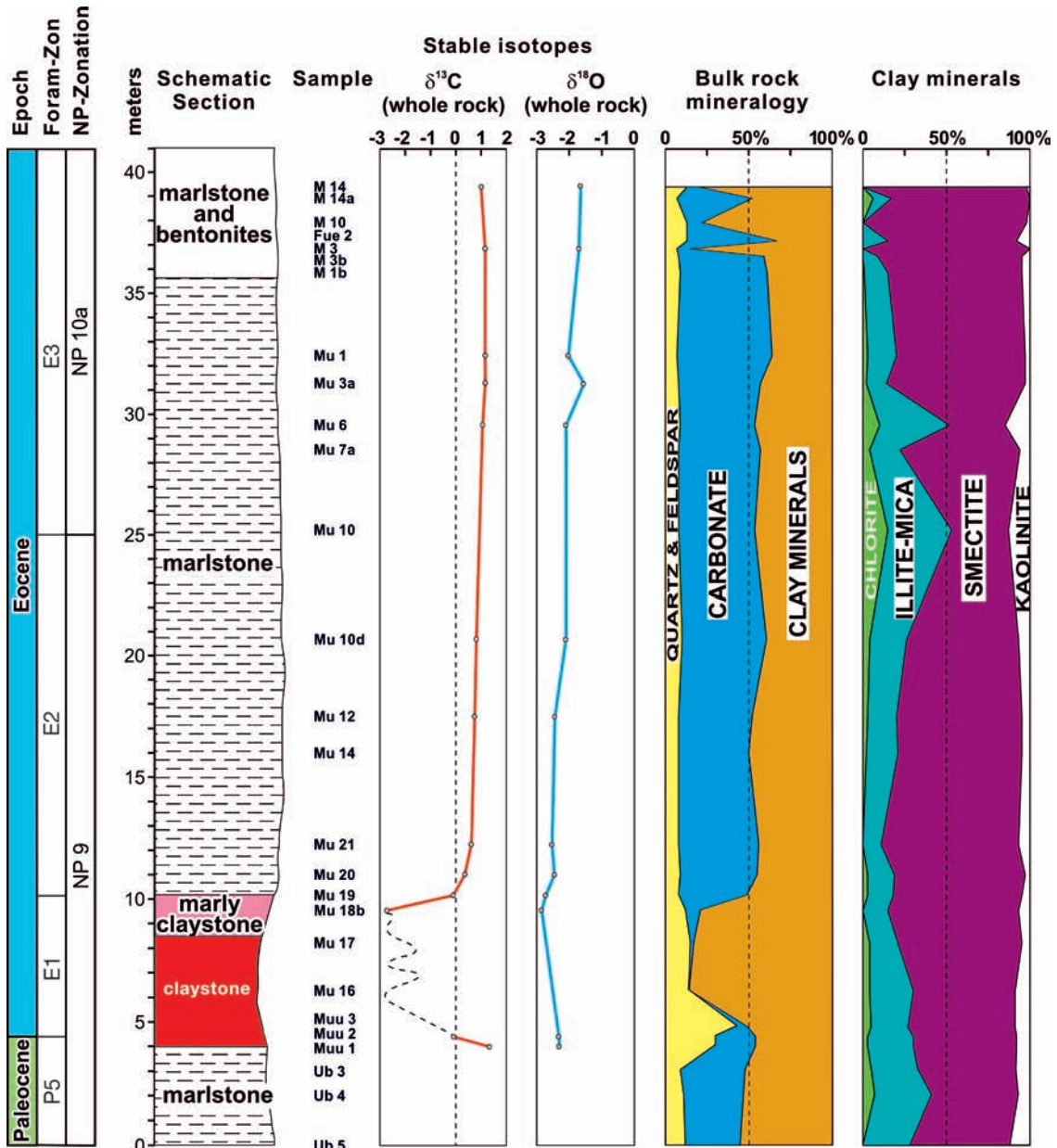


**Figure A1.4 ▲**  
Carbon isotope values, bulk rock mineralogy, and composition of clay mineral assemblages across the Paleocene–Eocene boundary.

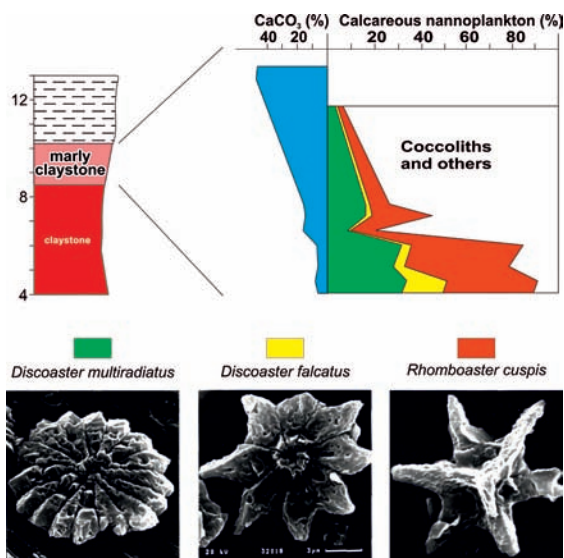


**Figure A1.5 ◀**  
Percentages of *Discoaster multiradiatus*, *Discoaster falcatus*, and *Rhomboaster cuspis* in the calcareous nannoplankton assemblages and calcium carbonate percentages at the top of the CIE-interval (scale bar represents 3  $\mu\text{m}$  and is valid for all photographs).

ples the majority of the specimens are slightly etched but all taxa can be easily identified and diversity is about 16 species per sample on average. In the poorly preserved samples, the majority of specimens are deeply etched, identification of taxa is difficult and the diversity is only about 6 species per sample.

Reworked specimens are present in the marlstone samples, with rare Cretaceous species appearing (less than 1% of the nannofossil assemblage). Reworking has affected mainly Upper Cretaceous deposits, indicated by the occurrences of *Micula decussata*, *Prediscosphaera cretacea*, *Lucianorhabdus cayeuxii*, *Broinsonia parca*, *Ceratolithoides aculeus*, *Uniplanarius trifidus* and *Arkhangelskiella cymbiformis*. In one sample (M3b) typical Lower Cretaceous species (*Micrantolithus hoschulzii* and *Nannococcus steinmannii*) were also found. However, the relatively common *Watznaueria barnesae* specimens in most samples may in part also originate from Lower Cretaceous deposits, as this species is abundant throughout the entire Cretaceous.

The Paleogene nannoflora is dominated by *Coccolithus pelagicus*, which usually accounts for about 90% of the nannoplankton assemblages, with the exception of the poorly preserved assemblages of the CIE-interval. *Discoaster multiradiatus*, the zonal marker of NP9, is another common species and the only species occurring in all samples. Species of the stratigraphically important genus *Fasciculithus* are rare in the Untersberg section, except in the samples from below the CIE. *Scapholithus apertus* is the only species which becomes extinct at the Palaeocene–Eocene boundary of the Untersberg section.

The first specimens of the genus *Rhombaster* occur just below the base of the CIE. There, short-armed specimens of *Rhombaster cuspis* are exceedingly rare. In contrast, in the samples from the top of the CIE-interval *Rhombaster cuspis* is the dominant species (up to 49% of the assemblages) followed by *Discoaster multiradiatus* and *Discoaster falcatus*. Rare specimens of *Discoaster araneus* occur. In other Tethyan sections *Discoaster anartios* (Bybell and Self-Trail, 1994) co-occurs with *Discoaster araneus*; however, this species has not been found at Untersberg. Coccoliths are absent or extremely rare in this CIE-assemblage.

The unusual composition of the nannoplankton assemblage of the marly claystone at the top of the CIE-interval is an effect of carbonate dissolution because, synchronously with increasing carbonate content, the calcareous nannoplankton shows better preservation and a higher diversity (Fig. A1.5). The species diversity in nannoplankton assemblages is, to large extent, controlled by selective dissolution of skeletal elements. Bukry (1971) recognized that *Discoaster* is the most dissolution-resistant genus among the Cenozoic genera, followed by the genus *Coccolithus*. At Untersberg, the high percentages of *Rhombaster* in the transition zone assemblages are most probably an effect of selective dissolution, indicating that *Rhombaster* has a similar resistance to dissolution as *Discoaster*.

## Foraminifera

Planktonic and benthic foraminifera are very abundant in most of the studied samples, although, as a result of carbonate dissolution, their preservation is poor across the CIE-interval. There, the assemblages are strongly dominated by agglutinating taxa. A specific determination was often difficult to make as many planktonic foraminifera specimens are corroded or deformed. For this reason no quantitative analysis of the foraminifera fauna was conducted, despite recording 191 different taxa in 19 samples, excluding species reworked from the Upper Cretaceous and Lower Paleocene (mainly Danian). The distribution of planktonic foraminifera is given in Tab. 1. The planktonic foraminiferal biozonation follows the criteria of Berggren & Pearson (2005).

Zone P5 (*Morozovella velascoensis* Partial-range Zone), the uppermost zone in the Paleocene, is defined by the highest occurrence (HO) of *Globanomalina pseudomenardii* and the lowest occurrence (LO) of *Acarinina sibaiyaensis*. At Untersberg, only reworked specimens of *G. pseudomenardii* occur, whereas *A. sibaiyaensis* is absent and has not been found in Eastern Alpine sections till now. The assignment of the lowermost part of the studied section to Zone P5 is due to the occurrence of *Morozovella subbotinae*, which has a stratigraphic range from Zone P5 to Zone E5. In this part of the section also *M. aequa* and *M. gracilis* occur.

Due to the scarcity of planktonic foraminifera in the claystone of the CIE-interval no zonal attribution was possible. In the overlying marlstone (sample MU 19/97) *Pseudohastigerina wilcoxensis* was found, indicating Zone E2 (*Pseudohastigerina wilcoxensis*/*Morozovella velascoensis* Concurrent-range Zone). This zone is defined as the interval between the LO of *P. wilcoxensis* and the HO of *M. velascoensis*.

UNTERSBERG KÜHLBACHGRABEN Planktonic Foraminifera	Ub 5/2003	Ub 4/2003	Ub 3/2003	Untersberg 1/10	MUU 2/99	MUU 3/99	Untersberg 2/10	Untersberg 2B/10	Untersberg 3/10	MU 17/97	Mu 18a/97	MU 18d/96	MU 19/97	MU 20/97	MU 21/97	MU 14/97	MU 12/97	MU 10d/97	MU 10/97	below MU 7/97	MU 6/97	below M 1	above M 14	Zonal Ranges acc. Olsson et al. 1999, Pearson et al. 2006	
	x	cf.		x																					
<i>Acarinina coalingensis</i> (CUSHMAN & HANNA)	x	cf.		x											x	x	x	x	cf.	x	x	x	x	P4c-E7	
<i>Acarinina mckannai</i> (WHITE)	x	x	x	x			x				x		x	x	x	cf.	cf.	cf.	x	x			x	x	P4a-b
<i>Acarinina nitida</i> (MARTIN)	x	x	x	x		x	x		x		x		x	x	x	x	x	x	x	x	x	x	x	x	P4
<i>Acarinina soldadoensis</i> (BRÖNNIMANN)	x	x		x			x										x	cf.	x	x	x	x	x	P4c-E7	
<i>Acarinina subsphaerica</i> (SUBBOTINA)	cf.	cf.		x		x	x						x											P4-E3	
<i>Subbotina cancellata</i> (BLOW)	cf.	x	x	x										x	x		cf.						cf.	P2-P4b	
<i>Subbotina triangularis</i> (WHITE)	x	x	x	x			x	x	x				x	x	x	x	x	x	x	x	x	x	x	P2-P5	
<i>Subbotina triloculinoides</i> (PLUMMER)	x	x	x	x		cf.	x			cf.	cf.							x						P1b-P4a	
<i>Subbotina velascoensis</i> (CUSHMAN)	x	x	x	x			x	x					x	x	x	x	x	x	x	x	x	x	x	P3b-E2	
<i>Morozovella acuta</i> (TOULMIN)	x																							P4b-E2	
<i>Morozovella aequa</i> (CUSHMAN & RENZ)	x	x	x	x									x	x	x			x	x	x	x	x		P4c-E5	
<i>Morozovella gracilis</i> (BOLLI)	cf.			cf.			x						x	x	x						x	x	x	P5-E5	
<i>Morozovella occlusa</i> (LOEBLICH & TAPPAN)	x	x	x						x				x	x				x						P4-P5	
<i>Morozovella subbotinae</i> (MOROZOVA)	x	x	x	x		x							x	x	x	x	x	x	x	x	x	x	x	P5-E5	
<i>Morozovella velascoensis</i> (CUSHMAN)	x	x	x	x									cf.	cf.	x	x	x	x			r			P3b-E2	
<i>Globanomalina pseudomenardii</i> (BOLLI)	x		cf.	x																				reworked	
<i>Praemurica</i> spp.	x	x	x	x																				reworked	
<i>Parvularugoglobigerina</i> sp.		x	x																					reworked	
<i>Parasubbotina pseudobulloidis</i> (PLUMMER)	x			x																				reworked	
<i>Parasubbotina varianta</i> (SUBBOTINA)		x	x	x																				P1c-E10	
<i>Acarinina strabocella</i> (LOEBLICH & TAPPAN)		x	x																					reworked	
<i>Igorina albeari</i> (CUSHMAN & BERMUDEZ)		x	x	x																				reworked	
<i>Morozovella pasionensis</i> (BERMUDEZ)				x	x																			P3b-E2	
<i>Globanomalina planocompressa</i> (PLUMMER)					x																			reworked	
<i>Globanomalina imitata</i> (SUBBOTINA)					x																			reworked	
<i>Morozovella marginodentata</i> (SUBBOTINA)					x			x										x	x			x	x	P5-E5	
<i>Subbotina incisa</i> (HILLEBRANDT)							x						x	x	x	x	x	x		x		cf.	cf.		
<i>Morozovella angulata</i> (WHITE)													cf.											P3-P4a	
<i>Morozovella apanthesma</i> (LOEBLICH & TAPPAN)													x	x										P3b-P4	
<i>Acarinina quetra</i> (BOLLI)										x			x	x					x	cf.	x	x		E3-E6	
<i>Globanomalina planoconica</i> (SUBBOTINA)													x	x					x		x	x		P4c-E6	
<i>Pseudohastigerina wilcoxensis</i> (CUSHMAN & PONTON)													x					x						E2-E10	
<i>Globanomalina chapmani</i> (PARR)															x									P3b-P5	
<i>Igorina broedermanni</i> (CUSHMAN & BERMUDEZ)															cf.						x		cf.	E1-E9	
<i>Acarinina pentacamerata</i> (SUBBOTINA)															cf.			x							
<i>Acarinina pseudotopilensis</i> SUBBOTINA																x	x							E1-E7	
<i>Subbotina linaperta</i> (FINLAY)																					x	x			
<i>Parasubbotina inaequispira</i> (SUBBOTINA)																						x	x	E1-E8	
<i>Acarinina wilcoxensis</i> (CUSHMAN & PONTON)																						x	x	P5-E5	
<i>Planorotalites pseudoscutula</i> (GLAESSNER)																						x	x	P5-E7	
<i>Igorina salisburgensis</i> (GOHRBANDT)																						x	x		
<i>Morozovella edgari</i> PREMOLI SILVA & BOLLI																							x	x	E2-E3
Upper Cretaceous	x	x		x	x	x							x	x	x	x	x	x	x	x	x	x	x	reworked	
Planktonic Foraminifera Zones	P5				E1 ?				E2				E3												

**Table 1 ▲**  
Planktonic foraminifera of the Untersberg section

*M. velascoensis* has its HO in sample MU 10d/97. Further up-section, rare specimens of this species (sample MU 6/97) are considered to be reworked. The LO of *Morozovella edgari* is used to assign the highest part of the section to Zone E3 (*Morozovella marginodentata* Partial-range Zone). This zone is defined by the HO of *M. velascoensis* and the LO of *M. formosa*, however, the latter species does not occur in our samples.

The distribution of calcareous benthic foraminifera is similar to those of other deep-water sections (see Thomas, 1998, for a review). *Gavelinella* cf. *beccariiformis* has its HO at the onset of the CIE. The post-extinction calcareous benthic foraminifera assemblages are dominated by *Nuttalides truempyii* (very small specimens), *Abyssamina poagi*, *Anomalinoidea nobilis*, *A. praeacutus*, *Oridorsalis* spp. and a number of pleurostomellids (e.g. *Ellipsoglandulina*, *Ellipsoidella*, *Ellipsopolymorphina*, *Nodosarella*, *Pleurostomella*). This assemblage is typical of lower bathyal to abyssal environments (van Morkhoven et al., 1986). For example, *Abyssamina poagi* occurs between 1700 m and 4000 m depth, and *Oridorsalis lotus* indicates a depth of between 800 m and 1900 m. This suggests a palaeodepth of about 2000 m (lower bathyal) for the deposition of Untersberg section.

The agglutinating foraminiferal fauna consists of 68 species, 25 of which (37% of the entire fauna) occur exclusively at the base of the succession and end within the CIE-interval. These species are *Ammodiscus cretaceus*, *Aschemocella carpathica*, *A. grandis*, *Bathysiphon? annulatus*, *Caudamina arenacea*, *C. excelsa*, *C. ovulum*, *Dorothia beloides*, *Glomospira diffundens*, *G. glomerata*, *G. serpens*, *Haplophragmoides walteri*, *Hormosinella distans*, *Hyperammina lineariformis*, *Karrerulina horrida*, *Psammodendron? gvidoensis*, *Psammosiphonella* sp., *Remesella varians*, *Rzehakina fissistomata*, *Saccamina grzybowskii*, *Silicobathysiphon* sp., *Subrheophax pseudoscalaris*, *S. splendidus*, *Trochamminoides folius*, and *T. subcoronatus*. In the upper part of the succession the typical assemblage with *Paratrochamminoides* and *Trochamminoides* has disappeared, but *Recurvoides gerochi* and *R. pseudoregularis* are still common. Within the CIE-interval the agglutinated assemblage is dominated by *Glomospira* spp. Such assemblages, similar to the „Biofacies B“ assemblage or to the „*Glomospira* event“ occur in the Cretaceous and in the Early Eocene of the North Atlantic and Tethys (comp. Kuhnt et al., 1989; Kaminski et al., 1996).

## Radiolarians

Occurrences of radiolarians are restricted to the lower part of the section, where they are abundant from samples Mu18a to Mu14 and common in samples Muu2, Mu10, and Mu10d. In the finest grained sieve-residue of sample Mu19, radiolarians are the dominant component. The radiolarians are all spheroidal spumellarians, but are taxonomically indeterminable, since their siliceous skeletons are poorly preserved, due to their replacement by smectite. The abundance of siliceous plankton indicates high nutrient levels in oceanic surface waters in the basal Eocene. A coeval increase in both sedimentation rates and the amounts of terrestrially derived quartz and feldspar suggests that this high primary productivity was the result of enhanced continental run-off. No radiolarians were found further up-section in outcrop 1b.



**Figure A1.6** ►  
Photograph of outcrop 1b  
at Untersberg displaying  
yellowish bentonite layers

### Outcrop 1b: Volcanic ash-layers in the Lower Eocene

Within grey marlstone (calcareous nannoplankton sub-Zone NP10a; planktonic foraminifera Zone E3 – s. Tab.1) thirteen light yellowish layers consisting essentially of smectite were found. These 0.2 cm to 3 cm thick bentonite layers are interpreted as volcanic ashes. No bentonites were found in either the lower part of zone NP9 or in the overlying sub-zone NP10b, which are exposed in other outcrops of the area. The occurrence of bentonites is therefore exclusively restricted to sub-zone NP10a.

Due to their complete conversion to smectitic clay the original chemical composition of the bentonites must have strongly changed. Consequently, only the immobile elements have been used to assess the composition of the original magma (Winchester and Floyd, 1977). The immobile element contents of most of these altered ash layers show very little variation: Nb  $28.3 \pm 4.7$  ppm, Zr  $259 \pm 104$  ppm, Y  $25.0 \pm 9.5$  ppm, and  $\text{TiO}_2$   $4.82 \pm 0.7$  wt% (see Fig. 5).

These samples plot in the discrimination diagram of different magma sequences in the field of alkali-basalts. Basaltic ashes are rare in the geological record as the generation of basaltic pyroclastics requires an interaction between basaltic lavas and meteoritic water (see Heister et al., 2001, for a review). Layer M3 (Fig. A1.8) has a totally different composition with highly enriched Nb and Zr, equal Y, and depleted  $\text{TiO}_2$  compared to the other bentonites. It is the oldest and thickest layer of the ash-series and plots at the border of trachyte and trachy-andesite.

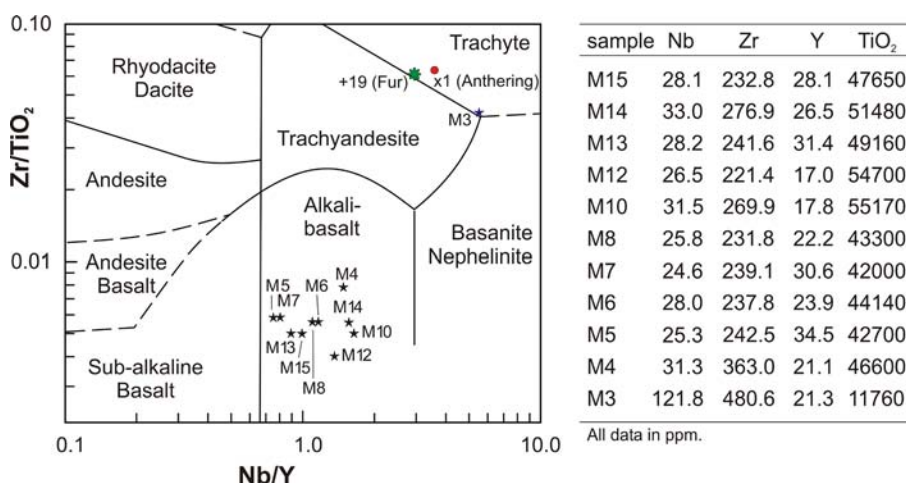


**Figure A1.7** ◀

Magma composition of different ash-layers by means of immobile element distribution (after Winchester and Floyd, 1977). For comparison, sample +19 from the Danish Fur Formation and sample X1, from the Austrian Anthering Formation, are plotted (from Egger et al., 2000).



**Figure A1.8** ◀

Photograph showing bentonite layer M3 at Untersberg

The biostratigraphical and geochemical correspondence of these tephras with ashes from the North Sea Basin suggests that these pyroclastic deposits are related to the continental breakup of Europe and Greenland (Egger et al, 2000; Huber et al., 2003; Egger & Brückl, 2006). There, the North Atlantic Igneous Province (NAIP), which is one of the largest basaltic lava accumulations on Earth, formed in the early Paleogene (62–53 Ma), prior to and during the continental break-up between Europe and Greenland (Eldholm & Grue 1994; Ritchie & Hitchen 1996; Ross et al. 2005). Beside voluminous flood basalts and associated igneous intrusions, it produced widespread pyroclastic deposits. From the early Eocene Fur Formation in Denmark more than 200 ash-layers of predominantly basaltic composition have been recorded from this explosive volcanic activity (Knox & Morton 1988; Heister et al. 2001). A numbering system for most of these layers was introduced by Bøggild (1918) and is still in use: The upper, closely spaced layers constitute the “positive series”, with layers numbered +1 to +140 in ascending order. The lower, more widely spaced and generally thinner layers make up the “negative series”, and are numbered -1 to -39 in descending order.

The paroxysm of this volcanic activity, the positive ash-series, consists of tholeiitic ferrobasaltic layers with the exception of layer +19. In the immobile element diagram of Floyd and Winchester (1976) this layer plots at the border between trachyte and trachyandesite, whereas more detailed geochemical investigations indicate a rhyolitic composition of the original magma (Huber et al., 2003; Larsen et al. 2003). Some of the ashes of the positive series have also been found at many other sites in Denmark, the North Sea, England, the Goban Spur southwest of Ireland, and the Bay of Biscay (Knox 1984). Based on detailed multi-stratigraphic and geochemical investigations, the most distal equivalents of layer +19 and 22 other layers have been identified in the Anthering and Untersberg outcrops (Fig. A1.3) of the Austrian Alps near Salzburg (Egger et al. 2000 and 2005; Huber et al. 2003).

It can be assumed that the ash-layers of the NAIP form important correlation horizons for lower Eocene deposits in large areas of Europe. In addition to the Austrian outcrops, reports of lower Eocene basaltic ash layers exist from Switzerland and Poland (Winkler et al. 1985; Waskowska-Oliwa & Lesniak 2002), although stratigraphic and geochemical information from these deposits is insufficient for a detailed correlation.

## ANTHERING SECTION

Hans Egger, Juliane Fenner, Claus Heilmann-Clausen, Fred Rögl, Birger Schmitz

### Topics:

Paleocene/Eocene-boundary section in a succession of deep-water turbidites and hemipelagites

### Tectonic unit:

Rhenodanubian Flysch Zone

### Lithostratigraphic units:

Rhenodanubian Group, Anthering Formation

### Chronostratigraphic units:

Upper Paleocene to Lower Eocene

### Biostratigraphic units:

Upper part of calcareous nannoplankton Zone NP9 to upper part of Zone NP10

### Location:

Outcrops in the Kohlbachgraben near Anthering

### Coordinates:

E 013° 01' 17", N 47° 53' 19"

### References:

Heilmann-Clausen & Egger, 1997, Egger, Heilmann-Clausen & Schmitz (2000), Crouch et al. (2001), Egger et al. (2003), Huber et al. (2003), Egger & Brückl (2006), Iakovleva & Heilmann-Clausen (2007), Egger, Heilmann-Clausen & Schmitz (2009)

From the carpark at the Reinthal inn it is an approx. 10 minutes walk on a small road to the first outcrop of the section, which is located along the course of the Kohlbach creek (no trail!). We examine the section (Fig. A1.9) walking up-stream from the lower Eocene (NP10) to the uppermost Paleocene (NP9).

The Anthering section is located about 18 km to the north of the Untersberg section as the Anthering and Untersberg sections are separated by the thrust between the Northern Calcareous Alps and the Rhenodanubian Flysch zone, the original palinspastic distance between them must have been much greater than at present. However, reliable data on this distance are lacking.

The 250 m thick upper Paleocene to lower Eocene deposits of the Anthering section, spanning calcareous nannoplankton Zones NP9 and NP10. These sediments comprise the youngest part of the Rhenodanubian Group. This group was deposited on the continental rise to the south of the European plate, which was the main source for the siliciclastic detritus entering the basin. The section is composed of calcareous mud-turbidites with intervening hemipelagic claystone indicating a deposition below the calcite compensation depth. The general sedimentary record of the Anthering-section is typical for an abyssal plain facies. Paleo-water depth estimations by Butt (1981), using foraminifera assemblages, range between 3000 to 5000 m.

In the Eocene part (Anthering Formation) of the section, the turbidite succession is characterized by the predominance of graded silty marlstone, which form about 85% of the succession (Anthering Formation). Occasionally, these turbiditic marlstone layers overlie silty to sandy beds deposited from the same turbidity current. The turbidites usually display base-truncated Bouma-sequences. Turbidites displaying complete Bouma-sequences are very rare. Single turbidite layers can reach thicknesses up to 2 m. The finegrained sand-fraction represents, on average, 5% of the sedimentary rocks and exceptionally up to 10%. The fine-grained (silty-clayey) sediment displays carbonate contents of 29% to 53%. The clay fraction is dominated by smectite.

Common intercalations of hemipelagic claystone occur between the individual mud-turbidite beds. The hemipelagic claystones prove a position of the basin-floor below the local calcite compensation depth. They are devoid of carbonate and display sharp contacts to the turbiditic marls. Usually the claystones show a greenish to greyish colour (0.15 wt% organic carbon on average) with a large number of dark spots as indications of intensive bioturbation. Only in the middle part of the section (outcrop E and one layer in outcrop D) darkgrey homogeneous claystones with abundant pyrite framboids and relatively high contents of organic carbon (0,94 wt% on average) occur. These black shales indicate an oxygen deficient environment at the basin floor. As they occur together with bentonite layers, volcanism might have led to eutrophic conditions and high plankton productivity responsible for the anoxic conditions.

In the lowermost Eocene (Subzone NP10a) at the Anthering section, 23 layers of altered volcanic ash (bentonites)

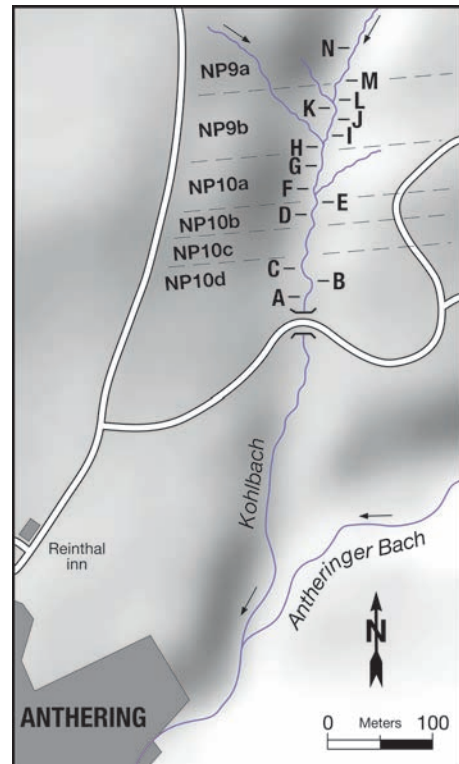


**Figure A1.9 ▲**  
Location of outcrops and biostratigraphy of the Anthering section near Anthering

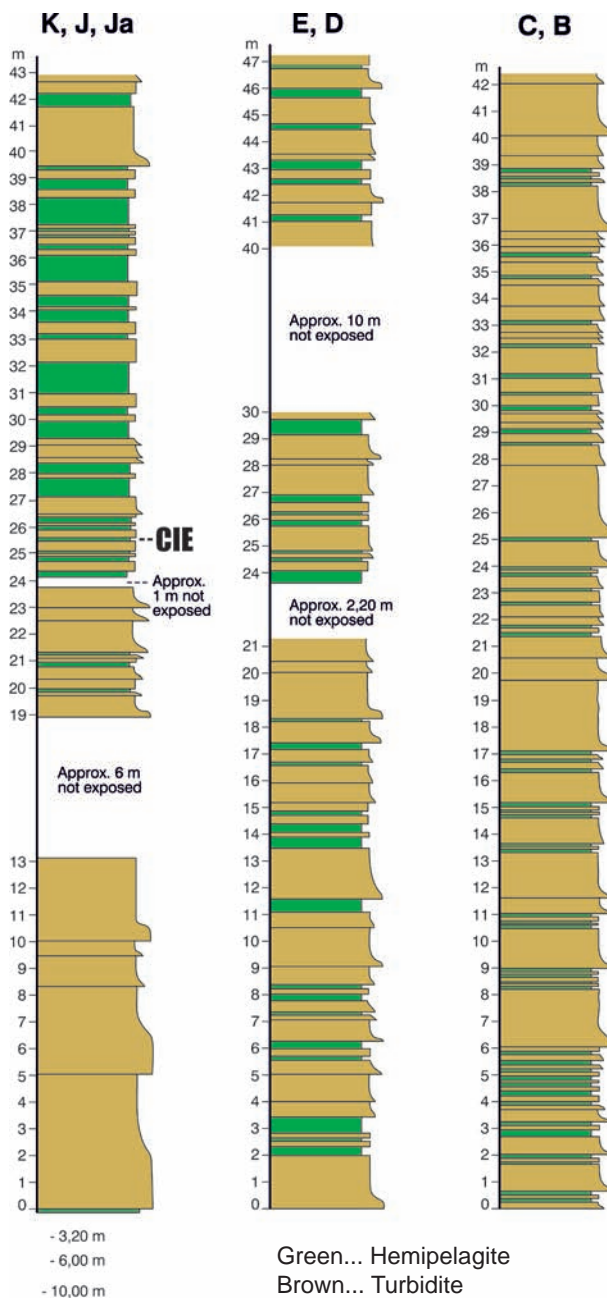
**Figure A1.10 ▼**  
Photograph of Outcrop B





**Figure A1.11 ▲**  
Detail outcrop B

**Figure A1.12 ▼**  
Lithologic logs of outcrops at Anthering



originating from the North Atlantic Igneous Province have been recorded, about 1,900 km away from the source area (Egger et al., 2000). The Austrian bentonites are between 1 mm and 30 mm thick and are considered to be distal equivalents of the “main ash-phase” in Denmark and the North Sea basin. Egger & Brückl (2006) have calculated the total eruption volume of this series as 21,000 km<sup>3</sup>, which occurred in 600,000 years. The most powerful single eruption of this series took place 54.0 million years ago (Ma) and ejected ca. 1,200 km<sup>3</sup> of ash material which makes it one of the largest pyroclastic eruptions in geological history. The clustering of eruptions must have significantly affected the incoming solar radiation in the early Eocene by the continuous production of stratospheric dust and aerosol clouds. This hypothesis is corroborated by oxygen isotope values which indicate a global decrease of sea surface temperatures between 1–2°C during this major phase of explosive volcanism.

The Anthering section displays the global negative carbon isotope excursion (CIE) and the acme of the dinoflagellate species *Apectodinium augustum* in the upper part of zone NP9 (Heilmann-Clausen and Egger, 1997; Egger et al. 2000; Crouch et al., 2001). The onset of the CIE is characterized by the presence of the thickest hemipelagic layers of the entire Anthering Section. About 45% of the rock is claystone, whereas the average percentage of claystone in the overlying NP10 is only 14%, and even less in the lower part of NP9. The CIE-interval attains a thickness of 15 m, comprising turbidites and hemipelagites. The thickness of the turbidites varies between 0.08 m and 2.25 m, although only the thickest layer exceeds 1 m thickness. The average thickness of the turbidite beds is 0.39 m and sand-grade material, which makes up 2% of this facies, occurs only in the thickest layers. Excluding the turbidites the remaining thickness of hemipelagic claystone is 8.4 m. Using Fe- and Ca-intensity curves which probably represent precessional cycles, Röhl et al. (2000) calculated that the CIE interval lasted for 170 ky. From this, a hemipelagic sedimentation rate of 49 mmky<sup>-1</sup> has been calculated for the compacted sediment across the CIE.

This value is ca. six times higher than the hemipelagic sedimentation rate in the Paleocene (Egger et al., 2009b). The increased rate of hemipelagic sedimentation at the CIE suggests a high input of siliciclastic suspension into the basin. At the level of the CIE clay mineral assemblages of hemipelagic claystone display a distinct increase of smectite and kaolinite at the expense of illite and chlorite (Egger et al., 2002). This indicates a decrease of bedrock erosion in the adjoining land areas. Well-developed smectitic soils with a mixture of kaolinite are mostly restricted to subtropical climates with a well-marked dry season (see Thiry, 2000 for a review). During the rainy season continental erosion of such areas is very pronounced (see van der Zwan, 2002, for a review) and will result in a strong increase in hemipelagic sedimentation rates (Schmitz et al., 2001).

Enhanced erosion of land areas around the CIE-interval can also be inferred from the composition of calcareous nannoplankton assemblages. Whereas, in general, reworked Cretaceous species form only 2–3% of the calcareous nannoplankton assemblages. Substantial Cretaceous admixtures are present in many samples from across the CIE (Fig. A1.15). The oldest nannoplankton assemblage showing a high percentage (>50%) of reworked specimens originates from a turbidite bed 22 m below the onset of the CIE. Three metres above the onset of this geochemical marker, the youngest assemblage with a similar percentage of reworked Cretaceous specimens has been found.

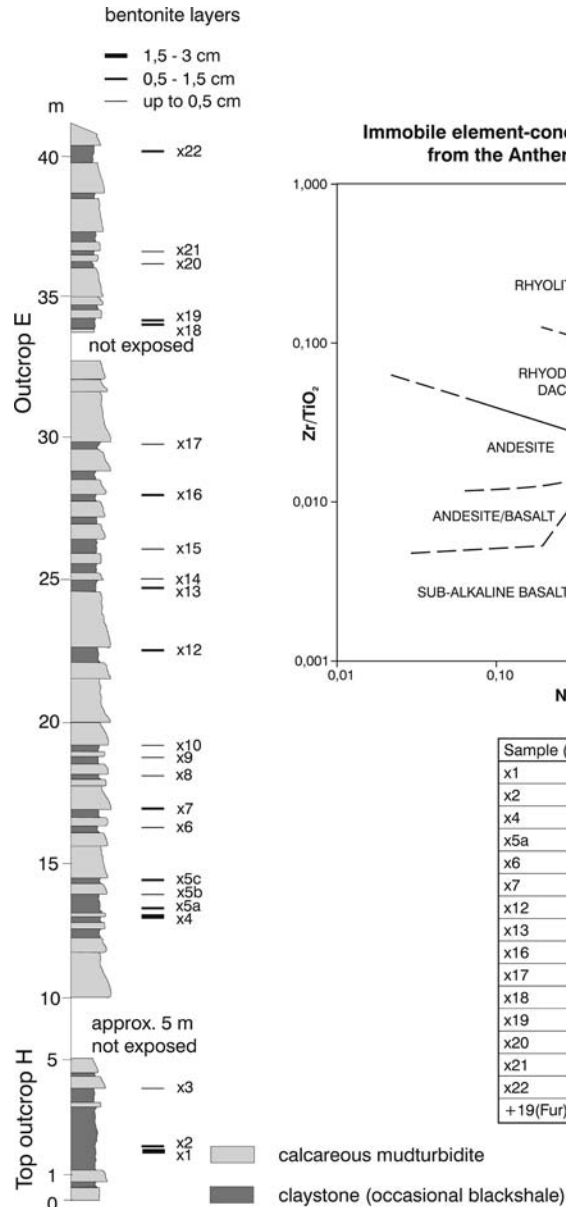


**Figure A1.13 ▲** Log of outcrop E showing positions of bentonites and immobile element-concentrations of bentonites

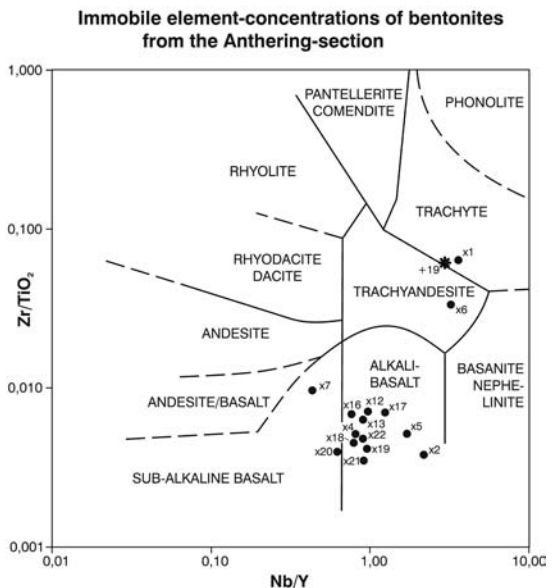


**Figure A1.14 ►** Two bentonite layers at outcrop E

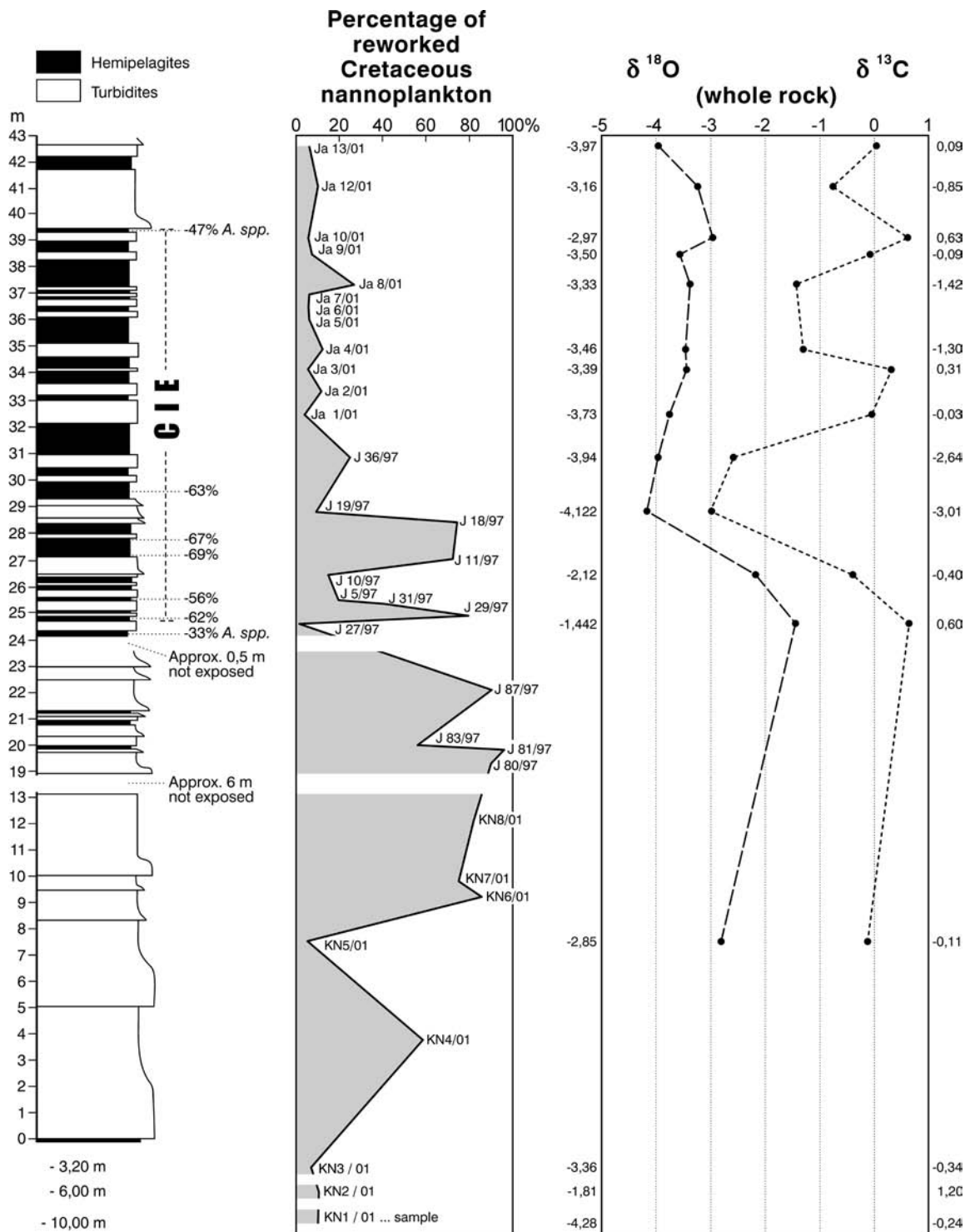


**Figure A1.15 ▲**

Lithostratigraphy percentages of redeposited Cretaceous nannoplankton and stable isotope record of oxygen and carbon across the CIE-interval at Anthering. A. spp. percentages of the genus *Apectodinium* in the dinoflagellate assemblages (Egger et al. 2009b)

Most of the reworked specimens consist of species with a long stratigraphic ranges (*Watznaueria barnesae*, *Micula staurophora*, *Retecapsa crenulata*, *Cribrosphaerella ehrenbergii*, *Eiffellithus turriseiffelii*). Biostratigraphically important species that were found in all of the counted samples include *Broinsonia parca*, *Arkhangeltskiella cymbiformis* (small specimens), *Calculites obscurus*, *Lucianorhabdus cayeuxii* and *Eiffellithus eximius* whilst *Marthasterites furcatus*, *Eprolithus floralis* and *Lithastrinus grillii* were found only occasionally. This assemblage suggests that predominantly lower to middle Campanian

deposits were reworked at the end of the Paleocene. Probably, the erosional area was the North-Helvetic shelf at the southern European Plate where the Middle Eocene is resting with an erosional unconformity on the Upper Cretaceous.

Substantial reworking of the Cretaceous started already in the latest Paleocene. At Anthering, the uppermost 20 m of the Paleocene succession are formed by the thickest turbidites (up to 5 m) of the entire section. The siliciclastic sand-fraction in the turbidites forms around 30% of the rocks in this part of the section (Aitlengbach Formation). This suggests that a sea-level drop took place shortly before the onset of the CIE. This is consistent with data from the Atlantic region (Heilmann-Clausen, 1995; Knox, 1998; Steurbaut et al., 2003; Pujalte and Schmitz, 2006; Schmitz and Pujalte, 2007). The synchronicity of this sea-level drop in the Atlantic and Tethys regions indicates a eustatic fluctuation. Starting with the onset of the CIE, mainly fine-grained suspended material came into the basin and caused an increase in hemipelagic sedimentation rates by a factor of 5 or 6. Such an increase associated with decreasing grain-sizes has already been reported from P/E-boundary sections elsewhere and interpreted as an effect of a climate change at the level of the CIE, affecting the hydrological cycle and erosion (Schmitz et al., 2001).

## DINOFLAGELLATE CYSTS

### General characteristics

Dinoflagellate cysts are present in all samples from the Anthering section. Preservation varies from good to moderate. There is a tendency to better preservation in samples from turbidites than in hemipelagic samples, perhaps due to sea-floor oxidation during slow, hemipelagic sedimentation.

Common genera and species occurring throughout the section are *Apectodinium* spp., *Spiniferites* spp., *Areoligera* spp. + *Glaphyrocysta* spp. (generally 2–15%), *Polyspaeridium zoharyi* (usually 1–5%), *Homotryblium tenuispinosum* (usually 1–5%), *Operculodinium* cf. *centrocarpum* (mostly 4–12%), and *Phthanoperidinium crenulatum* (mostly 1–3%). *Lingulodinium machaerophorum* occurs sporadically and

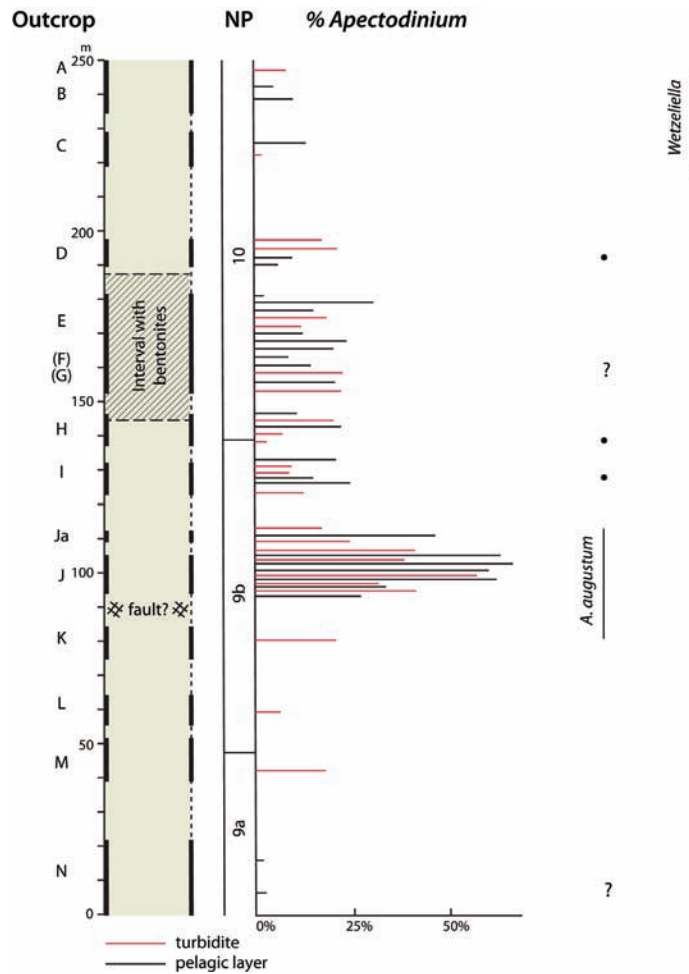


**Figure A1.16 ▲**

Distribution of the genera *Apectodinium* and *Wetzeliella* at Anthering. *Apectodinium* is shown as percentage of organic-walled microplankton. One fragmentary, possible specimen of *A. augustum* was recorded in outcrop N.

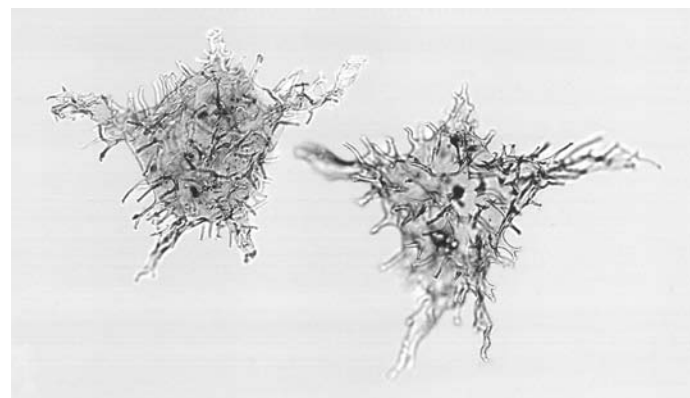


**Figure A1.17 ▲**

*Apectodinium augustum*. Left: specimen from Anthering, Outcrop J. Right: specimen from the CIE interval in Denmark (lowermost Ølst Formation, Viborg-1 borehole).

usually amounts to less than 1%. The overall composition of the dinoflagellate assemblages allows a simple subdivision of the section into three parts: The lower and upper intervals are characterized by a generally low dominance and relatively high species richness. These two intervals are separated by a middle interval coinciding with the CIE (outcrops J and JA). There the genus *Apectodinium* is dominant and reaches abundances up to 69% in hemipelagic samples (Fig. A1.16). Below and above this interval *Apectodinium* usually accounts for 5–20% of the dinoflagellate assemblages. The genus *Apectodinium* includes several intergrading species, the *Apectodinium*-plexus of Harland (1979). In spite of the strong dominance, the species richness remains relatively high within the CIE interval.

Quantitative dinoflagellate cyst data from hemipelagic layers of outcrop J reveal a 10-fold to 40-fold increase in the total number of cysts within the CIE interval (where *Apectodinium* dominates) (up to ca. 40.000 cysts/g) relative to pre-CIE samples. Above the CIE, counts reveal fluctuations in cyst numbers, but with a general trend towards smaller numbers of cysts.

### Paleoecology

Relying on information from modern cyst production (e.g., Dale, 1996), the Anthering section must have been deposited below neritic waters, or waters that originated in the neritic zone. The genus *Impagidinium*, which today is purely oceanic, is present in several samples (especially in outcrop N), but usually rarer than 1–2%. Such low occurrences indicate the neritic/oceanic boundary zone (Dale, 1996). Neritic cysts are today transported over long distances with currents, and are deposited in various basinal parts of the Atlantic Ocean (e.g., Dale, 1996). The continuous presence of *Polysphaeridium zoharyi* and *Homotryblium tenuispinosum* is evidence of a rather constant, and significant, mixing of the water masses at Anthering. *Polysphaeridium zoharyi* today mainly characterizes equatorial lagoons (Dale, 1996), and the extinct *Homotryblium* is a dominant form in several well-documented inner neritic, probably lagoonal settings of various ages (e.g., Köthe, 1990; Sluijs et al., 2005).

The acme of *Apectodinium* at the PETM is globally widespread (Crouch et al., 2001), however, the beginning of the acme in some sections precedes the global warming indicated by the CIE (Sluijs et

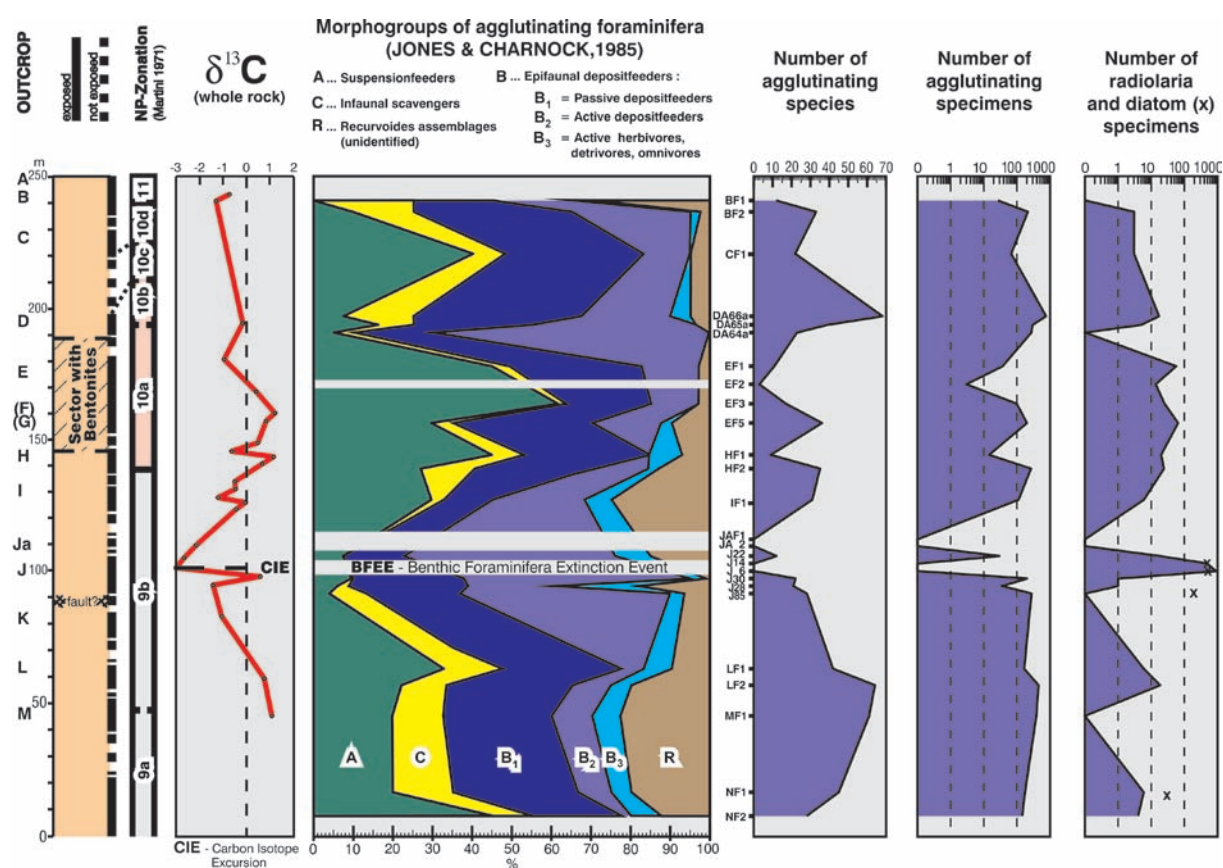


**Figure A1.18 ▲**

Distribution of agglutinating foraminifera and siliceous plankton in the Anthering section (modified from Egger et al. 2003)

al., 2007; 2011). The geographic and temporal distribution of *Apectodinium* shows that the genus was favoured by warm waters (Bujak & Brinkhuis, 1998), but the onset of the *Apectodinium* acme before the CIE in some areas shows that it was dependant on some other environmental factors too. Observations from the North Sea Basin clearly show that *Apectodinium* bloomed strongest in some marginal marine settings, where nearly monotypic assemblages may occur, e.g., in the Sparnacian facies of NW France. Observations from Anthering indicate that *Apectodinium* was associated with eutrophic waters (Egger et al., 2003).

#### *Apectodinium augustum*

The morphologically most extreme species of the *Apectodinium*-plexus is *A. augustum*. Typical specimens (Fig. A1.17) occur at Anthering, the first section from the western Tethys in which this species was recorded (Heilmann-Clausen & Egger, 2000; Egger et al., 2000). In the North Sea Basin of the North Atlantic realm *Apectodinium augustum* has only been recorded with certainty within the CIE interval (Heilmann-Clausen, 1985; Steurbaut et al., 2003; Schmitz et al., 2004). At Anthering the range likewise is closely related to the CIE interval, although a questionable earlier record cannot be excluded (Fig. A1.16).

#### *Comparison between hemipelagic and turbiditic samples*

A comparison between hemipelagic and turbiditic samples revealed no significant difference in the composition of the *in situ* cyst assemblages. A higher amount of older reworked cysts occur - as expected - in the turbidites, but in most turbidites the main part of the cysts are apparently of nearly the same age as the turbidites themselves. This indicates that the turbidites consist mainly of newly deposited sediment, or, if the proportion of older sediment is more substantial, it must be a sediment type poor in dinoflagellate cysts, like chalk and calcareous mud (Egger et al., 2000). The semi-contemporaneity of the turbidite-assemblages can be demonstrated by the fact that percentages of *Apectodinium* in the turbidites in the CIE-interval are higher than in all samples from the underlying strata (Fig. A1.16). They cannot, therefore be reworked from older levels. The similarity of the assemblages in hemipelagic and turbiditic layers indicates that the surface waters were similar over the basin slope where the turbidites originated, and over the basin floor.

#### *Biostratigraphic correlation of the interval with bentonites*

The first occurrence of the genus *Wetzeliiella* in the upper part of the Anthering section (Fig. A1.16) provides a tool for correlation to sections in the North Sea Basin recording the main ash series related to the opening of the NE Atlantic (Egger et al., 2000; Heilmann-Clausen & Egger, 2000). In the most offshore settings of the North Sea Basin, e.g. in Denmark, the main ash phase is bracketed by a strong *Apectodinium* acme (coinciding with the CIE) below, and by the first occurrence of *Wetzeliiella* spp. above. The bentonites in the Anthering section occur in the same position relative to these bracketing events, indicating that the bentonites are of similar age as the North Sea main ash phase, and thus may represent distal parts of the same ash layers.

## SILICEOUS PLANKTON

Throughout the Anthering section the fossil remains of siliceous plankton (radiolaria, diatoms as well as rare ebridians and silicoflagellates) have been replaced by pyrite. Silica dissolution prior to this replacement, and damage caused by the pressure of pyrite crystals growing inside the shells, can make identification difficult. In particular, radiolarians are very poorly preserved and are all taxonomically indeterminate spheroidal or lenticular spumellarians (Christopher Hollis, oral communication). If pyrite fillings only are preserved, the outline and shape of diatom frustules can be recognized, but a specific and often generic determination is impossible. However, in the more robust frustules, even relatively fine pores and cribra covering the areolae are preserved, and thus allow species determination.

Most samples have diatom floras dominated by the taxa *Paralia sulcata* var. *biseriata*, *Paralia sulcata* var. *crenulata*, *Coscinodiscus antiquus*, and by species of the genera *Auloplicata* and *Stephanopyxis*. The recent relatives of the latter two genera occur in coastal-neritic as well as in oceanic environments. This may also be the case for the less common species of the genera *Hemiaulus* (e.g. *H. peripterus*), *Actinoptychus* and *Sceptroneis*. Species of the genus *Trochosira*, which are also rather rare, are considered to have been fully planktonic, whereas specimens of *Craspedodiscus*, *Trinacria*, *Sheshukovia* and *Aulacodiscus* probably indicate a coastal-neritic environment. Other genera can be considered to

have been fully benthic, e.g. species of the genera *Auliscus* and *Arachnodiscus*. In neritic assemblages, resting spores should be abundant, but in the studied samples only single specimens of resting spores were found. These belong to the form groups *Xanthiopyxis*, *Pterotheca* and *Bicornis*. As resting spores are most resistant to dissolution, their scarcity indicates that the encountered diatoms represent an oceanic assemblage (Fenner, 1994). The minor admixture of coastal and neritic specimens may have been caused by storm events that whirled up freshly deposited sediment in shallow regions which thereafter settled out from suspension beyond the shelf edge.

The occurrence of *Craspedodiscus* spp. and *Trinacria* spp. in deep-water deposits at Anthering is highly remarkable as these genera are usually restricted to neritic environments. We can rule out redeposition of these specimens because in that case, resting spores and benthic species would have been redeposited in considerable amounts. This suggests that water-depth was not the limiting factor for the occurrence of *Craspedodiscus* spp. and *Trinacria* spp.. Probably, the preference of these genera for neritic settings was due to the higher level of dissolved nutrients in these areas.

## AGGLUTINATING FORAMINIFERA

Individual samples contain up to 65 species and more than 700 specimens (Fig. A1.18) of agglutinated foraminifera. More than 90 species were identified and grouped into four morphogroup assemblages (tubular genera, infaunal passive deposit feeders, active deposit feeders, epifaunal active herbivores and omnivores). Distributional patterns of morphogroups of agglutinating foraminifera are related, more or less directly, to food supply and food utilisation processes (Jones and Charnock, 1985).

At Anthering, tubular forms comprise the genera *Nothia*, *Rhabdammina*, *Rhizammina*, *Psammosiphonella* and *Bathysiphon*. These typical „fysch-type“ elements have been interpreted as sessile suspension feeders (morphogroup A of Jones and Charnock). However, the ecological interpretation of some of these deep-sea genera is still under discussion (Gooday et al. 1997), e.g. the life habitat of *Nothia* has been re-interpreted as epibenthic detritivore (Geroch and Kaminski, 1992). Epi- and infaunal passive deposit feeders (morphogroup B1) comprise *Saccamina*, *Psammosphaera*, *Hormosina*, *Hormosinella*, *Trochamminoides*, *Paratrochamminoides*, *Lituotuba*, *Hyperammina* and *Kalamopsis*. Another epifaunal and shallow infaunal group of active deposit feeders (morphogroup B2) corresponds to the *Ammodiscus* - *Glomospira* assemblage of „Biofacies B“ (Kuhnt et al., 1989). It consists of the genera *Ammodiscus*, *Glomospira* and *Rzehakina*. The B3 assemblage of epifaunal active herbivores and omnivores (*Haplophragmoides*, *Trochammina* s.l.) may be restricted to omnivores in this deep-sea environment. The C-morphogroup of infaunal forms (*Gerochammina*, *Karrerulina*, *Reophax*, *Subreophax*, *Spiroplectammina*) are negligible in the abyssal setting of the Anthering section. The genera *Recurvoides* and *Thalmanammina* were summarized as *Recurvoides*-assemblage. The microhabitat preferences of this assemblage are questionable. In the Cretaceous „Hatteras Fauna“ of the Fardes Formation in southern Spain it co-occurs with *Glomospira* and *Ammodiscus*, and might, therefore, be indicative of oxygen deficient conditions (Kaminski et al., 1999). In our samples we did not find this correlation because the highest percentages of the *Recurvoides*-assemblage occur in high diversity faunas without any indication of oxygen depletion. It is noteworthy, that the *Recurvoides*-assemblage usually forms more than 10% of the agglutinated faunas within nannoplankton zone NP9 whereas in zone NP10 this percentage is much lower.

The highest diversity and the highest abundance of agglutinated specimens occur in the lower part of the section (samples NF2 to LF1). These assemblages display balanced proportions of infaunal, epifaunal and suspension feeding species. The high diversity of these agglutinated faunas is seen as typical for oligotrophic, food-limited environments where the various microhabitats are fully occupied. Several taxa have their last occurrences in this part of the section: *Ammodiscus cretaceus*, *Aschemocella* cf. *carpathica*, *A. grandis*, *Haplophragmoides horridus*, *H. suborbicularis*, *Hormosina trinitatis*, *Karrerulina* cf. *coniformis*, *Paratrochamminoides heteromorphus*, *P. multilobus*, *Recurvoides walteri*, *Remesella varians*, *Rzehakina complanata*, *R. epigona*, *R. fissistomata*, *Spiroplectammina* cf. *dentata*, *Spiroplectammina spectabilis*, *Thalmanammina* n. sp., *Thurammina papillata*.

Further up-section (samples J85 to JaF1) impoverished faunas with a predominance of the genus *Glomospira* appear. This „*Glomospira* event“ has been observed at numerous localities in the Tethys and northern North Atlantic (see Kaminski et al., 1996 for a review). Kaminski et al. (1989) speculated that the predominance of *Glomospira* indicates areas of high surface productivity that caused low-oxygen

levels at the sea-floor. However, this assemblage occurs also in well oxidized sediments and, therefore, it may be opportunistic rather than a reliable indicator for high productivity (Galeotti et al., 2000; Kaminski et al., 1996). With the onset of the CIE, even this opportunistic assemblage disappeared and over a period of at least 180 000 years the benthic communities suffered severely from unfavorable habitat conditions.

Between samples HF2 to EF1 the majority of the hemipelagic layers have an organic carbon content between 0.14% and 0.17% (0.15% on average), but several black shale layers (up to 1.22% TOC) occur. This suggests periodic eutrophication of the sea water probably by volcanic ashfall as closely spaced bentonites were found in that part of the section (Egger et al., 2000a). The black shales are usually devoid of benthic foraminifera and contain common framboidal pyrite indicating anoxic conditions (Egger et al., 1997). The agglutinating faunas of these layers are not as rich and diverse as those from further down the section. *Glomospira glomerata* has its first appearance in this part of the section. The faunal assemblage changed to a predominance of passive deposit feeders (B1-assemblage) and tubular genera (A-assemblage). These assemblages are dominant along the continental rises where bottom currents or distal turbidity currents occur (Kaminski et al., 1996).

In the uppermost part of the Anthering section (samples DA64a to BF1) a strong increase in the number of species and specimens of the DWAF, with relatively balanced assemblages, occurs indicating the return of ecological conditions similar as those at the base of the section.

## STRUBACH SECTION

Hans Egger

**Topics:**

Hemipelagic sedimentation in the Paleocene

**Tectonic unit:**

Rhenodanubian Flysch Zone

**Lithostratigraphic units:**

Rhenodanubian Group, Acharting Formation, Strubach Tonstein

**Cronostratigraphic units:**

Danian to Thanetian

**Biostratigraphic units:**

Calcareous nannoplankton Zones NP3 to NP8

**Location:**

Strubach creek

**Coordinates:**

E 013° 01' 06", N 47° 54' 12"

**References:**

Egger 1995, Egger et al. 2005

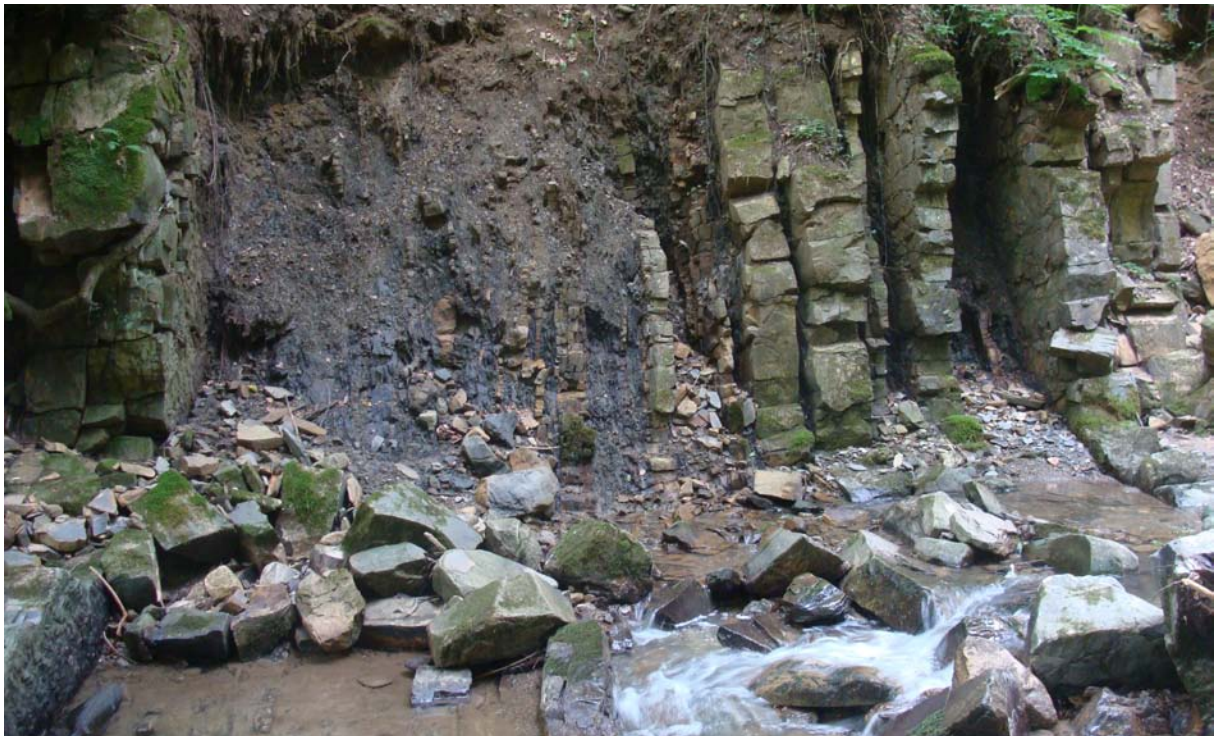


**Figure A1.19 ▲**  
Acharting member

In the upper Maastrichtian and Danian the Acharting Member of the Altlenbach Formation is characterized by thin- to medium-bedded turbidites which display base-truncated as well as complete Bouma sequences (Fig. A1.19). Usually the upper part of the Bouma sequences consist of medium-grey clayey marlstone, which represents c. 35 % of this member whereas the percentage of intervening green coloured hemipelagic claystone layers is less than 15%. A distinct feature of this turbidite facies is the intercalation of thick-bedded and coarse grained sandstones with high amounts of mica and quartz. These are marker beds for mapping the Altlenbach Formation. Calcareous nannoplankton zone NP3 was found in a sequence of very thin-bedded and fine-grained turbidites. Further up-section, hemipelagic claystone (Strubach Tonstein) becomes the dominant rock-type and turbidite layers are much less frequent than below. This 50 m thick claystone-rich interval is also regarded as part of the Acharting Member and comprises Zones NP3 to NP8.

Interestingly, clay mineral assemblages of the Strubach Tonstein display high amounts of chlorite indicating a strong increase in bed rock erosion. In addition, the bulk rock composition of the hemipelagic shales displays an increase in the percentages of detrital quartz and feldspar of about 10%. The concurrence of indications of increased mechanical erosion in the composition of interturbidite layers and a dearth of turbidite sedimentation indicates a steepening of relief and a synchronous change of drainage patterns. Tectonic uplift and associated block faulting, which cut off the basin from the source area of turbidity currents are the most likely interpretation of the observed sedimentary features (Egger et al., 2002). This interpretation is supported by the identification of slope basins in the Ultrahelvetic nappe complex (Egger & Mohamed, 2010 – Stop A2/4). These basins were formed from the Late Maastrichtian on and acted as sediment traps, which prevented the entering of turbidity currents into the main basin.



**Figure A1.20 ▲**  
Strubach Tonstein

## SOUTHERN SHELF OF THE EUROPEAN PLATE

Hans Egger, Claus Heilmann-Clausen

**Topic:**

The erosional unconformity between the Thanetian and Ypresian

**Tectonic unit:**

South Helvetic nappe complex

**Lithostratigraphic units:**

Kressenberg formation, Fackelgraben Member, Frauengrube Member

**Chronostratigraphic units:**

Thanetian and Ypresian

**Biostratigraphy:**

Calcareous nannoplankton Zones NP9 and NP12

**Location:**

Frauengrube quarry

**Coordinates:**

E 013° 00' 06", N 47° 56' 11"

**References:**

Egger et al., 2009b; Rasser & Piller, 1999 and 2001

### Outcrop 1 Frauengrube Section

In the Haunsberg area, the Frauengrube section and the immediately adjoining Kroisbach section are both part of the South-Helvetic Thrust Unit. The base of the succession is a grey mica-bearing marlstone of the Maastrichtian Gerhartsreit Formation, which is overlain by silty claystones and clayey siltstones of the Paleocene Olching Formation. Detailed nannoplankton studies at the Cretaceous/Paleogene-boundary indicate continuous sedimentation across the boundary, since the uppermost Maastrichtian (*Micula prinsii* Zone) and the lowermost Paleocene (*Markalius inversus* Zone) have been discovered (Stradner, pers. comm. 2005). Around the boundary, the amount of terrestrially-derived sediment input strongly increases at the expense of carbonate. This shift in the lithological composition defines the lithostratigraphic boundary between the Gerhartsreit and Olching formations.

The Olching Formation is overlain by the Kroisbach Member of the Kressenberg Formation. This member is characterized by glauconite-bearing quartz-sandstones with abundant brachiopods (*Crania austriaca* Traub) in the lower part and oysters (*Pycnodonte* spp.) in the upper part. The glauconitic matrix of the oyster-beds contains calcareous nannoplankton of the Upper Thanetian *Heliolithus riedelii* Zone (NP8) and very well preserved pollen and spores (Stradner, in Gohrbandt, 1963a; Kedves, 1980; Draxler, 2007).

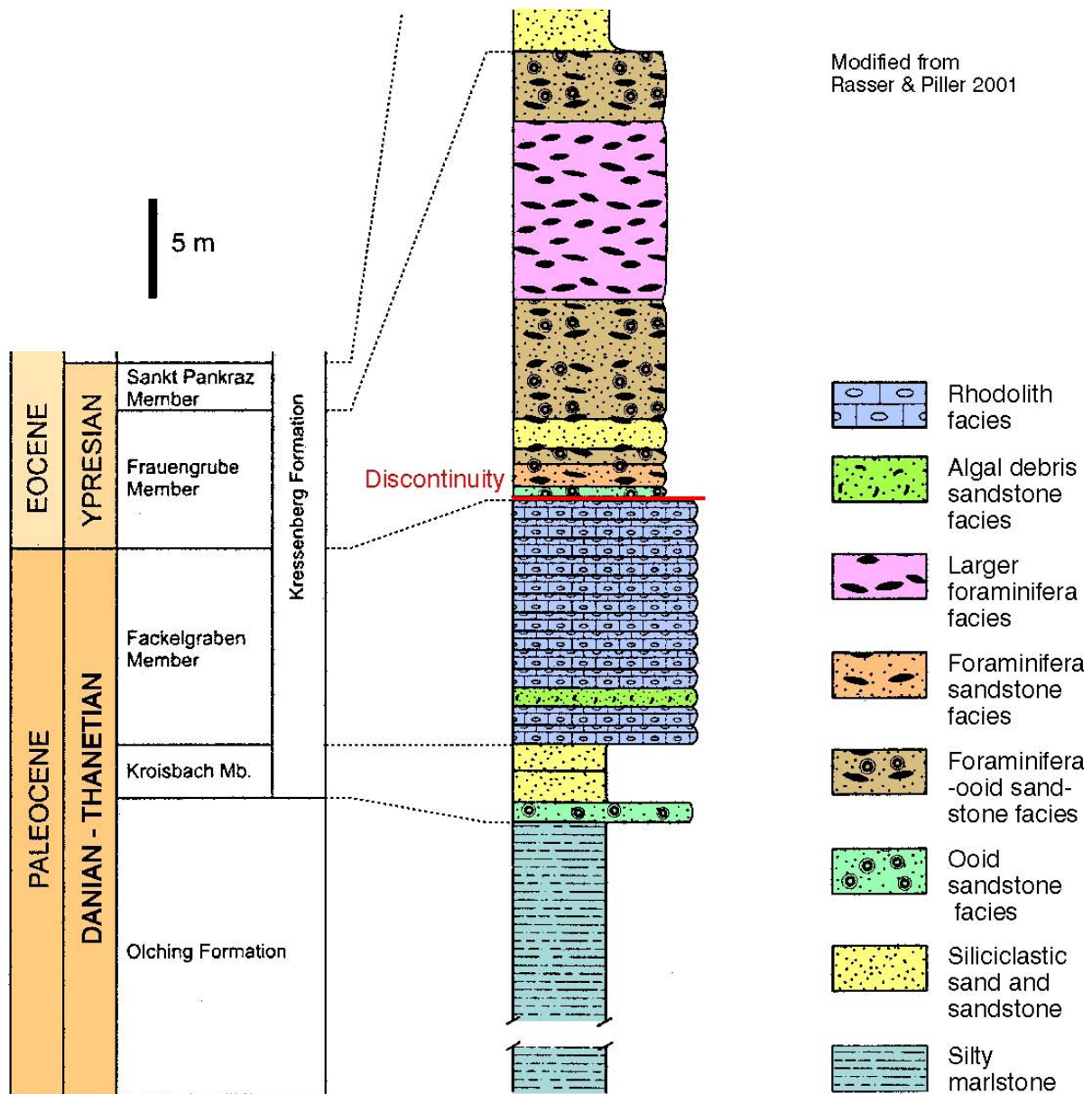


**Figure A1.21 ▲**  
Lithologic log of the south Helvetic succession

**Figure A1.22 ►**  
Glaucanitic sandstone of the Kroisbach Member containing abundant oysters

The Kroisbach Member is overlain by the rhodolithic limestone of the Fackelgraben Member. Samples from thin intervening marlstone layers in the upper part of this member contained poorly preserved calcareous nanoplankton of the *Discoaster multiradiatus* Zone (NP9), of latest Paleocene age: *Chiasmolithus* sp., *Coccolithus pelagicus*, *Discoaster falcatus*, *Discoaster mul-*



*tiradiatus*, *Discoaster mohleri*, *Fasciculithus tympaniformis*, *Neochiastozygus perfectus*, *Thoracosphaera* sp., *Toweius callosus*, *Toweius pertusus*. Reworking of Cretaceous species has not been observed.

The Fackelgraben Member and the overlying Frauengrube Member are separated by an irregular erosional surface (Rasser and Piller, 1999), that has been described previously from other outcrops in the Salzburg area (Vogeltanz, 1977). Clasts of the Fackelgraben Member are reworked in the basal part of the Frauengrube Member (Rasser and Piller, 2001), which comprises 0.5 m of brownish sandstone with a marly matrix, that contains poorly preserved calcareous nannoplankton. Reworked species from the Campanian and Maastrichtian make up about 5% of the nannoplankton assemblage (*Arkhangelskiella cymbiformis*, *Broinsonia parca*, *Cribrosphaerella ehrenbergii*, *Cyclagelosphaera reinhardtii*, *Eiffellithus eximius*, *Markalius inversus*, *Micula staurophora*, *Pre-discosphaera cretacea*, *Watznaueria barnesae*). The rest of the species observed have their first occurrence during the Paleocene (*Campylosphaera eodela*, *Chiasmolithus bidens*, *Chiasmolithus consuetus*, *Chiasmolithus danicus*, *Coccolithus pelagicus*, *Discoaster barbadiensis*, *Discoaster multiradiatus*, *Thoracosphaera* sp., *Toweius* spp.) or in the lower Eocene (*Neochiastozygus junctus*, *Pontosphaera versa*, *Pontosphaera duocava*, *Rhabdosphaera solus*, *Transversopontis pulcher*, *Zygrhablithus bijugatus*). Unfortunately, no marker species of the lowermost Eocene, in particular of the *Rhomboaster-Tribrachiatus* lineage, have been encountered in our samples. However, *Tribrachiatus orthostylus* (Type B = without bifurcated rays) has been described from the base of the Frauengrube Member from another outcrop in the Haunsberg area (Stradner in Gohrbandt, 1963b). This finding indicates that the onset of the transgression did not take place before the *Discoaster binodosus* Zone (NP11).

Beside calcareous nannoplankton, the samples from the base of the Frauengrube Member contain marine and terrestrial palynomorphs. The terrestrial flora indicates a subtropical to tropical climate containing Sapotaceae and Matixiaceae pollen among other floral elements (*Dictyophyllidites* sp., *Pityosporites* sp., *Nudopollis* sp., *Subtriporopollenites* sp., *Cupuliferoidaepollenites liblarensis*). Palmpollen have not been found (Draxler, pers. comm. 2006).

The marine flora contains very similar, relatively well preserved dinoflagellate assemblages dominated by *Homotryblium tenuispinosum* ("tasmaniense-type"), *Polysphaeridium zoharyi* and *Apectodinium* spp. (excluding *A. augustum*). The three taxa are equally common, and together are estimated to constitute 60–90% of the dinoflagellate assemblages. Of relevance for age-determination is the occurrence of the *Areoligera undulata* – *A. sentosa* group (present in each sample), *Glaphyrocysta* cf. *semitecta* (samples 1 and 3), *Deflandrea oebisfeldensis* (2 specimens in sample 1) and *Phthanoperidinium* cf. *echinatum* (1 or 2 specimens in sample 1). In addition to these taxa, the samples also include low abundances of several long ranging taxa without stratigraphic value. *Spiniferites* spp. and peridinioids, apart from *Apectodinium*, are rare.

The *Areoligera undulata* – *A. sentosa* group, *Glaphyrocysta* cf. *semitecta* and *Phthanoperidinium* cf. *echinatum* were not recorded in the Anthering Formation at Anthering, from where dinoflagellates were previously studied (Egger et al., 2000; 2003). This suggests a younger age for the Frauengrube Member. The *Areoligera undulata* – *A. sentosa* group is probably of inner neritic-lagoonal origin and has previously been recorded in the Lutetian in southern England (Eaton 1976; Bujak et al. 1980). Little is

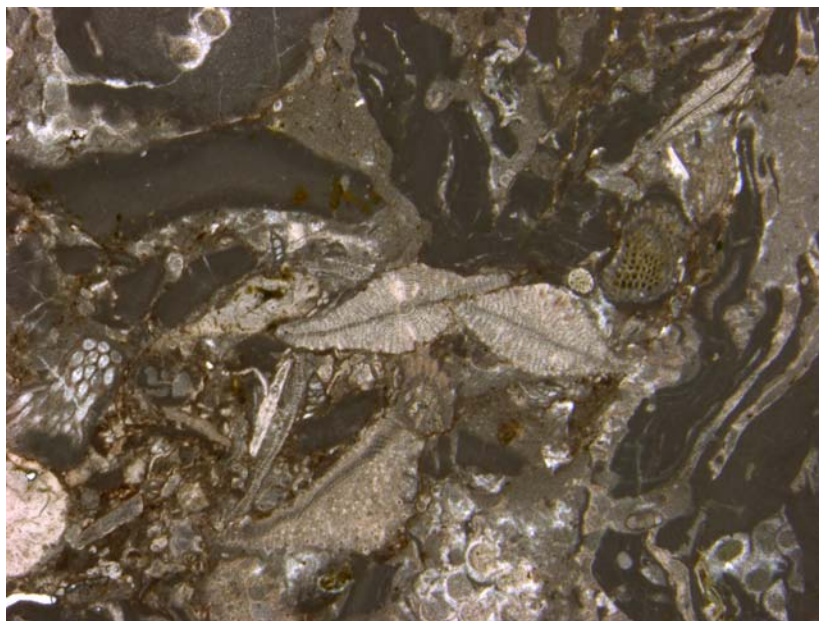


**Figure A1.23 ▲**

Image of a thin section of rhodolithic limestone with *Discocyclina* sp. (Fackelgraben member)



**Figure A1.24 ▲**

Photograph of the type locality of the Frauengrube Member (Note the erosional unconformity between the Fackelgraben Member (left) and the Frauengrube Member (right))

known about its stratigraphical distribution elsewhere. The several specimens of *Glaphyrocysta* (cf.) *semitecta* are very close to, but perhaps not identical with *Glaphyrocysta semitecta*, a taxon previously recorded from NP15 to near the Eocene/Oligocene boundary in NW Europe (e.g. Bujak et al. 1980; Heilmann-Clausen and Van Simaëys 2005). Nothing else in the samples suggests such a young age. The abundance of *Apectodinium* points to an age no younger than the Ypresian-Lutetian transition, most likely early Ypresian or older. The two specimens of *Deflandrea oebisfeldensis* also point to an early Ypresian or older age, as this form becomes extinct in the lower Ypresian in NW Europe (probably in or near top of NP11, e.g. Heilmann-Clausen and Costa 1989; Luterbacher et al. 2004).

In summary, the calcareous nannoplankton and dinoflagellate assemblages of the Frauengrube section indicate an erosional gap across the P/E-boundary, spanning the upper part of zone NP9, the entire zone NP10, and at least a large part of zone NP11.

**Outcrop 2: St. Pankraz Section****Topics:**

Palynology at the Paleocene-Eocene transition

**Tectonic unit:**

South-Helvetic nappe complex

**Lithostratigraphic unit:**

Claystone and marly claystone (not formalized)

**Chronostratigraphy:**

Upper Paleocene to lower Eocene

**Location:**

Hiking trail and creek south of St. Pankraz

Directly to the south of the St. Pankraz carpark, 8 m thick succession of grey claystone and marly claystone is exposed along a hiking trail. No macrofossils or indicators of bioturbation were observed in the claystone that consists of kaolinite (47 wt%), smectite (39 wt%) and illite (14 wt%). The claystone-rich succession is the tectonically truncated base of a small tectonic thrust unit of the south-Helvetic nappe complex. A higher part of this south-dipping succession outcrops ca. 20 m southward, in the course of a small creek. There, thick poorly sorted coarse-grained sandstone beds are alternating with the claystone. Most of the white to yellowish coloured sandstone beds show poor grain sorting. Occasionally parallel lamination occurs. The sandstone beds have sharp contacts to the pelitic rocks and often display rip-up clasts (up to 20 cm in diameter) indicating high energy erosive events. The claystone-sandstone-succession is overlain by a few meters of very pure quartz sandstone overlain by calcareous arenites



**Figure A1.25 ▲**  
Sharp contact between claystone and sand at the St. Pankraz section

rich in larger foraminifers. The St. Pankraz outcrop is interpreted to expose a general transgressive succession.

### Composition of the microflora

The claystone at St. Pankraz yields high percentages of the dinoflagellate genus *Apectodinium* including the species *Apectodinium augustum*. The range of this species is almost exclusively restricted to the negative carbon isotope excursion (CIE) at the base of the Eocene.

Gymnosperms are extremely rare, comprising only a few grains of Taxodiaceae/Cupressaceae s.l., Pinaceae (*Pinus*, *Abies*, *Cathaya*, and a *Tsuga*-type) and *Ephedra* (*Ephedrites*), whereas spores are relatively diverse but not common.

In contrast to the gymnosperms, angiosperms are far more abundant and dominate the assemblages: Prevailing are the *Triporopollenites* formgenus, the “*Normapolles*” s.l. group (*Nudopollis*, *Interpollis*, etc.), *Plicapollis* (Rhoipteleaceae), *Subtriporopollenites*- (Fig. A1.26, 4–6), *Triatriporopollenites*-species, *Platycaryapollenites*, and *Engelhardiapollenites* (all Juglandaceae). Fagaceae (*Trigonobalanopsis*, Fig. A1.26, 7–9), *Alnus* (Betulaceae), *Salix* (Salicaceae) and *Platanus* (Platanaceae, Fig. A1.26, 10–12) are much less common. The remaining eudicot taxa are all accessory elements (<1%) and include, for example, *Ilex*, *Parthenocissus*, *Vitis*, *Symplocos*, *Zanthoxylon* (Fig. A1.27, 7–9), *Euphorbia*-pollen and other rare elements. Most of the rare pollen taxa and some spore taxa (Schizaeales such as, *Ruffordia*, *Schizaea*, Fig. A1.26, 1–3) from the St. Pankraz claystone represent genera and families nowadays preferring warm temperate to (sub)tropical climates. This is particularly the case for genera that are affiliated with extant families that grow under present day megathermal conditions, such as Anacardiaceae (*Lansea*, Fig. A1.27, 4–6), Arecaceae (*Sabal* and *Aiphanes* type, Fig. A1.27, 10–15), Malvaceae (*Durio*-type and *Kostermansia*-type, *Craigia*, and a probable sterculoid gen. indet., Fig. A1.27, 1–3), Chloranthaceae (*Ascarina*), Icacinaceae (*Iodes*), Hamamelidaceae (cf. *Neostrearia*), Picodendraceae (*Aristogeiton*), Sapotaceae (*Palaquium* and gen. indet.) and are interpreted to originate mostly from East Asia (Manchester, 1999; Manchester et al., 2009) and to certain extent coming via Africa (*Aristogeiton*, Picodendraceae, Zetter and Hofmann, 2008). A few other rarer taxa, such as *Eotrigonobalanus*, *Euphorbia* type, *Ilex*, *Parthenocissus*, *Quercus*, *Symplocos*, *Vitis* etc. can also grow under more mesothermal conditions. Taxa such as *Alnus*, *Salix* and *Platanus* are not useful as palaeoclimate indicators. The helophytes such as *Sparganium*, *Lysichiton*, Restionaceae (a characteristic family of swamp inhabitants in the southern hemisphere) and a newly discovered Hydatellaceae (*Monosulcites rivularis*, Fig. A1.26, 13–15) are assumed to prefer humid, temperate to warm temperate conditions.

From the climatic point of view, the terrestrial palynomorphs of St. Pankraz are similar to palynofloras from the Thanetian Kroisbach Member of the same sedimentary succession (Draxler, 2007). The palynoflora indicates a climate warmer than the Cfa climate witnessed by Miocene microfloras from Austria and falls into the “warm temperate evergreen deciduous forest”, which is effectively a “subtropical flora with temperate elements”.

#### Figure A1.26 ►

all LM images x 1000, SEM overview bar = 10 µm, SEM detail bar = 1 µm

1–3. *Cicatricosisporites pseudodorogensis* (Schizales)

4–6. *Subtriporopollenites* sp. ? (Juglandaceae)

7–9. *Trigonobalanopsis* sp. (Fagaceae)

10–12. *Platanus* (Platanaceae)

13–15. *Monosulcites rivularis* (Hydatellaceae)

#### Figure A1.27 (Page 46)

all LM images x 1000, SEM overview bar = 10 µm, SEM detail bar = 1 µm

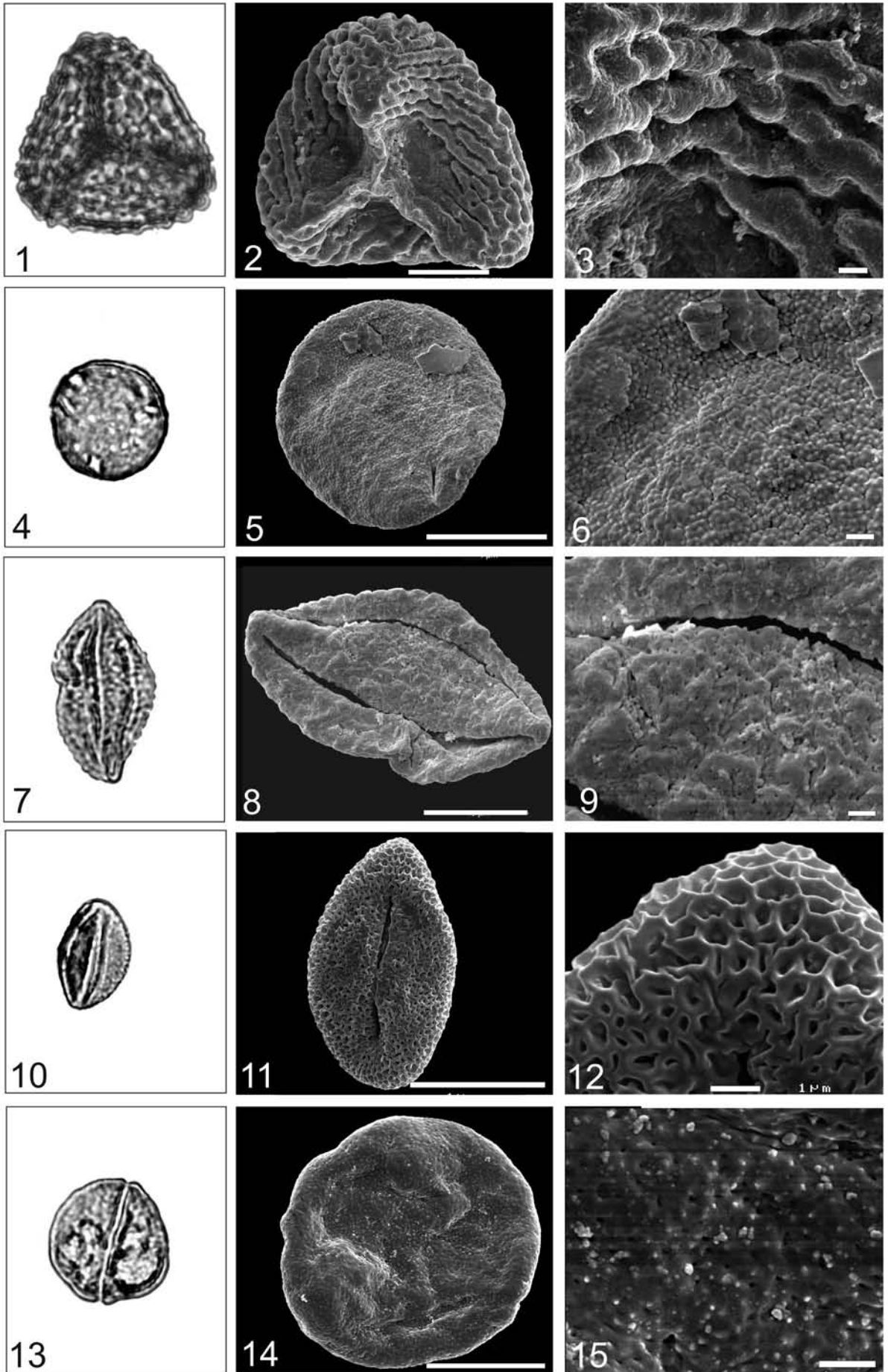
1–3. *Intratriporopollenites* sp. (? sterculoid Malvaceae)

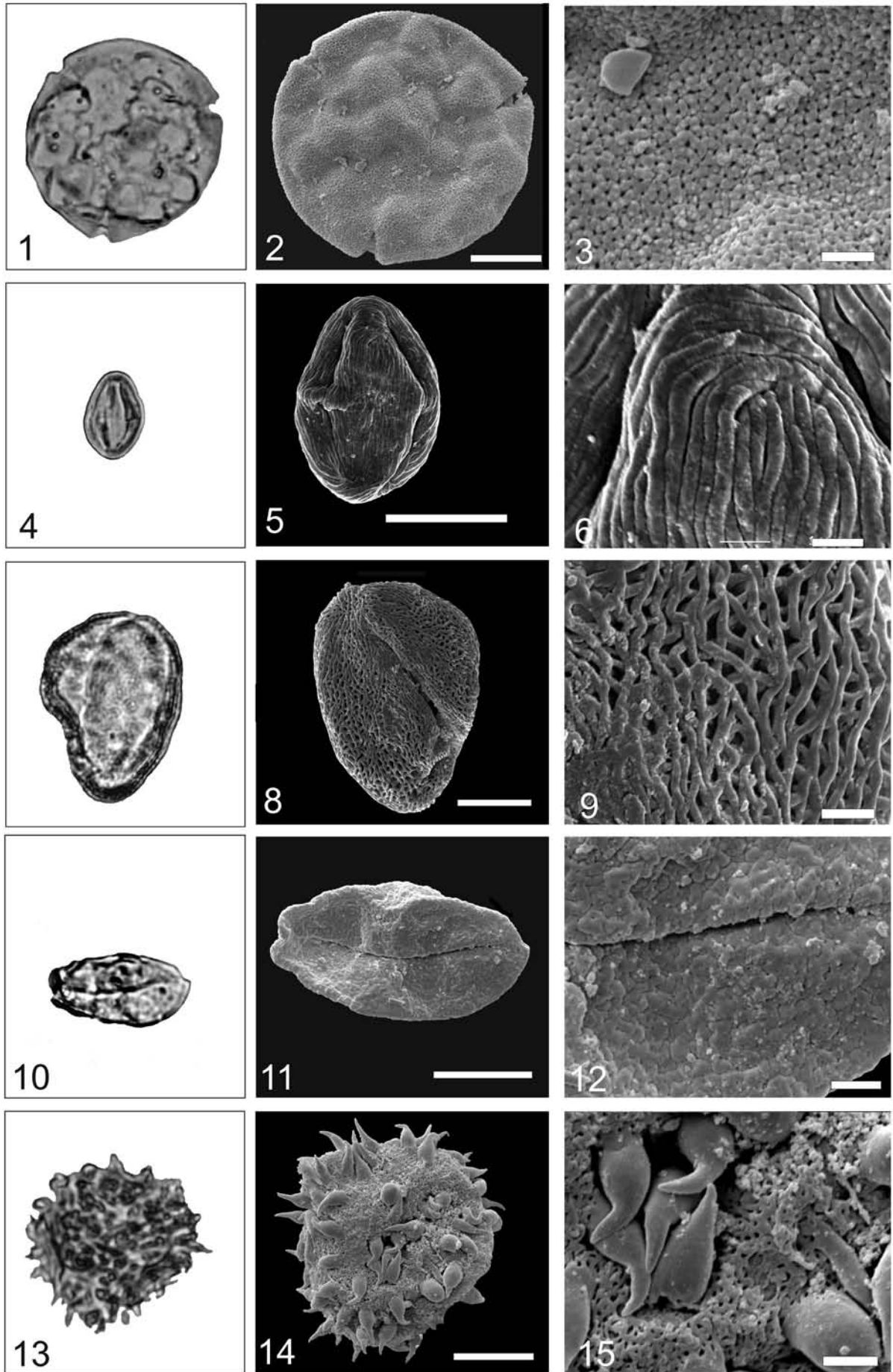
4–6. *Tricolporopollenites* cf. *solé de portai* (Anacardiaceae, *Lansea*-type)

7–9. *Tricolporopollenites* sp. ??? (Rutaceae, *Zanthoxylum* type)

10–12. *Arecipites* sp. (?Arecaceae)

13–15. *Monoporopollenites* sp. (Arecaceae, Bactridinae)





## Deep-water and shallow-water Lutetian deposits and a Cretaceous-Paleogene transitional section

### Introduction

Today we first head towards north to the small town of Mattsee at the eponymous lake. The town dates back into the 8th century but the area is inhabited since Neolithic times. The Mattsee castle was built in the 12<sup>th</sup> century. After visiting Lutetian deep-water deposits, we go back to south and then on the highway to reach Siegsdorf in Bavaria. We will have a packed lunch in the Siegsdorf museum and have the opportunity to have a look on the museum collection. After eating, we will see the Lutetian shallow-water deposits next to the mineral bottling plant at Bad Adelholzen. On the way back to Salzburg we stop to see the Cretaceous-Paleogene transition near Teisendorf. Arrival time at Salzburg ca. 5 p.m., the Ice Breaker party in the “Haus der Natur” starts at 7 p.m.

### Notes:

- Arrange your own breakfast and assemble at the carpark of St. Virgil (Ernst-Grein-Straße 14, 5026 Salzburg; Tel. +43-662-65901-516) for departure at 8.30 a.m. sharp.
- Packed lunch will be arranged at the Siegsdorf museum, which can be visited during the lunch break
- Route: Salzburg (St. Virgil) – Mattsee – Siegsdorf – Adelholzen – Teisendorf – Salzburg (St. Virgil)
- Accomodation at Salzburg has to be arranged by the participants.



Figure A2.1a ▲  
Mattsee



**Figure A2.1b ▲**  
Route map for Field Trip A2

## HOLZHÄUSL OUTCROP NEAR MATTSEE

Hans Egger, Fred Rögl, Peter Bijl, Henk Brinkhuis

### Topics:

Plankton assemblages of the lower Lutetian

### Tectonic unit:

Ultrahelvetic nappe complex

### Lithostratigraphic unit:

Buntmergelserie

### Chronostratigraphic unit:

Middle Eocene, Lutetian

### Biostratigraphic units:

planktic foraminifera Zone E8, calcareous nannofossil sub-Zones NP14b and NP15b

### Location:

Southern (coord.: 13° 07' 09" E, 47° 58' 26" N) and northern (coord.: 13° 07' 11" E, 47° 58' 23" N) Holzhäusl creeks near Mattsee

### References:

Rögl & Egger, 2010

The Holzhäusl section consists of a number of temporary outcrops resulting from the erosion of two small tributaries to Lake Mattsee and is located 20 km north of the town of Salzburg. In the southern gully calcareous nannoplankton sub-Zone NP15b (outcrop 1) was found. Along the course of the northern creek grey marlstone of calcareous nannoplankton sub-Zone NP14b (outcrop 2) is exposed. The bathyal marlstone (average carbonate content 58 wt%) of both outcrops is part of the informal lithostratigraphic unit "Buntmergelserie" and was deposited at approximately 35° northern paleolatitude. In the Oligocene, the slope deposits were detached from their substratum and became part of the Ultrahelvetic thrust unit, which tectonically overlies the sedimentary infilling of the Alpine Molasse Basin.

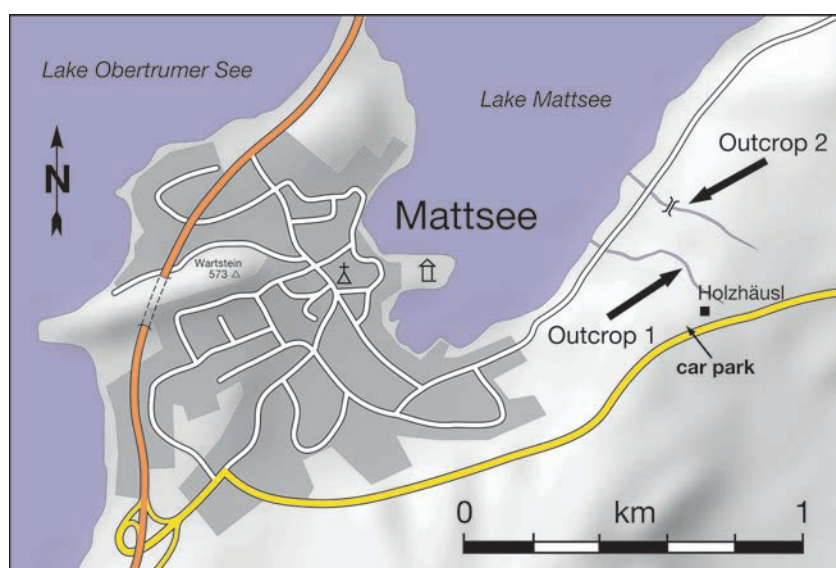


**Figure A2.2 ▲**  
Locations of outcrops near Holzhäusl

## Outcrop 1

The nannoplankton assemblages, which are dominated by *Reticulofenestra dictyoda*, *R. scrippsae*, *Coccolithus pelagicus*, and *Zygrhablithus bijugatus*, are diverse and show moderate preservation. Re-working of Cretaceous nannoplankton specimens is less than 1%. All samples display similar compositions of the assemblages (Fig. A2.3), which are characterized by the occurrences of *Blackites spinosus*, *Chiasmolithus consuetus*, *C. expansus*, *C. gigas*, *C. grandis*, *C. solitus*, *Coccolithus mutatus*, *Discoaster barbadiensis*, *D. gemmifer*, *D. saipanensis*, *D. tanii*, *D. wemmelensis*, *Nannotetrina fulgens*, *N. cristata*, *Reticulofenestra umbilicus* (> 14 µm), *Sphenolithus moriformis*, *S. spiniger*, *S. radians*.

This assemblage is typical for the *Nannotetrina fulgens* Zone, which is defined by the stratigraphic range of the marker fossil. The *N. fulgens* Zone represents Zone NP15 in the zonation scheme of Martini (1971) and Zone CP13 in the zonation scheme of Okada and Bukry (1980). The latter authors suggested a three-fold subdivision of the *Nannotetrina fulgens* Zone using the range of *Chiasmolithus gigas* (Fig. A2.6), which is restricted to the middle part (CP13b) of the *Nannotetrina fulgens* Zone. Aubry (1991) has defined Subzone NP15a as the interval between the FO of *Nannotetrina fulgens* and the FO of *Chiasmolithus gigas*, Subzone NP15b as the total range of *Chiasmolithus gigas*, and Subzone NP15c as the interval between the HO of *Chiasmolithus gigas* and the HO of *Rhabdosphaera gladius*. Using these criteria, the entire Holzhäusl section can be assigned to the *Chiasmolithus gigas* Subzone.

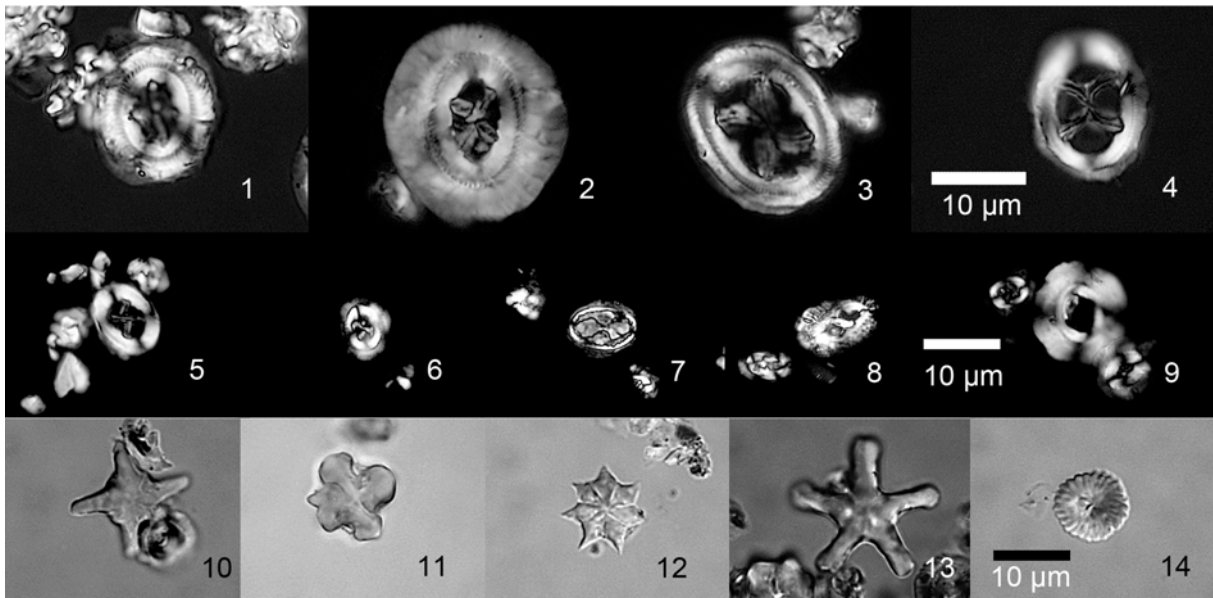


**Figure A2.3 ▲**

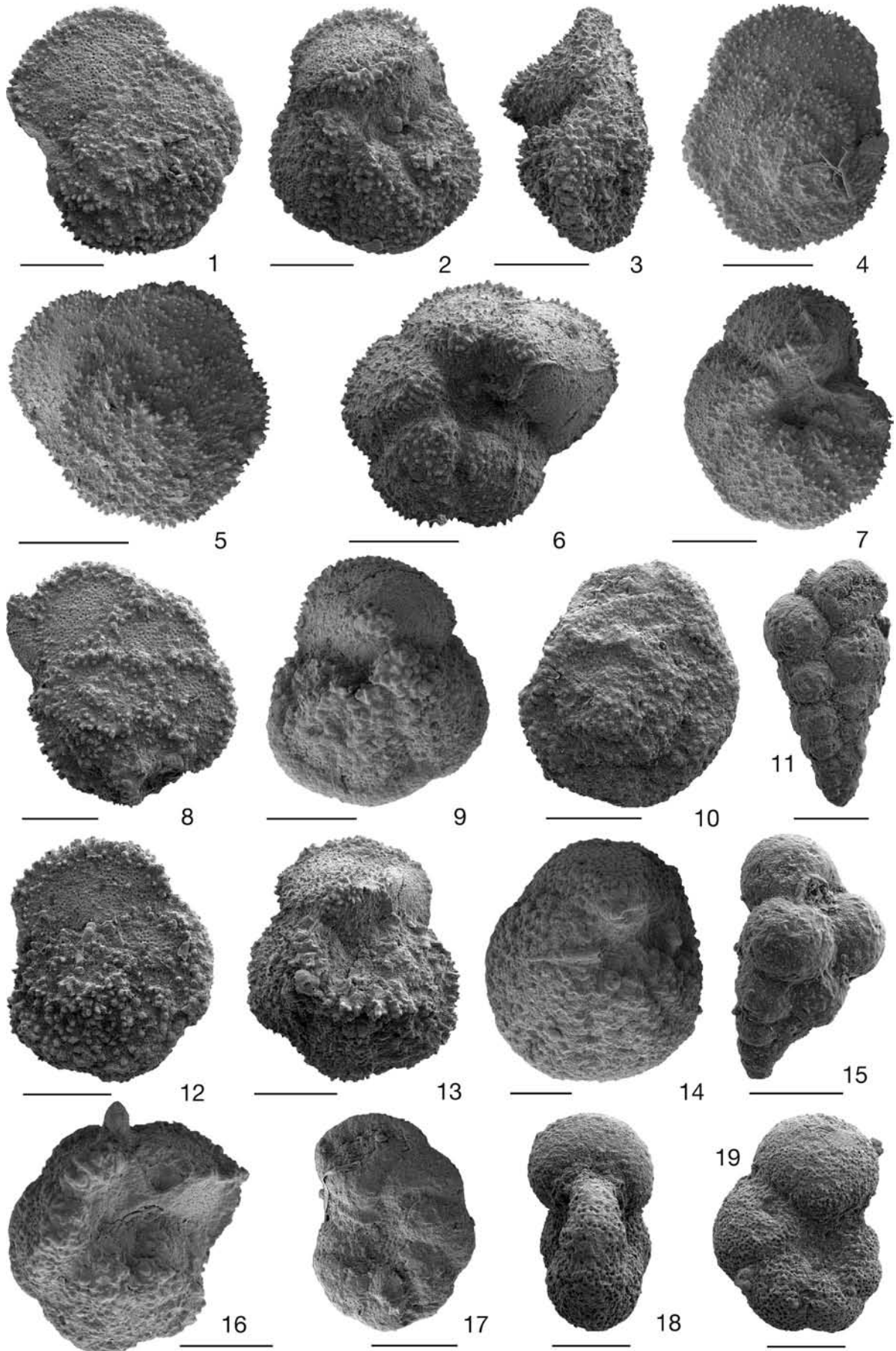
Selected calcareous nannoplankton from Holzhäusl outcrop 1

1 *Coccolithus mutatus*; 2 *Chiasmolithus gigas*; 3 *Chiasmolithus grandis*; 4 *Chiasmolithus expansus*; 5 *Chiasmolithus solitus*; 6 *Chiasmolithus nitidus*; 7 *Clausiococcus vanheckiae*; 8 *Helicosphaera bramlettei*; 9 *Reticulofenestra umbilicus*; 10 *Nannotetrina fulgens*; 11 *Nannotetrina cristata*; 12 *Discoaster saipanensis*; 13 *Discoaster tani*; 14 *Discoaster wemmelensis*.

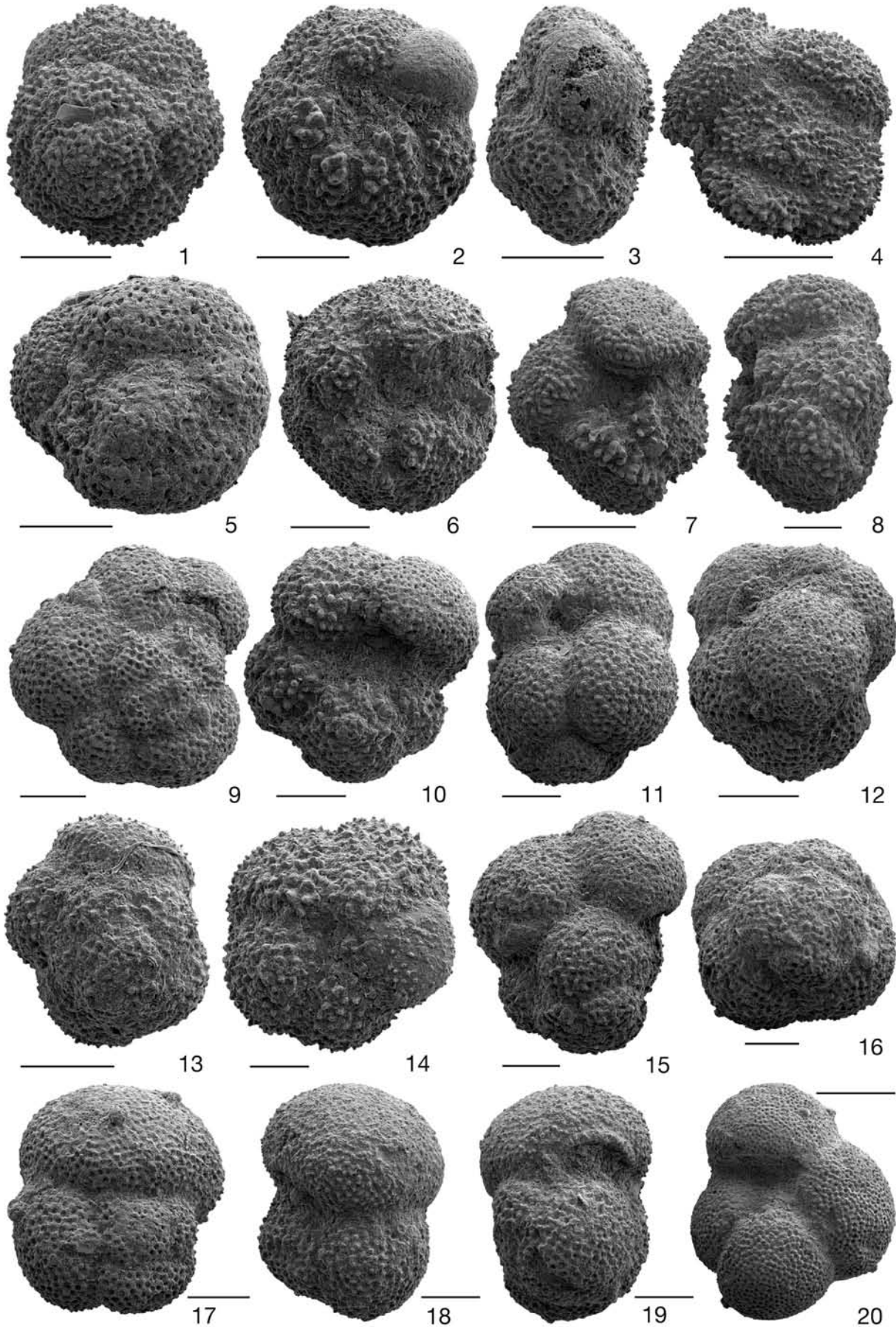
**Figure A2.4 ►**

1–3 *Morozovelloides crassatus* (Cushman). Section Holzhäusl-2, sample Rö 10-91.  
 4–7 *Morozovelloides coronatus* (Blow). Section Holzhäusl-2, sample Rö 10-91.  
 8–9 *Morozovella crater* (Hornibrook). Section Holzhäusl-2, sample Rö 10-91.  
 10, 14 *Morozovella aragonensis* (Nuttall). Section Holzhäusl-2, samples Rö 17-91 and Egger N2/09.  
 11 *Chiloguembelina ototara* (Finlay). Section Holzhäusl-2, sample Rö 10-91.  
 12–13 *Morozovella caucasica* (Glaessner). Section Holzhäusl-2, sample Rö 10-91.  
 15 *Jenkinsina triseriata* (Terquem). Section Holzhäusl-2, sample Rö 10-91.  
 16 *Morozovella caucasica* (Glaessner). Mattsee, centre, sample Gohrbandt 64/1-130.  
 17 *Planoglobanomalina pseudoalgeriana* Olsson & Hemleben. Section Holzhäusl-2, sample Egger N4/09.  
 18–19 *Pseudohastigerina wilcoxensis* (Cushman & Ponton). Section Holzhäusl-1, sample Egger 3b/04

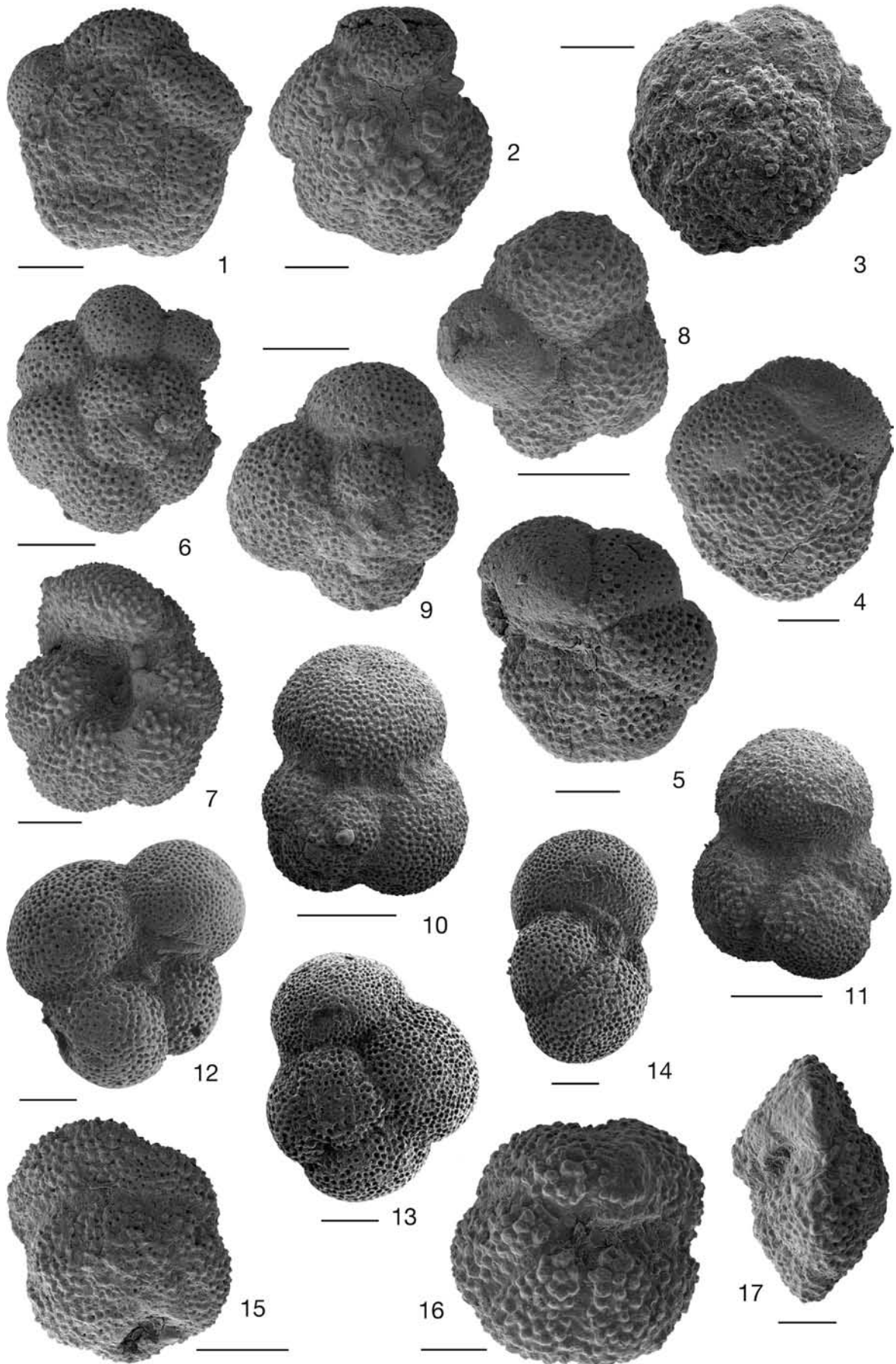
scale bar: figs 1–10, 12–13, 16 = 200 µm; figs 14, 17–19 = 100 µm; figs 11, 15 = 50 µm



1-10, 12-13, 16 = 200  $\mu\text{m}$  11,15 = 50  $\mu\text{m}$  14, 17-19 = 100  $\mu\text{m}$



1-3, 5-6,8-19 = 100  $\mu$ m 4,7,20 = 200  $\mu$ m



10-11 = 200  $\mu$ m 1-2,6-9,12-15 = 100  $\mu$ m 3-5,16-17 = 50  $\mu$ m

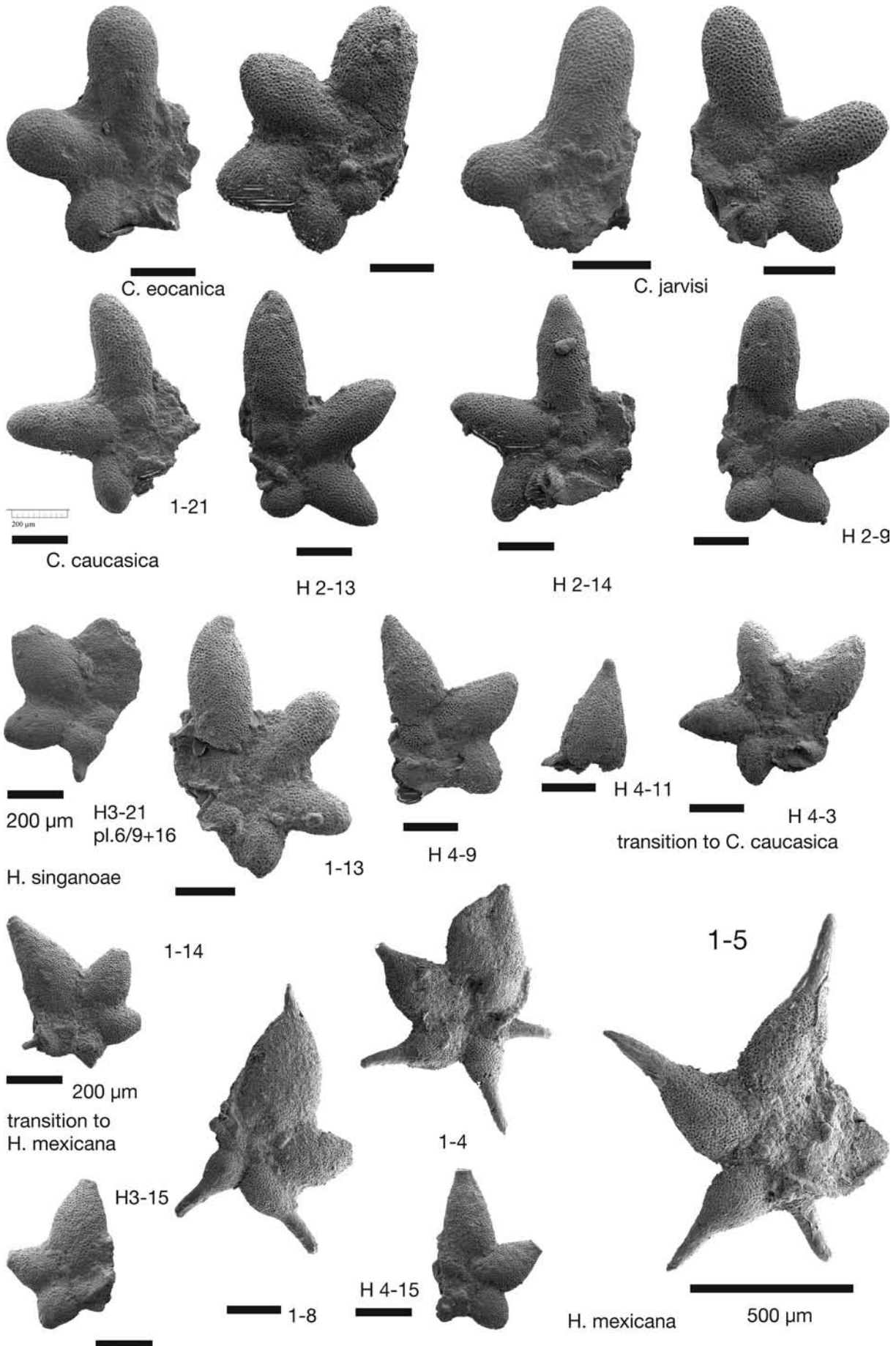


**Figure A2.5 (Page 52)**

- 1–3, 5–6 *Igorina broedermanni* (Cushman & Bermudez). Figs 1, 3 section Holzhäusl-2, sample Rö 10-91, figs 3, 5-6 section Holzhäusl-1, sample Egger 3b/04.
- 7–8 *Acarinina bullbrooki* (Bolli). Section Holzhäusl-2, sample Rö 10-91.
- 9–10 *Acarinina pentacamerata* (Subbotina). Section Holzhäusl-1, sample Egger 3b/04.
- 11–12, 15–16 *Guembeltrioides nuttalli* (Hamilton). Figs 11, 15-16 section Holzhäusl-1, sample Rö 1-98; fig. 12 section Holzhäusl-2, sample Rö 17-91.
- 13–14 *Acarinina collectea* (Finlay). Section Holzhäusl-1, sample Egger 3b/04.
- 17–19 *Turborotalia frontosa* (Subbotina). Section Holzhäusl-1, sample Egger 3b/04.
- 20 *Subbotina* cf. *eocaena* (Guembel). Section Holzhäusl-1, sample Egger 2b/04.

scale bar: figs 1–3, 5–6, 8–19 = 100 µm; figs 4, 7, 20 = 200 µm

**Figure A2.6 (Page 53)**

- 1–2 *Acarinina cuneicamerata* Blow. Mattsee, centre, sample Gohrbandt 64/1-130.
- 3–5 *Planorotalites capdevilensis* (Cushman & Bermudez). Fig. 3 section Holzhäusl-1, sample Egger 3b/04; figs 4-5 sample Gohrbandt 64/1-130.
- 6–7 *Acarinina aspensis* (Colom). Section Holzhäusl-2, fig. 6 sample Egger N2/09, fig. 7 sample Rö 10-91.
- 8–9 *Globorotaloides quadricameratus* Olsson, Pearson & Huber. Section Holzhäusl-2, sample Rö 10-91.
- 10–11 *Subbotina eocaena* (Guembel). Section Holzhäusl-1, sample Egger 2b/04.
- 12–14 *Parasubbotina hagni* (Gohrbandt). Section Holzhäusl-1, sample Gohrbandt 64/1-36-4a.
- 15–17 *Igorina salisburgensis* (Gohrbandt). Hochberg S of St. Pankraz, sample Gohrbandt 63/2-184-1.

scale bar: figs 10–11 = 200 µm; 1–2, 6–9, 12–15 = 100 µm; 3–5, 16–17 = 50 µm

**Figure A2.7 ◀**

- 1–2 *Clavigerinella eocanica* (Nuttall). Fig. 1 sample Gohrbandt 36/1, fig. 2 sample Egger A3/08.
- 3–4, 8 *Clavigerinella jarvisi* (Cushman). Fig. 3 sample Gohrbandt 36/0, figs 4,8 Egger B2/08.
- 5–7 *Clavigerinella caucasica* (Subbotina). Fig. 5 sample Egger B4/08, figs 6-7 sample Egger B2/08.
- 9–12 *Hantkenina gohrbandti* Rögl & Egger (in press). Figs 9, 11 sample Egger A2h, fig. 10 sample Gohrbandt 36/4b.
- 13 *Hantkenina mexicana* Cushman forma *nuttalli* Toumarkine. Sample Egger A1/08.
- 14 *Hantkenina mexicana* Cushman. Sample Rö 2-98.
- 15 *Hantkenina singanoae* Pearson & Coxall. Sample Egger B3/08.

All specimens from section Holzhäusl-1.

scale bar: figs 1–13, 15 = 200 µm; fig. 14 = 500 µm

About 90% of the foraminifera assemblage consist of planktonic species. Planktonic foraminiferal Zone E8 is indicated by the occurrences of *Guembeltrioides nuttalli* and *Globigerinatheka subconglobata*. Other stratigraphically important species are *Clavigerinella caucasica*, *Clavigerinella eocanica*, *Clavigerinella jarvisi*, *Hantkenina gohrbandti*, *Hantkenina mexicana*, and *Hantkenina singanoae* (Figs.A2.4–7). The evolutionary transition between *Clavigerinella* and *Hantkenina* was documented in this outcrop (Rögl & Egger, 2010). Remarkably, from the morozovellid assemblage only *Morozovella aragonensis* was found in small numbers.

Three samples were processed for palynology at Utrecht University following standard procedures of the Laboratory of Palaeobotany and Palynology (see, e.g., (Sluijs, Brinkhuis et al. 2003). Biostratigraphically important taxa include *Areosphaeridium diktyoplokum*, *Homotryblium floripes*, *Apectodinium homomorphum*, *A. hyperacanthum*, *Cordosphaeridium cantharellus* and *Wilsonidinium echinosuturatum*. The Wetzeliellid genera such as *Apectodinium* (Fig.A2.8/B) and *Wilsonidinium* (Fig.A2.8/J) places the section in the Eocene. The best calibrated dinocyst species is *Areosphaeridium diktyoplokum* (Plate 1, A; First Occurrence (FO) at 50.2 Ma in Northern mid-latitudes (Stover and Williams 1995; Williams, Brinkhuis et al. 2004)), which occurs throughout the section. That makes the maximum age for the section upper Ypresian. The consistent presence of *Homotryblium floripes* (Fig.A2.8/E) in all samples may indicate an age younger than 48 Ma, although the FO of this species is poorly calibrated, and may range slightly older in the Tethys Ocean. The FO of *Wilsonidinium echinosuturatum* (Fig.A2.8/J) is of

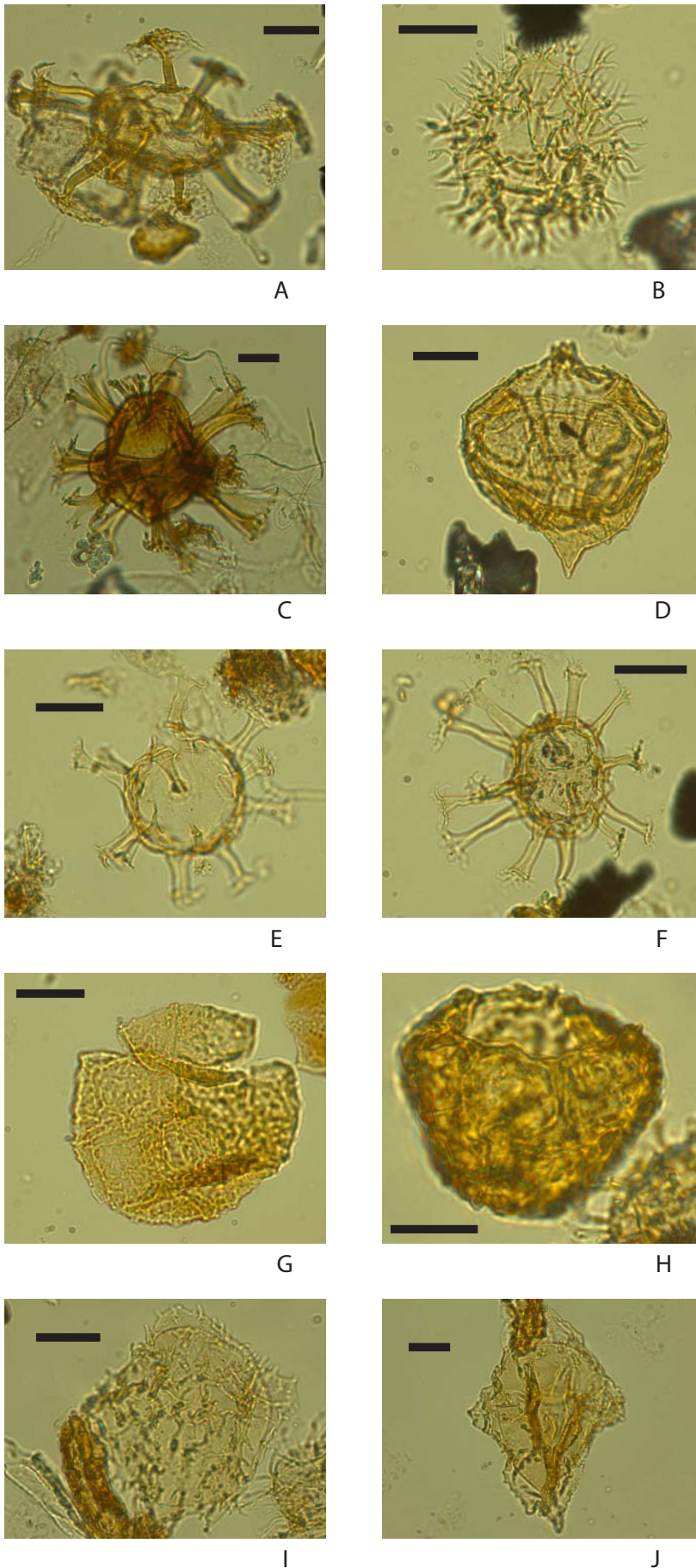


**Figure A2.8** ◀

A selection of (stratigraphically) important dinocyst species from the Holzhäusl sections.

Scale is 20µm

- A: *Areosphaeridium diktyoplokum*.
- B: *Apectodinium homomorphum*.
- C: *Cordosphaeridium cantharellus*.
- D: *Damassadinium* sp.
- E: *Homotryblium floripes* cpx.
- F: *Oligosphaeridium* sp.
- G: *Schematophora* cf. *obscura*.
- H: *Schematophora* cf. *obscura*.
- I: *Wetzeliella articulata*.
- J: *Wilsonidinium echinosutratum*

early Lutetian age in the Southwest Pacific Ocean (Brinkhuis, Sengers et al. 2003). *W. echinosuturatum* as well as *Cordosphaeridium cantharellus* (Fig. A2.8/C) have first occurrences within NP15 (magneto-chron C20r) in southwestern Siberia (Iakovleva and Heilmann-Clausen 2010), but these records are correlated from far outside the Tethys Ocean. In Northwestern Europe, *C. cantharellus* is found to have a first occurrence at around 40.1 Ma (Bujak, Downie et al. 1980), much younger than other sections. The LO of *Apectodinium* spp. was correlated to the Ypresian-Lutetian Boundary in the Southern Ocean (Brinkhuis, Sengers et al. 2003) and southwestern Siberia (Iakovleva and Heilmann-Clausen 2010), but no well-calibrated last occurrences are reported of *Apectodinium* from Tethyan successions, so it may very well be that the subtropical-tropical taxon *Apectodinium* spp. ranges much higher into the Lutetian in the likely warm Tethyan Ocean. The combined dinocyst events would thus tentatively place the entire section within the early Lutetian. One surprising finding is the common occurrence of a species closely resembling the early Eocene *Schematophora obscura* (Fig. 7, G, H) described from the Southern Ocean (Wilson 1988). There, this species has a short range in magnetochron C24n. Furthermore it has, to our recollection, not been recognized outside of the Southern Ocean thus far.

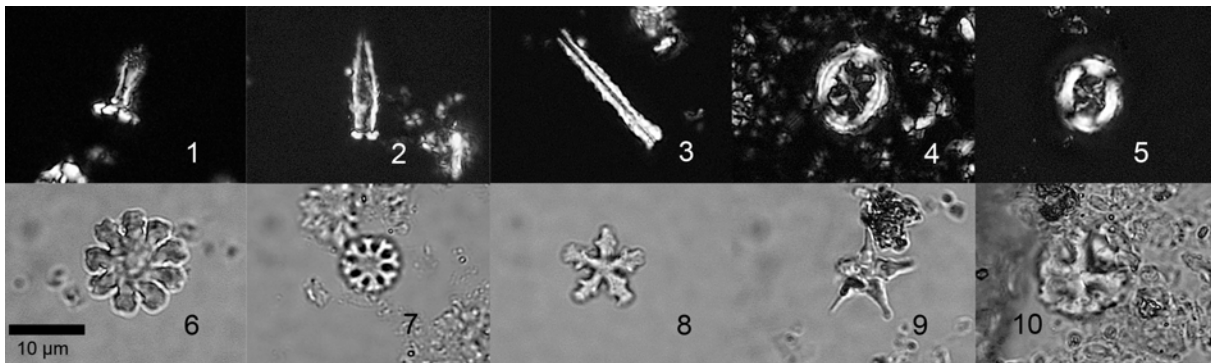


**Figure A2.9 ▲**

Selected calcareous nannoplankton from Holzhäusl outcrop 2

**1** *Blackites gladius*; **2** *Blackites inflatus*; **3** *Blackites stilus*; **4** *Chiasmolithus grandis*; **5** *Chiasmolithus solitus*; **6** *Discoaster deflandrei*; **7** *Discoaster nonaradiatus*; **8** *Discoaster tani nodifer*; **9** *Discoaster sublodoensis*; **10** *Nannotetrina cristata*.

## Outcrop 2

The nannoplankton assemblages, which are dominated by *Reticulofenestra dictyoda*, *R. scrippsae*, *Coccolithus pelagicus*, and *Zygrhablithus bijugatus*, are diverse and show moderate preservation. Re-working of Cretaceous nannoplankton specimens is less than 1%. Stratigraphically important species (Fig. A2.9) are *Blackites inflatus*, *B. gladius*, *Chiasmolithus solitus*, *C. grandis*, *Discoaster sublodoensis*, *Nannotetrina cristata* and *Sphenolithus spiniger*. This assemblage indicates the upper part of Sub-Zone NP14b. Interesting rare species are *Discoaster nonaradiatus* and *D. tani nodifer*.

The marlstone of outcrop 2 contains a rich planktonic fauna and a characteristic benthic deep-water assemblage. Stratigraphically important species are predominantly morozovellids with *Morozovella aragonensis* (E5-E9), *M. crater* (E4-E9), *M. caucasica* (E6-E8), *Morozovelloides bandyi* (E7-E10), *Ms. coronatus* (E8-E12), *Ms. crassatus* (E8-E13). The genus *Morozovelloides* is not as well developed as in Trinidad or in deep-sea drilling cores, tests are more blunt. Other important species are *Parasubbotina inaequispira* (E1-E8), *Turborotalia frontosa* (E7-E11), and in rare numbers *Pseudoglobanomalina pseudoalgeriana* (E6-E8). In the samples continuously *T. frontosa* is present, only in the uppermost part of the section *G. nuttalli* occurs but the occurrences of *Morozovelloides coronatus* and *Ms. crassatus* suggest an assignment to planktonic foraminiferal Zone E8. In contrast to outcrop 1, where only rare specimens of *Morozovella aragonensis* occur, specimens of *Morozovella* and *Morozovelloides* are common in all samples of outcrop 2.

The presence of *Oligosphaeridium* spp. (Fig. A2.8/F) in the dinoflagellate assemblage of this outcrop makes those samples older than 48.0 Ma when correlated to Northwestern European sections (Bujak and Mudge 1994; Williams, Brinkhuis et al. 2004). This species and *Wetzeliella articulata* were not found in the samples of outcrop 1. *Apectodinium homomorphum*, *Areosphaeridium diktyoplokum* and *Schematophora* cf. *obscura* occur in both outcrops.



## Stop A2/2

### SIEGSDORF MUSEUM (Lunch)

The museum of the small Bavarian town Siegsdorf ([www.museum-siegsdorf.de](http://www.museum-siegsdorf.de)) was founded in 1995 to document geological and paleontological features of southeastern Bavaria. Nowadays, the museum has about 50,000 visitors per year. The main trigger for the establishment of the museum was the finding of one of the best preserved mammoth skeletons in Central Europe in 1985. Together with the mammoth bones, the skeleton of a cave lion was found. These main attractions are now on display in the second floor of the museum together with other Pleistocene and Holocene items. On the first floor a fine selection of Lutetian fossils from the Adelholzen Formation is shown. Most of these specimens were collected during the construction of a new car park beside the Adelholzen mineral water plant (see Stop 4). Among the more spectacular pieces of this collection are shark vertebrae and a number of crabs (Fig. A2.11)



**Figure A2.10 ▲**  
Shark vertebrae from the upper part of the Adelholzen beds (Lutetian)



**Figure A2.11 ▲**  
Crab from the upper part of the Adelholzen beds (Lutetian)



## TYPE LOCALITY OF THE ADELHOLZEN BEDS (PRIMUSQUELLE BOTTLING PLANT) AN EOCENE (LUTETIAN, PRIABONIAN) DEEPENING SEQUENCE

Holger Gebhardt, Robert Darga, Stjepan Ćorić, Antonino Briguglio, Elza Yordanova, Bettina Schenk, Erik Wolfgring, Winfried Werner, Niels Andersen

### Topics:

Lithology, biostratigraphy (planktic foraminifera, calcareous nannoplankton, nummulitids), stable isotope stratigraphy, changing paleoenvironments, paleoproductivity.

### Tectonic unit:

North Helvetic Unit.

### Lithostratigraphic units:

Adelholzener Schichten (Adelholzen Beds), Stockletten.

### Chronostratigraphic units:

Lutetian, Priabonian

### Biostratigraphic units:

Planktonic foraminiferal zones P10-P115/16 (E8-E14/15), calcareous nannofossil zones NP15a-NP20 (CP13-CP15b), shallow benthic foraminifera zones SBZ 13-15.

### Location:

Primusquelle bottling plant southwest of Adelholzen, Siegsdorf, Bavaria.

### 1. Introduction

The section at Adelholzen is situated at the southwestern tip of the “Adelholzener Mineralwasser” bottling plant (Primusquelle, Fig.A2.12). The outcrop became accessible after excavations for the new plant. The steep slopes became overgrown and will be completely covered with grass and bushes in the near future. In 1996, the complete section was sampled with high resolution (20 cm-intervals).

Figure A2.13 shows the upper portion of the exposed rocks. The section covers the entire Lutetian and large parts of the Priabonian. It is

part of the Helvetic (tectonic) Unit and represents the sedimentary processes that took place on the southern shelf to upper bathyal of the European platform at that time. The nummulitic marls and sand

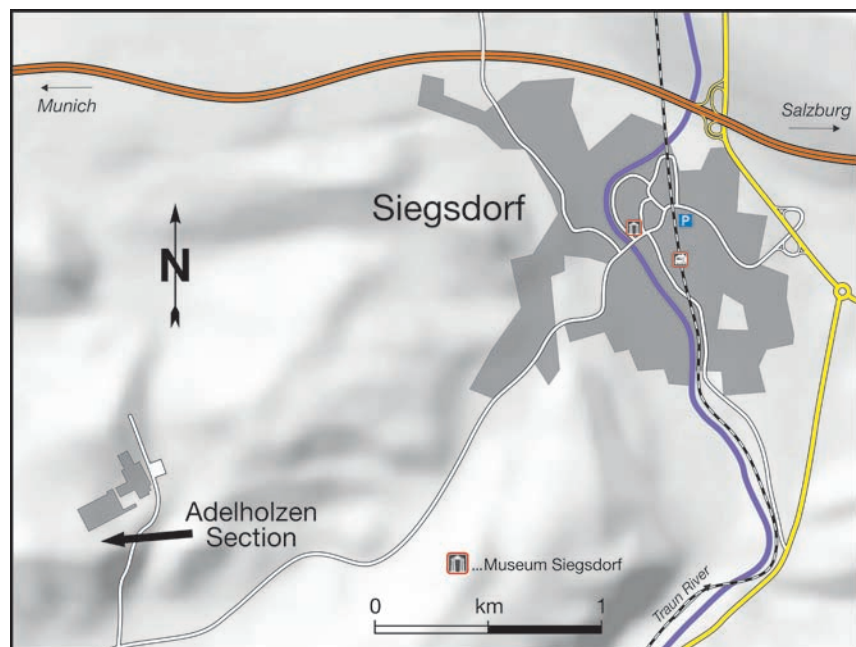


**Figure A2.12 ▲**  
Outcrop of Adelholzener Schichten



**Figure A2.13 ▲**

Outcrop of Adelholzener Schichten and Stockletten ("Globigerina"-Marls) behind the new bottling plant

of the area around Siegsdorf are famous for their high numbers of very large sized *Nummulites* and *Assilina*. Also in the Adelholzen Section, large specimens of these genera can be found in high numbers (Fig. A2.14).

## 2. Lithology

Six lithologic units occur in the Adelholzen-Section (Fig. A2.15). These lithologic units are, from base to top, 1) marly, glauconitic sands with predominantly *Assilina* (thickness exposed c. 4 m), 2) marly bioclastic sands with predominantly *Nummulites* (c. 4.5 m), 3) glauconitic sands (c. 0.6 m), 4) marls with *Discocyclina* (c. 4.2 m), and 5) marly brown sand (c. 1.1 m). The brown color of the latter unit results from its high content of sub-mm sized iron-hydroxide nodules. These units were combined as "Adelholzener Schichten" (Hagn et al., 1981) with unit 1 as "Untere Adelholzener Schichten" (lower Adelholzen Beds), unit 2 as "Mittlere Adelholzener Schichten" (middle Adelholzen Beds), and units 3 to 5 as "Obere Adelholzener Schichten" (upper Adelholzen Beds). For the sixth unit, Stockletten, no formal name has been established so far and the traditional name is still in use. Lateral equivalents in the west are called "Globigerina-Marls" (Hagn et al., 1981). The local name Stockletten refers to the sticky character of this marls (Letten = claystones, marls). The total thickness of all units exposed is about 18 m.

## 3. Biostratigraphy

The Adelholzen-Section is rich in planktonic foraminifera. Reworked specimens from older deposits commonly occur, whereas many zonal markers were not found within the investigated samples; other potential index species show a rather sporadic occurrence instead of a continuous record. Consequently, our age model is based mainly on calcareous nannofossils and nummulitids and one zonal boundary only is based on planktic foraminifera. Contrary to foraminifera, the nannoplankton samples are characterized by low percentages of reworked taxa. Nummulitids form the base for the biostratigraphic classification of the lower and middle Adelholzen Beds (units 1 and 2). Lack of first and last occurrences, evidence of stratigraphic gaps, and reworked planktonic foraminifera specimens complicate



**Figure A2.14 ▲**  
Close up of the basal nummulitic (Assilina, Nummulites) marlstone.

the construction of a consistent biostratigraphic framework. As reported from other sections elsewhere, planktic foraminifera, calcareous nannoplankton and larger benthic zonation did not always correlate well with established zonal schemes.

### 3.1 Planktonic foraminifera

Planktonic foraminifera form up to 80% of the total foraminiferal assemblages in the Stockletten, but also the basal nummulitic marls contain about 20% of planktonic species (see below). We dry sieved the total washed residue over a 0.250 mm sieve in order to concentrate the stratigraphically important species. Based on the occurring species we were able to recognize the planktonic foraminiferal zones P10 to P12 (according to Berggren et al., 1995) or E8 to E11 (according to Berggren and Pearson, 2005), and zones P15/16 (or E14/15) as shown in Figure 4. All species identified from the >0.250 mm fractions are shown in Figures A2.16 and A2.17.

The almost permanent occurrence of *Guembelitroides nuttalli* (Fig. A2.16/21, 22) characterizes Zone P10 (or E8) up to the E10-E11 boundary (within P12). Its disappearance indicates this boundary. *Globigerinatheka kugleri* (Fig. A2.16/31, 32) appears somewhat earlier and indicates the base of Zone P11 (E9). *Globigerinatheka index* (Fig. A2.16/27, 28) occurs first within the *Discocyclina*-marls and continues until the topmost sample. Its first occurrence, together with the first occurrence of *Turborotalia pomeroli* Fig. A2.17/28–30) points to the transition from Zone P11 (E9) to P12 (E10). Presence of *G. index* in the topmost sample indicates an age older than P17 (E16) for this sample. First occurrences of *Turborotalia cerroazulensis* (Fig. A2.17/31–33) point to the upper portion of zone P12.

The nannoplankton assemblages clearly indicate a long stratigraphic gap of at least 3 Ma (NP 17 is completely missing) within the lower portion of the Stockletten (Fig. A2.15). Consequently, indicators for P13 and 14 (E12, 13) cannot be found. This assumption is supported by the almost complete disappearance of acariniids in the overlying strata, pointing to a strong change in paleoceanography. Presence of *Turborotalia increbescens* (Fig. A2.17/34–36), supported by a few *Subbotina gortanii* (Fig. A2.17/14) is indicative for an interval covering P15 to 16 (E14-15). One found specimen of *Orbulinoides beckmanni* (Fig. A2.16/18, indicative of P13/E12) in sample AH-132 has apparently been reworked from eroded sediments.

In addition to these index species, the distribution of other occurring species has been considered. This includes several species of *Globigerinatheka*, *Turborotalia*, *Acarinina*, and *Morozovelloides*. However, because of the relatively shallow paleo-water depths, occurrences of species are not always continuous with respect to their total ranges. Conspicuous are the lack of *Acarinina* in the middle and upper parts of the Stockletten, its replacement by *Globigerinatheka*, and the almost complete absence of *Hantkenina* in the entire section.

The basal layers, and, but to a much lesser extent, the overlying rock units, contain a considerable amount of displaced planktic individuals, in particular from Zone P9. Many of them are in a good state of preservation and cannot be distinguished by this attribute alone from the autochthonous assemblage. Particularly frequent are: *Acarinina pentacamerala*, *A. quetra*, *Morozovella aequa*, *M. lensiformis*, and *M. subbotinae*.

### 3.2 Calcareous nannofossils

All investigated sediments contain very rich and well preserved calcareous nannoplankton assemblages, dominated by small reticulofenestrads (Fig. A2.18/28b), normal sized reticulofenestrads (Fig. A2.18/25, 26), and *Cyclicargolithus floridanus* (Fig. A2.18/27). Calcareous nannoplankton reworked

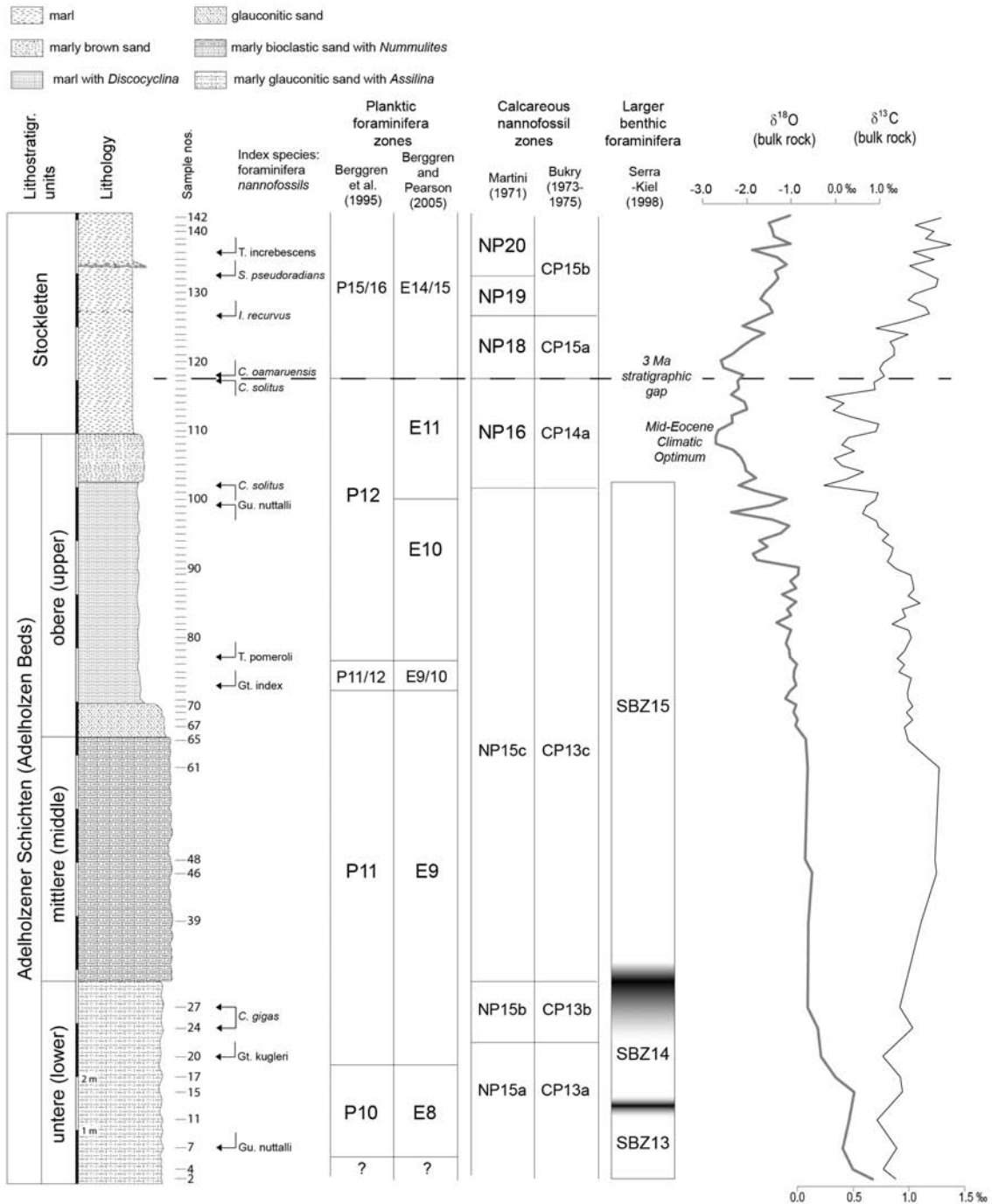
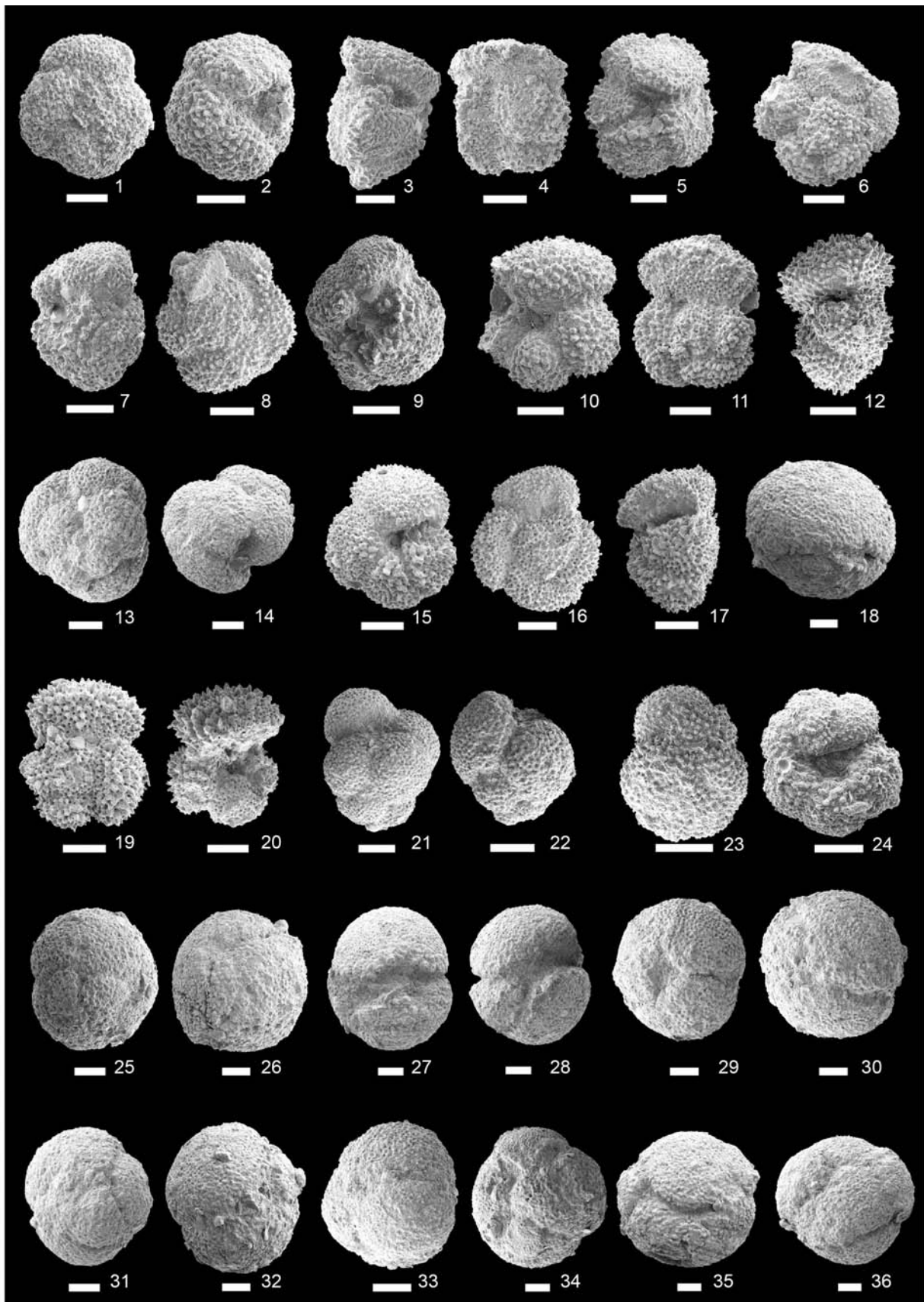


**Figure A2.15 ▲**  
Lithologic section of the section investigated, biostratigraphic zonation and δ<sup>13</sup>C-isotope curve.

**Figure A2.16 ►**  
Stratigraphically important planktic foraminiferal species from the >0.250 mm-fraction. **1, 2.** *Acarinina boudreauxi* (1 sample AH-95, 2 sample AH-99). **3–5.** *Acarinina bullbrooki* (sample AH-101). **6.** *Acarinina rohri* (sample AH-117). **7–9.** *Acarinina collactea* (7, 9 sample AH-97, 8 sample 101). **10–12.** *Acarinina praetopilensis* (10, 11 sample AH-101, 12 sample AH-115). **13, 14.** *Acarinina pseudosubphaerica* (sample AH-77). **15–17.** *Acarinina punctocarinata* (sample AH-116). **18.** *Orbulinoides beckmanni* (reworked specimen, sample AH-132). **19, 20.** *Acarinina topilensis* (sample AH-116). **21, 22.** *Guembelitroides nuttalli* (21 sample AH-77, 22 sample AH-99). **23, 24.** *Igorina broedermanni* (sample AH-95). **25, 26.** *Globigerinatheka euganea* (25 sample AH-133, 26 sample AH-132). **27, 28.** *Globigerinatheka index* (sample AH-129). **29, 30.** *Globigerinatheka korotkovi* (sample AH-129). **31, 32.** *Globigerinatheka kugleri* (sample AH-127). **33, 34.** *Globigerinatheka luterbacheri* (33 sample AH-139, 34 sample 133). **35, 36.** *Globigerinatheka subconglobata* (sample AH-129). Length of scale bars: 0.1 mm.

from older strata occurs with very low percentages. Nannoplankton zonation established by Martini (1971) and by Okada & Bukry (1980) were used for biostratigraphical subdivision of the section. Qualitative investigations on sediments allow us the subdivision of the section into five standard nanno-



plankton Zones (NP15-NP20) and three subzones (NP15a-c) as defined by Martini (1971), as well as three zones (CP13-CP15) with subzones (CP13a-c, and CP15a,b) as defined by Okada & Bukry (1980).

Sediments of the Adelholzen beds can be attributed to Nannoplankton Zone NP15 (*Nannotetrina fulgens* Zone) and the lower part of NP16. *Blackites inflatus*, its last occurrence (LO) marks the NP14/NP15 boundary, was not found in the sediments analysed. The zonal marker for NP15 *Nannotetrina fulgens* (Fig. A2.18/22) is present but very scarce, whereas *Blackites gladius* occurs continuously throughout this part of the section. Some additional zonal markers as *Lophodolichus rotundus* (Fig. A2.18/1) and *L. acutus* (Fig. A2.18/2) observed in this part of the section confirm this stratigraphic attribution. *Chiasmolithus gigas* (Fig. A2.18/43, 44) with its short stratigraphic range defines the limits of Nannoplankton Zone NP15b (CP13b) and was observed in samples AH-24 and AH-27. Thus, the marly glauconitic sand with *Assilina* ("Lower Adelholzen beds"), can be assigned to subzones NP15a (CP13a) and NP15b (CP13b). The "Middle Adelholzen beds" can be completely attributed to the lower part of NP15c (CP13c). The "Upper Adelholzen beds" belong stratigraphically to the upper NP15c (CP13c) and the lowermost part of *Discoaster tanii nodifer* Zone NP16. The NP15/NP16 boundary, defined by the LO of *Blackites gladius* (sample AH-102), can be placed within marly brown sand layer of the "Upper Adelholzen beds". The first occurrence (FO) of *Reticulofenestra umbilicus* (Fig. A2.18/23) defines the lower boundary of CP14a. Rare specimens of *R. umbilicus* were observed below the NP15/16 boundary. Continuous occurrences of this large reticulofenestrids were observed from above the CP13c/CP14a boundary.

The Stockletten comprises nannoplankton zones upper NP16, NP18, NP19 and NP20 (CP14b–CP15b). Zone NP17 (*Discoaster saipanensis* Zone) which is defined as the period between LO of *Chiasmolithus solitus* (Fig. A2.18/36) and FO of *Chiasmolithus oamurensis* (Fig. A2.18/45, 46) could not be documented in the Adelholzen section. The LO of *Chiasmolithus solitus* was observed in sample AH-117, whereas next sample AH-118 already contains *Chiasmolithus oamaruensis*. This long sedimentation gap within the lower part of the Stockletten is placed between samples AH-117 and AH-118. The NP18/19 (CP15a/CP15b) boundary is marked by the first occurrence of the easily recognizable *Isthmolithus recurvus* (Fig. A2.18/10, 11). This form with its LO in the lower Oligocene continuously occurs from sample AH-127 throughout the upper part of the profile. Due to restricted occurrences of *S. pseudoradians* and taxonomic difficulties, the nannoplankton zones NP19 (*Isthmolithus recurvus* Zone) and NP20 (*Sphenolithus pseudoradians* Zone) usually cannot be distinguished. Nevertheless, the FO of *S. pseudoradians* was observed in sample AH-135 and therefore the NP19/NP20 boundary was tentatively placed below this sample within the uppermost portion of the Stockletten.

### 3.3. Nummulitids

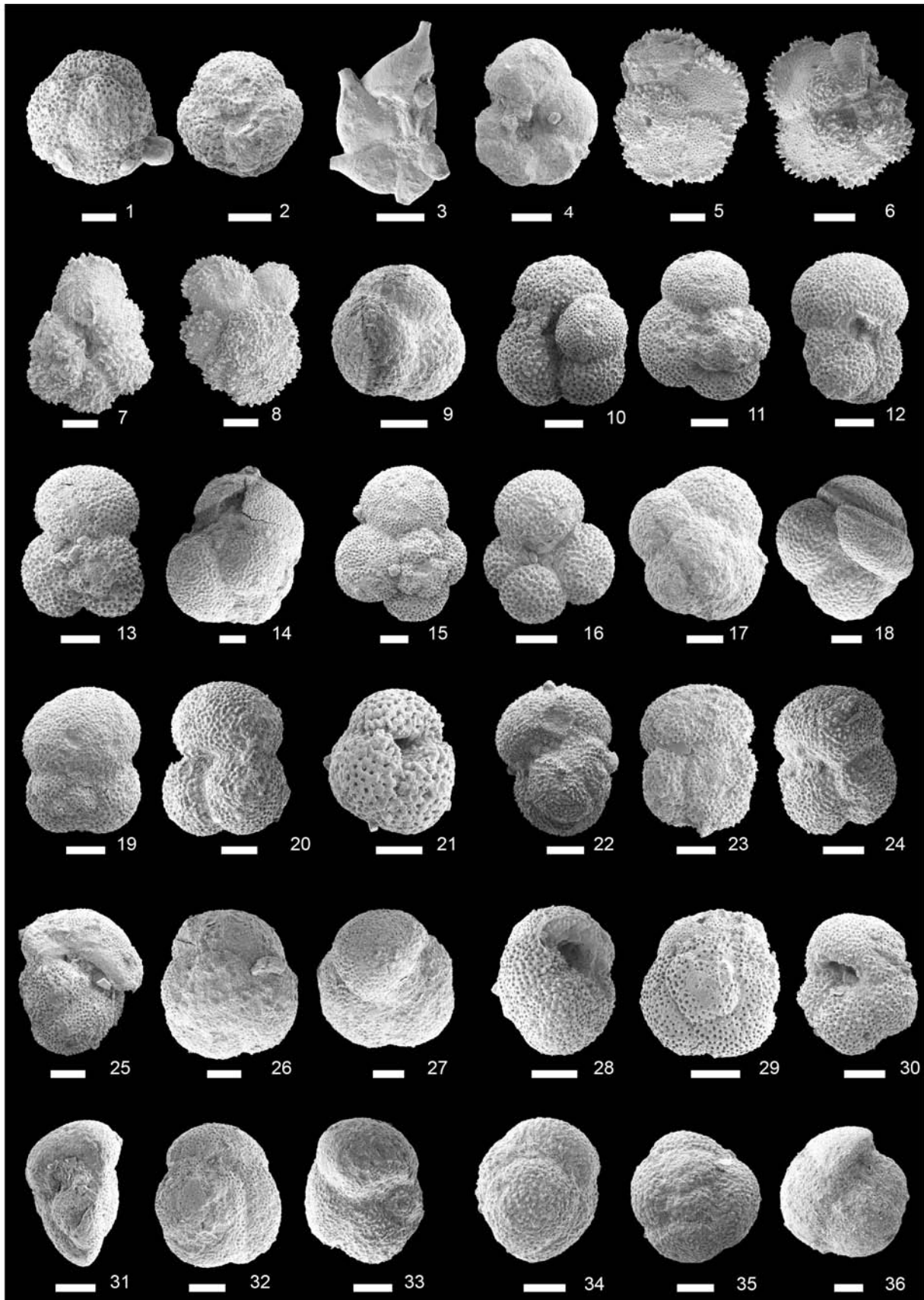
The lower part of the presented profile is rich in Larger Benthic Foraminifera (LBF). The abundant fauna is mainly composed by the genera *Assilina*, *Nummulites* and *Discocyclina* (Fig. A2.19). Taxa belonging to the lineage of *Assilina exponens*, the most abundant within the sediment, allow the biostratigraphic determination of the shallow benthic zones (SBZ) from SBZ 13 to SBZ 15 (*sensu* Serra-Kiel et al., 1998) along the profile.

The limits between these Opperl-zones have been observed by biometric determination of the investigated taxa. Specimens of *Assilina tenuimarginata*, abundant in both A and B forms in the lowest part of the profile indicate lowermost Lutetian with probably some reworked specimens (*A. cuvillieri*) from the uppermost SBZ12 (uppermost Ypresian). *A. tenuimarginata* is further above replaced by *A. ex-*

#### Figure A2.17 ►

Stratigraphically important planktic foraminiferal species from the >0.250 mm-fraction (continuation). **1, 2.** *Catapsydrax unicavus* (sample AH-75). **3.** *Hantkenina liebusi* (sample AH-93). **4.** *Pseudohastigerina wilcoxensis* (sample AH-101). **5, 6.** *Morozovelloides coronatus* (5 sample AH-77, 6 sample AH-101). **7, 8.** *Morozovelloides lehneri* (7 sample AH-79, 8 sample AH-89). **9.** *Subbotina angiporoides* (sample AH-139). **10, 11.** *Subbotina corpulenta* (sample AH-101). **12.** *Subbotina cruciapertura* (sample AH-97). **13.** *Subbotina eocaena* (sample AH-115). **14.** *Subbotina gortanii* (sample AH-142). **15, 16.** *Subbotina hagni* (15 sample AH-115, 16 sample AH-116). **17, 18.** *Subbotina jacksonensis* (17 sample AH-141, 18 sample AH-137). **19, 20.** *Subbotina linaperta* (19 sample AH-139, 20 sample AH-101). **21.** *Subbotina senni* (sample AH-2). **22–24.** *Turborotalia frontosa* (22, 24 sample AH-97, 23 sample AH-101). **25–27.** *Turborotalia possagnoensis* (25 sample AH-113, 26, 27 sample AH-129). **28–30.** *Turborotalia pomeroli* (sample AH-116). **31–33.** *Turborotalia cerroazulensis* (sample AH-135). **34–36.** *Turborotalia increbescens* (34, 35 sample AH-139, 36 sample AH-137). Length of scale bars: 0.1 mm.

*ponens*, which remains abundant within the sediments of all the lower part of the presented profile and indicates middle to late Lutetian and Bartonian age (SBZ 14-17). With the samples AH24 and 27 some larger specimens belonging to *A. exponens* have been found. They are up to 15 mm large in diameter for



8 or 9 whorls in A forms; no B forms have been found. Multispiral growth is evident as well as opposite growth direction.

Specimens belonging to the genus *Nummulites* are lower in abundance along the profile. All the investigated specimens belong to the phylum of *N. distans - millecaput* (*sensu* Schaub, 1981). In the lower part of the profile (samples 4–17) *N. cf. kaufmanni* and *N. alponensis* are present. The proloculus diameter, very small in size, measured on the investigated specimens is a clear indication for the species preceding *N. millecaput* and later on *N. maximus*. In fact, *N. millecaput* starts to be present from sample 24 and later became abundant indicating SBZ 15 (upper, but not uppermost, Lutetian). The species *N. millecaput* is present as A and B forms until the sample 61, which is the last sample where LBF have been investigated. The largest B forms belonging to *N. millecaput* are 6 cm in diameters for more than 45 whorls. Other specimens have a radius of 20–24 mm for 34–42 whorls. Specimens from the last nummulitid-bearing sample (101, top *Discocyclina*-marls) are not younger than SBZ 15.

Bioturbation (microborings?) occurred abundantly and mainly on discocyclinids. More than 50 specimens have been sectioned on the equatorial plane revealing a completely bioturbated embryonic apparatus. Therefore a consistent taxonomy on such forms has not been provided.

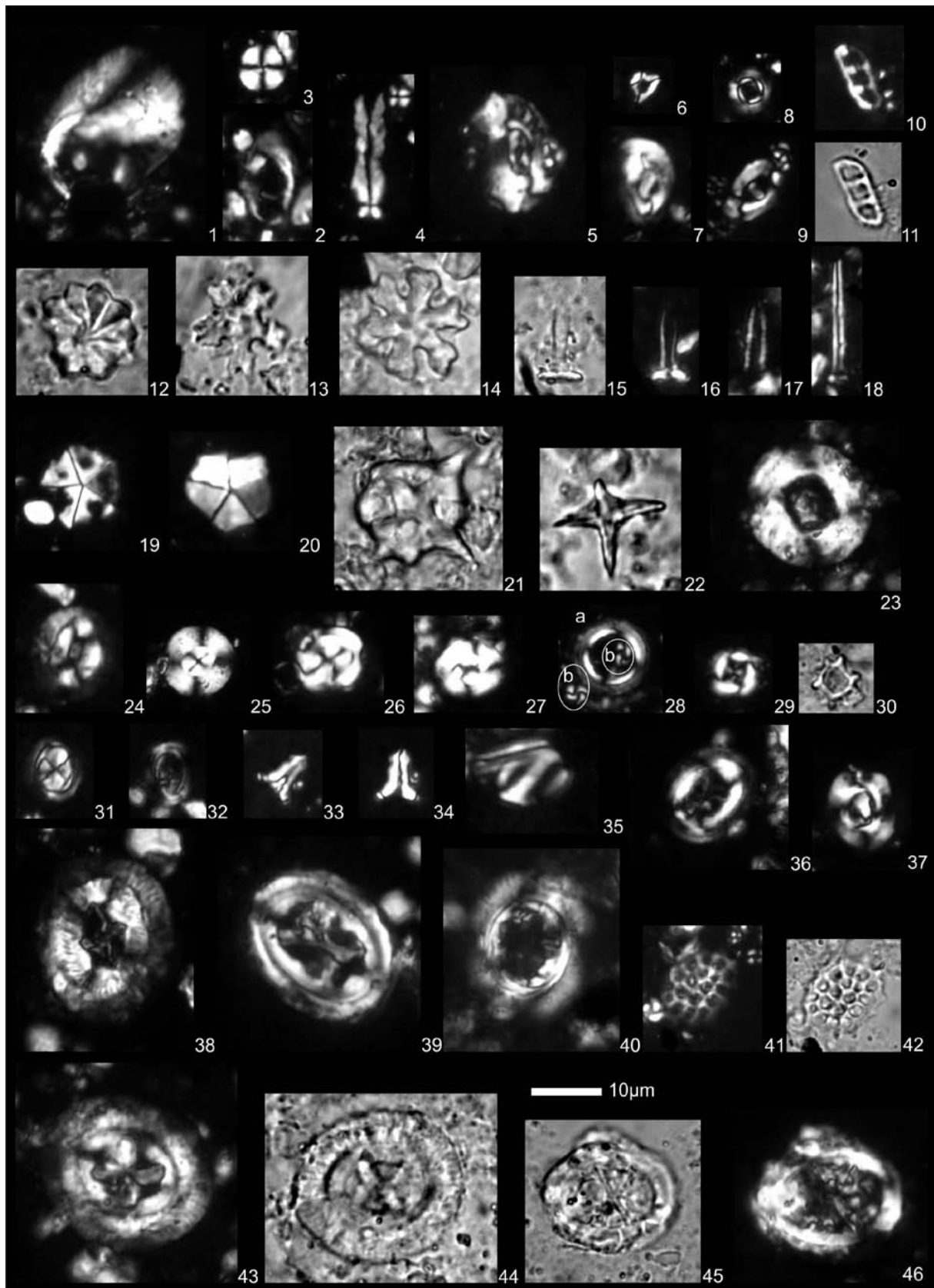
#### 4. Stable O and C-isotope stratigraphy, age model and sedimentation record

In order to refine the stratigraphic resolution of the Adelholzen Section, we measured bulk rock stable isotope ratios ( $\delta^{13}\text{C}$ ,  $\delta^{18}\text{O}$ ). The resulting curves are shown in Figure A2.15. We then subdivided the  $\delta^{13}\text{C}$ - and  $\delta^{18}\text{O}$  curves into five subsequences according to the nannoplankton and planktic foraminiferal zones and correlated these units with characteristic curve patterns of a global stack published in Hancock & Dickens (2005). The zonal boundaries used are P11/P12, E10/E11, NP16/NP18, and NP19/NP20. Despite the prominent (at least) 3 Ma years long stratigraphic gap represented by the completely missing nannoplankton zone NP17 within the lower Stockletten, another stratigraphic gap of c. 0.4 Ma within the upper zone P11 (i.e., within the glauconitic sands, base of “obere Adelholzener Schichten”) appears plausible as additional peaks show up in the  $\delta^{13}\text{C}$  reference record.

##### Figure A2.18 ►

Stratigraphically important calcareous nanofossils. **1.** *Lophodolichus rotundus* Bukry & Percival, 1971; Sample AH-2; NP15a. **2.** *Lophodolichus acutus* Bukry & Percival, 1971; Sample AH-2; NP15a. **3.** *Cyclicargolithus luminis* (Sullivan, 1965) Bukry, 1971; Sample AH-2; NP15a. **4.** *Sphenolithus furcatolithoides* Locker, 1967; Sample AH-7; NP15a. **5.** *Helicosphaera lophota* Bramlette & Sullivan, 1961; Sample AH-27; NP15b. **6.** *Lanternithus minutus* Stradner, 1962; Sample AH-140; NP20. **7.** *Helicosphaera bramlettei* Müller, 1970; Sample AH-108; NP16. **8.** *Calcidiscus? protoannulus* (Gartner, 1971) Loeblich & Tappan, 1978; Sample AH-80; NP15c. **9.** *Helicosphaera seminulum* Bramlette & Sullivan, 1961; Sample AH-2; NP15a. **10, 11.** *Isthmolithus recurvus* Deflandre, 1954; Sample AH-130; NP19. **12.** *Discoaster barbadiensis* Tan, 1927; Sample AH-2; NP15a. **13.** *Discoaster distinctus* Martini, 1958; Sample AH-108; NP16. **14.** *Discoaster deflandrei* Bramlette & Riedel, 1954; Sample AH-27; NP15b. **15, 16.** *Blackites gladius* (Locker, 1967) Varol, 1989; Sample AH-7; NP15a. **17.** *Blackites virgatus* Bown, 2005; Sample AH-27; NP15b. **18.** *Blackites spinosus* (Deflandre & Fert, 1954) Hay & Towe, 1962; Sample AH-108; NP16. **19.** *Pemma basquensis* (Martini, 1959) Báldi-Beke, 1971; Sample AH-80; NP15c. **20.** *Braarudosphaera bigelowii* (Gran & Braarud, 1935) Deflandre, 1947; Sample AH-117; NP16. **21.** *Nannotetrina cristata* (Martini, 1958) Perch-Nielsen, 1971; Sample AH-77; NP15c. **22.** *Nannotetrina fulgens* (Stradner, 1960) Achuthan & Stradner, 1969; Sample AH-27; NP15b. **23.** *Reticulofenestra umbilicus* (Levin, 1965) Martini & Ritzkowski, 1968; Sample AH-108; NP16. **24.** *Coccolithus cachaoui* Bown, 2005; Sample AH-27; NP15b. **25.** *Reticulofenestra bisecta* (Hay, Mohler & Wade, 1966) Roth, 1970; Sample AH-135; NP20. **26.** *Reticulofenestra scrippsae* (Bukry & Percival, 1971) Roth, 1973; Sample AH-135; NP20. **27.** *Cyclicargolithus floridanus* (Roth & Hay, 1967) Bukry, 1971; Sample AH-80; NP15c. **28.** a) *Coronocyclus bramlettei* (Hay & Towe, 1962) Bown, 2005; b) *Reticulofenestra minuta* Roth, 1970; Sample AH-115; NP16. **29.** *Criboecentrum reticulatum* (Gartner & Smith, 1967) Perch-Nielsen, 1971; Sample-AH 110; NP16. **30.** *Corannulus germanicus* Stradner, 1962; Sample AH-108; NP16. **31.** *Clausiococcus fenestratus* (Deflandre & Fert, 1954) Prins, 1979; Sample AH-75; NP15c. **32.** *Campylosphaera dela* (Bramlette & Sullivan, 1961) Hay & Mohler, 1967; Sample-AH 90; NP15. **33, 34.** *Zygrhablithus bijugatus* (Deflandre, 1954) Deflandre, 1959; Sample AH-80; NP15c. **35.** *Pontosphaera exilis* (Bramlette & Sullivan, 1961) Romein, 1979; Sample AH-27; NP15b. **36.** *Chiasmolithus solitus* (Bramlette & Sullivan, 1961) Locker, 1968; Sample AH-117; NP16. **37.** *Reticulofenestra dictyoda* (Deflandre, 1954) Stradner, 1968; Sample AH-140; NP20. **38.** *Coccolithus mutatus* (Perch-Nielsen, 1971) Bown, 2005; Sample AH-27; NP15b. **39.** *Chiasmolithus grandis* (Bramlette & Riedel, 1954) Radomski, 1968; Sample AH-27; NP15b. **40.** *Pontosphaera formosa* (Bukry & Bramlette, 1969) Romein, 1979; Sample AH-108; NP16. **41, 42.** *Clathrolithus ellipticus* Deflandre, 1954; Sample AH-110; NP16. **43, 44.** *Chiasmolithus gigas* (Bramlette & Sullivan, 1961) Radomski, 1968; Sample AH-27; NP15b. **45, 46.** *Chiasmolithus oamaruensis* (Deflandre, 1954) Hay, Mohler & Wade, 1966; Sample AH-140; NP20.

The correlation of the Adelholzen record to the reference curve suggests a largely complete and even sedimentation without larger stratigraphic gaps in addition to the gaps indicated above. This appears to be particularly valid for the "obere Adelholzener Schichten" and the Stockletten.



Both the  $\delta^{13}\text{C}$ - and  $\delta^{18}\text{O}$  curves show the characteristic peak successions of the reference curve. Consequently, we were able to identify prominent isotopic and climatic events such as the Middle Eocene Climatic Optimum (MECO), which is positioned within the marly brown sand (E11, NP16). However, diagenetic overprint lead to exceptional low  $\delta^{13}\text{C}$ -values, in particular in the marly nummulitic sands up to the basal Stockletten. Diagenetic overprint is even more prominent in the  $\delta^{18}\text{O}$ -curve. Values down to -3‰ during MECO are far beyond any temperature signal. However, peak positions correspond perfectly to those in the reference curve.

The overall sediment-accumulation rate was about 1.8 mm per 1000 years. However, sedimentation rates were much higher during deposition, in particular for the nummulitid-sands and *Discocyclina*-marls in the lower part of the Adelholzen Section.

## 5. Macrofossils

Despite the larger foraminifera *Nummulites* and *Assilina* in the lower and middle Adelholzen Beds, a number of other macro-faunal elements has been found at Adelholzen. The lower Adelholzen Beds contain articulated large oysters (*Pycnodonte gigantea*), spondylids with preserved spines, sea urchin remains, and occasionally internal molds of bivalves. The middle Adelholzen beds contain only a few serpulids grown on *Nummulites* and some sea urchin remains. In the three units of the upper Adelholzen Beds, various macrofossils were found. Glauconitic sands: free serpulids, oysters (*Pycnodonte* sp.), large but rare crabs; marls with *Discocyclina*:sea urchins (*Conoclypeus* sp.), spines of *Spondylus* sp., crabs with preserved limbs, free serpulids, and nodular bryozoan colonies; marly brown sand: crabs, partly with limb preservation, spondylids, shark teeth, rare amber, and lumachelles at the very top of this unit. The Stockletten are almost free of macrofossils, only at its base a few tiny bivalves can be found.

## 6. Changing water depths

The ratio of planktic to benthic foraminifera (P/B-ratio or percent planktic foraminifera) is proportional to water depth in modern oligotrophic open marine settings (e.g., van der Zwaan et al., 1990). It is considered to be a good estimator also for paleo-water depth estimations at least during the Cenozoic. The percentage of planktic foraminifera in the assemblages is displayed in Figure 9 together with rough absolute water depth estimates. Our absolute estimates are based on the P/B-ratio and range from 50 m (inner shelf) at the base of the section to a maximum of c. 600 m (upper bathyal) in the Stockletten. Nummulitids and macrofossil assemblages (oysters, spondylids, sea urchins, serpulids, crabs, bryozoans, shark teeth) however point to shallower paleo-water depths, in particular for the basal and middle lithologic units.

The P/B-ratio shows several distinct increases in paleo-water depth (transgressive phases). The corresponding lowstands (Lu2-4, Pr2) fit well with global sequence boundaries (Luterbacher et al., 2004).

## 7. Changing paleo-productivity

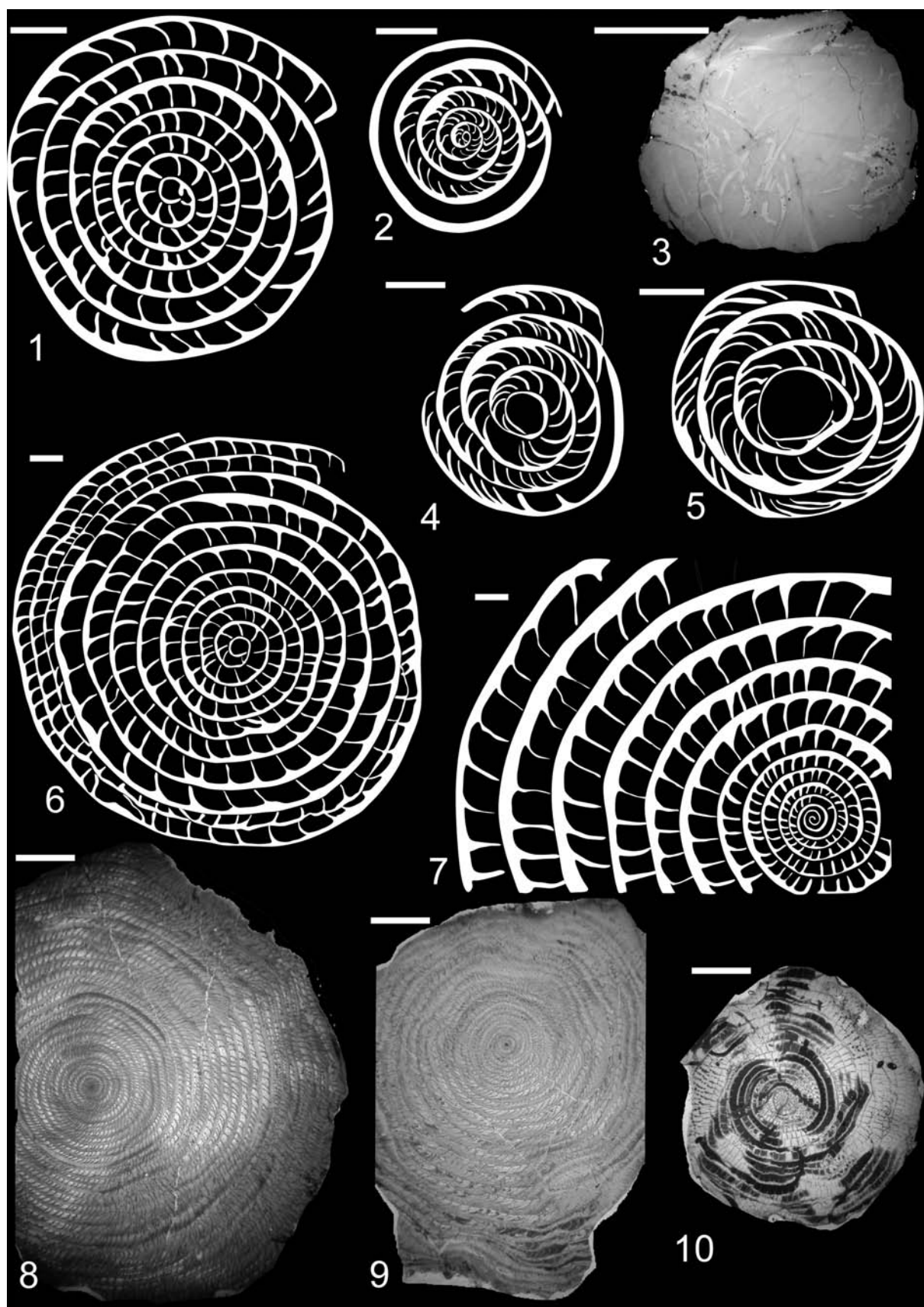
The number of heterotrophic planktic and benthic foraminifera is largely coupled to primary surface productivity as these groups either feed directly on diatoms, coccolithophores or other algae (planktic foraminifera, e.g., Hemleben et al, 1989) or depend on the organic rain that reaches the seafloor (benthic foraminifera, e.g., Gooday, 2003). Foraminiferal abundance is therefore a good estimator for paleo-productivity of ancient eco-systems. Figure 9 shows rather parallel curves for planktic and benthic foraminiferal abundance, pointing to at several transgressive phases that resulted in increased nutrient

### Figure A2.19 ►

Stratigraphically important nummulitids. 1. *Assilina cuvillieri*, A-form, scale bar; 1 mm (sample AH-2). 2. *Nummulites alponensis*, A-form, scale bar; 1 mm (sample AH-15). 3. *Discocyclina* sp. with bioturbation, scale bar; 10 mm (sample AH-11). 4. *Nummulites millecaput* A-form, scale bar; 1 mm (sample AH-27). 5. *Nummulites millecaput* A-form, scale bar; 1 mm (sample AH-61). 6. *Assilina exponens* (larger specimen), A-form, scale bar; 1 mm (sample AH-24). 7. *Assilina tenuimarginata*, B-form, scale bar; 1 mm (sample AH-7). 8. *Nummulites millecaput*, B-form, scale bar; 5 mm (sample AH-39). 9. *Nummulites millecaput*, B-form, scale bar; 5 mm (sample AH-65). 10. *Assilina exponens*, B-form, scale bar; 5 mm (sample AH-65).

mobilization and subsequent increased numbers of foraminifera. The highest foraminiferal abundance (planktic as well as benthic) was reached shortly after the MECO-event.

The benthic assemblages are dominated by rather large planoconvex or lenticular species (*Cibicid*



*doides*, *Planulina*, *Lenticulina* etc.). Dominance of these genera points to oxic conditions at the seafloor (Kaiho, 1999).

All samples from the section contain very rich calcareous nannoplankton with the dominance of small reticulofenestrads, *Reticulofenestra dictyoda* and *Cyclicargolithus floridanus*. Small reticulofenestrads generally dominate nannoplankton assemblages along continental margins. High amounts of *Reticulofenestra minuta* can be interpreted as indicator of a warm, well stratified water column. Low percentages of *Coccolithus pelagicus* point to oligotrophic paleoenvironments and are in good agreement with the foraminiferal interpretations.

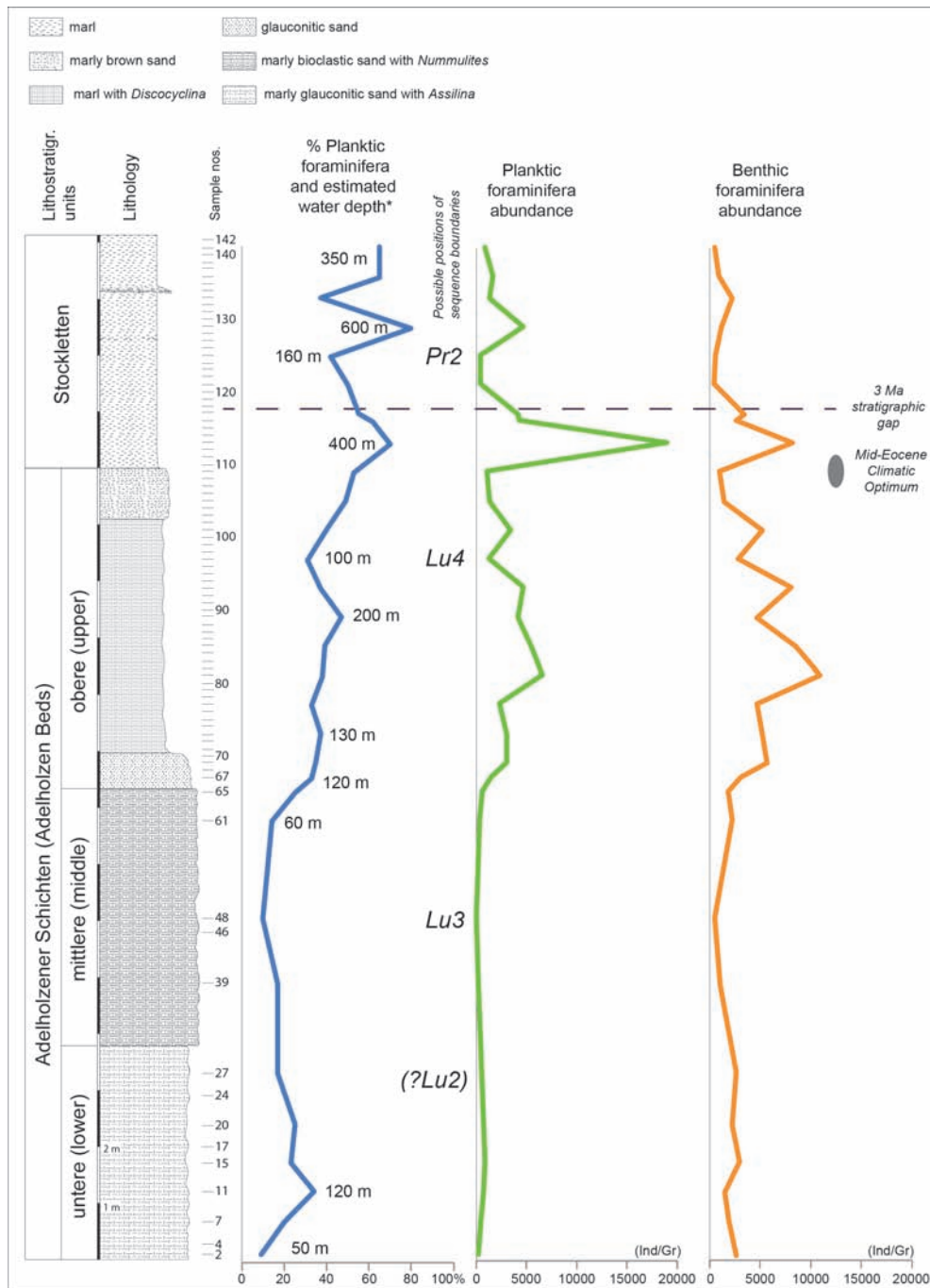


**Figure A2.20 ▲** Water depths estimations according to percent planktic foraminifera and frequency of planktic and benthic Foraminifera (individuals per gram dry sediment). Percentage peaks in planktic foraminifera may represent transgressive cycles (*Lu*, *Pr*) as indicated. \*) Estimates appear to be too high with respect to macrofauna, see text for further details.

## MAASTRICHTIAN TO YPRESIAN SLOPE-BASIN DEPOSITS OF THE ULTRAHELVETIC NAPPE COMPLEX (ACHTHAL FORMATION)

Hans Egger, Omar Mohamed

### Topics:

Cretaceous-Paleogene transition in an active tectonic deep-water setting. Slope basin formation on the bathyal to abyssal southern slope of the European Plate.

### Tectonic unit:

Ultrahelvetic nappe complex

### Lithostratigraphic units:

Buntmergelserie, Achthal Formation (type locality)

### Chronostratigraphic units:

Upper Maastrichtian to Lower Eocene

### Biostratigraphic units:

Calcareous nannoplankton zones CC26 to NP11

### Location:

Stecherwald southwest of Teisendorf (Bavaria)

Coordinates:

Base of the section: E 012° 47' 42", N 47° 50' 51"; Top of the section: E 012° 48' 02", N 47° 50' 48"

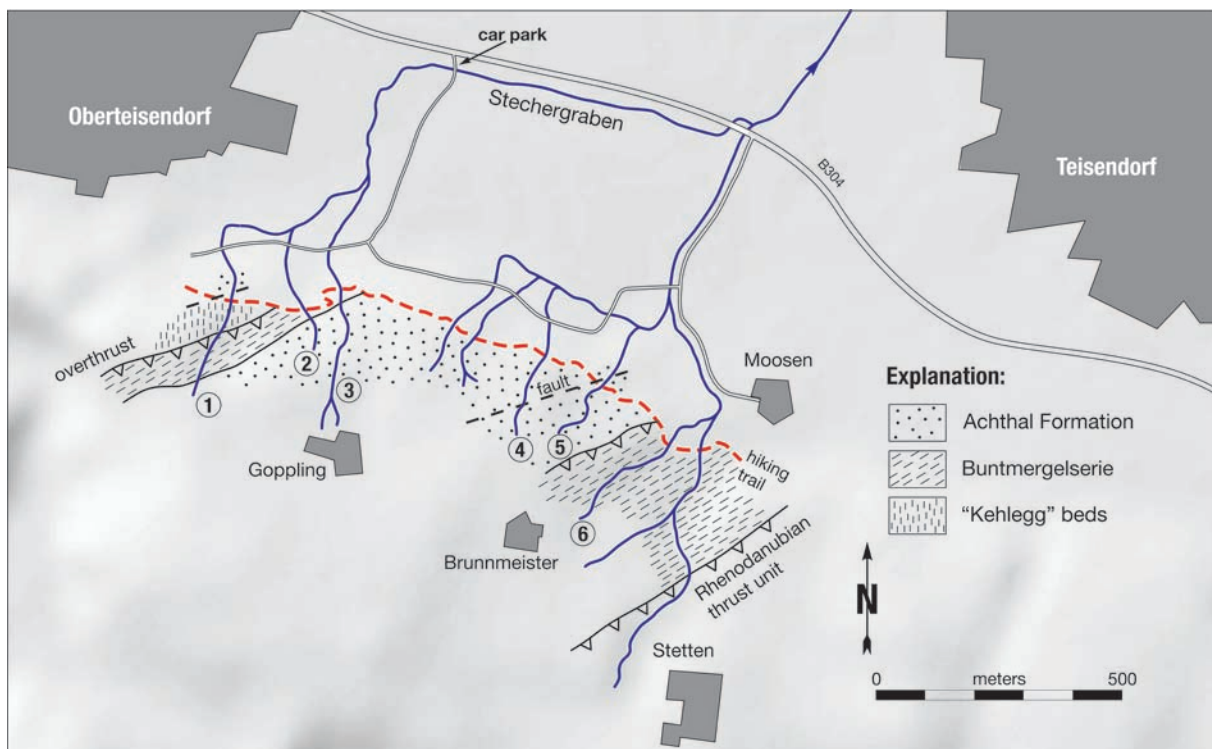
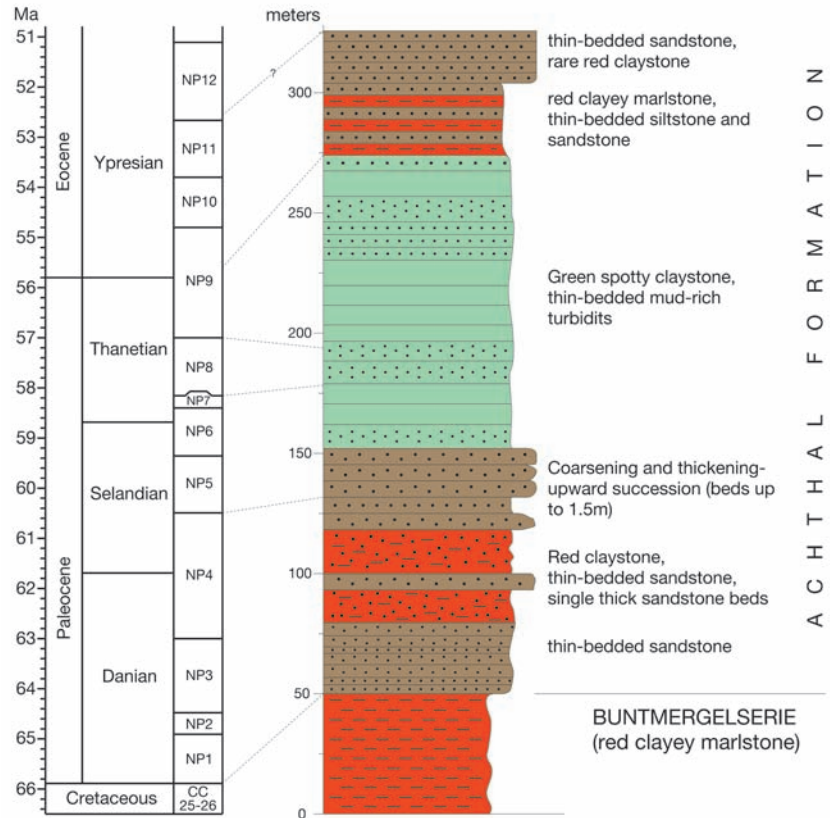


**Figure A2.21 ▲**

Sketch map of the area investigated. Numbers indicate the most important creek sections mentioned in the text.

**Figure A2.22** ►  
Composite log of the Achthal Formation in the type area (Stecherwald near Teisendorf).



The type area of the Achthal Formation is the forest (“Stecherwald”) southwest of Teisendorf. The base of the composite type section of the Achthal Formation (Goppling section) is located in creek 3 (“Gopplingbach”), ca. 15 m south of the hiking trail bridge. Further up-stream the Danian, Selandian and lower Thanetian all show excellent exposures, which end at the hamlet of Goppling. The upper Thanetian is seen only in small and poor exposures, in the two gullies east of creek 3 (Fig. A2.21). The Eocene part of the section is well exposed along creek 4, with the first outcrop ca. 20 m downstream from the hiking trail.

The lithostratigraphic term “Achthaler Sandstein” dates back to Gümbel (1862, p.616). Although Schlosser (1925, p.167) mentioned a Thanetian macrofauna from this unit (“Achthaler Grünsand”), it can be assumed that these fossils originated from the tectonically neighbouring shallow-water deposits of the south-Helvetic thrust unit. Ganss and Knipscheer (1956) report on Paleocene foraminifera faunas and interpreted the outcrops as a special facies (Teisendorf facies) of the Helvetic sedimentation area. Hagn (1960 and 1967) recognized the deep-water character of the deposits and assigned them to the southern part of the Ultrahelvetic sedimentation area, which interpretation is adopted by Egger & Mohamed (2010), who introduced the term “Achthal Formation” for the deep-water turbidite succession.

The base of the Achthal Formation, which conformably overlies the Buntmergelserie, is defined by the onset of turbiditic sedimentation in the uppermost Maastrichtian. The stratigraphic top is unknown because of the tectonic truncation of the Goppling section. However, deposition of the Achthal Formation probably ended in the Ypresian because grey calcareous marlstone of early Lutetian age occurs in the Ultrahelvetic thrust unit at Mattsee in Austria (Rögl and Egger, 2010 – STOPA2/1), only ca. 25 km northeast of Teisendorf.

**Figure A2.23** ►

Sedimentary facies at the Goppling section. **1** Buntmergelserie, Upper Maastrichtian (CC25), creek 3; **2** Sandstone beds of lower Danian age, creek 3; **3** and **4** Danian sandstone and intervening red claystone, creek 3; **5** The highest red claystone layers, upper Danian (NP3-4), creek 3. Note the flute casts at the base of the sandstone indicating paleotransport parallel to the trend of the strike; **6** Thick-bedded sandstone, Selandian (NP5); **7** Mud-rich facies with abundant bioturbated green hemipelagic claystone and thin turbiditic sandstone. Note the erosional channels perpendicular to the trend of the strike (Selandian-Thanetian), creek 3; **8** Bioturbated red marlstone and thin-bedded silt turbidites, Ypresian (NP11), creek 4.



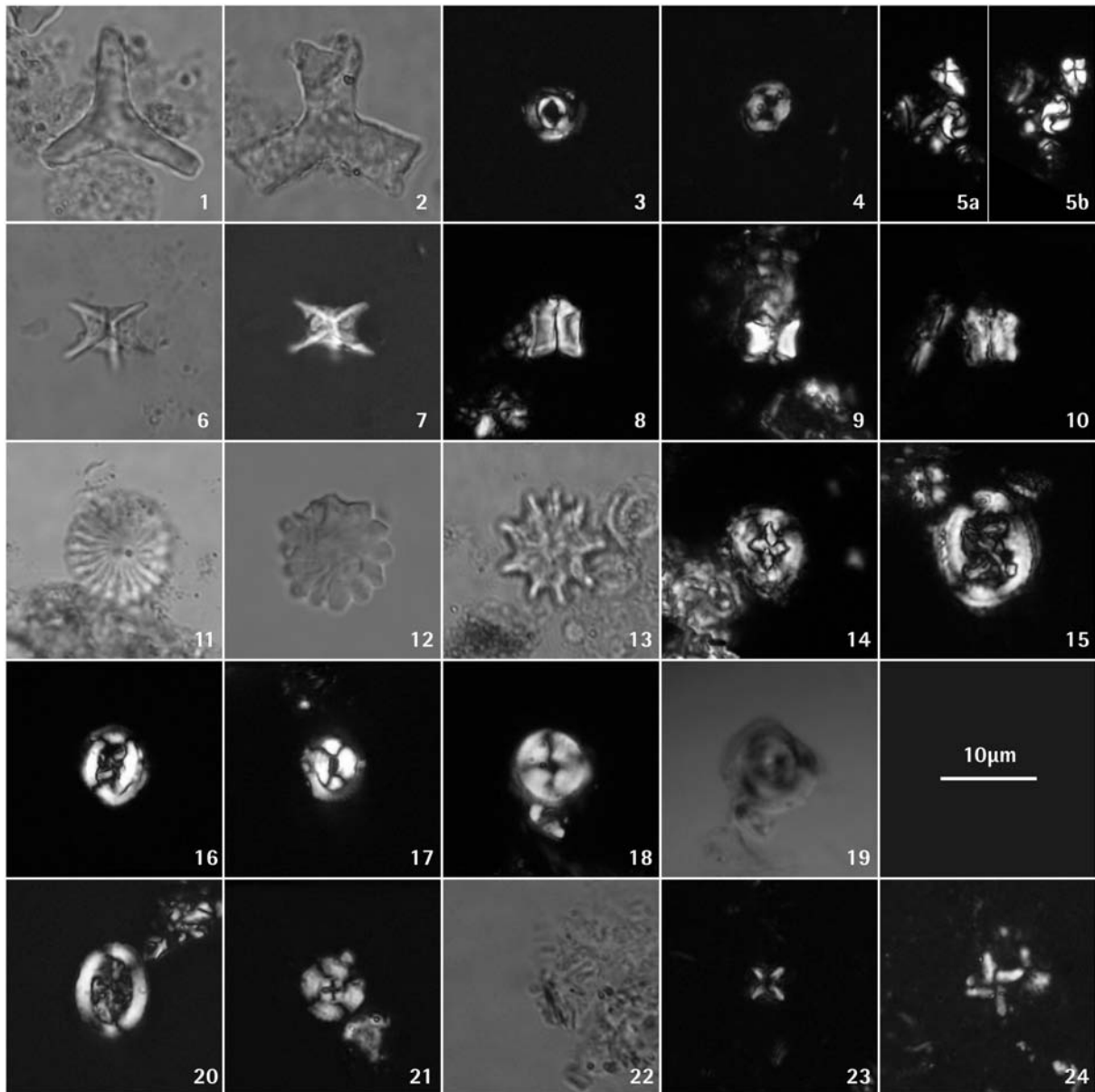


**Figure A2.24 ▲**

Calcareous nannoplankton from the Goppling section.

Paleogene species: **1** *Tribrachiatus orthostylus* - Gstetten18/09; **2** *Tribrachiatus digitalis* – Gstetten10/09; **3** *Toweius callosus* – Gstetten22/09; **4** *Toweius occultatus* - Gstetten22/09; **5 a and b** *Sphenolithus anarrhopus* – Achthal 12/09; **6 and 7** *Rhomboaster cuspis* – Gstetten22/09; **8** *Fasciculithus tympaniformis* – Achthal12/09; **9** *Fasciculithus billii* – Achthal28/09; **10** *Fasciculithus ulii* – Achthal28/09; **11** *Discoaster multiradiatus* – Gstetten13/09; **12** *Discoaster mohleri* - Achthal12/09; **13** *Discoaster falcatus* - Gstetten13/09; **14** *Cruciplacolithus tenuis* – Achthal12/09; **15** *Chiasmolithus bidens* – Achthal12/09; **16** *Chiasmolithus danicus* - Achthal12/09; **17** *Coccolithus pelagicus* - Achthal12/09; **18 and 19** *Bomolithus elegans* - Achthal28/09.

Maastrichtian: **20** *Arkhangelskiella cymbiformis* - Achthal18/09; **21** *Ceratolithoides cf. kamptneri* - Achthal18/09; **22** *Cyclagelosphaera reinhardtii* - Achthal18/09; **23** *Micula staurophora* - TS10/09; **24** *Micula prinsii* - TS10/09.

The deep-water system of the Achthal Formation is interpreted to have initially filled a slope depression lying above a subsiding basement fault block. Initial subsidence occurred in the latest Maastrichtian and continued into the early Paleogene. Synsedimentary tectonic activity was the primary control on the depositional evolution of the slope-basin.

In the forest south of Teisendorf and Oberteisendorf, a number of small creeks have created excellent exposures of the Achthal Formation. Almost all such outcrops lie to the south of the hiking trail running between the two villages. For better orientation, the more important creeks have been numbered (Fig. A2.21). The Ultrahelvetic nappe complex in the area is composed of three tectonic slices exposing beds con-

tinuously dipping to the southeast. During the field trip we will see part of the ca. 320 m thick sedimentary succession of the Goppling slice, which comprises Maastrichtian to lower Eocene deposits (Fig. A2.22).

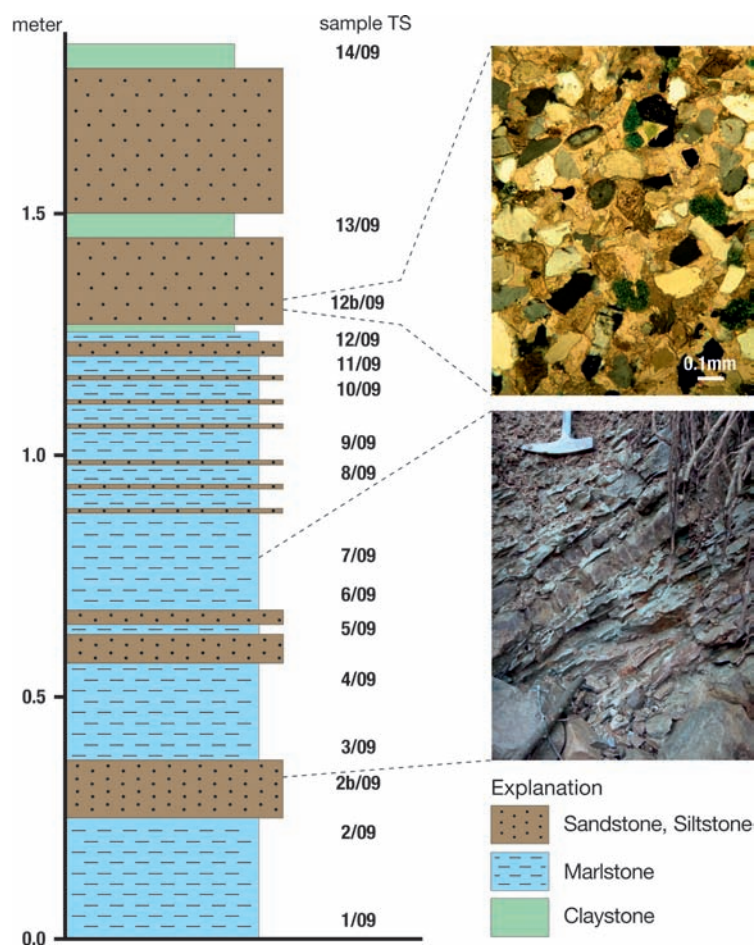
## STRATIGRAPHIC FRAMEWORK OF THE GOPPLING SECTION

### Maastrichtian

The basal part of the Goppling section is formed by ca. 50 m of bioturbated red clayey marlstone, which is assigned to the Buntmergelserie. The top of this red-bed succession is exposed in creek 3 ("Goppling creek"), immediately south of the hiking trail bridge (Fig. A2.23/1). There, the marlstone contains 19 wt% carbonate. The nannoplankton assemblages are dominated by *Micula staurophora*, whereas all other species are rare and most specimens are preserved only as fragments. Apart from *Lithraphidites quadratus*, the zonal marker for the upper Maastrichtian Zone CC25, *Arkhangelskiella cymbiformis* (Fig. A2.24/20), *Cyclagelosphaera reinhardtii* (Fig. A2.24/22), *Eiffellithus turriseiffeli*, *Micula staurophora*, *Prediscosphaera cretacea*, *Retecapsa crenulata*, and *Watznaueria barnesae* occur. At the top of the red marlstone outcrop, small specimens of *Ceratolithoides cf. kamptneri* were observed (Fig. A2.24/21), indicating already Zone CC26.

Two samples for foraminifera studies were taken from the red marlstone at the outcrop in creek 3 outcrop. The assemblages consist essentially of a rich agglutinated fauna and a small number of calcareous benthic species. Very small planktic species were found only in one sample and display excellent grain-size sorting suggesting reworking by current activity.

Predominant dissolution-resistant species in the calcareous nannoplankton assemblages and the composition of foraminifera assemblages indicate sedimentation of the Maastrichtian red clayey marlstone in a deep-water environment. The absence of an autochthonous planktic fauna indicates deposition below the foraminiferal lysocline, where all planktic foraminifera are dissolved. Below the lysocline and above the calcite compensation depth (CCD) calcareous nannoplankton form coccolith ooze, because in spite of their small size, some coccoliths are more dissolution-resistant than foraminifera (see Hay, 2004, for a review).



In the latest Maastrichtian (*Micula prinsii*-Zone), rapid subsidence brought the Ultrahelvetic sea-floor to below the CCD. The red marlstone transitionally passes into ca. 5 m of grey marlstone with intercalated thin carbonate-cemented parallel-laminated turbiditic siltstone and sandstone beds (Fig. A2.25). The best outcrop of these rocks was found in creek 2 about 10 m south of the hiking trail. In the lower part of this out-

**Figure A2.25** ◀

Log of the upper Maastrichtian (*Micula prinsii*-Zone) in the creek 2 section. The lower photograph shows grey to pale red marlstone displaying carbonate contents of ca. 20 wt% and intervening calcite cemented fine-grained turbiditic sandstone beds. The upper photograph is the image of a thin-section of such a sandstone. Calcite replacement affected the components (predominantly single-crystal quartz grains displaying straight extinction, small amounts of K-feldspar and glauconite, very rare mica and cherts) and a possible matrix. The composition of the original sandy fraction cannot be assessed due to the strong diagenetic alteration.

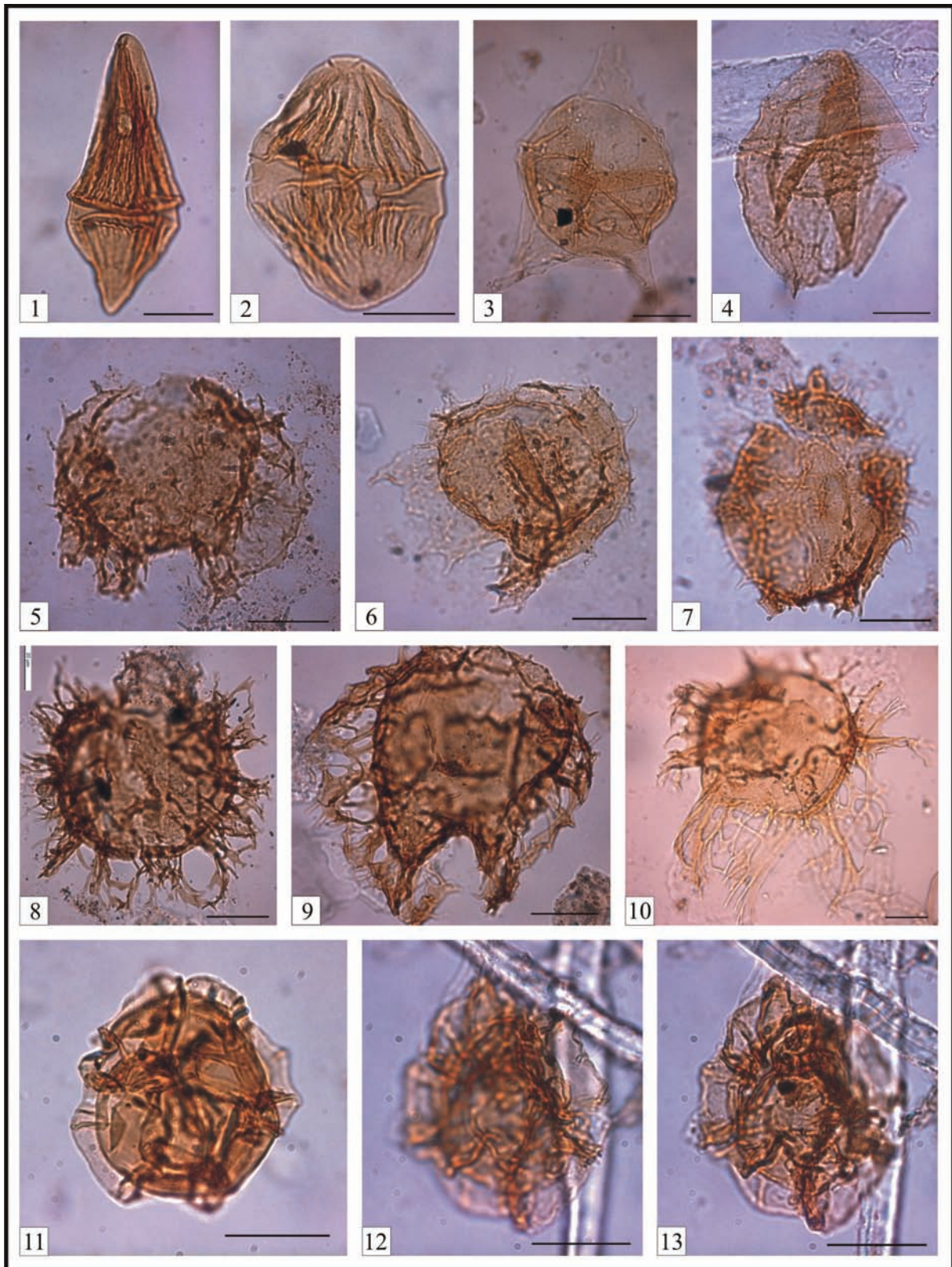


**Figure A2.26 ▲**

Dinoflagellate taxa from the Goppling section. The species name is followed by sample location and England Finder coordinates (for localization of the specimen on the slide). Scale is 20  $\mu\text{m}$ . **1** *Dinogymnium acuminatum* - TS11/09/a, O24; **2** *Dinogymnium* sp., TS11/09/a, F7/3; **3** *Cerodinium* sp, TS11/09/a, X16/3; **4** *Trithyrodinium* *suspectum* - TS8/09/a, B24/2; **5** *Palynodinium grillator* - TS13/09/a, C40; **6** *Palynodinium grillator* - TS11/09/a, W36; **7** *Palynodinium minus* - TS13/09/b, Y27; **8** *Areoligera volata* - Ach.2/09/a, G12; **9** *Areoligera coronata* - Ach.1/09/a, A3; **10** *Areoligera gippingensis* - TS11/09/a, X34; **11** *Pterodinium cingulatum* subsp. *cingulatum* - TS12/09/a, W33/4; **12** and **13** *Pterodinium aliferum* - TS8/09/a, D6/1.

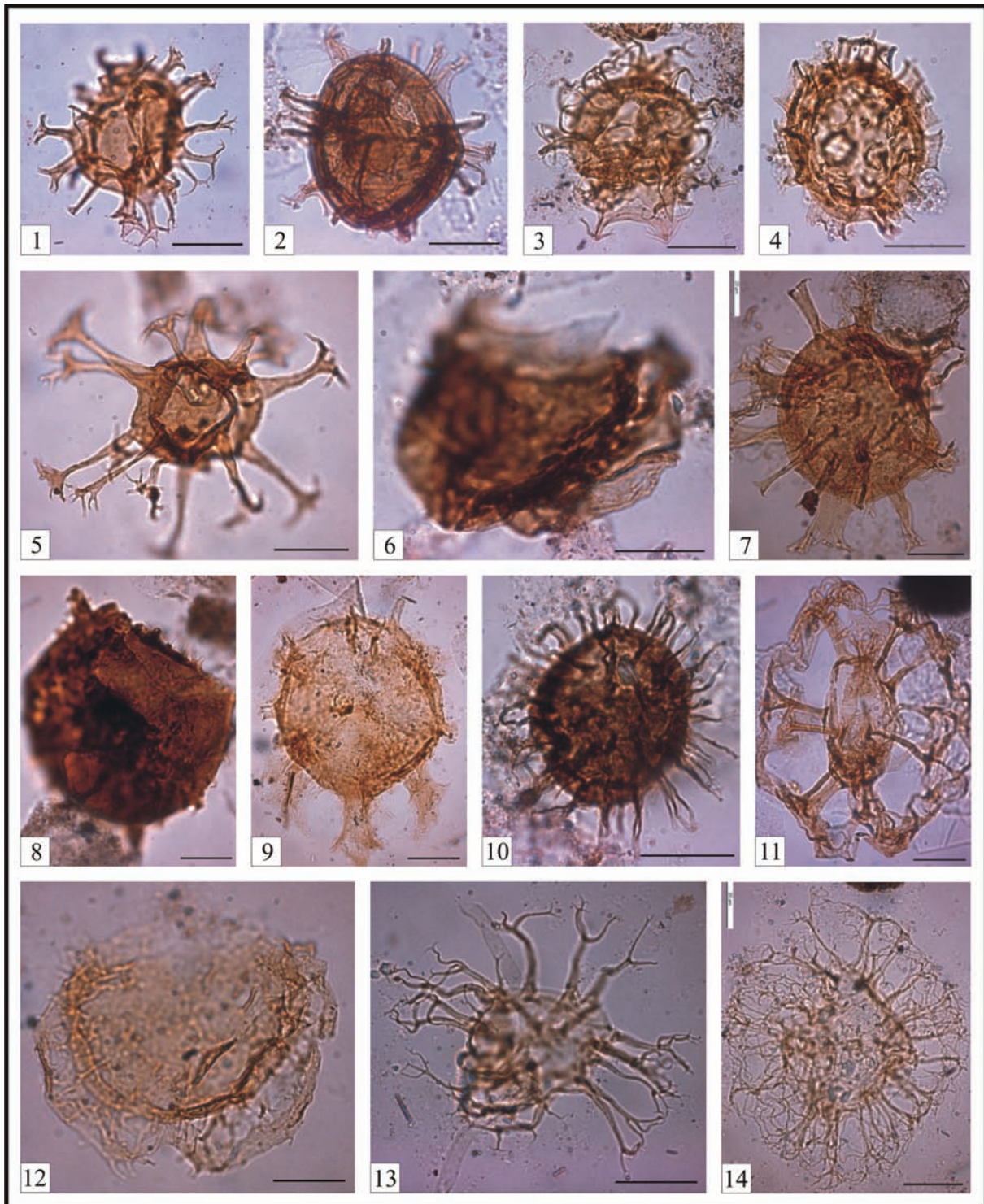


**Figure A2.27 ▲**

Dinoflagellate taxa from the Goppling section (continuation). The species name is followed by sample location and England Finder coordinates (for localization of the specimen on the slide). Scale is 20  $\mu$ m. **1** *Achomosphaera* cf. *alcicornu* - TS13/09/b, N5; **2** *Spiniferites pseudofurcatus* - TS4/09/b, X51/1; **3** *Hystrichostrogylon membraniphorum* - TS12/09/a, N24/2; **4** *Achilleodinium biformoides* - TS11/09/a, X8; **5** *Oligosphaeridium complex* - Ach. 2/09/a, G12; **6** *Senoniasphaera inornata* - Ach. 2/09/b, F40; **7** *Cordosphaeridium fibrospinosum* - TS12/09/a, B36/3; **8** *Carpatella cornuta* - Ach.1/09/b, K16; **9** *Damassadinium californicum* - TS11/09/a, P10; **10** *Operculodinium centrocarpum* - Ach.2/09/b, B25/4; **11** *Rigaudella aemula* - TS4/09/b, D18/1; **12** *Glaphyrocysta perforate* - TS11/09/a, S14/1; **13** *Surculosphaeridium longifurcatum* - TS11/09/a, M46/2; **14** *Trabeculidium quinquetrum* - TS12/09/a, D34/2.

crop, carbonate values of three samples (TS2/09, TS7/09 and TS9/09) range between 20.8 wt% and 21.5 wt%. In the upper part carbonate values decrease to 9.4 wt% (TS10/09) and finally to less than 2 wt% (TS12/09, TS13/09 and TS14/09). Dinoflagellate cyst assemblages indicate a Maastrichtian age of the claystone as in the uppermost sample *Dinogymnium acuminatum* occurs (Fig. A2.26/1), which does not cross the K/Pg-boundary (e.g. Stover et al. 1996).

Associated with this regional subsidence along the southern continental margin of the European Plate, was the onset of turbidite sedimentation. Turbidity currents running parallel with the strike of the slope indicate an opposing topographic high, which caused deflection of the down slope sediment transport (Kneller and McCaffrey, 1999). Subsidence of the sea-floor associated with the deposition of sediment-gravity flows and the coeval generation of a sea-ward bounding topographic high suggest the formation of an intra-slope basin on subsiding crustal fault blocks.

## Danian

Danian and Selandian deposits are almost continuously exposed in the Goppling creek gully. Due to the carbonate depletion, no calcareous plankton could be found in the siliciclastic succession, although dinoflagellate assemblages of samples Ach1/09 and Ach2/09 (see Tab. 1 and Fig. A2.27/6, 8 and 9) contain *Carpatella cornuta*, *Damassadinium californicum* and *Senoniasphaera inornata*, which have their first appearance date in the early Danian. *Palynodinium grallator* (Fig. A2.26/5 and 6) has its highest occurrence in the lowermost Danian planktonic foraminiferal Zone P1a (Habib et al., 1996; Dam et al., 1998; Brinkhuis et al., 1998). The samples were taken at the base (Ach1/09) and top (Ach2/09) of the same outcrop (Fig. A2.23/2). Consequently, this outcrop can be assigned to Zone P1a in the zonation of Berggren et al. (1995).

The Danian shows a two-fold lithological subdivision. The 30 m thick lower part is dominated by thin-bedded (< 40 cm) parallel-laminated sandstone turbidites, that rarely show thin capping mudstone (Fig. A2.23/2). In contrast to the Maastrichtian turbidites, the Danian ones are not calcite cemented and do not contain carbonate at all. They are fine-grained (grain diameters up to 0.2 mm), show clast supported fabrics, and have a quartzarenitic composition. Beside quartz (ca. 90% of the grains), feldspar, chert and glauconite occur as components. Freimoser (1972) noted that the heavy mineral assemblages of these Paleocene sandstones are essentially composed of zircon, tourmaline and rutile (together about 90% of the assemblage). Hemipelagic claystone between the turbidite beds is rare and when present only a few millimeters thick indicating that (1) turbidity currents entered the basin with a high frequency and (2) deposition took place below the local CCD.

In the 40 m thick upper part of the Danian, hemipelagic layers are common and often display red colors (Fig. A2.23/3 and 4). Packages of red hemipelagic claystone contain thin base truncated turbiditic siltstone to sandstone beds. These packages are separated by single thick (> 0.5 m) medium to coarse-grained sandstone beds showing grain diameters up to 1.0 mm. As in the lower Danian, only K-feldspar components can be observed and plagioclase is entirely absent. The beds are either massive or show stratification defined by 2–5 cm thick laminae. Graded (Ta) and parallel laminated (Tb) Bouma divisions form the major parts of these beds. Small-sized terrestrial plant remnants are commonly concentrated in horizontal Td-layers near the top of the beds and indicate a derivation of the turbidite material from land areas. Submarine erosion is evidenced by flute casts, which indicate sediment transport predominantly from the west, parallel to the approximately east-west trending slope (Fig. A2.23/5).

One sample (Ach3/09) of the red claystone was studied for dinoflagellates but contained only *Areoligera senonensis*, which has a range from the Cretaceous to the Paleogene. Together with the last red hemipelagites, grey turbiditic clayey marlstones occur, containing strongly corroded nannoplankton assemblages. Beside substantial admixtures of Cretaceous species, *Chiasmolithus danicus*, *Cruciplacolithus tenuis*, *Coccolithus pelagicus* and *Toweius spp.* are indicative for the Danian (*Chiasmolithus danicus* Zone, NP3). However, the absence of *Ellipsolithus macellus*, the zonal marker for Zone NP4, might only be a consequence of the poor preservation in this sample.

## Selandian

About 10 m up-section from the above mentioned Danian sample, nannoplankton assemblages contain *Fasciculithus tymaniformis*, the zonal marker for the calcareous nannoplankton Zone NP5 of earli-

est Selandian age. With the disappearance of red hemipelagites the discrimination between turbiditic and non-turbiditic rocks becomes difficult. Single turbidites show a distinct pelitic component (Bouma T<sub>d</sub>) in this part of the Goppling section, with approximately the same thickness as the sandy part of the turbidite. This turbiditic mudstone only occasionally contains carbonate. In most cases it is devoid of carbonate and displays the same grey color as the supposed hemipelagic mudstone.

The Selandian, which forms the morphologically steepest part in the course of creek 3, is composed of a ca. 25 m thick thickening and coarsening upward succession. In the lower part of this succession decimeter-scale turbidites occur. Continuing up the exposure, the bed thicknesses gradually increase up to 1.5 m at the top of the succession (Fig. A2.23/6). These sandstone beds are the thickest beds in the entire Achthal Formation and do not display turbiditic mudstone. In part, they contain intraformational mudstone clasts with diameters up to 0.2 m. Flute casts indicate paleotransport from west to east and thus an orientation parallel to the trend of the paleoslope (Fig. A2.28).

### Thanetian

In spite of excellent exposures along creek 3, the boundary between the Selandian and Thanetian is difficult to fix precisely due to carbonate depletion and the lack of calcareous plankton. Ca. 20 m downstream from the confluence in the uppermost part of creek 3 (Fig. A2.21), *Fasciculithus billii* is indicative for the upper part of Zone NP5. From here on upstream, a ca. 40 m thick part of the section is characterized by abundant olive-green strongly bioturbated „spotty“ claystone. Probably, the majority of the oval spots in these hemipelagic deposits represent cross sections of the trace fossils *Planolites* and *Thalassinoides* (Uchman, 1999). *Thalassinoides* ispp. and a strongly fragmented specimen of ?*Scolica strozzii* were found also as semi-reliefs at the base of turbidite beds (Fig. A2.29/4, 5 and 6).

The turbidites intervening with the claystone are mostly thin bedded and occasionally display substantial amounts of glauconite, resulting in green rock colors. Glauconite was deformed during burial and flowed around adjacent quartz grains. This is indicated by the patchy distribution of glauconite-filled areas, which are much larger than normal pores.

Some beds show a lenticular shape. The orientation of paleoflow indicators (flute casts and erosional channels) suggest paleotransport from north to south, following the gradient of the south-facing paleoslope (Fig. A2.23/7 and Fig. A2.30). *Discoaster mohleri* (Fig. A2.23/12) indicative of Thanetian zone NP7, was found in the eastern branch of creek 3, about 50 m up-stream from the confluence with the western branch (Fig. A2.21). *Discoaster multiradiatus* (Fig. A2.24/11), the zonal marker of Zone NP9, was found in the uppermost part of the western branch.



**Figure A2.28** ◀  
Flute casts at the base of a south-dipping bed indicating longitudinal paleotransport from west to east (creek 3)

## Ypresian

The Ypresian of the Goppling section shows a two-fold lithological subdivision. The lower part consists of a ca. 50 m thick succession of decimeter-scale turbiditic sandstone and siltstone beds alternating with red colored marly claystone (Fig. A2.23/8). The latter rock is often bioturbated and probably represents hemipelagic non-turbiditic material. As its carbonate values range between 4 wt% and 8 wt%, sedimentation slightly above the CCD can be assumed.

Samples containing *Rhomboaster cuspis* (Fig. A2.24/6 and 7) were found in the lower part of creek 5, about 20 m to the north of the hiking trail. *R. cuspis* has its first appearance date at the Paleocene/

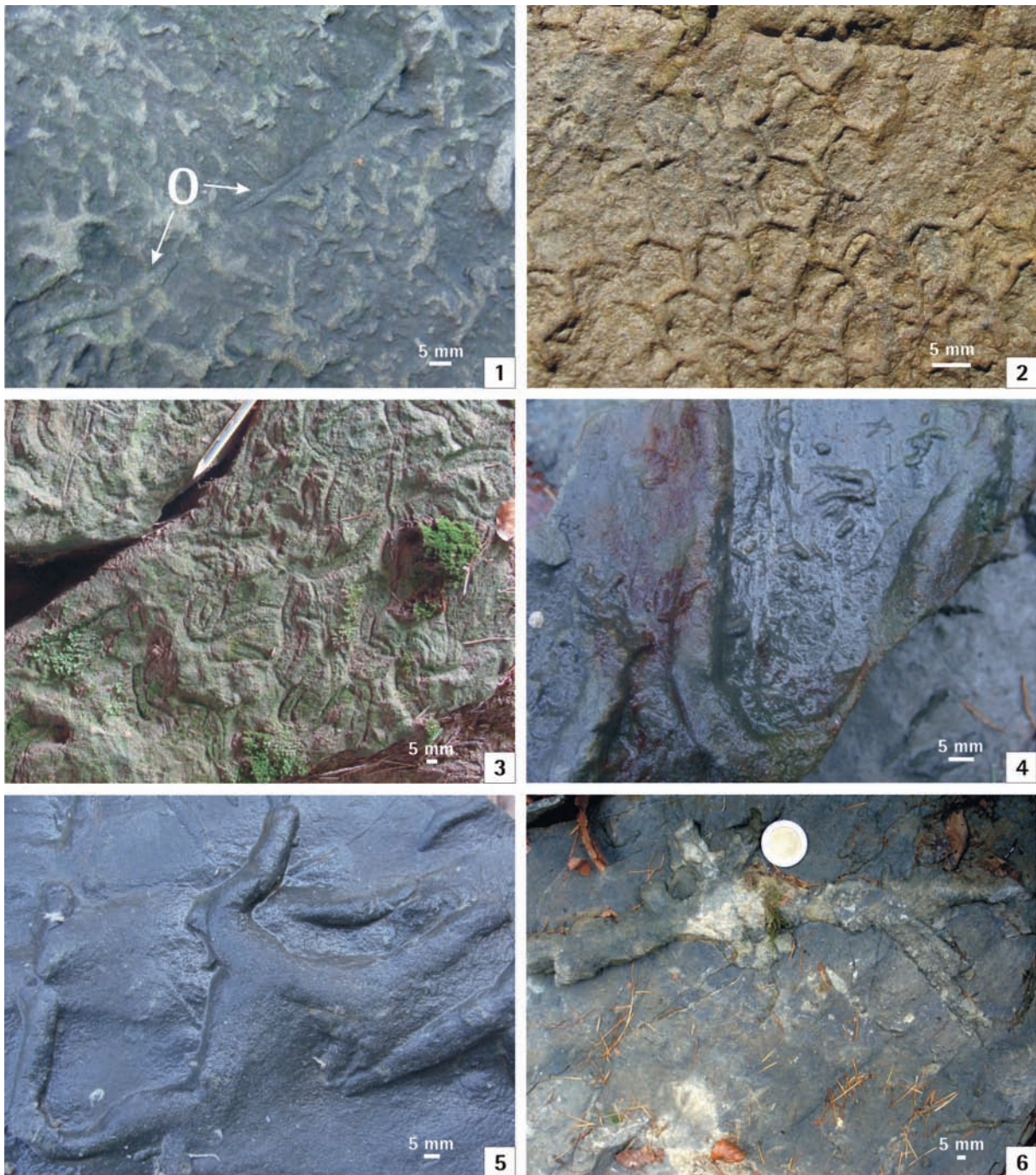


**Figure A2.29 ▲**

Ichnofossils from the Thanetian (creek 3) and Ypresian (creek 4) of the Goppling section 1) *Ophiomorpha annulata* (O) and ? *Protopaleodictyon* isp. – creek 3; 2) *Paleodictyon majus*.- creek 4; 3) *Scolicia prisca* – creek 4; 4) ? *Scolicia strozzii* – creek 3; 5) *Thalassinoides* isp. – creek 3; 6) *Thalassinoides* isp. – creek 3.



**Figure A2.30 ▲**

Flute casts at the base of a south-dipping bed indicating transverse paleotransport from north to south (creek 3).

by a fault from the underlying part of the succession in creek 4. In this gully, the topographically lowest outcrops lie just down-stream the hiking trail (Fig. A2.23/8). *T. orthostylus* with pointed rays (Fig. A2.24/1) co-occurs with *Chiasmolithus bidens*, *Coccolithus pelagicus*, *Discoaster barbadiensis*, *D. multiradiatus*, *Ellipsolithus macellus* and *Sphenolithus primus*. Whereas the robust and dissolution resistant *Tribrachiatulus* specimens may be common in the samples, the other species, in particular the discoasterids, are exceedingly rare due to dissolution. Carbonate values of two samples from this outcrop were 4.2 wt% and 4.8 wt%.

A few meters up-stream from the hiking trail the red bed facies in creek 4 shows a sharp sedimentary contact to an overlying ca. 60 m thick sand-rich and thin-bedded turbidite succession that displays only rare and very thin carbonate depleted hemipelagic layers. This suggests that the upper part of the Ypresian succession was deposited below the CCD and hence another subsidence pulse can be assumed. This interpretation is supported by the orientation of flute casts, which indicate paleoflow directions from west to east.

This part of the Goppling section commonly contains trace fossils (e.g. *Paleodictyon majus* and *Scolicia prisca*, see Fig. A2.29/2 and 3). According to Uchman (1999) the ichnogenus *Paleodictyon* probably reflects a moderate shortage of food. These generally oligotrophic conditions were interrupted by periodic accumulation of organic detritus (e.g. plant detritus) by turbidity currents. These more eutrophic episodes favored the ichnogenera *Ophiomorpha* and *Scolicia*. In the Rhenodanubian Group (Egger and Schwerd, 2008) of the adjacent abyssal Penninic basin, the ichnogenera *Ophiomorpha*, *Paleodictyon* and *Scolicia* are known exclusively from the Greifenstein Formation of Eocene age (Uchman, 1999).

## DEPOSITIONAL EVOLUTION

Due to the lack of information about the three-dimensional geometry of the basin-fill, the scale and shape of this basin is unknown. It can be assumed that it was a narrow elongate, structurally controlled depression where tectonic activity was the primary control on sedimentation. Presumably, this confined basin was too small for the development of a large-scale deep-sea fan. Instead a channelized deep-water system could be expected, with the bounding slopes of the basin acting as channel walls (Fig. A2.31). Gravity-induced flows entering a sub-basin drop their sediment load and prograde across the depression forming a thickening and coarsening upward succession (Anderson et al., 2006; Shultz and Hubbard, 2005).

At the front of this prograding lobe-like body the thin-bedded sand-rich turbidite succession of early Danian age was deposited (e.g. Crabaugh and Steel, 2004). The lack of muddy tops can be interpreted as an effect of flow-stripping of the fine-grained component of the turbidity currents (e.g. Piper and Normark, 1983; Sinclair and Tomasso, 2002). This indicates that during this early stage of basin evolution,

Eocene-boundary, which is situated in the upper third of Zone NP9. About 25 m to the south of the hiking trail, *Tribrachiatulus digitalis* (Fig. A2.24/2) occurs, the marker fossil of sub-Zone NP10b in the refined zonation scheme of Aubry (1992). About 15 m further up-section, another outcrop of the red bed facies occurs and provided *Tribrachiatulus orthostylus* (Fig. A2.24/1), whereas *T. contortus*, which has its highest occurrence at the NP10/NP11-boundary is absent. Therefore these samples can be assigned to the lower part of NP11 (*Discoaster binodosus*-Zone). Thus, in summary, the red bed facies encompasses the upper part of NP9 to the lower part of NP11.

Along strike to west, red beds containing *R. cuspis* were found in the upper part of creek 4. These deposits are separated

the confining sill was still low. Hence it could be surmounted by the lower-density fraction of the turbidity currents, while the coarse-grained higher density portions of the flows were deflected and preserved upstream of the barrier. The rare and thin hemipelagites indicate the existence of high-frequency trigger mechanisms (e.g. earthquakes) for turbidity currents during the onset of basin formation.

In a conventional fan model, the upper Danian packages of thin-bedded turbidites and red hemipelagic mudstone, which are separated by single thick sandstone beds, can be interpreted as interchannel deposits. In such a model, the thin-bedded turbidites are thought to result from low-density currents overflowing adjacent active channels, while the thicker beds are explained as the result of crevasses in the channel levee, which let high density turbidity currents (Lowe, 1982) escape to the basin floor (e.g. Mutti, 1977). This model implies the existence of subordinate fairways within the slope-basin.

Alternatively, the upper Danian facies can be seen as the result of an episode of comparatively tectonic quiescence. Siliciclastic material accumulated at the shelf edge over time and larger turbidity currents triggered by earthquakes or gravity load entered the slope-basin with low periodicity. This is indicated by the common occurrence of intervening hemipelagic red claystone as their deposition indicates very low sedimentation rates. The lack of muddy tops of the thick-bedded turbidites can again be explained as a result of flow-stripping as flow thickness was determined as the primary control of the run-up distance of a turbidity current onto the opposing slope (Muck and Underwood, 1990). It is assumed, that high-density currents (Lowe, 1982) lost their fine-grained component by down-spill, so that only their coarse-grained material is preserved in the sub-basin. Low-density currents had not the potential to surmount the bounding slope and remained completely in the sub-basin.

Increased subsidence at the end of the Danian caused ponding of the turbidity currents, which display a distinct pelitic component. However, sedimentation rates quickly outpaced subsidence rates and deposition reduced the relief sufficiently to allow spill down-slope. The filling up of the basin to the spill-point is indicated by downslope paleotransport directions in the upper Selandian and Thanetian. Due to the gradient reduction in the area of the former basinal structure turbidites were deposited on this flat surface and the ca. 95 m thick basin-fill succession of Danian and Selandian age became buried by slope deposits developing into a healed slope (e.g. Smith, 2004).

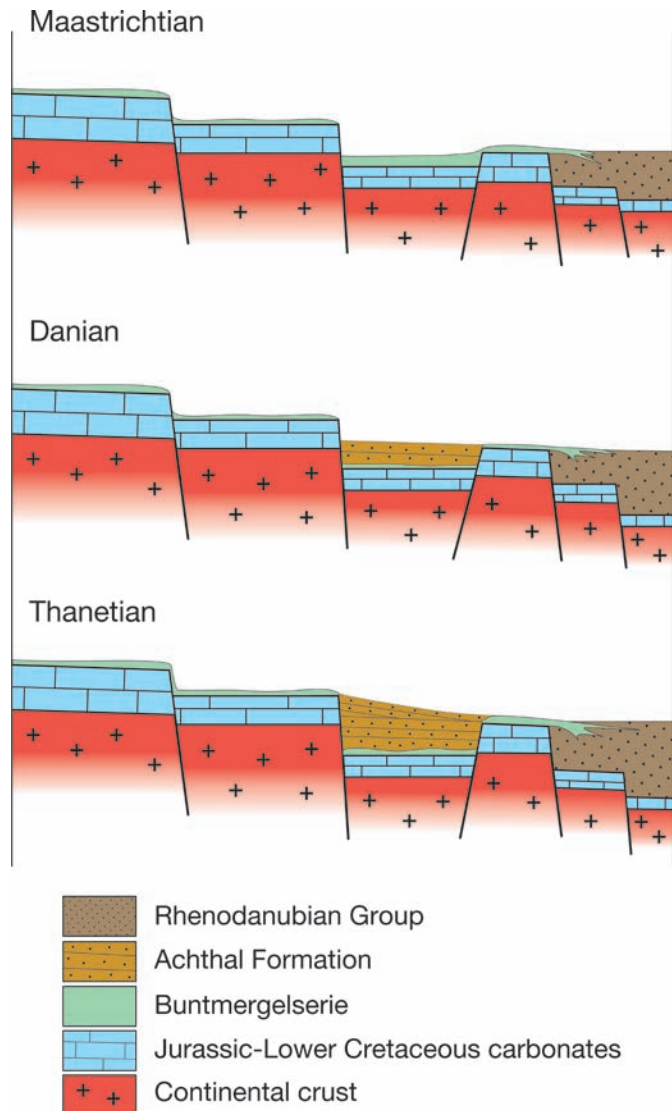


**Figure 11 ▲**  
Slope basin model for the deposition of the Achthal Formation.

## Cretaceous/Paleogene-boundary and Paleocene/Eocene-boundary sections at Gams and Lower Eocene at Krappfeld

### Introduction

Today we start with a 3 hours bus drive, passing by two lakes (Mondsee and Attersee) in the Salzkammergut area and then going through the Gesäuse-Gorge of the Enns river. This scenic drive will bring us to Gams, a small village that is the centre of the only Geopark in Austria. During the lunch break, we will have time to visit the exhibition in the Geopark museum. Among other items of geological interest, a polished block of the K/Pg-boundary from the Knappengraben section is on display. We will not visit this outcrop, but will have our first stop after the lunchbreak at the better exposed and less remote Gamsbach section. From there, we will walk to the Pichler section where the Paleocene/Eocene section crops out. After visiting these two outcrops, we have another bus ride, of about 3 hours, to the hotel in the convent of St. Georgen, at Längsee (Fig. A3.1). On the way, we will make a photo stop at Erzberg, which is the largest open cast mine in Austria.

On Friday, our first stop will be a photo stop near the Hochosterwitz fortress. Then we will examine lower Eocene outcrops in the Fuchsofen quarry and the Höhwirt sections, both of which are very rich in the larger foraminifera. After eating, we will go back to Salzburg on the motorway crossing the Central Eastern Alps. For participants who want to get off at Villach to catch a train towards the south, we will make a short stop at the railway station.

### Notes:

- Arrange your own breakfast and assemble at the carpark of St. Virgil (Ernst-Grein-Straße 14, 5026 Salzburg; Tel. +43-662-65901-516) for departure at 8.30 a.m. sharp.
- Lunches will be arranged at Gams and Guttaring. Dinner will be at the Hotelrestaurant at St. Georgen (Stift St. Georgen am Längsee, Schlossallee 6, A-9313 St. Georgen am Längsee; Tel+43-4213-2046; office@stift-stgeorgen.at).
- Route: Salzburg (St. Virgil) – Gams – Erzberg – St. Georgen am Längsee (Overnight) – Klein St. Paul – Guttaring – Villach ( – Salzburg)
- Accommodation at Salzburg (arrival time ca. 4 pm) has to be arranged by the participants.



Figure A3.1 ◀  
Convent of St. Georgen



**Figure A3.2 ▲**  
Route map for Field Trip A3

## GEOCENTRE AT GAMS



**Figure A3.3 ▲**  
Exhibition hall at the GeoCentre Gams

The Nature Park Eisenwurzen, located in the Austrian state of Styria, is situated in the Northern Calcareous Alps. Geotourism has a long tradition in the area. As early as 1892 the Kraus Cave of Gams, one of the most splendid gypsum-bearing caves of Europe and the first one in the world with electric light, was opened to the public. In recent times, the adventure of experiencing 250 million years of Alpine history has given new impulses to tourism in the region, which has suffered from extreme depopulation in the past decades.

Scientists have been aware of the magnificent geology of the region since the early 19th century. The Anisian stage of the Triassic period has been named after a section of rocks close to the Enns River, which was called Anisius fluvius in Roman times. Geotouristic activities are the domain of GeoLine ([www.geoline.at](http://www.geoline.at)), the geological branch of the Nature Park. These comprise two permanent exhibitions: the museum of the Second Vienna Water Supply Line, which benefits from karstic springs in the area, and the GeoCentre of Gams, which provides an overview of the regional geology. The GeoTrail and GeoBike, a demanding bicycle trail, provide in-situ evidence of geological phenomena. This most powerful of all geological agents may be explored in the Water Park of St. Gallen and at GeoRafting, which combines science with adventure. The GeoWorkshop serves all activities related to the preparation of geological items.

The recognition as a member of the European Geoparks Network in 2002 has provided new momentum. Funded by the EC programme LEADER+, challenging geotouristic projects are established in all communities of the Nature Park. This will be an important step towards a sustainable development of the region.



## THE CRETACEOUS-PALEOGENE (K/PG) BOUNDARY AT THE GAMSBACH SECTION (GAMS, STYRIA)

Hans Egger, Christian Koeberl, Omar Mohamed, Christoph Spöttl, Michael Wagreich

### Topics:

Cretaceous/Paleogene-boundary, nannoplankton, dinoflagellates, geochemistry

### Tectonic unit:

Northern Calcareous Alps

### Lithostratigraphic unit:

Nierental Formation

### Chronostratigraphic units:

Upper Maastrichtian to lowermost Paleocene

### Biostratigraphic units:

Calcareous nannoplankton Zones CC26 and NP1

### Location:

Gamsbach to the east of Haid (Gams, Styria)

### Coordinates:

E 014° 51' 50" N 47° 39' 51"

### References:

Egger et al., 2009c

### Introduction

In the area east of Gams (Styria, Austria), the Cretaceous/Paleogene boundary has been recognized in the Gamsbach section, which comprises the upper part of the Cretaceous *Nephrolithus frequens* Zone (CC26) and the lower part of the Paleocene *Markalius inversus* Zone (NP1). The 6.5 m long section is part of the Nierental Formation of the Gosau Group of the Northern Calcareous Alps.

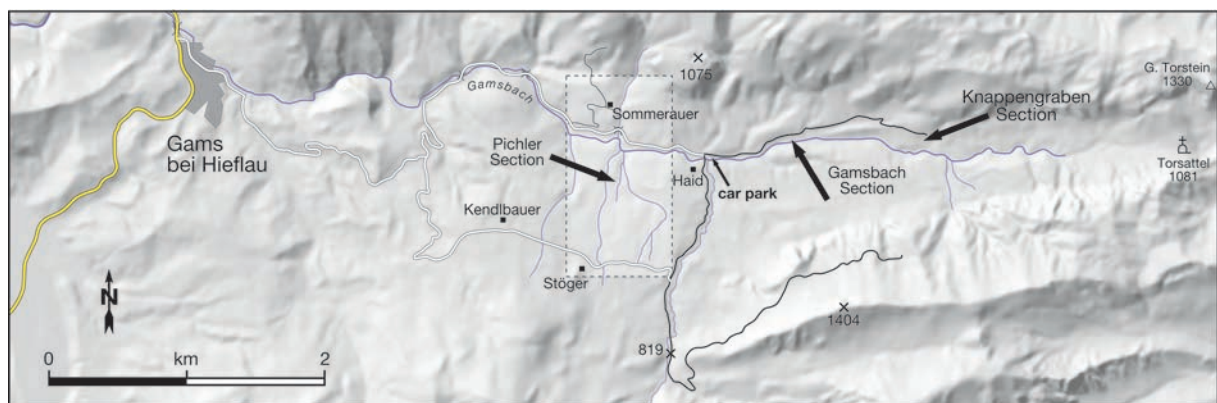


**Figure A3.4 ▲**

Positions of the Gamsbach (Stop A3/2), Pichler (Stop A3/3) and Knappengraben sections.

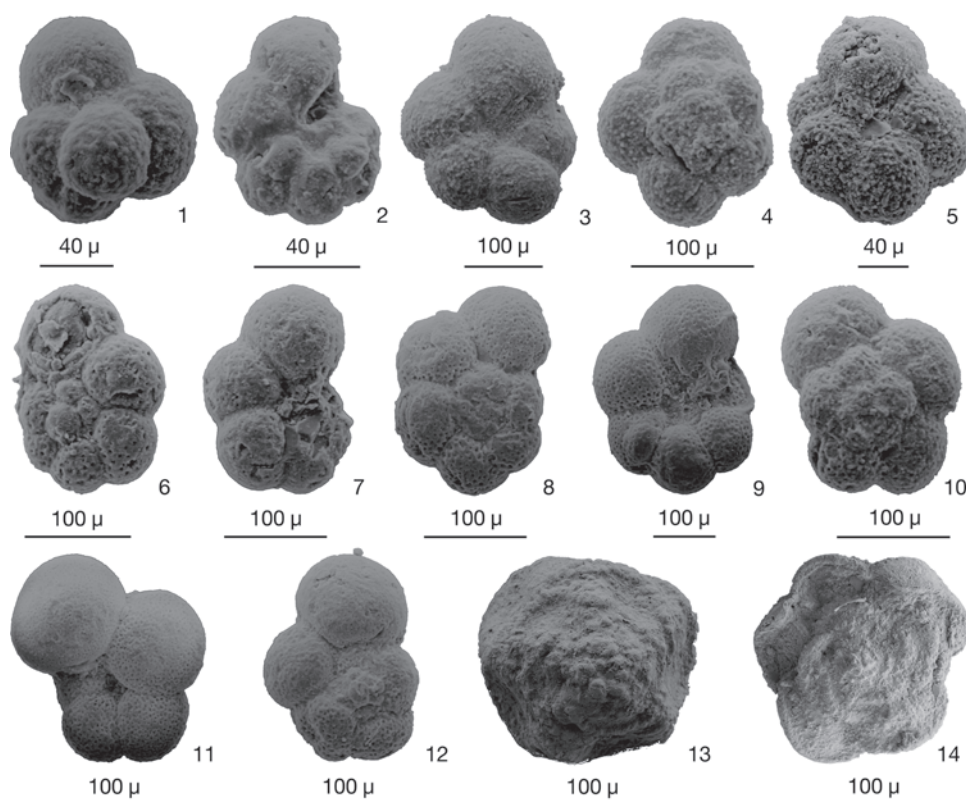


sponds to the top of calcareous nannoplankton Zone NP1. The duration of Biochron NP1 has been estimated at about 700 ky (Berggren et al. 2000; Gradstein et al. 2004). During this time 805 cm of turbidites, slumps, and hemipelagites were deposited at the Knappengraben section (Lahodinsky 1988b). This suggests a sedimentation rate of  $11 \text{ mmky}^{-1}$  in the earliest Paleocene.

### Lithology of the Gamsbach section

The Gamsbach section (Figs A3.6 and A3.7) consists mainly of fine-grained pelitic rocks. Below the K/Pg light to medium gray marlstones and marly limestones occur (mean carbonate content of 11 samples is 54.9 wt.%; mean content of total organic carbon is 0.18 wt.%), which are interbedded with thin (< 15 cm) sandstone turbidites. Dark gray mottles due to bioturbation are present especially in more indurated marly limestone beds. *Chondrites*- and *Zoophycos*-type burrows were identified. The top of the Maastrichtian consists of 50 cm thick well indurated, bioturbated marly limestone with an irregular, wavy upper surface. Above this surface, 0.2 to 0.4 cm of yellowish clay marks the base of the Paleocene. The yellowish clay is overlain by gray clay with a maximum carbonate content of about 13 wt.% in the upper part of the layer. The overlying 200 cm thick middle to dark gray marl to marlstone contains ca. 20–50 wt.% carbonate (mean content of total organic carbon 0.23 wt.%). Twelve thin (0.5 to 5 cm) sandy to silty turbidite layers are intercalated in the first 9 cm of this marlstone. The color of the marls and marlstones changes up-section from light to medium gray, and they are interbedded with brown to reddish layers. Turbiditic beds become thicker there (up to 14 cm). A variegated marl/marlstone bed (40 cm thick) occurs at 323 cm. It contains clasts of red and brown marly limestone up to 15 cm in diameter and some slump folds. Above this mass-flow bed, the grayish-red marl-marlstone succession extends to the top of the section, 400 cm above the K/Pg boundary.

The marly Cretaceous limestones are regarded largely as hemipelagites deposited above the local calcite compensation depth. Turbidity currents disturbed the fine-grained pelagic sedimentation from time to time, delivering sandy and pelitic material into the basin. The less indurated marl beds were deposited by fine-grained tails of sandy-silty turbidity currents or by mud-rich turbidites. This sedimentation pattern continues after the K/Pg boundary with the deposition of marls and thin sandstone turbidites. No clear-cut distinction can be made between turbidite pelites and hemipelagites due to the overall decrease in carbonate content.



Gams, Knappengraben K/T

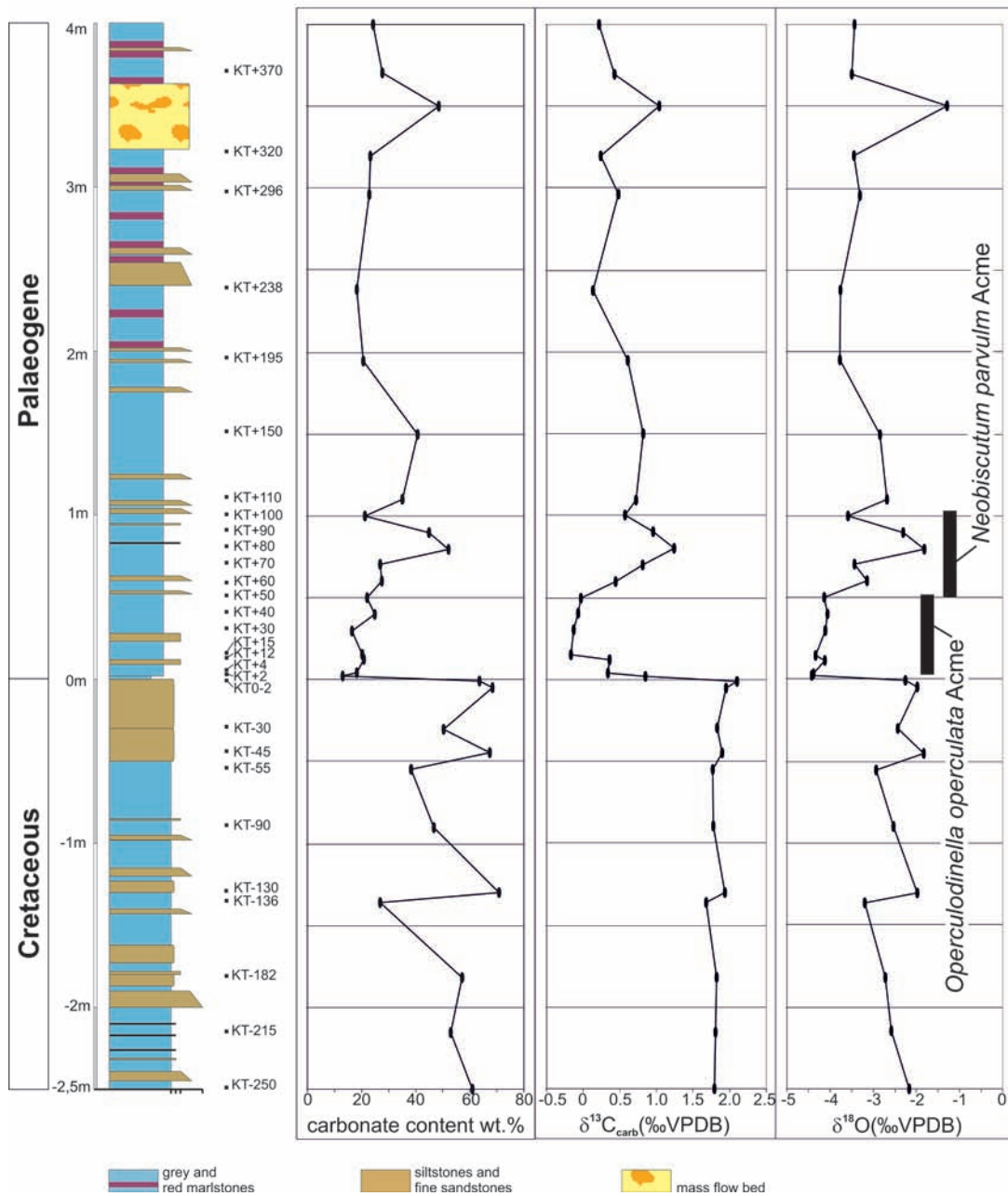
**Figure A3.6** ▶

Photograph of the Gamsbach section. Note that due to higher carbonate contents the Maastrichtian deposits are more resistant to erosion than the Danian ones.

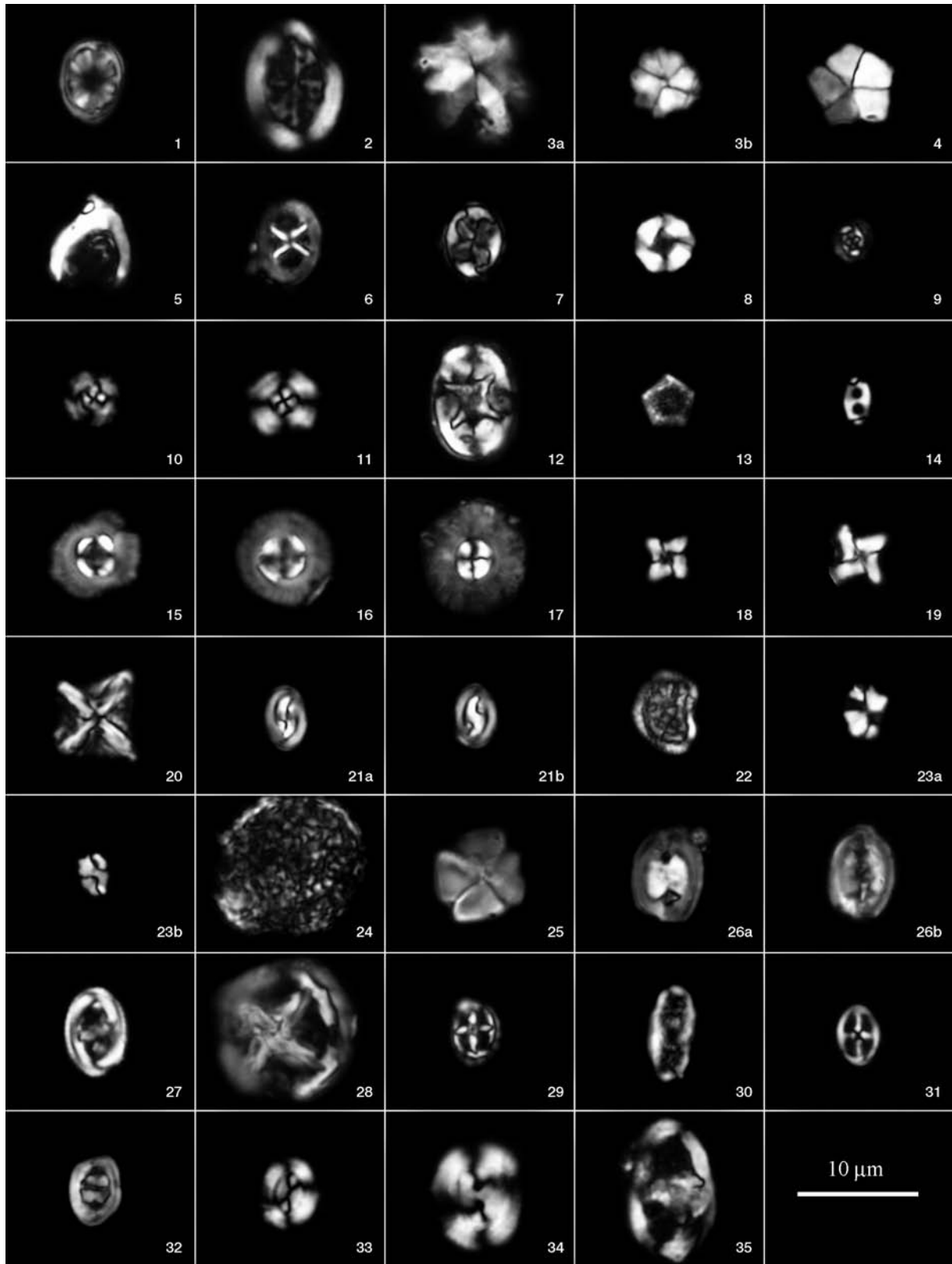


**Figure A3.7** ▼

Stratigraphic log of the Gamsbach section, with carbonate content and variation in the stable isotope abundances.







### Calcareous nannoplankton

The distribution of calcareous nannoplankton species in 9 samples below and 21 samples above the K/Pg boundary is given in Table 1. Figure A3.7 shows the more important species encountered in the Gamsbach section. The reader is referred to Perch-Nielsen (1985) and Burnett (1998) for taxonomy. The zonal schemes of Martini (1971) and Sissingh (1977) have been used for the Cretaceous and

**Figure A3.8** ◀

Calcareous nannoplankton species of the Gamsbach section. All figures were taken with cross-polarized light.

1	<i>Ahmuellerella regularis</i> (Gorka 1957) Reinhardt 1966	KT +370cm
2	<i>Arkhangelskiella cymbiformis</i> Vekshina 1959	KT +4cm
3a	<i>Biantholithus cf astralis</i> Bramlette and Martini 1964	KT +238cm
3b	<i>Biantholithus sparsus</i> Bramlette and Martini 1964	KT +238cm
4	<i>Braarudosphaera bigelowii</i> (Gran and Braarud 1935) Deflandre 1947	KT +80cm
5	<i>Ceratolithoides kamptneri</i> Bramlette and Martini 1964	KT +370cm
6	<i>Chiastozygus amphipons</i> (Bramlette and Martini 1964) Gartner 1968	KT -0.3cm
7	<i>Chiastozygus ultimus</i> Perch-Nielsen 1981	KT +90cm
8	<i>Cribracorona gallica</i> (Stradner 1963) Perch-Nielsen 1973	KT +370cm
9	<i>Cruciplacolithus primus</i> Perch-Nielsen 1977	KT +4cm
10	<i>Cyclagelosphaera alta</i> Perch-Nielsen 1979	KT +50cm
11	<i>Cyclagelosphaera reinhardtii</i> (Perch-Nielsen 1968) Romein 1977	KT +60cm
12	<i>Eiffelithus turriseiffeli</i> (Deflandre 1954) Reinhardt 1965	KT +238cm
13	<i>Goniolithus fluckigeri</i> Deflandre 1957	KT +40cm
14	<i>Lanternithus duocavus</i> Locker 1967	KT +370cm
15	<i>Markalius apertus</i> Perch-Nielsen 1979	KT +370cm
16	<i>Markalius astroporus</i> (Stradner 1963) Hay and Mohler 1967	KT +370cm
17	<i>Markalius inversus</i> (Deflandre 1954) Bramlette and Martini 1964	KT +90cm
18	<i>Micula murus</i> (Martini 1961) Bukry 1963	KT -0.3cm
19	<i>Micula prinsii</i> Perch-Nielsen 1979	KT -0.3cm
20	<i>Micula staurophora</i> (Gardet 1955) Stradner 1963	KT +50cm
21 a,b	<i>Neocrepidolithus cohenii</i> (Perch-Nielsen 1968) Perch-Nielsen 1984	KT +90cm
22	<i>Nephrolithus frequens</i> Gorka 1957	KT +12cm
23 a	<i>Octolithus multiplus</i> (Perch-Nielsen 1973) Romein 1979	KT +370cm
23 b	<i>Octolithus multiplus</i> (Perch-Nielsen 1973) Romein 1979	KT +80cm
24	<i>Operculodinella operculata</i> (Bramlette and Martini 1964) Hildebrand-Habel, Willems and Versteegh 1999	KT +40cm
25	<i>Petrarhabdus copulatus</i> (Deflandre 1959) Wind and Wise 1983	KT +12cm
26 a,b	<i>Podorhabdus? elkefensis</i> Perch-Nielsen 1981	KT +12cm
27	<i>Placozygus fibuliformis</i> (Reinhardt 1964) Hoffmann 1970	KT +70cm
28	<i>Prediscosphaera grandis</i> Perch-Nielsen 1979	KT +40cm
29	<i>Prediscosphaera spinosa</i> (Bramlette and Martini 1964) Gartner 1968	KT -0.3cm
30	<i>Rhagodiscus angustus</i> (Stradner 1963) Reinhardt 1971	KT +296cm
31	<i>Staurolithites crux</i> (Deflandre and Fert 1952) Caratini 1963	KT +238cm
32	<i>Tranolithus orionatus</i> (Reinhardt 1966) Perch-Nielsen 1968	KT +80cm
33	<i>Watznaueria barnesae</i> (Black 1959) Perch-Nielsen 1968	KT -0.3cm
34	<i>Watznaueria biporta</i> Bukry 1969	KT -136cm
35	<i>Zeugrhabdotus embergeri</i> (Noel 1958) Perch-Nielsen 1984	KT +50cm

Paleogene deposits, respectively. The Maastrichtian deposits belong to the upper part of the *Nephrolithus frequens* Zone (Zone CC26), which is defined by the co-occurrence of *Nephrolithus frequens* and *Micula prinsii*. The base of the Paleocene consists of the *Markalius inversus* Zone (Zone NP1), which comprises the interval from the lower occurrence (LO) of *Biantolithus sparsus* and/or *Cyclagelosphaera alta* and/or an increased abundance of the calcareous dinoflagellate cyst *Operculodinella operculata* to the LO of *Cruciplacolithus intermedius* (Bernaola and Monechi 2007).

The carbonate values of the Cretaceous samples are about twice as high as those of the Paleogene samples (52 vs 25 wt.% on average). The negative aspects of carbonate-rich lithologies on the taphonomy of calcareous nannoplankton are reasonably well known (see Bown et al. 2008, for a review). As a result of post-depositional recrystallization small calcite crystals can be selectively dissolved and larger ones overgrown. These processes may be responsible for the scarcity of small nannoplankton species (e.g., *Biscutum constans*) in the Maastrichtian part of the Gamsbach section, and for the low abundances of calcareous nannoplankton there, ranging from 3 to 14 specimens per field of view. Thirty-three species were identified in total in the Maastrichtian samples. The most abundant species is *Micula staurophora*, followed by *Watznaueria barnesae*. Both species are relatively resistant to dissolution and their large numbers are probably an effect of preservational conditions.

The preservation of the Maastrichtian nannoflora is worse than that of the lower Danian where even very small coccoliths (1–3 µm) are well preserved (Fig. A3.9). There, clays isolate nannofossils within an impermeable medium, preventing or inhibiting recrystallization. Due to this better preservation and due to a higher abundance of reworked Campanian species species richness increases from thirty-three species in the Upper Maastrichtian to fifty-five species in the lowermost Paleocene (Table 2). Five new species appear after the terminal Cretaceous event. These new species are *Cyclagelosphaera alta* (LO +2 cm), *Markalius astroporus* (LO +4 cm), *Lanternithus duocavus* (LO +12 cm), *Biantholithus sparsus* (LO +30 cm), and *Markalius apertus* (LO +100 cm). *Zeugrhabdotus sigmoides*, another marker spe-

cies for the basal Paleocene, was encountered only in two samples at the Gamsbach section (Table 1). Similar to the North Sea basin, this species seems to be extremely rare in the lower part of Zone NP1 (e.g., Perch-Nielsen 1979; Lottaroli and Catrullo 2000). Other species such as *Cruciplacolithus primus* and *Neobiscutum parvulum*, previously thought to be indicative of the basal Paleocene, have their first appearance date already in the Maastrichtian (Gardin 2002; Mai et al. 2003; Schulte et al. 2006).

The understanding of nannoplankton survivorship is hampered by uncertainties due to massive reworking of Cretaceous species in the Paleocene. In most K/Pg boundary sections reworking of Cretaceous species is clearly restricted to the basal few centimeters of the Danian (Perch-Nielsen 1985). In the Gamsbach section reworked Campanian species were found in all Paleocene samples with the exception of sample KT+350 cm, which originates from a slump. In the other samples the occurrences of *Broinsonia parca parca* and *Eiffellithus eximius* together with *Calculites obscurus*, *Ceratolithoides aculeus*, *Lucianorhabdus cayeuxii*, *Manivitella pemmatoidea*, *Petrarhabdus copulatus*, *Uniplanarius gothicus* and *Uniplanarius trifidus* indicate erosion of Upper Campanian strata at and above the K/Pg boundary. None of these species has been found in the Maastrichtian samples.

Reworking at the Gamsbach section prevents unequivocal differentiation between survivors and victims of the ecological catastrophe at the end of the Mesozoic. Good indicators for survivorship of taxa are atypical abundances of species, reflecting the ecological stress after the rapid environmental changes at the K/Pg boundary (Perch-Nielsen 1985). Albeit scarcely, the calcareous dinoflagellate cyst *Operculodinella operculata* appears regularly in the Maastrichtian samples but exhibits an unprecedented increase in abundance immediately following the K/Pg event. This corresponds to the “*Thora-cosphaera*” bloom, which has often been reported in studies of the K/Pg boundary. The cyst-producing genus *Operculodinella* was apparently well adapted to the environmental conditions at and just above the boundary (Hildebrand-Habel et al. 1999).

The maximum abundance of *Operculodinella operculata* in the Gamsbach section is between +12cm and +60cm. Within this interval dominant *Operculodinella* specimens are associated with a significantly increased number of the survivor species *Cyclagelosphaera reinhardtii*.

The *Operculodinella operculata* acme is followed by an acme of *Neobiscutum parvulum* (Fig. A3.9 and Table 2). This species becomes very abundant between +70 cm and +110 cm. More than 100 specimens of this small coccolith species occur per field of view, which is the highest total abundance of calcareous nannoplankton in the entire Gamsbach section. In the other samples the total abundance of *Neobiscutum parvulum* is low varying between 2 and 15 specimens per field of view. *Neobiscutum romeinii* was not recognized at Gams. This may be due to the very small size and low birefringence of this species, which makes it difficult to distinguish it from other *Neobiscutum* specimens.

This distribution pattern of *Operculodinella operculata* and *Neobiscutum parvulum* at the Gamsbach section is similar to that observed at other low-paleolatitude sites (Gardin and Monechi 1998; Gardin 2002; Tantawy 2003; Schulte et al. 2006). A bloom of *Braarudosphaera bigelowii* subsequent to the *Operculodinella* bloom has been described from a number of other K/Pg boundary sites (see Hildebrand-Habel and Streng 2003, for a review). *Braarudosphaera* is a genus, probably favored by high nutrient levels in up-welling or near-shore areas (Kelly et al. 2003; Bown 2005). This paleologic preference may explain the rare occurrence of *Braarudosphaera* specimens in the samples of the bathyal Gamsbach section. The open marine environment can also explain the sporadic occurrence of holococcoliths, because this group prefers neritic settings (Perch-Nielsen 1985). More than 178 dinoflagellate species and subspecies were identified from 89 rock samples concentrated

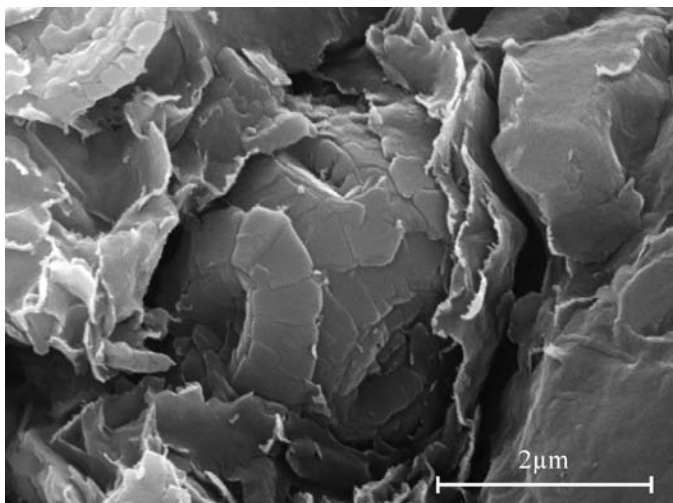


**Figure A3.9 ▲** Scanning electron image of a coccosphere of *Neobiscutum parvulum* (Romein 1979) Varol 1989. Note the clay layers coating the fossil. (sample KT+80cm at the Gamsbach section).

around the K/Pg boundary. In most samples the dinocysts are moderate to well preserved but associated with reworked material. The dinoflagellate cyst assemblages from most samples are dominated (more than 90%) by gonyaulacoid cysts (e.g., *Spiniferites*, *Areoligera*, *Achomosphaera*, *Hystrichosphaeridium*, *Adnatosphaeridium*, *Pterodinium*). Peridinioid cysts occur in low and variable concentrations.

Some well known dinocyst marker species around the K/Pg boundary such as *Carpatella cornuta*, *Spongodinium delitiense*, *Trithyrodinium evittii*, *Palynodinium grillator*, *Manumiella druggii*, *Cordosphaeridium fibrospinosum*, *Membranilarnacia? tenella*, *Senoniasphaera inornata*, *Damassadinium californicum*, and *Dinogymnium acuminatum* are recorded in the studied samples. These marker species can be correlated with other dinocyst bioevents around the K/Pg boundary in the northern and southern hemisphere. In addition to these, *Trabeculidinium quinquetrum*, *Lejeunecysta izerzenensis*, *Batiacasphaera rifensis*, *Impagidinium maghribensis*, and *Cyclonophelium compactum* represent local markers. A *Spongodinium delitiense* acme is recorded in both studied sections (from 80 cm to 180 cm in Gamsbach section and from 100 cm to 220 cm in Knappengraben section above the K/Pg boundary) and is interpreted as a transient cooling event of oceanic surface waters. The stratigraphic distribution of the dinocyst species indicates that dinocysts have not been seriously affected by the mass extinction event at the K/Pg boundary.

### Stable isotopes

Due to the scarcity of marlstone beds in the overall pelitic succession only a moderately high resolution could be achieved for the stable isotope evolution across the K/Pg boundary. No attempt was made to analyze calcareous microfossils separately and we assume that the measured isotope values reflect primarily that of calcareous nannofossils (cf. Perch-Nielsen et al. 1982) plus variable amounts of diagenetically formed calcite cement.

**Table 3** ►

Geochemical data for Gams K/Pg boundary samples. Data by neutron activation analysis. (All data in ppm, except as indicated. Samples: KT0-2a and 2b: shale-textured and compact bulk samples, respectively (thickness about 5cm) just below the K/T-boundary clay; KTK-3 and -4: 2 and 1 cm below the boundary clay, respectively; KTP-5 and 6: 1 and 2 cm above the boundary clay; KTG-7 and -8: duplicate samples of the boundary clay).

	KT0-2a	KT0-2b	KTK	KTK	KTP	KTP	KTG	KTG
	1	2	3	4	5	6	7	8
<b>Na (wt%)</b>	0.27	0.22	0.19	0.19	0.63	0.62	0.32	0.32
<b>K (wt%)</b>	1.25	0.89	0.86	0.92	2.38	2.50	1.60	1.58
<b>Sc</b>	9.87	7.94	6.37	7.59	16.2	16.6	12.7	12.3
<b>Cr</b>	64.0	48.1	31.3	45.0	121	125	136	131
<b>Fe (wt%)</b>	2.98	2.32	1.50	1.87	4.29	4.42	3.89	3.72
<b>Co</b>	8.67	6.25	18.9	20.8	20.1	20.6	57.2	55.7
<b>Ni</b>	52	46	32	44	74	64	79	84
<b>Zn</b>	94	51	49	60	140	141	129	124
<b>As</b>	2.36	2.63	7.41	7.68	6.90	6.96	42.7	42.3
<b>Se</b>	<1.4	<1.2	<1.1	<1.3	0.69	<0.9	<1.8	<1.2
<b>Br</b>	0.7	0.6	0.5	0.7	0.5	0.6	0.7	0.8
<b>Rb</b>	75.8	57.9	33.1	55.0	143	137	87	85
<b>Sr</b>	825	712	615	773	239	240	429	390
<b>Zr</b>	141	105	76	117	188	194	161	143
<b>Sb</b>	0.55	0.45	0.54	0.43	1.42	1.14	1.43	1.61
<b>Cs</b>	4.66	3.61	3.08	3.46	8.28	8.16	5.29	5.15
<b>Ba</b>	189	127	97	115	252	249	148	149
<b>La</b>	25.4	22.0	20.0	21.8	23.8	23.1	18.7	18.5
<b>Ce</b>	53.4	46.4	33.5	46.0	46.5	45.6	39.1	38.6
<b>Nd</b>	25.1	21.0	19.5	21.6	21.0	19.2	17.7	18.6
<b>Sm</b>	5.36	4.50	4.10	4.56	4.50	4.28	3.73	3.72
<b>Eu</b>	1.28	1.12	1.03	1.10	0.98	0.96	0.91	0.88
<b>Gd</b>	5.27	4.26	2.97	3.50	4.24	3.75	3.73	3.69
<b>Tb</b>	0.80	0.70	0.48	0.68	0.64	0.60	0.55	0.55
<b>Tm</b>	0.33	0.28	0.25	0.31	0.32	0.31	0.28	0.27
<b>Yb</b>	1.93	1.76	1.57	1.72	1.92	1.84	1.51	1.45
<b>Lu</b>	0.29	0.25	0.23	0.25	0.29	0.29	0.23	0.22
<b>Hf</b>	2.05	1.58	1.28	1.63	4.43	4.71	2.85	2.83
<b>Ta</b>	0.62	0.44	0.34	0.44	1.31	1.27	0.80	0.79
<b>W</b>	1.6	1.4	1.0	1.3	2.8	2.2	2.7	3.0
<b>Os</b>	<0.2	<0.2	<0.2	<0.2	<0.3	<0.2	<0.3	<0.3
<b>Ir (ppb)</b>	1.67	0.37	0.34	0.84	4.61	4.25	6.05	5.80
<b>Au (ppb)</b>	0.4	0.4	0.4	0.4	1.5	1.7	2.7	2.6
<b>Th</b>	7.20	5.37	3.66	5.22	13.4	12.9	9.10	9.01
<b>U</b>	0.96	0.71	0.75	0.83	1.75	1.57	1.21	1.20

The  $\delta^{13}\text{C}$  values in the uppermost Maastrichtian carbonate beds are rather uniform (ca. +1.8‰) and drop down to values as low as -0.2‰ at the K/Pg boundary. The  $\delta^{13}\text{C}$  values subsequently increase reaching a maximum of +1.2‰ at +80 cm (Fig. 4). Values then decrease up-section. Higher values are only recorded in components embedded in a slump deposit near the top of the studied section interpreted as reworked Cretaceous sediments.

A similar conspicuous negative shift of 2‰ in  $\delta^{13}\text{C}$  has been observed in many K/Pg boundary sections, both locally (Gosau basin: Peryt et al. 1997), regionally (Lattengebirge: Perch-Nielsen et al. 1982; Piave River Valley: Fornaciari et al. 2007) and globally (e.g., Zachos et al. 1989; Corfield 1994). This shift implies a rapid and complete collapse of the ocean's bioproductivity which in a normal biologically productive ocean gives rise to a characteristic  $\delta^{13}\text{C}$  depth gradient, i.e., deep waters being enriched in  $^{12}\text{C}$  (e.g., Zachos et al. 1989; Corfield 1994; Kaiho et al. 1999). This earliest Paleocene C isotope minimum is also observed in terrestrial organic matter reflecting a decrease in  $\delta^{13}\text{C}$  values of atmospheric carbon dioxide (e.g., Maruoka et al. 2007 and references therein).

The  $\delta^{13}\text{C}$  values largely follow the carbonate content in Gamsgraben, i.e., low  $\delta^{13}\text{C}$  values coincide with carbonate-poor marls (Fig. 4). The classic model of a 'Strangelove' ocean (Hsü and McKenzie 1985) subsequent to the K/Pg boundary provides an explanation for this correlation, inasmuch as a low-productivity ocean gives rise to a significantly reduced carbonate accumulation rate (cf. Zachos et al. 1989).

The oxygen isotope data show a pattern that is strikingly similar to that of  $\delta^{13}\text{C}$  (Fig. 4). Maastrichtian  $\delta^{18}\text{O}$  values (-3.2 to -1.8‰) drop sharply at the K/Pg boundary down to -4.4‰ and remain low in the first 50 cm above the boundary. The values then increase parallel to the  $\delta^{13}\text{C}$  data (with a maximum at 80 cm) and decrease gradually thereafter. A high degree of covariation between both isotope data is commonly regarded as diagnostic of diagenetic alteration, in particular when bulk samples are analyzed. Indeed, scanning electron microscopy has shown that calcareous nannoplankton species from the Maastrichtian of the Gamsbach section commonly exhibit recrystallization and secondary overgrowth. Thus, isotopic reequilibration is implied for that part of the section.

### Trace element geochemistry

Eight samples of the boundary section were analyzed by neutron activation analysis. The results are shown in Table 2. Changes in the contents and ratios of other trace elements, such as the rare earth elements (REE), are evident in the layer that marks the K/Pg boundary. The compositions of the samples do not in general change significantly, and most elemental abundance ratios, as well as the chondrite-normalized REE abundance patterns, show values indicative of an upper crustal source. The samples from the boundary clay display relatively lower REE contents than those above and below it, and the boundary sample itself has the lowest Eu value of all of the samples. This was earlier interpreted by Koeberl and Sigurdsson (1992) as being due to REE mobility during palagonitization of the original impact glass spherules deposited after the impact event, and is somewhat similar to the situation described by MacLeod et al. (2007) for the marine K/Pg section at Demerara Rise.

The siderophile elements show a clear maximum at the K/Pg boundary, with maximum values of about 6 ppb Ir, 56 ppm Co, 80 ppm Ni, and 130 ppm Cr. These values are significantly higher than background values below the boundary, and are higher than these in the samples taken just above the boundary clay. The Ir and Co contents indicate about 1 percent by mass of a chondritic component in the sample. The Ni content is somewhat lower than expected, probably due to post-depositional alteration.

### Summary

The K/Pg-boundary at the Gamsbach section is characterized by (1) an enrichment of the contents of the siderophile elements Ir, Co, Ni, and Cr compared to the background and continental crustal values, (2) a sudden decrease of carbon and oxygen isotope values, (3) a sudden decrease of carbonate content, and (4) an acme of the calcareous dinoflagellate cyst *Operculodinella operculata*, which is succeeded by an acme of the small coccolith species *Neobiscutum parvulum*. The *Neobiscutum* acme is associated with a positive excursion of  $\delta^{18}\text{O}$  indicating a transient cooling of ocean surface waters due to short-lived changes in the configuration of ocean circulation after the impact.

## PICHLER SECTION (GAMS)

Michael Wagreich, Hans Egger, Holger Gebhardt, Omar Mohamed

**Topic:**

Paleocene/Eocene-boundary in a deep-water turbidite setting

**Tectonic unit:**

Northern Calcareous Alps

**Lithostratigraphic unit:**

Gosau Group, Zwieselalm Formation

**Chronostratigraphic units:**

Upper Paleocene to Lower Eocene

**Biostratigraphic units:**

Calcareous Nannoplankton Zones NP9 and NP10

**Location:**

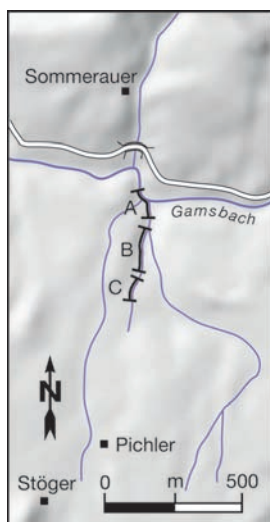
Southern tributary of the Gamsbach (Krautgraben) to the west of Haid (Gams, Styria)

**Coordinates:**

014° 50' 26" E, 47° 39' 49" N

**References:**

Egger et al., 2009; Wagreich et al., 2011.



In the area of Gams, the Danian deposits of the Nierental Formation are characterized by the predominance of red and grey pelagic to hemipelagic marlstones and marly limestones with thin turbidites and single debris flows (Egger et al. 2004, 2009a). This interval is followed by a turbidite-dominated unit assigned to the Zwieselalm Formation (Wagreich et al. 2009). Within this formation, a continuous Paleocene/Eocene boundary section is exposed in a creek in the eastern part of the Gams basin (Egger et al., 2009; Wagreich et al., 2011).

The creek forms a southern tributary of the Gamsbach (Krautgraben) to the west of Haid, south of farm house Sommerauer. The base of the Pichler section is located at the confluence of the Gamsbach and the tributary creek including the cut bank of the Gamsbach itself (section A, Fig. A3.10; Fig. A3.11)

**Figure A3.10** ◀  
Sketch map indicating detailed location of the investigated sections A, B, and C.

with a ca. 34 m thick section. Above a few meters covered by debris and vegetation, a continuous, ca. 43 m-thick section starts within the western branch of the creek (section B, Fig. A3.10), which

includes the Paleocene/Eocene boundary interval indicated by the presence of the dinoflagellate cyst *Apectodinium augustum* and the calcareous nannoplankton species *Discoaster araneus*. Additionally, a negative carbon isotope excursion can be interpreted as the CIE-interval at the base of the Eocene. Using the isotope and paleontological records the thickness of the CIE-interval can be estimated as at least 40 m.

Overlying section B, above a 10m unexposed interval, section C exposes another 27 m of section. The top is overlain by Quaternary moraine.



**Figure A3.11 ▲**  
Section A at the bank of the Gamsbach

**Lithology**

The Pichler section is dominated by sandy to silty turbidites. Significant differences in rock composition result from variations in carbonate content and the presence and absence of conspicuous marl layers. Based on these features, a lower carbonate-bearing and coarser grained interval can be recognized, followed by a carbonate-poor, finer-grained interval around the Paleocene/Eocene boundary that again grades into a more carbonate-rich interval at the top of the section (Fig. A3.12). Transitions from one interval to the other occur over several meters to tens of meters. Therefore, no exact positions of boundaries between those facies types can be given within the section.

The lowermost ca. 13 m of the section (section A, outcrop at cut bank of Gamsbach) are characterized by several up to 110 cm-thick sandy turbidites with clear grading from a gravel-dominated base (components up to 7 cm) to a fine sandstone/siltstone top. Bouma intervals T<sub>a</sub> to T<sub>e</sub> are present, sometimes with prominent convolute lamination (Fig. A3.13). The sandy parts of the turbidite beds grade within a few centimeters into dark grey silty claystones. Thin turbidite

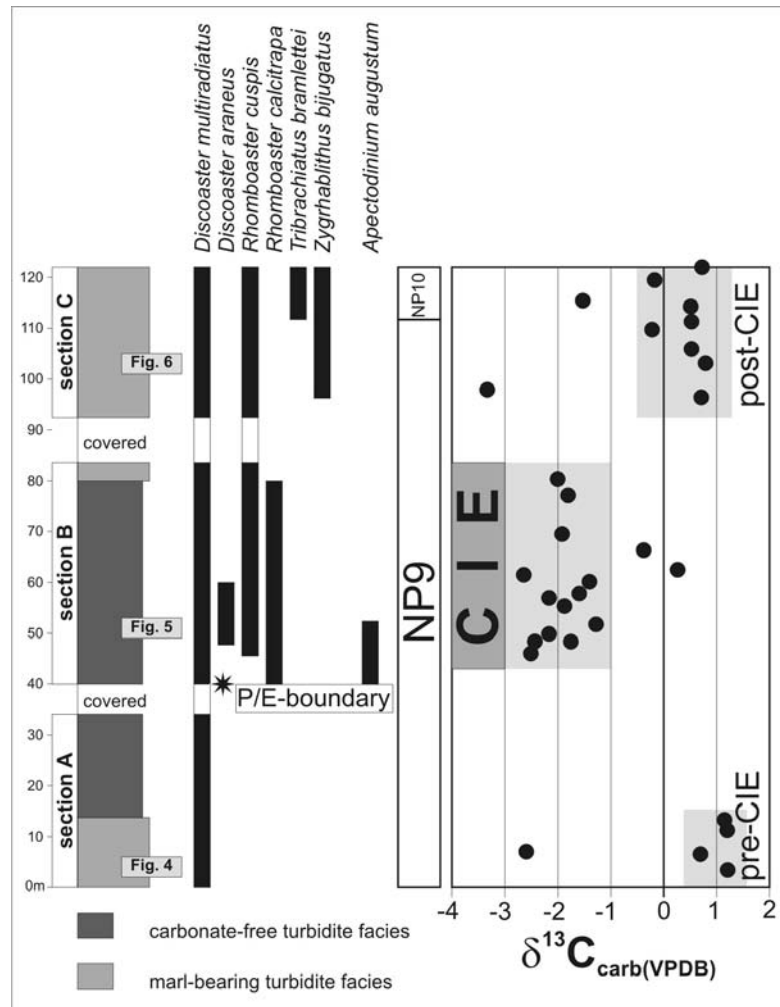


**Figure A3.12 ▲**  
Detailed composite overview log of the studied section with sections A, B and C marked, main biostratigraphic markers (nannofossils, dinoflagellates) recognized, and carbon isotope data of bulk carbonate. Positions of detailed sections of figs. 4 to 6 indicated in log.

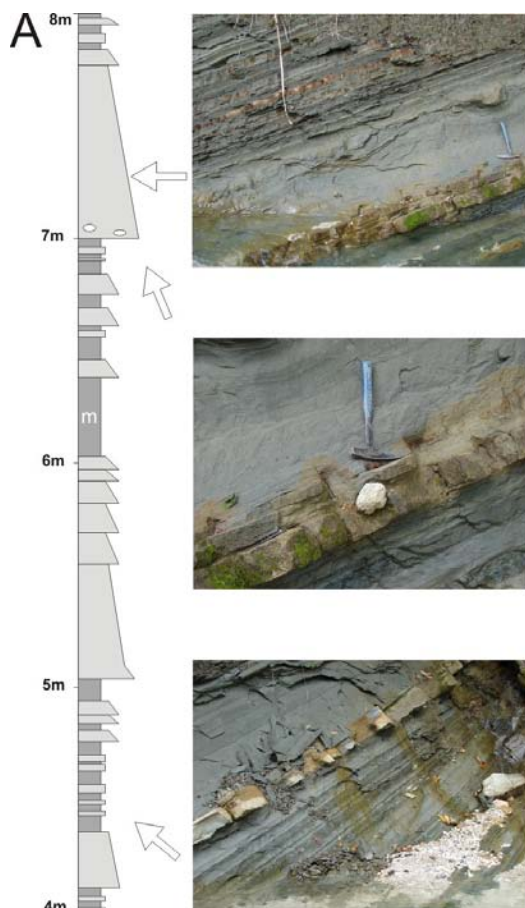
sandstone to coarse siltstone beds (0.5 to 30 cm) are present between these thick beds which constitute the majority of the turbidites present. Thicker beds display complete Bouma sequences whereas thin beds mostly show the Bouma interval  $T_{cde}$ . Amalgamation of several turbidite beds to single thick beds is a common feature. Some clasts of Paleocene platform limestones are present in the turbidite layers.

A 15 cm-thick mud-supported debris flow bed with a silty-clayey matrix and clasts up to 5 cm in diameter is present. Another conspicuous feature of this basal part are up to 80 cm-thick marl beds (mean carbonate content of five samples 12.4 wt%, maximum 16.7 wt%) without any visible bedding. The top parts of these marl beds as well as some of the dark grey thin silt-clay layers show downward bioturbation by mainly *Chondrites*-type burrows. Sandstone/pelite ratios are between 1:1 to 2:1. The turbidites, especially the thin sandy layers, display only weak cementation due to a low carbonate content. Turbiditic shales are dark grey, mainly only a few centimeters thin, and largely devoid of carbonate. No clear fining- or coarsening-upward cycles could be recognized; only at meter 5 of the section a 1 m-thick succession of six amalgamated turbidite beds display a fining-upward and thinning-upward trend.

The turbidite facies is characterized by classical sandy turbidites showing both complete and incomplete, base-truncated Bouma sequences. This corresponds to facies C and D of Walker (1978) and, according to the classification of Pickering et al. (1989), these sandstones fall into the classical turbidite facies C2 (organized sand-mud couplets – classic turbidites). The thick sandstone beds show characteristics for transitional deposition from relatively low- to high-concentrated and high-density turbidity currents. The dark grey clays are interpreted as representing the fine-grained portion of the turbidites. The thicker marl beds present may be interpreted either as (fine-grained) turbidites or hemipelagites. Several observations argue for an origin as a turbidity current: (1) these marl beds follow directly above turbiditic sandstone beds, (2) at 2.5 m in the section 15 cm-thick pebbly mudstone directly grades into

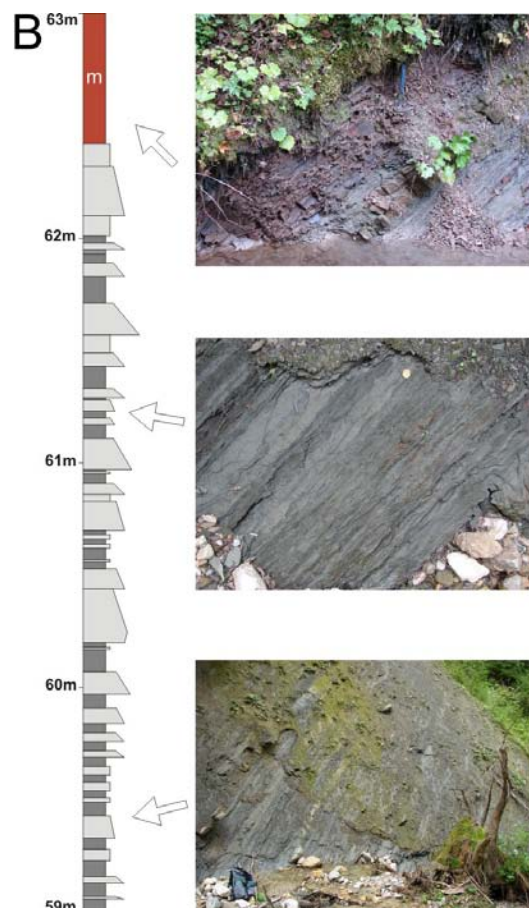
**Figure A3.13** ▼

Detailed sedimentological log from the lower part of section A (4.00 to 8.00 m; white m denotes marl beds) and photographs of typical facies types from this section (arrows point to position of photographs within the section).



**Figure A3.14** ▼

Detailed sedimentological log from the middle part of section B (59.00 to 63.00 m; white m denotes reddish marl bed) and photographs of typical facies types from this section (arrows point to position of photographs within the section).



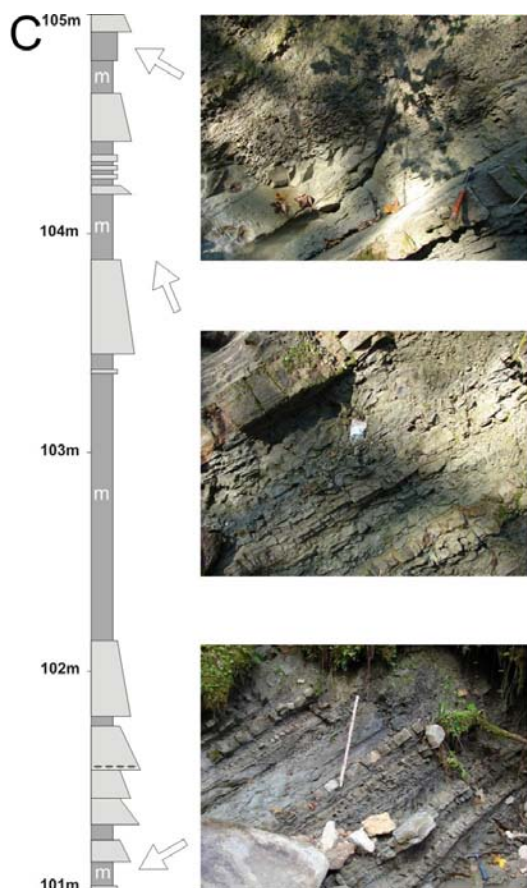


**Figure A3.15** ◀

Detailed sedimentological log from the middle part of section C (101.00 to 105.00 m; white m denotes marl bed) and photographs of typical facies types from this section (arrows point to position of photographs within the section; scale in lower right 90 cm).

a 80 cm-thick marl bed; (3) foraminiferal data also support a transported microfauna and thus argue against a hemipelagic deposition of these marl beds.

This marl-bearing interval grades in the top part of section A into an interval without distinctive marl beds, which ranges up to the upper part of section B, up to ca. section meter 80. There, thin-bedded sandy- to silty turbidites with thin, dark-grey silty claystone intervals prevail. Claystones to marly claystones have carbonate contents of 0 to 6.4 wt% (mean of 28 samples 1.9 wt%). A few sandstone beds up to 48 cm are present but the majority of sandstone layers are only a few centimeters thin. Grading is ubiquitous and thicker sandstones show complete  $T_{a-e}$  Bouma sequences; thinner beds often show only  $T_{cd}$  intervals. Two distinctive reddish brown marly claystone to marl beds (22.9 and 34.2 wt% carbonate content) of up to 85 cm thickness are present at 62 and 66 m of the section. Bioturbation has only very rarely been observed.

Sandstone/pelite ratios are between 2:1 to 5:1. This facies is interpreted as mainly thin-bedded classical turbidites in the sense of Walker (1978: facies D) and Pickering et al. (1989; facies C2.2 and C2.3). The lack of identifiable hemipelagic layers and the high proportion of sand suggests a high-frequency turbidite environment. The reddish claystone layers probably also represent turbidites, i.e. mud turbidites, as also suggested by a transported and poor microfauna (see below).

A prominent feature of the Paleocene/Eocene-boundary interval are siderite concretions, which are conspicuous in outcrops due to their hardness and rusty color (Fig. A3.16). Concretions occur within several levels both in sandy-silty and in silty-clayey material, especially in the middle part of the section. Both, layers enriched in disseminated siderite cement and platy to rounded ellipsoid siderite nodules

Both, layers enriched in disseminated siderite cement and platy to rounded ellipsoid siderite nodules

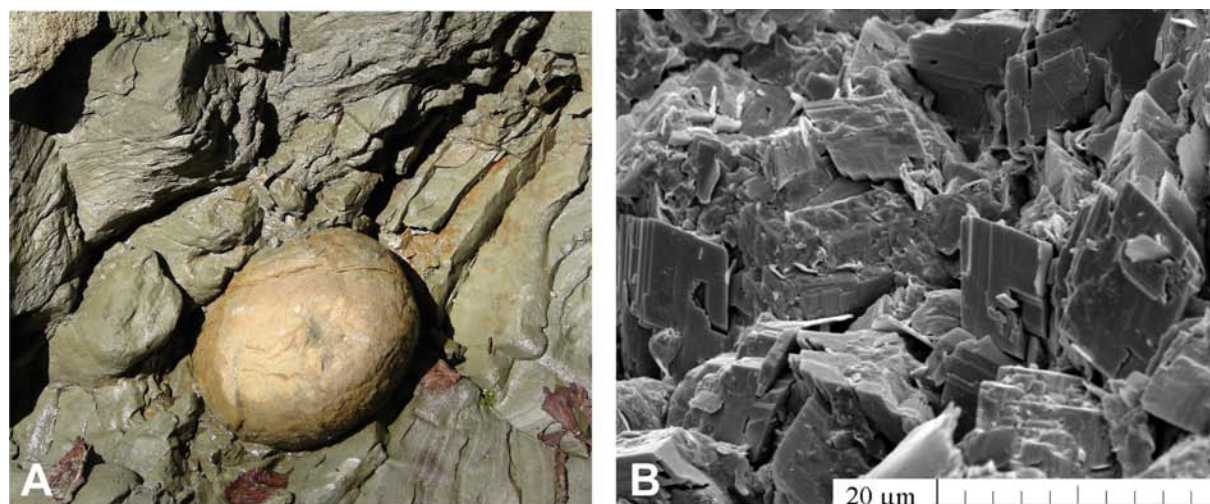


**Figure A3.16** ▲

Siderite concretion (13 cm in diameter), outcrop in middle part of section B, within largely carbonate-free turbidites. 7B. REM picture of diagenetic siderite from concretion in section B.

up to 30 cm in diameter are present. Siderite ranges up to a maximum of 66 wt% within the concretions (41.1 wt% FeO). Mudstones embedding the concretions show FeO values around 6–8 wt%. No significant enrichment in minor elements was observed. A pre-compaction origin of the concretions is evident by the presence of squeezed sedimentary layering around the nodules. Although detailed investigations are missing, an early diagenetic origin of the siderite is probable (e.g. Laenen & De Craen 2004).

Starting at around 80 m in the section, light grey to slightly greenish grey marly claystones and marl beds again occur and become significant, and sandstone beds become thicker again (up to 80 cm). This facies resembles largely the basal interval; however, the carbonate contents rises significantly: the mean of nine samples of marl layers above 90 m in the section is 19.7 wt% and the maximum is 29.0 wt%. Although cm-thick sandstone turbidite beds are still present, thicker sandstones and marls predominate the topmost part of the section above 100 m. Convolute bedding and structures indicative of water-escape processes such as flame and ball-and-pillow structures are often present in the sandstones. Amalgamation of beds is commonly observed. Flute casts indicate a paleotransport direction from SW to NE. Marl beds up to 120 cm thick are intercalated. Foraminiferal data indicate that at least some of the marl beds represent hemipelagites as suggested by an autochthonous foraminiferal assemblage with abundant planktic foraminifera.

### Carbon isotope stratigraphy

Stable isotope measurements of whole-rock samples (Fig.A3.12) are influenced by diagenesis and the small amount of carbonate of the samples, which can be as low as 0.1%. The oxygen isotope values range between -1.0 and -5.5‰ and are considered to be strongly influenced by diagenesis as no systematic variation could be recognized within the section. Carbon isotope values range from +1.2 to -8.9‰. This large variation is considered to be also influenced by diagenesis and the low carbonate content and highly negative values below -8‰ are not considered further. However, except for a few outliers, a clear trend can be seen in the section. The lower part (up to 15 m) is characterized by values around 0.5‰ (mean of six samples 0.43‰). A gap with virtually no carbonate occurs up to ca. 45 m. The following ca. 40 m-thick interval is characterized by slightly negative values around -2‰ (mean of 15 samples -1.7‰). After another gap due to a covered section interval, above 90 m, values increase again to ca. 0.5‰ (mean of 10 samples -0.14‰).

Based on these data and the extended stratigraphic range of marker species we speculate that the CIE of the PETM (e.g. Zachos et al. 2007) is represented by a strongly expanded section of at least 35 ms and present between 45.7 and 80 m. As no isotope data are available from the 33 m-thick interval below 45.7 m due to the lack of carbonate and a covered section interval, the CIE may well comprise an interval thicker than 35 m.

### Biostratigraphy

The biostratigraphic evaluation of the Pichler section is handicapped by the presence of two unexposed intervals, the paucity of carbonate especially in the middle part of the section, and the predominance of turbidites, which result in mostly allochthonous microfossil assemblages. Therefore, both calcareous nanofossil biostratigraphy and especially planktic foraminiferal zonations had to be applied with caution. In addition, some of the samples, especially around the suspected P/E-boundary, were also tested for dinoflagellates. The characteristic dinoflagellate *Apectodinium augustum* (Fig.A3.17) was found in several samples from 40 to 52.50 m (Fig.A3.12), a clear indicator of the P/E-boundary interval (Egger et al. 2000; Crouch et al. 2001; Sluijs et al. 2006,



**Figure A3.17 ▲**  
*Apectodinium augustum* (Harland, 1979) Lentin & Williams, 1981, a dinoflagellate typical for the Paleocene/Eocene-boundary interval; Pichler section, 40 m. Scale bar = 20 µm.

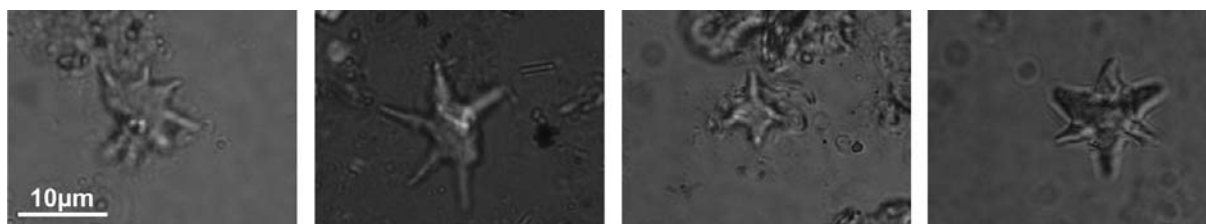


**Figure A3.18 ▲**

Nannofossil marker species from the Pichler section (light microscope, magnification 1000x, all same scale): A. *Discoaster araneus* Bukry, 1971 (sample PE4-07, 57.62 m), B. *Rhomboaster calcitrapa* Gartner, 1971 (sample PE7-07, 51.66 m), C. *Rhomboaster cuspis* Bramlette & Sullivan, 1961 (sample PE14-08, 109.50 m), D. *Tibrachiatus bramlettei* (Brönnimann & Stradner, 1960) Proto Decima et al., 1975 (sample PE18-08, 115.14 m).

2007b, 2008), thus providing additional biostratigraphic information for the nearly carbonate-free interval at the base of section B.

The distribution of nannofossil marker species (Fig. A3.18) indicates the presence of the *Discoaster multiradiatus* Zone (Zone NP9) and the *Tibrachiatus contortus* Zone (Zone NP10) in the the Standard Tertiary zonation of Martini (1971) (Fig. A3.12). In the lower part of the section *Discoaster multiradiatus* occurs regularly. Above a 6 m long unexposed interval, the first *Rhomboaster calcitrapa* was found at 40.40 m and the first *Rhomboaster cuspis* at 45.70 m. The first occurrence of the genus *Rhomboaster* is in the upper third of Zone NP9 and coincides with the onset of the CIE-interval (e.g. Aubry 1996) and, therefore, is a good tool to recognize the P/E-boundary. Another indicator for the CIE-interval is the asymmetrical *Discoaster araneus* whose stratigraphic range is restricted to this interval (e.g. Tremolada & Bralower 2004). *Discoaster araneus* appears for the first time at 47.76 m and ends at 59.92 m of the section. *Zygrhablithus bijugatus*, a holococcolith species, has its first occurrences in the upper part of Zone NP9 (Bown 2005) but becomes common not before the P/E-boundary (Bralower 2002). At the Pichler section, this species is common from 96.20 m to the top of studied section. The base of NP10 was identified by the first appearance of *Tibrachiatus bramlettei* at 110.90 m.

Only two samples are considered to represent almost completely autochthonous foraminiferal assemblages. Sample PEG-36 from near the base of the section at 10.3 m contains a number of rather large agglutinated foraminifera (Fig. A3.19). Some of the species provide limited biostratigraphic control in flysch deposits (Geroch & Nowak 1983). *Reophax subnodulosus* points to an Eocene age.

Sample PEG-05 from the upper portion of the section at c. 110.96 m contains a number of planktic foraminifera that were used for age classification (Fig. A3.20). In particular the concurrent presence of the species *Subbotina velascoensis*, *Acarinina soldadoensis*, *Morozovella acuta*, *M. aequa*, *M. apanthesma*, *M. occlusa*, *M. gracilis* and *M. subbotinae* point to the latest Paleocene - earliest Eocene planktic Zone P5 (Olsson et al. 1999; Pearson et al. 2006) as defined in Berggren et al. (1995). We could not apply the revised zonation of Berggren & Pearson (2005) because index species such as *Acarinina sibaiyaensis* or *Pseudohastigerina wilcoxensis* were not found in the samples. From the foraminiferal point of view, it remains unclear whether this sample is of Paleocene or of Eocene age. The benthic *Aragonia velascoensis* restricts the youngest possible age to zone P5 (Tjalsma & Lohmann 1983).

### Sedimentation rates

Given a 40 m-thick interval that marks the CIE in the Pichler section and the 170 to 210 kyr duration of that interval (Röhl et al. 2000, 2007; Abdul Aziz et al. 2008; Westerhold et al. 2009; Murphy et al. 2010) a sediment accumulation rate of 19 to 23.5 cm/kyr can be calculated. Even higher accumulation rates are calculated by applying shorter duration estimates as reported recently by Sluijs et al. (2007a: 90–140 kyrs; see also Westerhold et al. 2009). Accumulation rates can be compared to those from the terrestrial record of the Bighorn Basin, USA (Sluijs et al. 2007a, Abdul Aziz et al. 2008), but are at least one magnitude larger than accumulation rates in pelagic sections, e.g., in the Belluno Basin in northern Italy (Dallanave et al. 2009). By counting the sandy turbidites within this interval (240 layers) a periodicity of ca. 700 yrs (170 kyrs duration) can be reconstructed for turbidity currents entering the basin. The pronounced input of sand fraction is different from most other sections showing the Paleocene-Eocene transition (e.g. Schmitz & Pujalte 2007) and can be interpreted as a result of regional tectonic activity overprinting the effects of global environmental perturbations.

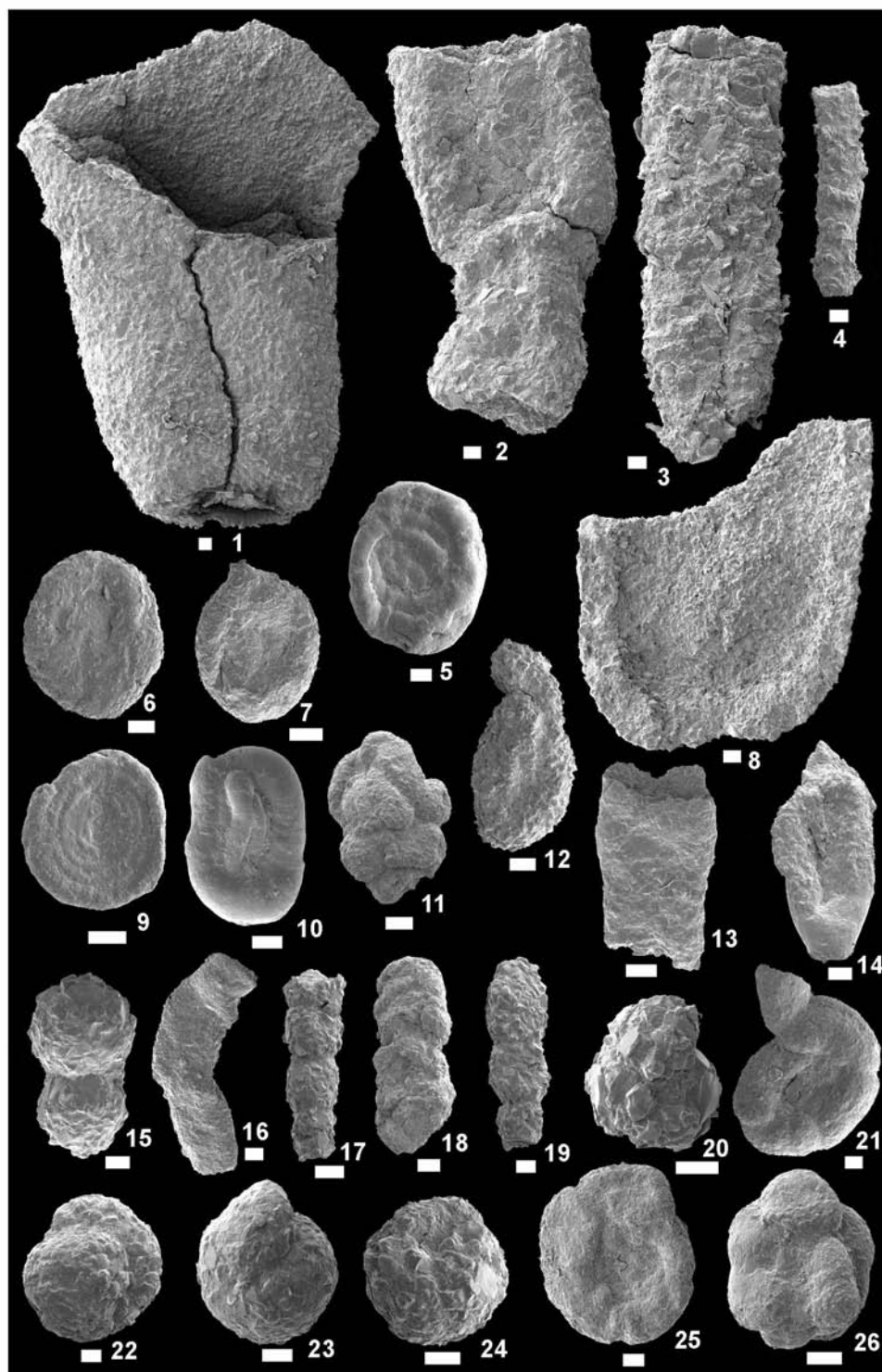


**Figure A3.19 ▲**

Agglutinated foraminifera

1, 2, 8: *Arthrodendron diffusum* (Ulrich, 1904); 3: ?*Nothia* sp.; 4: *Psammosiphonella cylindrica* (Glaessner, 1937); 5: *Ammodiscus glabratus* Cushman & Jarvis, 1928; 6: *Psammosphaera fusca* Schulze, 1875; 7: *Placentammina placenta* (Grzybowski, 1898); 9: *Ammodiscus siliceus* (Terquem, 1862); 10: *Glomospirella gaultina* (Berthelin, 1880); 11: „*Glomospira*” irregularis (Grzybowski, 1898); 12: *Dolgenia* sp.; 13: *Kalamopsis grzybowskii* (Dylasanka, 1923); 14: *Hyperammina* cf. *nuda* Subbotina, 1950; 15: *Reophax duplex* Grzybowski, 1896; 16: *Subreophax* sp.; 17: *Reophax* cf. *minuta* Tappan, 1940; 18: *Hormosina velascoensis* (Cushman, 1926); 19: *Reophax subnodulosus* Grzybowski, 1898; 20: *Trochammina* sp.; 21: *Trochamminoides dubius* (Grzybowski, 1901); 22: *Recurvoides* sp.; 23, 24: *Thalmanammina subturbinata* (Grzybowski, 1898); 25: *Trochamminoides proteus* (Karrer, 1866); 26: *Trochamminoides variolaris* (Grzybowski, 1898); All from sample PEG 36, length of scale bars 0.1 mm.

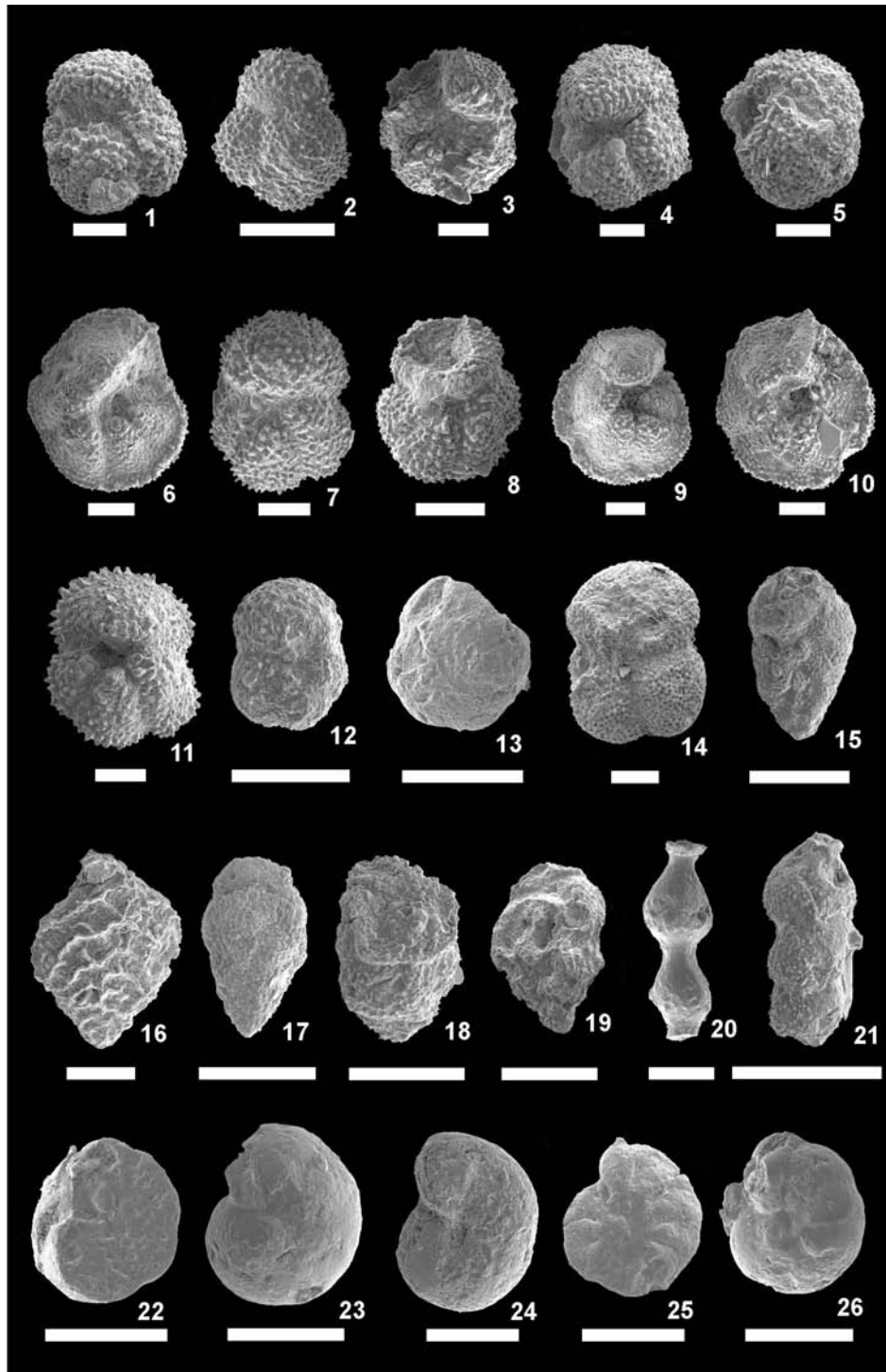


**Figure A3.20 ▲**

Planktic and calcareous benthic foraminifera

1: *Acarinina coalingensis* (Cushman & Hanna, 1927); 2: *Acarinina* cf. *esnaensis* (LeRoy, 1953); 3: *Acarinina nitida* (Martin, 1943); 4: *Acarinina soldadoensis* (Brönnimann, 1952); 5: *Acarinina subsphaerica* (Subbotina, 1947); 6: *Morozovella acuta* (Toulmin, 1941); 7: *Morozovella aequa* (Cushman & Renz, 1942); 8: *Morozovella apantesma* (Loeblich & Tappan, 1957); 9: *Morozovella gracilis* (Bolli, 1957); 10: *Morozovella occlusa* (Loeblich & Tappan, 1957); 11: *Morozovella subbotinae* (Morozova, 1939); 12: *Parasubbotina varianta* (Subbotina, 1953); 13: *Planorotalites pseudoscitula* (Glaessner, 1937); 14: *Subbotina triangularis* (White, 1928); 15: *Chiloguembelina trinitatis* (Cushman & Renz, 1942); 16: *Aragonia velascoensis* (Cushman, 1925); 17: *Bolivina midwayensis* Cushman, 1936; 18: *Bulimina* sp. (?cf. *bradbury* Martin, 1943); 19: *Bulimina* cf. *trinitatis* Cushman & Jarvis, 1928; 20: *Stilostomella gracillima* (Cushman, 1933); 21: *Stilostomella subspinosa* (Cushman, 1943); 22, 23: *Cibicidoides tuxpamensis* (Cole, 1928); 24: *Gavelinella danica* (Brotzen, 1940); 25: *Gavelinella* cf. *micra* (Bermudez, 1949); 26: *Hanzawaia cushmani* (Nuttall, 1930); All from sample PEG 05, except 16 (PEG 04), length of scale bars 0.1 mm.

## PHOTOSTOP AT OPEN CAST MINE ERZBERG



**Figure A3.21 ▲**  
Photograph of the Erzberg mine

Along the road from Gams to the south we will pass the town Eisenerz and the Erzberg ("iron mountain" of about 1500 m altitude). Numerous siderite mineralizations of various sizes occur in the Eastern Alps. Nowadays only the Erzberg mine is still operating with an iron ore production of about 1.4 million tons a year (Ebner et al., 2000). The total ore reserves of Erzberg are estimated as 200 million tons. Mining activities in the area date back to the 3<sup>rd</sup> century A.D. The open cast mine is situated in Paleozoic rocks of the Noric nappe complex of the Greywacke Zone, which forms the basement of the Northern Calcareous Alps. The majority of the ore are metasomatic bodies in Devonian limestones. The mineralizing event must have been post-Variscan as Permian conglomerates were affected by hydrothermal features. The ore bodies are cut off by thrust planes of late Early Cretaceous age. An early Triassic age of the mineralization has been proposed (Ebner et al., 2000).



## PHOTOSTOP AT THE HOCHOSTERWITZ CASTLE



**Figure A3.22 ▲**  
Photograph of the Hochosterwitz castle ([www.kaernten.at](http://www.kaernten.at))

The castle Hochosterwitz at St. Georgen is one of the landmarks of Carinthia. It dates back to the 9<sup>th</sup> century but its appearance today is the result of a major enlargement of the fortification in the 16<sup>th</sup> century. Since then, the castle is the private property of the Khevenhüller family.



## PEMBERGER AND FUCHSOFFEN QUARRIES TO THE WEST OF KLEIN ST. PAUL

Katica Drobne, Hans Egger, Christa Hofmann, Omar Mohamed, Franz Ottner, Fred Rögl

### Topics:

Shallow water limestone with larger foraminifera

### Tectonic unit:

Gurktal nappe complex

### Lithostratigraphic units:

Gutting Group, Holzer Formation, Sittenberg Formation, Dobranberg Formation

### Chronostratigraphic units:

middle Cuisian to middle Lutetian

### Biostratigraphic units:

SBZ10 to SBZ14

### Location:

Fuchsofen Quarry at Dobranberg

### References:

Hillebrandt 1993

The transgression of the Eocene on the Upper Cretaceous was exposed in the Pemberger quarry (Fig. A3.23). Unfortunately, this outcrop was recultivated and destroyed during the last winter. In this outcrop, Upper Campanian marlstone (*Tranolithus phacelosus* Zone, CC23a) of the Pemberger Formation was overlain with an 8 m-thick soft clay of the Holzer Formation. This green and red clay consists essentially of kaolinite (between 73 wt% and 78 wt%) and contains coal lenses and a rich terrestrial palynoflora whereas marine fossils are absent. The top of the clay is formed by 0.5 m of black shale containing 7.6 wt%  $C_{org}$  (Fig. A3.24). This organic rich deposits are the base of the Eocene transgression and yield rich and excellent preserved marine and terrestrial palynofloras. More than 90% of the dinoflagellate assemblage are formed by specimens of the peridinoid genus *Apectodinium* (*A. homomorphum*, *A. parvum*, *A. paniculatum*, and *A. spp.*). Beside these taxa *Homotryblium pallidum* and *Spinidinium echinoideum* occur (see Figs. A3.25 and A3.26).

The terrestrial palynomorph assemblages from the Krapfeld are relatively well preserved and terrestrial pollen and spores are preserved with *Botryococ-*

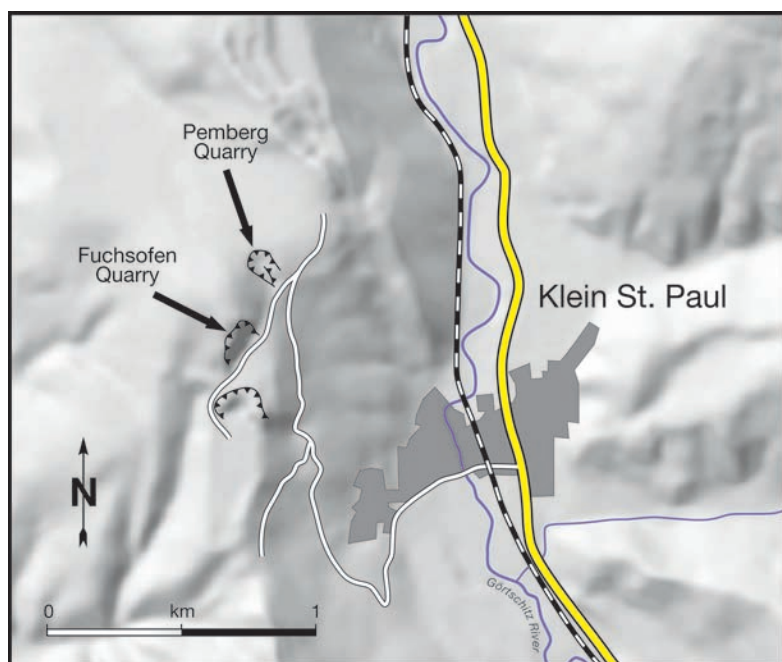


**Figure A3.23 ▲**  
Location of the outcrops to the west of Klein St. Paul

*cus* colonies. Most common elements are angiosperm pollen from families such as Myricaceae, Juglandaceae (various *Normapolles*, *Engelhardia*, *Platycarya*, *Plicatopollis*, *Subtriporopollenites*), Rhoipteleaceae (*Plicapollis plicatus*, Figure A3.27, 1–3), Fagaceae (*Lithocarpus*, *Eotrigonobalanopsis*), Sapotaceae (5 taxa), Araceae (*Proxapertites operculatus*) and Arecaceae (e.g., *Nypa*, Arecoideae various calamoid palms, Plate A3.28, 10–15) and Restoniaceae. Less common to very rare megathermal elements are Anacardiaceae (e.g., cf. *Spondias*, *Lansea*, Plate A3.27, 7-9), Avicenniaceae (black mangrove, *Avicennia*, Plate A3.27, 10–12), Hamamelidaceae (*Corylopsis*, *Tetrathyrum*), Icacinaceae, Malvaceae (e.g., *Kostermannsia*-type, *Adansonia*-type, Plate A3.28, 1–6), Olacaceae, Picrodendraceae (*Aristogeitonia*-type), Rutaceae (*Zanthoxylon*-type, Plate A3.27, 4–6), Styracaceae (*Styrax*, Plate A3.28, 7–9), Theaceae (two *Camellia*-types, Plate A3.27, 13–15), Thymelaceae (*Wikstroemia*), *Alangium* and many more tropical elements.



**Figure A3.24 ▲**  
The base of the transgressive black shale at Pemberger quarry resting on kaolinitic red claystone.

Generally, in term of taxa diversity, floral composition and temperature affinities of the taxa, the lower Eocene of the London Clay (Collinson, 1996) and the Krappfeld area are very similar, although the former is a macroflora.

In the Pemberger quarry, from the lower part of the marine deposits of the Sittenberg Formation *Asilina placentula*, *Nummulites burdigalensis kuepperi*, *Nummulites increscens*, and *Nummulites bearnensis* have been described (Schaub, 1981; Hillebrandt, 1993). This fauna is indicative of the lower part

**Figure A3.25 ►**

(The species name is followed by sample location and England Finder coordinates)

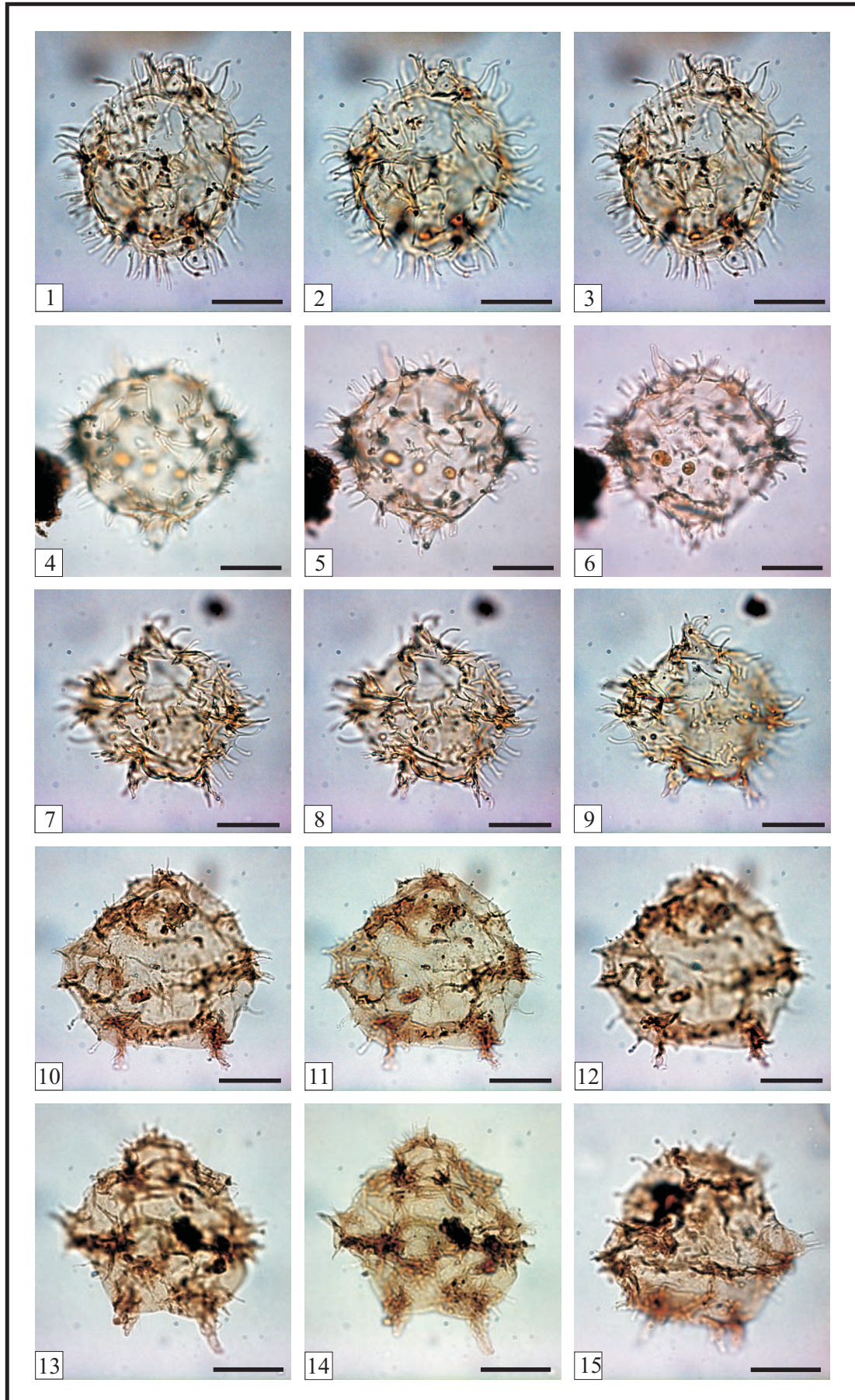
- 1–3 *Apectodinium homomorphum* (Deflandre & Cookson, 1955) Lentin & Williams, 1977; TQ8-10/E, M28/1.
- 4–6 *Apectodinium homomorphum* (Deflandre & Cookson, 1955) Lentin & Williams, 1977; TQ8-10/E, R7/4.
- 7–9 *Apectodinium paniculatum* (Costa & Downie, 1976) Lentin & Williams, 1977; TQ8-10/ G, W24/3.
- 10–12 *Apectodinium parvum* (Alberti, 1961) Lentin & Williams, 1977; TQ8-10/E, B22.
- 13–14 *Apectodinium parvum* (Alberti, 1961) Lentin & Williams, 1977; TQ8-10/E, H21/2.
- 15 *Apectodinium parvum* (Alberti, 1961) Lentin & Williams, 1977; TQ8-10/E, M2.

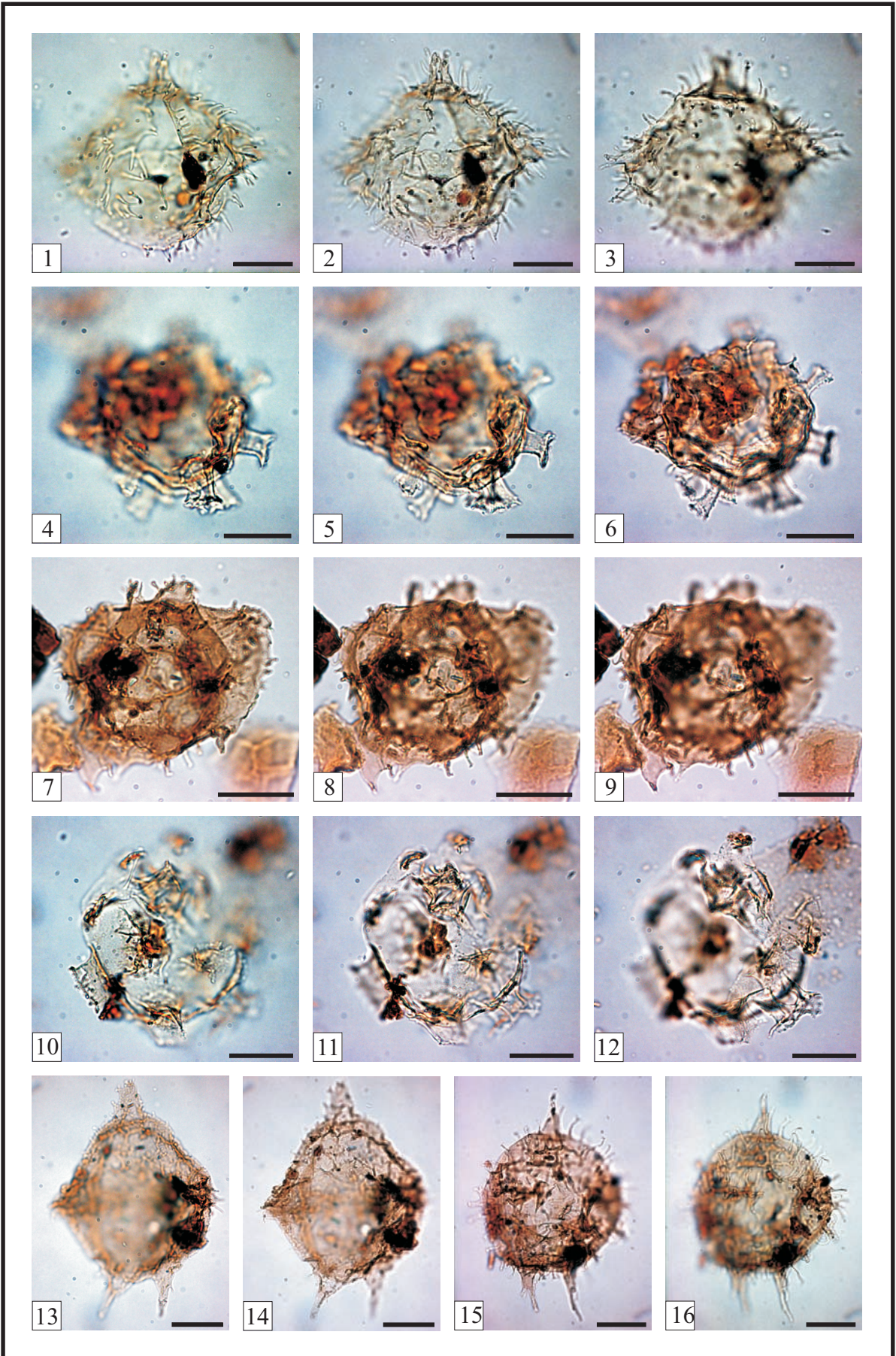
**Figure A3.26 (Page 114)**

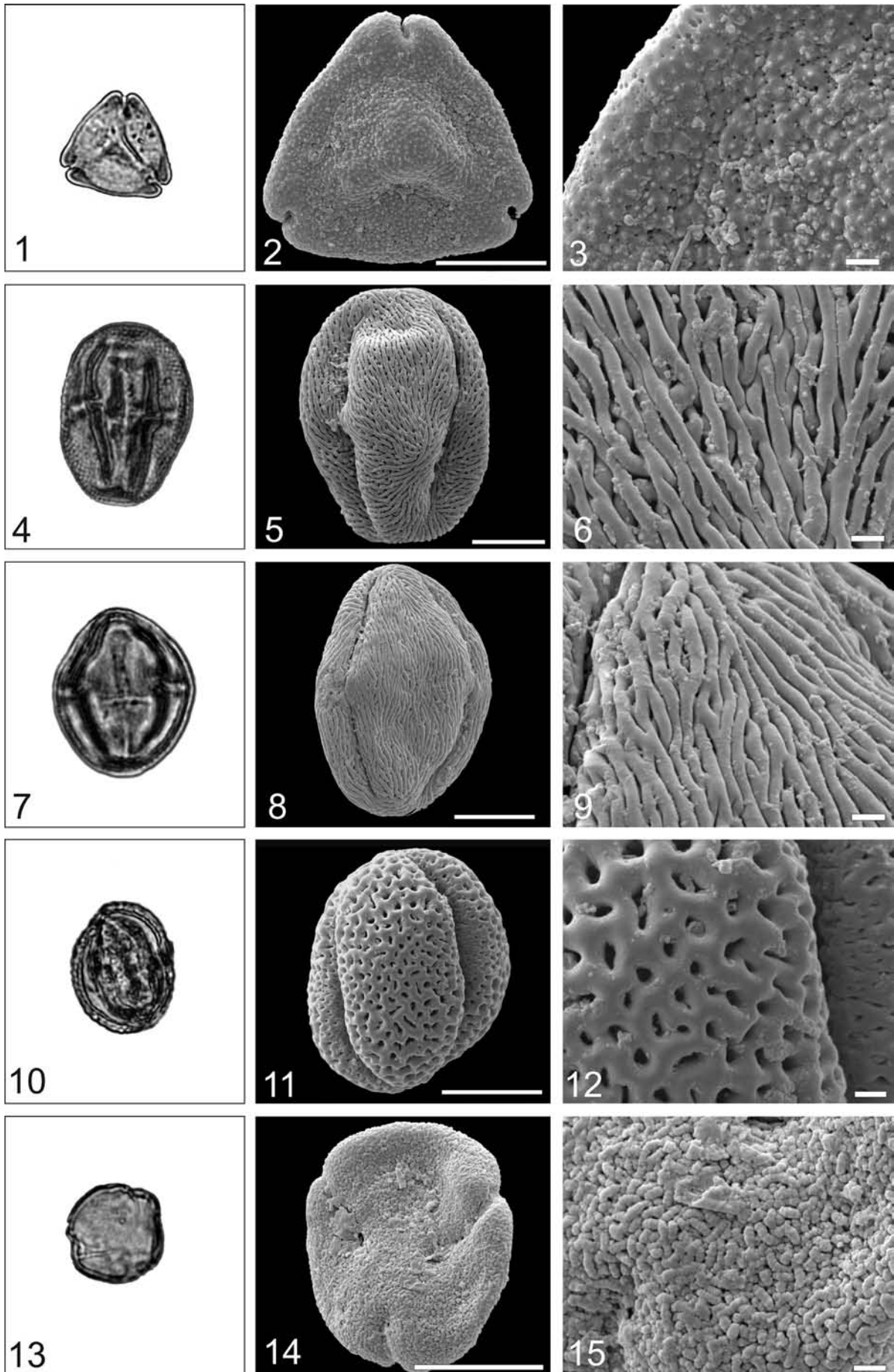
(The species name is followed by sample location and England Finder coordinates)

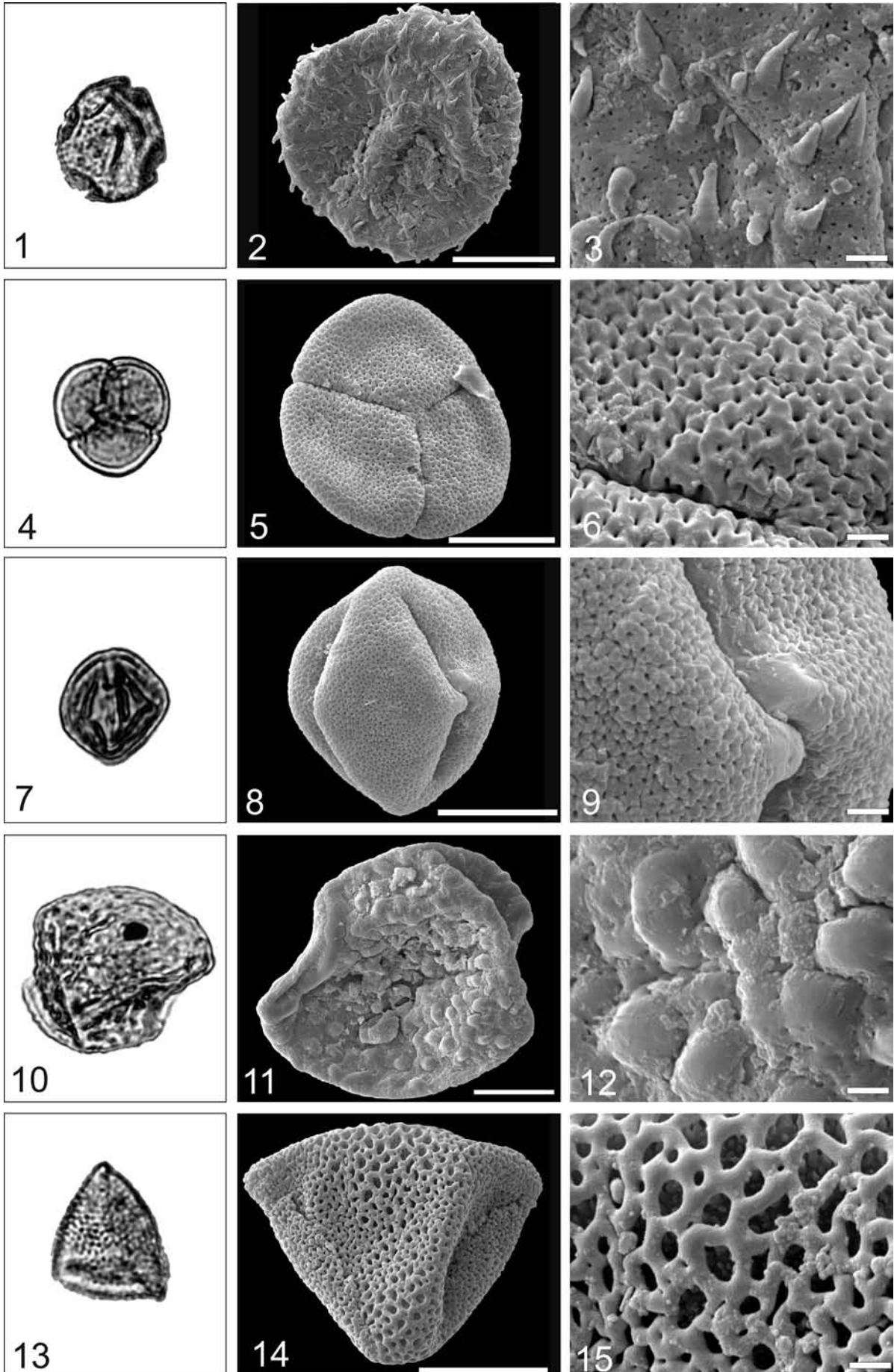
- 1–3 *Apectodinium* spp.; TQ8-10/E, Y43.
- 4–6 *Homotryblium pallidum* Davey & Williams, 1966; TQ8-10/E, L38.
- 7–9 *Palynodinium grillator* Gocht, 1970a; TQ8-10/A, D19.
- 10–12 *Damassadinium californicum* (Drugg, 1967) Fensome et al., 1993b; TQ8-10/E, J30-3.
- 13–14 *Spinidinium echinoideum* (Cookson and Eisenack, 1960a) Lentin & Williams, 1976. Emendation: Sverdlove & Habib, 1974; TQ8-10/E, T8-1.
- 15–16 *Spinidinium* sp.; TQ8-10/E, L27-3.

Plate 1









**Figure A3.27 (Page 115)**

all LM images x 1000, SEM overview bar = 10 µm, SEM detail bar = 1 µm

- 1–3 *Plicapollis plicatus* (Rhoipteliaceae)
- 4–6 *Tricolporopollenites* sp. (Rutaceae)
- 7–9 *Tricolporopollenites* sp. (Anacardiaceae)
- 10–12 *Tricolporopollenites* sp. (Avicenniaceae, Avicennia)
- 13–15 Theaceae, *Camellia*-type

**Figure A3.28 ◀**

all LM images x 1000, SEM overview bar = 10 µm, SEM detail bar = 1 µm

- 1–3 Malvaceae, *Adansonia*-type
- 4–6 *Bombacidites* (Malvaceae, *Kostermannsia*-type)
- 7–9 Styracaceae, *Styrax*
- 10–12 *Diporites*, Arecaceae, Calamae
- 13–15 *Dicolpopollis*, Arecaceae, Calamae

of shallow benthic zone SBZ10, which has been correlated with calcareous nannoplankton Zone NP12 (Serra-Kiel et al. 1998). This suggests that the marine transgression took place within this biochron.

The clay-rich deposits of the Sittenberg Formation are overlain by the pure limestone of the Dobranberg Formation, which is excellently exposed about 300 m to the south, in the Fuchsofen quarry (Fig.A3.29). The limestone is quarried for the cement plant at Wietersdorf. In the lower quarry limestone particularly rich in *Alveolina* spp. occurs (Fig.A3.30). *Alveolina distefanoi* and *A. schwageri* (deter. Drobne) indicate the lower to middle Cuisian (SBZ10-11). For the detrital and partly rhodolithic limestone in the northern part of the upper quarry *Nummulites burdigalensis* cf. *cantabricus* and *Aspilina laxispira* indicate a middle Cuisian age. The limestone in the southern part of the upper quarry is assigned to the Middle Lutetian due to the occurrences of *Nummulites beneharnensis*, *N. hilarionis*, and *N. krappfeldensis* (Hillebrandt, 1993).

The sedimentation of the Gosau Group at Krappfeld ended in the Lutetian. Hillebrandt (1993) reported both *Nummulites hilarionis* and *Nummulites boussaci*, which indicate shallow benthic zone SBZ14, and *Nummulites millecaput* evidencing shallow benthic zone SBZ15. These foraminiferal zones can be correlated with the upper part of calcareous nannoplankton zone NP15 and the lower part of zone NP16 (Serra-Kiel et al., 1998).

It is interesting to compare the Krappfeld outcrops with the Eocene in Slovenia. There, next to the Ivartnik and Kogovnik farm estates, 24 species of alveolinas and 12 species of nummulites were found. Cuisian age was assigned to the samples from Ivartnik and Lutetian age to those from Kogovnik. The presence of several species was also confirmed in cobblestones collected between Mežica, Slovenj Gradec, along the SW foot of Pohorje mountains and Stranice near Slovenske Konjice (Drobne et al., 1977, Pavlovec, 2005). These sites prove the original wide distribution of Eocene marine deposits in this area.



**Figure A3.29 ▲**  
Photograph of the Fuchsofen Quarry (view towards north).

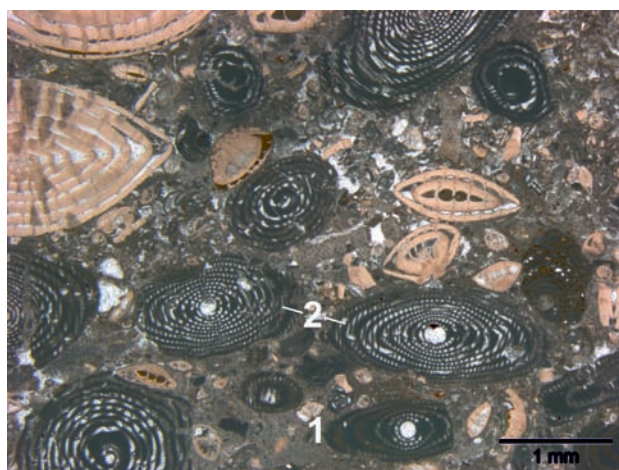


**Figure A3.30 ▲**  
Image of a thin-section of a limestone with nummulites and alveolinas (1... *A. distefanoi* Checchia-Rispoli, 2...*A. schwageri* Checchia-Rispoli), Fuchsofen quarry.



## OUTCROPS ALONG THE SONNBERG FOREST ROAD NEAR GUTTARING

Stjepan Ćorić, Hans Egger, Fred Rögl

### Topics:

Marlstone and limestone with larger foraminifera and calcareous nannoplankton

### Tectonic unit:

Gurktal nappe complex

### Lithostratigraphic unit:

Sittenberg Formation

### Chronostratigraphic unit:

Ypresian

### Biostratigraphic unit:

calcareous nannoplankton Zone NP12

### Location:

Forest road to the west of Guttaring

### References:

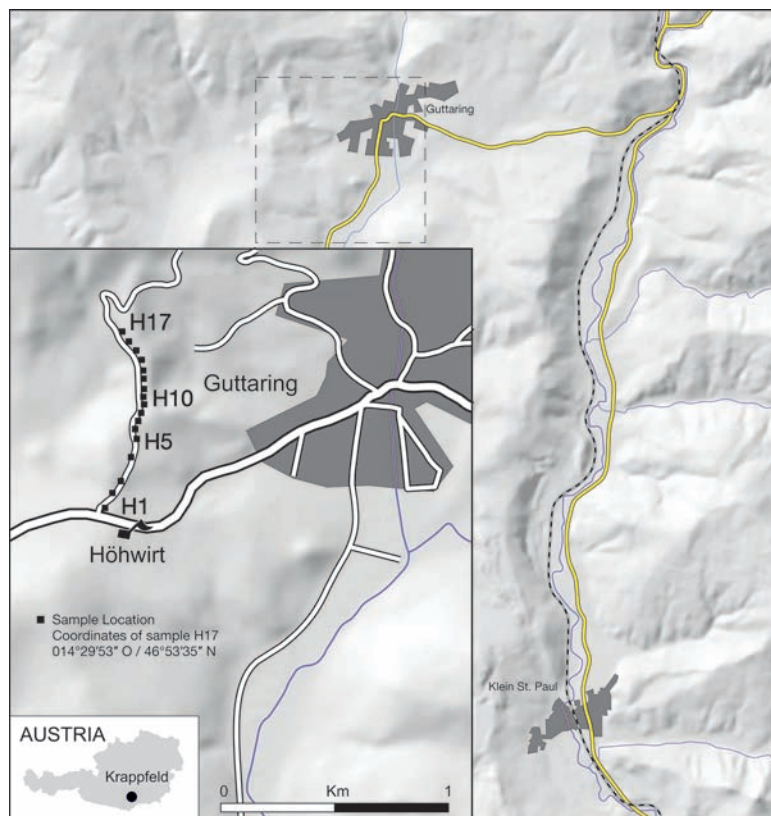
van Hinte 1963; Egger et al., 2009, Wilkens, 1989

Along the first part of the forest road red claystone indicates the presence of the terrestrial Holzer Formation. Actually, in this area coal seams with a thickness of up to almost 2 meters were mined till the 1950s. The Holzer Formation is about 100 m thick in the Sonnberg region, whereas its thickness in the Dobranberg area is only 8 m. The facies of the Eocene in both regions is also different. Predominant marlstone suggests that deposition in the northern Krappfeld (Sonnberg) took place in deeper water than in the southern part (Dobranberg). Few limestone beds consist essentially of nummulites (Fig. A3.32)

Nineteen samples were analyzed for calcareous nannoplankton from the forest road section.

### Figure A3.31 ►

Location of outcrops and sample points along the Sonnberg forest road



The lowermost sample (Höhwirt 1) is barren, whereas the other samples contain moderately to well preserved nannofossils. Regularly occurring nannoplankton taxa are: *Campylosphaera dela* (Bramlette & Sullivan, 1961) Hay & Mohler, 1967, *Coccolithus formosus* (Kamptner, 1963) Wise 1973, *Coccolithus pelagicus* (Wallich, 1877) Schiller, 1930, *Coronocyclus bramlettei* (Hay & Towe, 1962) Bown 2005, *Pontosphaera exilis* (Bramlette & Sullivan, 1961) Romein, 1979, *Pontosphaera pulchra* (Deflandre in Deflandre & Fert, 1954) Romein, 1979, *Pontosphaera versa* (Bramlette & Sullivan, 1961) Sherwood, 1974, *Reticulofenestra minuta* Roth, 1970, *Sphenolithus editus* Perch-Nielsen in Perch-Nielsen et al. 1978, *Sphenolithus moriformis* (Brönnimann &



**Figure A3.32 ▲**

Image of a thin-section from the uppermost limestone bed at the Sonberg section with nummulitids and discocyclinas.

Stradner, 1960) Bramlette & Wilcoxon, 1967, *Sphenolithus radians* Deflandre in Grassé 1952, *Thoracosphaera saxea* Stradner, 1961, *Toweius* spp. and *Zygrhablithus bijugatus* (Deflandre, 1954) Deflandre, 1959. Discoasterids are presented by *Discoaster barbardiensis* Tan, 1927, *D. kuepperi* Stradner, 1959, *D. lodoensis* Bramlette & Riedel, 1954 and scarce *D. salisburgensis* Stradner, 1961. Also occur: *Blackites herculesii* (Stradner, 1969) Bybell & Self-Trail, 1997, *Braarudosphaera bigelowii* (Gran & Braarud, 1935) Deflandre, 1947, *Chiasmolithus consuetus* (Bramlette & Sullivan, 1961) Hay & Mohler, 1967, *Ch. grandis* (Bramlette & Riedel, 1954) Radomski, 1968, *Coronocyclus nitescens* (Kamptner 1963) Bramlette & Wilcoxon 1967, *Lophodolichus reniformis* Bramlette & Sullivan, 1961 etc. Stratigraphical important *Tribrachiatulus orthostylus* Shamrai, 1963 occurs sporadically in the studied samples.

Co-occurrence of *T. orthostylus*, *D. lodoensis* and *D. kuepperi* allow the stratigraphical attribution to nannoplankton Zone NP12 (Martini, 1971) for the whole succession.

The poor planktonic foraminifera assemblage consists predominantly of acarinids: *Subbotina triloculinoides* (Plummer, 1926), *Parasubbotina varianta* (Subbotina, 1953), *Acarinina coalingensis* (Cushman & Hanna, 1922), *Acarinina esnaensis* (LeRoy, 1953), *Acarinina esnehensis* (Nakkady, 1950), *Acarinina pseudotopilensis* Subbotina 1953, *Acarinina soldadoensis* (Brönnimann, 1952), *Acarinina wilcoxensis* (Cushman & Ponton, 1932), *Acarinina* cf. *subsphaerica* (Subbotina, 1947), *Morozovella gracilis* (Bolli, 1957) and *Morozovella marginodentata* (Subbotina, 1953). This indicates a deposition in the Ypresian within the range of planktonic foraminifera Zones P5 to E5.

1	2	3	4	5	6	7	8	9	10	11	12	13	14	15	16	17	Samples
barren	GM	GM	GM	P	GM	GM	G	GM	GM	G	GM	G	GM	GM	G	G	preservation
	F	R	F	R	F	F	F	F	R	F	R	F	F	F	C	C	abundance
	x					x		x		x		x			x	x	<i>Blackites herculesii</i>
																x	<i>B. creber</i>
														x			<i>B. vitreus</i>
												x				x	<i>Blackites truncatus</i>
	x					x	x			x		x	x	x	x		<i>Braarudosphaera bigelowii</i>
								x				x					<i>Braarudosphaera</i> sp.
								x					x				<i>Calcidiscus pacificanus</i>
		x	x		x	x	x					x	x	x	x	x	<i>Calcidiscus</i> sp.
	x	x	x		x	x	x	x		x	x	x	x	x	x	x	<i>Campylosphaera dela</i>
		x															<i>Chiasmolithus bidens</i>
							x	x		x		x	x			x	<i>Ch. consuetus</i>
	x		x			x							x	x	x	x	<i>Ch. grandis</i>
	x																<i>Clathrolithus ellipticus</i>
	x	x	x														<i>Coccolithus foraminis</i>
	x	x	x		x	x	x					x	x	x	x	x	<i>C. formosus</i>
								x					x			x	<i>C. latus</i>
	x	x	x	x	x	x	x	x		x	x	x	x	x	x	x	<i>C. pelagicus</i>
	x																<i>Coccolithus</i> sp.
		x	x		x	x		x		x	x	x	x	x	x	x	<i>Coronocyclus bramlettei</i>
			x		x	x	x				x		x	x		x	<i>C. nitescens</i>
		x							x				x				<i>Coronocyclus</i> sp.
																x	<i>Cyclicargolithus luminis</i>
			x		x					x		x	x		x	x	<i>Discoaster barbardiensis</i>
		x	x		x	x	x	x		x			x	x	x	x	<i>D. kuepperi</i>
	x		x		x					x			x				<i>D. lodoensis</i>
	x																<i>D. salisburgensis</i>
	x			x	x		x						x		x	x	<i>Discoaster</i> sp.
												x				x	<i>Lophodolichus acutus</i>
												x			x		<i>L. mochloporus</i>
									x								<i>L. nascens</i>
										x		x		x	x		<i>L. reniformis</i>
			x												x		<i>Lophodolichus</i> sp.
		x	x	x		x							x		x	x	<i>Markalius inversus</i>
													x				<i>Micrantholithus cf. astrum</i>
							x					x				x	<i>Micrantholithus attenuatus</i>
							x						x				<i>M. excelsus</i>
													x			x	<i>Micrantholithus</i> sp.
		x	x	x	x		x		x	x	x	x	x	x	x	x	<i>Micula decussata</i>
	x		x				x	x	x	x		x	x		x	x	<i>Pontosphaera exilis</i>
			x					x				x		x	x		<i>P. plana</i>
					x	x	x			x		x		x			<i>P. pulchra</i>
		x	x			x	x	x		x		x	x		x	x	<i>P. versa</i>
	x	x	x	x	x	x	x	x	x	x	x	x	x	x	x		<i>Pontosphaera</i> sp.
	x	x	x	x	x	x	x	x	x	x	x	x	x	x	x		<i>Reticulofenestra minuta</i>
			x		x	x	x							x			<i>Sphenolithus acervus</i>
		x	x		x	x	x	x		x	x	x	x	x	x	x	<i>S. editus</i>
	x	x	x		x	x	x	x			x	x	x	x	x	x	<i>S. moriformis</i>
	x	x	x	x	x	x	x					x		x	x	x	<i>S. radians</i>
	x						x			x			x	x			<i>Sphenolithus</i> sp.
	x		x			x	x	x		x			x		x	x	<i>Thoracosphaera heimii</i>
	x	x	x		x	x	x	x	x	x	x	x	x	x	x	x	<i>Th. saxea</i>
	x		x	x	x	x	x	x	x	x	x	x	x	x	x	x	<i>Toweius</i> spp.
	x									x						x	<i>Tribrachiatus orthostylus</i>
												x				x	<i>Triquetrorhabdus carinatus</i>
													x				<i>Trochoaster operosus</i>
			x					x		x		x	x		x	x	<i>Umbilicosphaera jordanii</i>
					x												<i>Zygodiscus adamas</i>
x	x		x		x		x	x	x	x	x	x	x	x	x	x	<i>Zygrhablithus bijugatus</i>
		x					x	x		x	x	x		x	x	x	<i>Zygrhablithus</i> sp.

**Table 1** ◀ Distribution of calcareous nannoplankton in the samples from the Sonnberg section

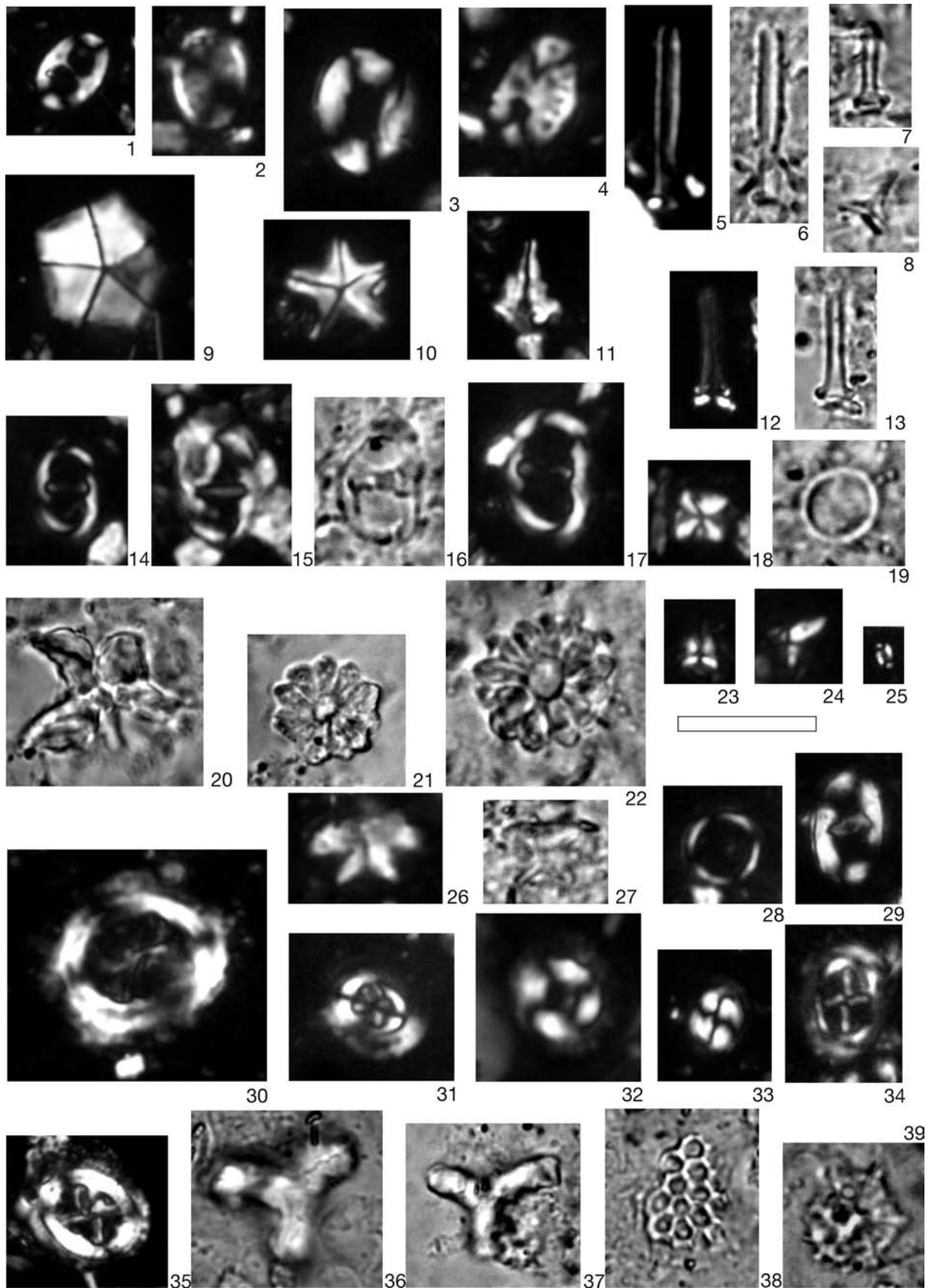


**Figure A3.33** ◀ = Plate Calcareous nannoplankton from the Sonnberg section

Lower Eocene calcareous nanofossils from the Sonnberg section

- Fig. 1 *Pontosphaera exilis* (Bramlette & Sullivan, 1961) Romein, 1979; Sample Höhwirt 2.  
 Fig. 2 *Pontosphaera versa* (Bramlette & Sullivan, 1961) Sherwood, 1974; Sample Höhwirt 4.  
 Fig. 3 *Pontosphaera rimosa* (Bramlette & Sullivan, 1961) Roth & Thierstein, 1972; Sample Höhwirt 15.  
 Fig. 4 *Pontosphaera pulchra* (Deflandre in Deflandre & Fert, 1954) Romein, 1979; Sample Höhwirt 6.  
 Figs. 5, 6 *Blackites herculesii* (Stradner, 1969) Bybell & Self-Trail, 1997; Sample Höhwirt 7.  
 Fig. 7 *Blackites creber* (Deflandre in Deflandre & Fert, 1954) Sherwood, 1974; Sample Höhwirt 2.  
 Fig. 8 *Blackites vitreus* (Deflandre, 1954) Shafik, 1981; Sample Höhwirt 15.  
 Fig. 9 *Braarudosphaera bigelowii* (Gran & Braarud, 1935) Deflandre, 1947; Sample Höhwirt 2.  
 Fig. 10 *Micrantholithus cf. astrum* Bown, 2005; Sample Höhwirt 14.  
 Fig. 11 *Zygrhablithus bijugatus* (Deflandre in Deflandre & Fert, 1954) Deflandre, 1959; Sample Höhwirt 2.  
 Figs. 12, 13 *Blackites truncatus* (Bramlette & Sullivan, 1961) Varol, 1989; Sample Höhwirt 2.  
 Fig. 14 *Lophodolithus acutus* Bukry & Percival 1971; Sample Höhwirt 8.  
 Fig. 15 *Lophodolithus mochlophorus* Deflandre in Deflandre & Fert, 1954; Sample Höhwirt 8.  
 Figs. 16, 17 *Lophodolithus reniformis* Bramlette & Sullivan, 1961; Sample Höhwirt 15.  
 Fig. 18 *Micula decussata* Vekshina 1959; Sample Höhwirt 4.  
 Fig. 19 *Coronocyclus nitescens* (Kamptner 1963) Bramlette & Wilcoxon 1967; Sample Höhwirt 4.  
 Fig. 20 *Discoaster lodoensis* Bramlette & Riedel, 1954; Sample Höhwirt 2.  
 Fig. 21 *Discoaster barbadiensis* Tan, 1927; Sample Höhwirt 17.  
 Fig. 22 *Discoaster salisburgensis* Stradner, 1961; Sample Höhwirt 4.  
 Figs. 23, 24 *Sphenolithus editus* Perch-Nielsen, 1978; Sample Höhwirt 4.  
 Fig. 25 *Reticulofenestra minuta* Roth, 1970; Sample Höhwirt 2.  
 Figs. 26, 27 *Discoaster kuepperi* Stradner, 1959; Sample Höhwirt 4.  
 Fig. 28 *Coronocyclus bramlettei* (Hay & Towe, 1962) Bown 2005; Sample Höhwirt 4.  
 Fig. 29 *Zygodiscus adamas* Bramlette & Sullivan, 1961; Sample Höhwirt 6.  
 Fig. 30 *Chiasmolithus grandis* (Bramlette & Riedel, 1954) Radomski, 1968; Sample Höhwirt 15.  
 Fig. 31 *Chiasmolithus consuetus* (Bramlette & Sullivan, 1961) Hay & Mohler, 1967 Sample Höhwirt 11.  
 Fig. 32 *Coccolithus formosus* (Kamptner, 1963) Wise 1973; Sample Höhwirt 15.  
 Fig. 33 *Coccolithus pelagicus* (Wallich, 1877) Schiller, 1930; Sample Höhwirt 2.  
 Fig. 34 *Campylosphaera dela* (Bramlette & Sullivan, 1961) Hay & Mohler, 1967; Sample Höhwirt 14.  
 Fig. 35 *Chiasmolithus bidens* (Bramlette & Sullivan, 1961) Hay & Mohler, 1967; Sample Höhwirt 3.  
 Figs. 36, 37 *Tribrachiatus orthostylus* Shamrai, 1963; Sample Höhwirt 2 (Fig. 36); Sample 17 (Fig. 37).  
 Fig. 38 *Clathrolithus ellipticus* Deflandre, 1954; Sample Höhwirt 2.  
 Fig. 39 *Trochoaster operosus* (Deflandre, 1954) Martini & Stradner, 1960; Sample Höhwirt 14.



# References

- Abdul Aziz, H., Hilgen, F.J., van Luijk, G.M., Sluijs, A., Kraus, M.J., Pares, J.M. & Gingerich, P.D. (2008): Astronomical climate control on paleosol stacking patterns in the upper Paleocene - lower Eocene Willwood Formation, Bighorn Basin, Wyoming. - *Geology*, 36, 531–534.
- Anderson, K.S., Graham, S.A. and Hubbard, S.M., 2006. Facies, architecture, and origin of a reservoir-scale sand-rich succession within submarine canyon fill: insights from Wagon Caves Rock (Paleocene), Santa Lucia Range, California, U.S.A. *Journal of Sedimentary Research*, 76, 819–838.
- Aubry, M.-P. (1996): Towards an upper Paleocene-lower Eocene high resolution stratigraphy based on calcareous nannofossil stratigraphy. - *Israel Journal of Earth Sciences*, 44, 239–253.
- Berggren, W.A. and Pearson, P.N., 2005. A revised tropical to subtropical Paleogene planktonic foraminiferal zonation. - *Journal of Foraminiferal Research*, 35, 279–298.
- Berggren, W.A., Kent, D.V., Swisher, C.C. and Aubry, M.P., 1995. A revised Cenozoic Geochronology and Chronostratigraphy. Society for Sedimentary Geology Special Publication, 54, 129–212.
- Berggren, W.A., Aubry, M.-P., Fossen van, M., Kent, D.V., Norris, R.D. and Quillevère, F., 2000. Integrated Paleocene calcareous plankton magneto-biochronology and stable isotope stratigraphy: DSDP Site 384 (NW Atlantic Ocean). *Palaeogeography, Palaeoclimatology, Palaeoecology*, 159, 1–51.
- Bernaola, G. and Monechi, S., 2007. Calcareous nannoplankton extinction and survivorship across the Cretaceous-Paleogene boundary at Walvis Ridge (ODP Hole 1262C, South Atlantic Ocean). *Palaeogeography, Palaeoclimatology, Palaeoecology*, 255, 132–156.
- Bown, P.R., 2005. Palaeogene calcareous nannofossils from the Kilwa and Lindi areas of coastal Tanzania (Tanzania Drilling Project 2003-4). *Journal of Nanoplankton Research*, 27, 21–95.
- Brinkhuis, H., Bujak, J.P. and Versteegh, G.J.M., and Visscher, H., 1998. Dinoflagellate-based sea surface temperature reconstructions across the Cretaceous-Tertiary boundary. *Palaeogeography, Palaeoclimatology, Palaeoecology*, 141, 67–83.
- Brinkhuis, H., S. Sengers, A. Sluijs, J. Warnaar and G.L. Williams, 2003. Latest Cretaceous to earliest Oligocene, and Quaternary dinoflagellates from ODP Site 1172, East Tasman Plateau. *Proceedings of the Ocean Drilling Program, Scientific Results*, Volume 189. N. Exon and J. P. Kennett. College Station, Texas, U.S. Government Printing Office.
- Brückl, E., Behm, M., Decker, K., Grad, M., Guterch, A., Keller, G.R. and Thybo, H., 2010. Crustal structure and active tectonics in the Eastern Alps. *Tectonics* 29, doi:10.1029/2009TC002491.
- Bujak, J.P. and D.C. Mudge, 1994. A high-resolution North Sea Eocene dinocyst zonation. *J. Geol. Soc. London* 151, 449–462.
- Bujak, J.P., and Brinkhuis, H., 1998, Global warming and dinocyst changes across the Paleocene/Eocene Epoch boundary, in Aubry, M.P., et al., eds., *Late Paleocene–early Eocene biotic and climatic events in the marine and terrestrial records*: New York, Columbia University Press, pp. 277–295.
- Bujak, J.P., Downie, C., Eaton, G.L., and Williams, G.L., 1980. Dinoflagellate cysts and acritarchs from the Eocene of Southern England. *Special Papers in Palaeontology*, 24, 3–100.
- Bukry, D., 1971. Cenozoic calcareous nannofossils from the Pacific ocean. *Transactions San Diego Society of Natural History*, 16, 303–328.
- Bukry, D., 1973. Low-latitude biostratigraphic zonation. - *Initial Reports of the Deep Sea Drilling Project*, U.S. Government Printing Office, Washington D.C., 15, 685–703.
- Bukry, D., 1975. Coccolith and silicoflagellate stratigraphy, northwest Pacific Ocean, Deep Sea Drilling Project Leg 32. - *Initial Reports of the Deep Sea Drilling Project*, U.S. Government Printing Office, Washington D.C., 32, 677–701.
- Burnett, J.A., with contributions by Gallagher, L.T., and Hampton, M.J., 1998. Upper Cretaceous. In: Bown, P.R. (ed.): *Calcareous Nannofossil Biostratigraphy*, 132–199, Cambridge (Chapman and Hall)
- Butt, A., 1981, *Depositional environments of the Upper Cretaceous rocks in the northern part of the Eastern Alps*: Cushman Foundation Foraminiferal Research, Special Publication, 20, 121 p.
- Collinson, M.E., 2000. Fruit and seed floras from the Palaeocene/Eocene transition and subsequent Eocene in southern England: Comparison and palaeoenvironmental implications. In: Schmitz, B., Sundquist, B., Andreasson, F.P. (eds.). *Early Paleogene Warm Climates and Biosphere Dynamics*, *GFF (Journal of the Geological Society of Sweden)*, 122, 36–37.
- Corfield, R.M., 1994. Palaeocene oceans and climate: an isotopic perspective. *Earth Science Review*, 37, 225–252.
- Crouch, E. M., Heilmann-Clausen, C., Brinkhuis, H., Morgans, H.E.G., Rogers, K.M., Egger, H. and Schmitz, B., 2001. Global dinoflagellate event associated with the Late Paleocene Thermal Maximum: *Geology*, 29, 315–318.

- Dale, B., 1996, Dinoflagellate cyst ecology: modelling and geological applications: In: Jansonius, J. and McGregor, D.C. (eds.), *Palynology: principles and applications*; American Association of Stratigraphic Palynologists Foundation, 3, 1249–1275.
- Dam, G., Nøhr-Hansean, H. and Kennedy, W. J., 1998. The northernmost marine Cretaceous-Tertiary boundary section: Nuussuaq, West Greenland. *Geology of Greenland Survey Bulletin* 180, 138–144.
- Decker, K. and Peresson, H., 1996. Tertiary kinematics in the Alpine-Carpathian-Pannonian system: links between thrusting, transform faulting and crustal extension.- In: Wessely, G. and Liebl, W.: *Oil and gas in Alpidic thrustbelts and basins of central and eastern Europe.- EAGE Special Publication*, 5, pp. 69–77.
- Draxler, I., 2007. Significant Palynomorphs from the Thanetian Kroisbach-Member in Salzburg (Eastern Alps, Austria). *Jahrbuch der Geologischen Bundesanstalt*, 147, 357–377 (Vienna).
- Drobne, K., Pavlovec, R., Drobne F. 1977. Paleogene Larger Foraminifera from the area between Mežica and Slovenj Gradec (NW Yugoslavia). *Razprave, 4. razr.SAZU*, 20, 1–88, 23 pls, Ljubljana.
- Eaton, G.L. 1976. Dinoflagellate cysts from the Bracklesham Beds (Eocene) of the Isle of Wight, Southern England. *Bulletin of the British Museum of Natural History and Geology*, 26, 227–332.
- Egger, H., 1995, Die Lithostratigraphie der Altlengbach-Formation und der Anthering-Formation im Rhodanubischen Flysch (Ostalpen, Penninikum): *Neues Jahrbuch für Geologie und Paläontologie Abhandlungen*, v. 196, p. 69–91.
- Egger, H. and Wagreich, M., 2001. Upper Paleocene – Lower Eocene nannofossils from the Gosau Group of Gams/Styria (Austria). – *Österreichische Akademie der Wissenschaften, Schriftenreihe der Erdwissenschaftlichen Kommissionen*, 14, 465–472.
- Ebner, F., Cerny, I., Eichhorn, R., Götzinger, M., Paar, W.H., Prochaska, W., Weber, L., 2000. Mineral resources in the Eastern Alps and adjoining areas. *Mitteilungen österreichische Geologische Gesellschaft* 92, 157–184.
- Egger, H. and Brückl, E., 2006: Gigantic volcanic eruptions and climatic change in the early Eocene. *International Journal Earth Sciences*, 95, 1065–1070.
- Egger, H. and Schwerd, K., 2008. Stratigraphy and sedimentation rates of Upper Cretaceous deep-water systems of the Rhodanubian Group (Eastern Alps, Germany). *Cretaceous Research*, 29, 405–416.
- Egger, H. and Mohamed, O., 2010. A slope-basin model for early Paleogene deep-water sedimentation (Achthal Formation nov. nom.) at the Tethyan continental margin (Ultrasubalpine realm) of the European Plate (Eastern Alps, Germany). *Austrian Journal of Earth Sciences* 103, 121–137.
- Egger, H., Bichler, M., Homayoun, M., Kirchner, E.C., and Surenian, R., 1996. Spätpaleozäne Bentonite aus der Gosau des Untersberg-Vorlandes (Nördliche Kalkalpen, Salzburg). *Jahrbuch Geologische Bundesanstalt* 139, 13–20.
- Egger H., Lobitzer, H., Polesny, H. and Wagner, L.R., 1997. Trip#1 - Cross section through the oil and gas-bearing Molasse basin into the alpine units in the area of Salzburg, Austria-Bavaria). *Guidebook AAPG International Conference and Exhibition*, 104p.
- Egger, H., Heilmann-Clausen, C. and Schmitz, B., 2000. The Paleocene/Eocene-boundary interval of a Tethyan deep-sea section and its correlation with the North Sea Basin. *Société Géologique de France Bulletin*, 171, 207–216.
- Egger, H., Homayoun, M. and Schnabel, W., 2002. Tectonic and climatic control of Paleogene sedimentation in the Rhodanubian Flysch basin (Eastern Alps, Austria). *Sedimentary Geology*, 152, 247–262.
- Egger, H., Fenner, J., Heilmann-Clausen, C., Rögl, F., Sachsenhofer, R.F. and Schmitz, B., 2003. Paleoproductivity of the northwestern Tethyan margin (Anthering Section, Austria) across the Paleocene-Eocene transition. In: Wing, S.L., Gingerich, P., Schmitz, B., Thomas, E. (eds.), *Causes and Consequences of Globally Warm Climates in the Early Paleogene*, Geological Society of America Special Paper, 369, 133–146.
- Egger, H., Rögl, F., Wagreich, M., 2004: Biostratigraphy and facies of Paleogene deep-water deposits at Gams (Gosau Group, Austria). *Annalen Naturhistorisches Museum Wien*, 106A, 281–307.
- Egger, H., Homayoun, M., Huber, H., Rögl, F. and Schmitz, B., 2005. Early Eocene climatic, volcanic, and biotic events in the northwestern Tethyan Untersberg section, Austria. *Palaeogeography, Palaeoclimatology, Palaeoecology*, 217, 243–264.
- Egger, H., Koeberl, C., Spötl, C., Wagreich, M., Mohamed, O., 2009a: Paleogene deep-water deposits at Gams (Austria): From the K/Pg-boundary to the P/E-boundary in a Tethyan setting.- In: Crouch, E.M., Strong, C.P., Hollis, C.J. (eds.): *Climatic and Biotic Events of the Paleogene (CBEP 2009)*, extended abstracts volume, 49–52.
- Egger, H., Heilmann-Clausen, C., Schmitz, B., 2009b. From shelf to abyss: Record of the Paleocene/Eocene-boundary in the Eastern Alps (Austria). *Geologica Acta*, 7, 215–227.
- Egger, H., Koeberl, C., Wagreich, M. and Stradner, H., 2009c. The Cretaceous-Paleogene (K/Pg) boundary at Gams, Austria: Nannoplankton stratigraphy and geochemistry of a bathyal northwestern Tethyan setting. *Stratigraphy*, 6, 333–345.
- Eldholm, O. and Grue, K., 1994. North-Atlantic Volcanic Margins: Dimensions and Production-Rates. *Journal Geophysical Research*, 99, 2955–2968.
- Fornaciari, E., Giusberti, L., Luciani, V., Tateo, F., Agnini, C., Backman, J., Oddone, M. and Rio, D., 2007. An expanded Cretaceous-Tertiary transition in a pelagic setting of the Southern Alps (central-western Tethys). *Palaeogeography, Palaeoclimatology, Palaeoecology*, 255, 98–131.
- Freimoser, M., 1972. Zur Stratigraphie, Sedimentpetrographie und Faziesentwicklung der Südbayerischen Flyschzone und des Ultrasubalpinen zwischen Bergen / Obb. und Salzburg. *Geologica Bavarica*, 66, 7–91.
- Frisch, W., 1979. Tectonic progradation and plate tectonic evolution of the Alps. *Tectonophysics* 60, 121–139.
- Galeotti, S., Angori, E., Coccioni, R., Ferrari, G., Galbrun, B., Monechi, S., Premoli-Silva, I., Speijer, R. and Turi, B., 2000. Integrated stratigraphy across the Paleocene/Eocene boundary in the Contes-

- sa Road section, Gubbio (central Italy). *Société Géologique de France Bulletin*, 171, 355–366.
- Ganss, O. and Knipscheer, H.C.G., 1956. Die Maastricht-Eozän-Folge des Helvetikums im Sprunggraben bei Oberteisendorf (Obb.) und ihre Gliederung mit Hilfe pelagischer Foraminiferen. *Geologisches Jahrbuch*, 71, 617–630.
- Gardin, S., 2002. Late Maastrichtian to early Danian calcareous nannofossils at Elles (Northwest Tunisia): A tale of one million years across the K-T boundary. *Palaeogeography, Palaeoclimatology, Palaeoecology*, 178, 211–231.
- Gardin, S. and Monechi, S., 1998. Palaeoecological change in middle to low latitude calcareous nannoplankton at the Cretaceous/Tertiary boundary. *Société Géologique de France Bulletin*, 169, 709–723.
- Geroch, S. & Nowak, W. (1983): Proposal of zonation for the Late Tithonian - Late Eocene, based upon arenaceous foraminifera from the Outer Carpathians, Poland. - Benthos '83; 2nd International Symposium on Benthic Foraminifera (Pau, April 1983), pp. 225–239, Pau.
- Geroch, S. and Kaminski, M. A., 1992. The morphology, paleoecology and systematics of *Nothia excelsa* (Grzybowski), a deep-water agglutinated foraminifer. *Annales Societas Geologorum Poloniae*, 62, 255–265.
- Gooday, A. J., 2003. Benthic Foraminifera (Protista) as tools in deep-water palaeoceanography: environmental influences on faunal characteristics. *Advances in Marine Biology*, 46, 1–90.
- Gooday, A. J., Shires, R. and Jones, A.R., 1997. Large, deep-sea agglutinated foraminifera: two different kinds of organization and their possible ecological significance. *Journal of Foraminiferal Research*, 27, 278–291.
- Gohrbandt, K., 1963a. Paleozän und Eozän des Helvetikums nördlich von Salzburg (Haltepunkte DI/1-DI/5). In: Grill, R., Kollmann, K., Küpper, H., Oberhauser, R. (eds.). *Exkursionsführer für das achte mikropaläontologische Kolloquium in Österreich*, 47–57. (Vienna)
- Gohrbandt, K., 1963b. Zur Gliederung des Paläogen im Helvetikum nördlich Salzburg nach planktonischen Foraminiferen. *Mitteilungen der Geologischen Gesellschaft in Wien*, 56, 1–116.
- Grachev, A.F., Korchagin, O.A., Kollmann, H.A., Pechersky, D.M., Tselmovich, A., 2005. A new look at the nature of the transitional layer at the K/T boundary near Gams, Eastern Alps, Austria, and the problem of the mass extinction of the biota. *Russian Journal of Earth Sciences*, 7, 1–45.
- Grachev, A.F., Korchagin, O.A., Tselmovich, V.A., Kollmann, H.A., 2008. Cosmic dust and micrometeorites in the transitional clay layer at the Cretaceous-Paleogene boundary in the Gams Section. *Physics of the Solid Earth*, 44, 555–569.
- Grachev, A.F. (ed.), 2009. The K/T boundary of Gams (Eastern Alps, Austria) and the nature of terminal Cretaceous mass extinction. *Abhandlungen Geologische Bundesanstalt*, 63, 1–199.
- Gradstein, F., Ogg, J. and Smith, A., 2004. *A Geologic Time Scale*, 589 p. (Cambridge University Press).
- Graup, G., and Spettel, B., 1989. Mineralogy and phase-chemistry of an Ir-enriched pre-K/T layer from the Lattengebirge, Bavarian Alps, and significance for the KTB problem. *Earth and Planetary Science Letters* 95: 271–290
- Gümbel, C.W., 1862. *Geognostische Beschreibung des bayerischen Alpengebirges und seines Vorlandes*. 950 p., Gotha (Justus Perthes).
- Habib, D., Olsson, R.K., Liu, C. and Moshkovitz, S., 1996. High-resolution biostratigraphy of sea-level low, biotic extinction, and chaotic sedimentation of the Cretaceous-Tertiary boundary in Alabama, north of the Chicxulub crater. In: Ryder, G., Fastovsky, D. and Gartner, S. (Eds.), *The Cretaceous/Tertiary Event and Other Catastrophes in Earth history*. Geological Society of America, Special Paper, 307, pp. 243–252.
- Hagn, H., 1960. Die stratigraphischen, paläogeographischen und tektonischen Beziehungen zwischen Molasse und Helvetikum im östlichen Oberbayern. *Geologica Bavarica*, 44, 5–208.
- Hagn, H., 1967. Das Alttertiär der Bayerischen Alpen und ihres Vorlandes. *Mitteilungen Bayerische Staatssammlung Paläontologie und historische Geologie*, 7, 245–320.
- Hagn, H., Costa, L.I., Herm, D., Hillebrandt, A. v., Höfling, R., Lindenberg, H.G., Malz, H., Martini, E., Moussavian, E., Perch-Nielsen, K., Pfeil, F.H., Risch, H., Schaub, H., Schmidt, K., Schroeder, R., Urlichs, M., Voigt, E., Wehner, H., Weiss, W., Witt, W., 1981. Die Bayerischen Alpen und ihr Vorland in mikropaläontologischer Sicht (Exkursionsführer 17. europäisches Mikropaläontologisches Kolloquium. *Geologica Bavaria* 82, 1–408.
- Hancock, H.J.L. & Dickens G.R. (2005): Carbonate dissolution episodes in Paleocene and Eocene sediment, Shatsky Rise, West-Central Pacific. -In Bralower et al. (Eds.) *Proc. ODP, Sci. Results*, 198, 1–24 (online).
- Harland, R., 1979. The *Wetzeliella* (Apectodinium) homomorphus plexus from the Paleogene/earliest Eocene of North-West Europe. IV International Palynological Conference, Lucknow (1976-1977), 2, 59–70.
- Hay, W.W., 2004. Carbonate fluxes and calcareous nannoplankton. In: Thierstein, H.R. and Young, J.R. (eds.): *Coccolithophores*, pp.509–528 (Springer).
- Heilmann-Clausen, C., 1985. Dinoflagellate stratigraphy of the uppermost Danian to Ypresian in the Viborg 1 borehole, central Jylland, Denmark: *Danmarks Geologiske Undersøgelse, ser. A*, 7, 1–69.
- Heilmann-Clausen, C. and Costa, L.I., 1989. Dinoflagellate Zonation of the Uppermost Paleocene? to Lower Miocene in the Wursterheide Research Well, NW Germany. *Geologisches Jahrbuch, Ser. A*, 111, 431–521.
- Heilmann-Clausen, C. and Egger, H., 1997. An ash-bearing Paleocene/Eocene sequence at Anthering, Austria: biostratigraphical correlation with the North Sea Basin. *Danmarks og Grønlands undersøgelse rapport*, 1997/87, 13.
- Heilmann-Clausen, C. and Egger, H., 2000. The Anthering outcrop (Austria), a key section for correlation between Tethys and northwestern Europe near the Paleocene/Eocene boundary: *GFF (Journal of*

- the Geological Society of Sweden), 122, 69.
- Heilmann-Clausen, C. and Van Simaey, S., 2005. Dinoflagellate cysts from the Middle Eocene to ?lowermost Oligocene succession in the Kysing research borehole, central Danish Basin. *Palynology*, 29, 141–204.
- Heister, L.E., O'Day, P.A., Brooks, C.K., Neuhoﬀ, P.S. and Bird, D.K., 2001. Pyroclastic deposits within the East Greenland Tertiary flood basalts. *Journal Geological Society London*, 158, 269–284.
- Hemleben, C., Spindler, M. & Anderson, O.R. (1989): *Modern planktonic foraminifera*. Springer Verlag, New York, 363 pp.
- Herm, D., Hillebrandt, A. and Perch-Nielsen, K., 1981. Die Kreide/Tertiärgrenze im Lattengebirge (Nördliche Kalkalpen) in mikropaläontologischer Sicht. *Geologica Bavarica*, 82: 319–344.
- Hesse, R., 1973. Flysch-Gault und Falknis–Tasnagault (Unterkreide): Kontinuierlicher Übergang von der distalen zur proximalen Flyschfazies auf der penninischen Trogebene der Alpen. *Geologica et Palaeontologica*, Sonderband 2, 90p., Marburg.
- Hesse, R., 1975. Turbiditic and non-turbiditic mudstone of Cretaceous flysch sections of the East Alps and other basins. *Sedimentology*, 22, 387–416.
- Hildebrand-Habel, T., Willems, H. and Versteegh, G.J.M., 1999. Variations in calcareous dinoflagellate associations from the Maastrichtian to Middle Eocene of the western South Atlantic Ocean (Sao Paulo Plateau, DSDP Leg 39, Site 356). *Review of Palaeobotany and Palynology*, 106, 57–87.
- Hildebrand-Habel, T. and Streng, M., 2003. Calcareous dinoflagellate associations and Maastrichtian-Tertiary climatic change in a high-latitude core (ODP Hole 689B, Maud Rise, Weddell Sea). *Palaeogeography, Palaeoclimatology, Palaeoecology*, 197, 293–321.
- Hillebrandt, A. v., 1962. Das Paleozän und seine Foraminiferenfaunen im Becken von Reichenhall und Salzburg. *Bayerische Akademie der Wissenschaften mathematisch-naturwissenschaftliche Klasse Abhandlungen*, 108, 1–113.
- Hillebrandt, A.v., 1993. Nummuliten und Assilinen aus dem Eozän des Krappfeldes in Kärnten (Österreich). *Zitteliana*, 20, 277–293.
- Hsü, K.J. and McKenzie, J.A., 1985. A 'Strangelove' ocean in the earliest Tertiary. In: Sundquist, E.T. and Broecker, W.S. (eds.), *The carbon cycle and atmospheric CO<sub>2</sub>: natural variations, Archean to Present*. *Geophysical Monographs*, 32, 487–492.
- Huber, H., Koeberl, C. and Egger, H., 2003. Geochemical study of Lower Eocene volcanic ash layers from the Alpine Anthering Formation, Austria. *Geochemical Journal*, 37, 123–134.
- Iakovleva, A.I. & Heilmann-Clausen, C., 2007. *Wilsonidium pechoricum* new species – a new dinoflagellate species with unusual asymmetry from the Paleocene/Eocene transition. *J. Paleont.* 8, 1020–1030.
- Iakovleva, A.I. and C. Heilmann-Clausen, 2010. Eocene dinoflagellate cyst biostratigraphy of research borehole 011-BP, Omsk region, southwestern Siberia. *Palynology* 34, 195–232.
- Jones, R.W. and Charnock, M.A., 1985, „Morphogroups“ of agglutinating foraminifera. Their life positions and feeding habits and potential applicability in (paleo)ecological studies. *Revue Paleobiologique*, 4, 311–320.
- Kaiho, K., 1999. Effect of organic carbon flux and dissolved oxygen on the benthic foraminiferal oxygen index (BFOI). *Marine Micropaleontology*, 37, 67–76.
- Kaminski, M.A., Kuhnt, W., and Radley, J.D., 1996. Palaeocene–Eocene deep water agglutinated foraminifera from the Numidian Flysch (Rif, Northern Morocco): their significance for the palaeoceanography of the Gibraltar gateway. *Journal of Micropalaeontology*, 15, 1–19.
- Kedves, M., 1980. Palynological investigations on Austrian Upper Cretaceous and Lower Tertiary sediments. *Acta Biologica Szeged*, 26, 63–77.
- Kelly, D.C., Norris, R.D. and Zachos, J.C., 2003. Deciphering the paleoceanographic significance of Early Oligocene *Braarudosphaera* chalks in the South Atlantic. *Marine Micropaleontology*, 49, 49–63.
- Kley, J. and Voigt, T., 2008. Late Cretaceous intraplate thrusting in central Europe: Effect of Africa-Iberia-Europe convergence, not Alpine collision. *Geology*, 36, 839–842.
- Kneller, B. and McCaffrey, W., 1999. Depositional effects of flow nonuniformity and stratification within turbidity currents approaching a bounding slope: deflection, reflection and facies variation. *Journal of Sedimentary Research*, 69, 980–991.
- Knox, R. W. O'B. and Morton, A. C., 1988. The record of early Tertiary North Atlantic volcanism in sediments from the North Sea Basin. Early Tertiary Volcanism and the Opening of the NE Atlantic (Morton, A. C. and Parson, L. M., eds.), *Geological Society London Special Publication*, 39, 407–419.
- Kollmann, H.A., 1964. *Stratigraphie und Tektonik des Gosaubeckens von Gams (Steiermark, Österreich)*. *Jahrbuch Geologische Bundesanstalt*, 107, 71–159.
- Köthe, A., 1990. Paleogene Dinoflagellates from Northwest Germany. *Geologisches Jahrbuch, Serie A*, 118, 3–111.
- Kuhn, W. and Weidich, K.F., 1987. Neue mikropaläontologische Ergebnisse aus dem Paleozän des Haunsberg-Helvetikums (Salzburg, Österreich). *Paläont. Zeitschrift* 61, 181–201.
- Kuhnt, W., Kaminski, M.A. and Mouflade, M., 1989. Late Cretaceous deep-water agglutinated foraminiferal assemblages from the North Atlantic and its marginal seas. *Geologische Rundschau*, 78, 1121–1140.
- Lahodinsky, R., 1988. Lithostratigraphy and sedimentology across the Cretaceous/Tertiary Boundary in the Flyschgosau (Eastern Alps, Austria). - *Revista Española Paleontología Special Volume*, 1988: 73–82.
- Larsen, L.M., Fitton, J.G. and Pedersen, A.K., 2003. Paleogene volcanic ash layers in the Danish Basin: compositions and source areas in the North Atlantic Igneous Province. *Lithos*, 71, 47–80.
- Lottaroli, F. and Catrullo, D., 2000. The calcareous nanofossil biostratigraphic framework of the Late Maastrichtian–Danian North Sea chalk. *Marine Micropaleontology*, 39, 239–263.
- Lowe, D.R., 1982. Sediment gravity flows: II. Depositional models with special reference to the depos-

- its of high-density turbidity currents. *Journal of Sedimentary Petrology*, 52, 279–297.
- Luterbacher, H. P., Ali, J. R., Brinkhuis, H., Gradstein, F.M., Hooker, J.J., Monechi, S., Ogg, J.G., Powell, J., Röhl, U., Sanfilippo, A. and Schmitz, B., 2004. The Paleogene Period. In: Gradstein, F.M., Ogg, J.G., Smith, A.G., (eds.). *A Geologic Time Scale 2004*. Cambridge University Press, pp. 384–408.
- MacLeod, K.G., Whitney, D.L., Huber, B.T., and Koberl, C., 2007. Impact and extinction in remarkably complete Cretaceous-Tertiary boundary sections from Demerara Rise, tropical western North Atlantic. *Bulletin of the Geological Society of America*, 119, 101–115.
- Mai, H., Speijer, R.P., and Schulte, P., 2003. Calcareous index nannofossils (coccoliths) of the lowermost Paleocene originated in the late Maastrichtian. *Micropaleontology*, 49, 189–195.
- Martini, E., 1971. Standard Tertiary and Quaternary calcareous nannoplankton zonation.- In: Farinacchi (ed): *Proceedings II Planktonic Conference*, Roma 1970, 2, 739–785.
- Menkveld-Gfellner, U., 1997. Die Bürgen-Fm. Und die Klinsenhorn-Fm.: Formelle Definition zweier lithostratigraphischer Einheiten des Eozäns der helvetischen Decken. *Eclogae geol. Helv.* 90, 245–261.
- Muck, M.T. and Underwood, M.B., 1990. Upslope flow of turbidity currents: A comparison among field observations, theory, and laboratory models. *Geology*, 18, 54–57.
- Mutti, E., 1977. Distinctive thin-bedded turbidite facies and related depositional environments in the Eocene Hecho Group (South-central Pyrenees, Spain). *Sedimentology*, 24, 107–131.
- Murphy, B.H., Farley, K.A. & Zachos, J.C. (2010): An extraterrestrial  $^3\text{He}$ -based timescale for the Paleocene-Eocene thermal maximum (PETM) from Walvis Ridge, IODP Site 1266. - *Geochimica Et Cosmochimica Acta*, 74: 5098–5108.
- Nachtmann, W. and Wagner, L., 1987. Mesozoic and early Tertiary evolution of the Alpine foreland in Upper Austria and Salzburg, Austria. *Tectonophysics*, 137, 61–76.
- Neubauer, F., Genser, J. and Handler, R., 2000. The Eastern Alps: Result of a two-stage collision process. *Mitteilungen österreichische geologische Gesellschaft*, 92, 117–134.
- Oberhauser, R., 1991. Erläuterungen zur geologischen Karte der Republik Österreich 1:25.000 Blatt 110 St. Gallen Süd und 111 Dornbirn Süd. 72 pp., Vienna (Geologische Bundesanstalt).
- Okada, H., and Bukry, D., 1980. Supplementary modification and introduction of code numbers to the low-latitude coccolith biostratigraphy zonation (Bukry, 1973; 1975). *Marine Micropaleontology*, 5, 321–325.
- Olsson, R.K., Hemleben, C., Berggren, W.A. and Huber, B.T., 1999. Atlas of Paleocene planktonic foraminifera. *Smithsonian Contributions Paleobiology*, 85, 1–252.
- Perch-Nielsen, K., 1985. Cenozoic calcareous nannofossils. In: Bolli, H.M., Saunders, J.B. and Perch-Nielsen, K. (eds.). *Plankton Stratigraphy*, Cambridge University Press, pp. 427–554.
- Perch-Nielsen, K., McKenzie, J., He, Q., 1982. Biostratigraphy and isotope stratigraphy and the „catastrophic“ extinction of calcareous nannoplankton at the Cretaceous/Tertiary boundary.- In: Silver, L.T. and Schultz, P.H. (eds.): *Geological Implications of Impacts of Large Asteroids and Comets on the Earth*. Geological Society of America Special Paper, 190: 353–371.
- Peryt, D., Lahodynsky, R., Rocchia, R., Boclet, D., 1993. The Cretaceous/Paleogene boundary and planktonic foraminifera in the Flyschgosau (Eastern Alps, Austria). *Palaeogeography, Palaeoclimatology, Palaeoecology*, 104, 239–252.
- Peryt, D., Lahodynsky, R. and Durakiewicz, T., 1997. Deep-water agglutinated foraminiferal changes and stable isotope profiles across the Cretaceous-Paleogene boundary in the Rotwand section, Eastern Alps (Austria). *Palaeogeography, Palaeoclimatology, Palaeoecology*, 132, 287–307.
- Pickering, K.T., Hiscott, R.N. and Hein, F.J. (1989). *Deep-marine environments*. 416 p., London (Unwin Hyman).
- Piper, D.J.W. and Normark, W.R., 1983. Turbidite-deposits, patterns and flow characteristics, Navy Submarine Fan, California borderland. *Sedimentology*, 30, 681–694.
- Preisinger, A., Zobetz, E., Gratz, A., Lahodynsky, R., Becke, M., Mauritsch, H.J., Eder, G., Grass, F., Rögl, F., Stradner, H. and Surenian, R., 1986. The Cretaceous/Tertiary boundary in the Gosau Basin, Austria. *Nature*, 322, 797–799.
- Prey, S., 1952. Aufnahmen in der Flyschzone auf den Blättern Gmunden-Schafberg (4851) und Kirchdorf/Krems (4852) (Gschlifgraben), sowie den Blättern Ybbs (4754) und Gaming-Mariazell (4854) (Rogatsboden).-*Verhandlungen der Geologischen Bundesanstalt*, 1952, 41–45.
- Prey, S., 1957. Ergebnisse der bisherigen Forschungen über das Molassefenster von Rogatsboden (NÖ.). *Jahrbuch der Geologischen Bundesanstalt* 100, 299–358.
- Pujalte, V. and Schmitz, B., 2006. Abrupt climatic and sea level changes across the Paleocene-Eocene boundary, as recorded in an ancient coastal plain setting (Pyrenees, Spain). *Climate and biota of the Early Paleogene Abstracts*, p. 103 (Bilbao).
- Rasser, M.W. and Piller, W.E., 1999. Kroisbachgraben und Frauengrube: Lithostratigraphische Typuslokalitäten für das paläogene Helvetikum in Salzburg. *Abhandlungen Geologische Bundesanstalt*, 56, 713–722.
- Rasser, M.W. and Piller, W.E., 2001. Facies patterns, subsidence and sea-level changes in ferruginous and glauconitic environments: The Paleogene Helvetic shelf in Austria and Bavaria. *Österreichische Akademie der Wissenschaften Schriftenreihe der Erdwissenschaftlichen Kommissionen*, 14, 77–110.
- Rögl, F. and Egger, H., 2010. The missing link in the evolutionary origin of the foraminiferal genus *Hantkenina* and the problem of the lower-middle Eocene boundary. *Geology*, 38, 23–26.
- Ritchie, J. D. and Hitchen, K., 1996. Early Paleogene offshore igneous activity to the northwest of the UK and its relationship to the North Atlantic igneous province. Correlation of the Early Paleogene in Northwest Europe (Knox, R. W. O'B., Corfield, R. M. and Dunay, R. E., eds.), *Geological Society*

- London Special Publication, 101, 63–78.
- Rögl, F. and Egger, H., 2010. The missing link in the evolutionary origin of the foraminiferal genus *Hantkenina* and the problem of the lower-middle Eocene boundary. *Geology*, 38, 23–26.
- Röhl, U., Bralower, T.J., Norris, R.D. and Wefer, G., 2000. New chronology for the late Palaeocene thermal maximum and its environmental implications. *Geology*, 28, 927–930.
- Ross, P.S., Ukstins, A., Peate, I., McClintock, M.K., Xu, Y.G., Skilling, I.P., White, J.D.L. and Houghton, B.F., 2005. Mafic volcanoclastic deposits in flood basalt provinces: A review. *Journal of Volcanology Geothermal Research*, 145, 281–314.
- Schaub, H., 1981. *Nummulites et Assilines de la tethys paleogene, taxonomie, phylogenese et biostratigraphie*. *Memoires Suisses de Paleontologie* 104, 1–236
- Schlosser, M., 1925. *Die Eocänfaunen der bayerischen Alpen*. 1. Teil: Die Faunen des Unter- und Mitteleocän. *Abhandlungen Bayerische Akademie der Wissenschaften, Mathematisch-naturwissenschaftliche Abteilung*, 30, 1–207.
- Schmitz, B. and Pujalte, V., 2007. Abrupt increase in extreme seasonal precipitation at the Paleocene-Eocene boundary. *Geology*, 35, 215–218.
- Schmitz, B., Pujalte, V. and Nunez-Betelu, K., 2001. Climate and sea-level perturbations during the Initial Eocene Thermal Maximum: evidence from siliciclastic units in the Basque Basin (Ermua, Zumaia and Trabakua Pass), northern Spain. *Palaeogeography, Palaeoclimatology, Palaeoecology*, 165, 299–320.
- Schmitz, B., Peucker-Ehrenbrink, B., Heilmann-Clausen, C., Åberg, G., Asaro, F. & Lee, C.-T. A., 2004: Basaltic volcanism, but no comet impact, at the Paleocene/Eocene boundary: high-resolution chemical and isotopic records from Egypt, Spain and Denmark. *Earth and Planetary Science Letters*, 225, 1–17.
- Schulte, P. Speijer, R., Mai, H. and Kontny, A., 2006. The Cretaceous-Paleogene (K-P) boundary at Brazos, Texas: Sequence stratigraphy, depositional events and the Chicxulub impact. *Sedimentary Geology*, 184, 77–109.
- Schwerd, K., 1996. *Ultrahelvetikum*. In: Freudenberger, W. and Schwerd, K.: *Erläuterungen zur Geologischen Karte von Bayern 1:500 000*, pp. 205–210.
- Serra-Kiel, J., Hottinger, L., Caus, E., Drobne, K., Fernandez, C., Jaurhi, A.K., Less, G., Pavlovec, R., Pignatti, J., Samso, J.M., Schaub, H., Sirel, E., Strougo, A., Tambareau, Y., Tosquella, J., Zakrevskaya, E., 1998. Larger foraminiferal biostratigraphy of the Tethyan Paleocene and Eocene. *Société Géologique de France Bulletin*, 169, 281–299.
- Shultz, M.R. and Hubbard, S.M., 2005. Sedimentology, stratigraphic architecture, and ichnology of gravity-flow deposits partially ponded in a growth-fault-controlled slope minibasin, Tres Pasos Formation (Cretaceous). *Journal of Sedimentary Research*, 75, 440–453.
- Sinclair, H.D. and Tomasso, M., 2002. Depositional evolution of confined turbidite basins. *Journal of Sedimentary Research*, 72, 451–456.
- Sissingh, W., 1977. Biostratigraphy of Cretaceous calcareous nannoplankton. *Geologie en Mijnbouw*, 56, 37–65.
- Sluijs, A., H. Brinkhuis, C.E. Stickley, J. Warnaar, G.L. Williams and M. Fuller, 2003. Dinoflagellate cysts from the Eocene - Oligocene transition in the Southern Ocean: Results from ODP Leg 189. *Proceedings of the Ocean Drilling Program, Scientific Results*. N. Exon and J. P. Kennett. College Station, Texas, U.S. Government Printing Office 189.
- Sluijs, A., Pross, J. and Brinkhuis, H., 2005: From greenhouse to icehouse; organic-walled dinoflagellate cysts as paleoenvironmental indicators in the Paleogene. *Earth Science Reviews*, 68, 281–315.
- Sluijs, A., Brinkhuis, H., Schouten, S., Bohaty, S.M., John, C.M., Zachos, J.C., Reichart, G.-J., Sinninghe Damsté, J.S., Crouch, E.M. and Dickens, G.R., 2007a. Environmental precursors to light carbon input at the Paleocene/Eocene boundary. *Nature*, 450, 1218–1221.
- Sluijs, A., Bowen, G.J., Brinkhuis, H., Lourens, L.J., Thomas, E., 2007b. The Paleocene-Eocene Thermal Maximum super greenhouse: biotic and geochemical signatures, age models and mechanisms of global change. In: Williams, M., Haywood, A.M., Gregory, J. and Schmidt, D.N. (eds.): *Deep-Time Perspectives on Climate Change: Marrying the Signal from Computer Models and Biological Proxies*. The Micropalaeontological Society, Special Publications, pp. 323–349, London (Geological Society London).
- Sluijs, A., Brinkhuis, H., Crouch, E.M. et al. (2008): Eustatic variations during the Paleocene-Eocene greenhouse world. - *Paleoceanography*, 23: PA4216.
- Sluijs, A., Bijl, P.K., Schouten, S., Röhl, U., Reichart, G.-J. and Brinkhuis, H., 2011: Southern ocean warming, sea level and hydrological change during the Paleocene-Eocene thermal maximum. *Climate of the Past*, 7, 47–61.
- Smith, R., 2004. Silled sub-basins to connected tortuous corridors: sediment distribution systems on topographically complex sub-aqueous slopes. In: Lomas, S.A. and Joseph, P. (Eds.): *Confined Turbidite Systems*. Geological Society London Special Publication, 222, pp.23–43.
- Stampfli, G.M., Mosar, J., Marquer, D., Marchant, R., Baudin, T., Borel, G., 1998. Subduction and obduction processes in the Swiss Alps. *Tectonophysics*, 296, 159–204.
- Stampfli, G.M., Borel, G., Marchant, R., Mosar, J., 2002. Western Alps geological constraintson western Tethyan reconstructions. *Journal virtual explorer* 8, 77–106.
- Steinmetz, J.C., 1979. Calcareous nannofossils from the North Atlantic ocean, Leg 49, Deep Sea Drilling Project. *Initial Reports of the Deep Sea Drilling Project*, 49, 519–531.
- Steurbaut, E, Magioncalda, R., Dupuis, C, Van Simaey, S., Roche, E., Roche, M., 2003. Palynology, paleoenvironments, and organic carbon isotope evolution in lagoonal Paleocene-Eocene boundary settings in North Belgium. In: Wing, S.L., Gingerich, P., Schmitz, B., Thomas, E. (eds.), *Causes and Consequences of Globally Warm Climates in the Early Paleogene*, Geological Society of America Special Paper, 369, 291–317.
- Stover, L.E. and G.L. Williams, 1995. "A revision of the Paleogene dinoflagellate genera *Areosphaeridi-*

- um Eaton 1971 and *Eatonicysta* Stover and Evitt 1978." *Micropaleontology* 41, 97–141.
- Stradner, H., Eder, G., Grass, F., Lahodynsky, R., Mauritsch, H.J., Preisinger, A., Rögl, F., Surenian, R., Zeissl, W. and Zobetz, E., 1987. New K/T boundary sites in the Gosau Formation of Austria. *Terra cognita*, 7, 212 (Paris).
- Tantawy, A.A.A.M., 2003. Calcareous nannofossil biostratigraphy and paleoecology of the Cretaceous-Tertiary transition in the central eastern desert of Egypt. *Marine Micropaleontology*, 47, 323–356.
- Tjalsma, R.C. & Lohmann, G.P. (1983): Paleocene-Eocene bathyal and abyssal benthic foraminifera from the Atlantic Ocean. - *Micropaleontology Special Publication*, 4: 1–90.
- Thomas, E., 1998. Biogeography of the Late Paleocene benthic foraminiferal extinction. – In: Aubry, M.-P., Lucas, S. and Berggren, W.A. (editors). *Late Paleocene-Early Eocene climatic and biotic events in the marine and terrestrial records*. 214–243. – New York (Columbia University Press).
- Tremolada, F. & Bralower, T.J. (2004): Nannofossil assemblage fluctuations during the Paleocene-Eocene Thermal Maximum at Sites 213 (Indian Ocean) and 401 (North Atlantic Ocean): palaeoceanographic implications. - *Marine Micropaleontology*, 52: 107–116.
- Uchman, A., 1999. Ichnology of the Rhenodanubian Flysch (Lower Cretaceous-Eocene) in Austria and Germany. *Beringeria*, 25, 67–173.
- van der Zwaan, D.J., Jorissen, F.J., de Stigter, H.C., 1990. The depth dependency of planktonic/benthic foraminiferal ratios: Constraints and applications. *Marine Geology*, 95, 1–16.
- Vogeltanz, R., 1977. Geologie des Wartstein-Straßentunnels, Umfahrung Mattsee (Land Salzburg). *Verhandlungen der Geologischen Bundesanstalt, Jahrgang 1977*, 279–291.
- Wagreich, M., 1993. Subcrustal tectonic erosion in orogenic belts - A model for the Late Cretaceous subsidence of the Northern Calcareous Alps (Austria). *Geology*, 21, 941–944.
- Wagreich, M. (ed.) (2009): *Rapid Environmental/Climate Changes and Catastrophic Events in Late Cretaceous and Early Paleogene*. RECCCE Workshop Abstracts and Excursion Guide. – *Berichte der Geologischen Bundesanstalt*, 78: 74 pp.
- Wagreich, M., Egger, H., Gebhardt, H., Mohamed, O., Spötl, C., Koukal, V., Hobiger, G., 2011. A new expanded record of the Paleocene-Eocene transition in the Gosau Group of Gams (Eastern Alps, Austria). *Annalen Naturhistorisches Museum Wien, Serie A*, 113, 35–65
- Walker, R.G. (1978): Deep water sandstone facies and ancient submarine fans: models for exploration of stratigraphic traps. - *AAPG Bulletin*, 62: 932–966.
- Waskowska-Oliwa, A. and Lesniak, T., 2002. Lower Eocene Tuffites in the Zegocina Zone (Polish Flysch Carpathians). *Geologica Carpathica*, 53, 45–47.
- Weidich, K.F. and Schwerd, K., 1987. Über den Feuerstätter Flysch im Allgäu. *Neues Jahrbuch für Geologie und Paläontologie Abhandlungen*, 174, 193–212.
- Wessely, G., 1987. Mesozoic and Tertiary evolution of the Alpine-Carpathian foreland in eastern Austria. *Tectonophysics*, 137, 45–59.
- Westerhold, T., Röhl, U., McCarren, H.K. & Zachos, J.C. (2009): Latest on the absolute age of the Paleocene-Eocene Thermal Maximum (PETM): New insights from exact stratigraphic position of key ash layers +19 and –17. - *Earth and Planetary Science Letters*, 287: 412–419.
- Wicher, C.A., 1956. Die Gosau-Schichten im Becken von Gams (Österreich) und die Foraminiferengliederung der höheren Oberkreide in der Tethys. – *Paläontologische Zeitschrift*, 30, 87–136.
- Williams, G.L., H. Brinkhuis, M.A. Pearce., R.A. Fensome and J.W. Weegink, 2004. Southern Ocean and global dinoflagellate cyst events compared: Index events for the Late Cretaceous - Neogene. *Proceedings of the Ocean Drilling Program, Scientific Results* 189. N. F. Exon, J. P. Kennett and M. J. Malone, 189, 1–98.
- Winchester, J.A. and Floyd, P.A., 1977. Geochemical discrimination of different magma series and their differentiation products using immobile elements. *Chemical Geology*, 20, 325–343.
- Winkler W., Galetti G. and Maggetti, M., 1985. Bentonite im Gurnigel-, Schlieren- und Wägital-Flysch: Mineralogie, Chemismus, Herkunft. *Eclogae Geologicae Helvetiae*, 78, 545–564.
- Zachos, J.C., Röhl, U., Schellenberg, S.A., Sluijs, A., Hodell, D.A., Kelly, D.C., Thomas, E., Nicolo, M., Raffi, I., Lourens, L.J., McCarren, H. and Kroon, D., 2005. Rapid acidification of the ocean during the Paleocene-Eocene thermal maximum. *Science*, 308, 1611–1615.
- Zetter, R. and Hofmann, Ch.-Ch., 2001. New aspects of the palynoflora of the lowermost Eocene (Krapfeld Area, Carinthia). In: Piller, W.E., Rasser, M.W. (eds.). *Paleogene of the Eastern Alps*, Österreichische Akademie der Wissenschaften Schriftenreihe der Erdwissenschaftlichen Kommissionen, 14, 473–507.
- Zachos, J.C., Arthur, M.A. and Dean, W.E., 1989. Geochemical evidence for suppression of pelagic marine productivity at the Cretaceous/Tertiary boundary. *Nature*, 337, 61–64.
- Zachos, J.C., Bohaty, S.M., John, C.M., McCarren, H., Kelly, C.C. & Nielsen, T. (2007): The Palaeocene-Eocene carbon isotope excursion: constraints from individual shell planktonic foraminifer records. - *Philosophical Transactions of the Royal Society A*, 365: 1829–1842.
- Ziegler, P.A., 1987. Late Cretaceous and Cenozoic intra-plate compressional deformations in the Alpine foreland – a geodynamical model. *Tectonophysics*, 137, 389–420.
- Ziegler, P.A., Bertotti, G., and Cloething, S., 2002. Dynamic processes controlling foreland development - the role of mechanical (de)coupling of orogenic wedges and forelands. In: Bertotti, G. et al. (eds.): *Continental collision and the tectono-sedimentary evolution of forelands*. EGU Stephan Müller Special Publication Series 1, pp.17–56.